Development of Novel Synthetic Strategies for Iminosugar-Based Glycomimetics

by

Krishnakumar K A

10CC18J39003

A thesis submitted to the

Academy of Scientific & Innovative Research for the award of the degree of

DOCTOR OF PHILOSOPHY

in

SCIENCE

Under the supervision of

Dr. Ravi Shankar Lankalapalli

CSIR-National Institute for Interdisciplinary Science and Technology (CSIR-NIIST)
Thiruvananthapuram-695019

Academy of Scientific and Innovative Research

AcSIR Headquarters, CSIR-HRDC campus
Sector 19, Kamla Nehru Nagar,
Ghaziabad, U.P. – 201 002, India

June 2024

सीएसआईआर - राष्ट्रीय अंतर्विषयी विज्ञान तथा प्रौद्योगिकी संस्थान
रसायन विज्ञान तथा प्रौद्योगिकी प्रभाग
विज्ञान तथा प्रौद्योगिकी मंत्रालय, भारत सरकार
इंडस्टिरयल इस्टेट पी.ओ., तिरुवनंतपुरम, भारत 695 019

CSIR - NATIONAL INSTITUTE FOR INTERDISCIPLINARY SCIENCE &TECHNOLOGY
Chemical Sciences and Technology Division
Ministry of Science and Technology, Govt. of India
Industrial Estate P.O., Thiruvananthapuram, Kerala – 695019 INDIA

डॉ. रवि शंकर एल.
प्रधान वैज्ञानिक एवं सह-आचार्य (एसीएसआईआर)
Dr. Ravi Shankar L.
Principal Scientist & Associate Professor (AcSIR)

CERTIFICATE

This is to certify that the work incorporated in this Ph.D. thesis entitled, ***"Development of Novel Synthetic Strategies for Iminosugar-Based Glycomimetics"*** submitted by ***Mr. Krishnakumar K A*** to the Academy of Scientific and Innovative Research (AcSIR) in fulfillment of the requirements for the award of the Degree of ***Doctor of Philosophy in Science***, embodies original research work carried out by the student. We further certify that this work has not been submitted to any other university or Institution in part or full for the award of any degree or diploma. Research materials obtained from other sources and used in this research work have been duly acknowledged in the thesis. Images, illustrations, Figures, tables, etc., used in the thesis from other sources have also been duly cited and acknowledged.

Signature of the student
Name : Krishnakumar K A
Date :18-06-2024

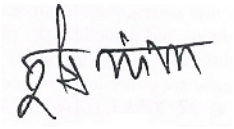

Signature of the supervisor
Name : Dr. Ravi Shankar L
Date :18-06-2024

STATEMENTS OF ACADEMIC INTEGRITY

I **Krishnakumar K A**, a Ph.D. student of the Academy of Scientific and Innovative Research (AcSIR) with Registration No.**10CC18J39003,** hereby undertake that the thesis entitled **"Development of Novel Synthetic Strategies for Iminosugar-Based Glycomimetics"** has been prepared by me and that the document reports original work carried out by me and is free of any plagiarism in compliance with the UGC regulations on *"Promotion of Academic Integrity and Prevention of Plagiarism in Higher Educational Institutions (2018)" and the CSIR Guidelines for Ethics in Research and in Governance (2020)".*

Signature of the student
Date :18-06-2024
Place : Thiruvananthapuram

It is hereby certified that the work done by the student, under my/our supervision, is plagiarism-free in accordance with the UGC Regulations on *"Promotion of Academic Integrity and Prevention of Plagiarism in Higher Educational Institutions (2018)" and the CSIR Guidelines for Ethics in Research and in Governance (2020)".*

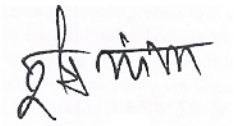

Signature of the supervisor
Name : Dr. Ravi Shankar Lankalapalli
Date :18-06-2024
Place : Thiruvananthapuram

DECLARATION

I, **Krishnakumar K A**, bearing AcSIR Registration No. **10CC18J39003,** declare:

a) that the plagiarism detection software is currently not available at work-place institute.

b) that my thesis entitled, **"Development of Novel Synthetic Strategies for Iminosugar-Based Glycomimetics"** is plagiarism free in accordance with the UGC Regulations on *"Promotion of Academic Integrity and Prevention of Plagiarism in Higher Educational Institutions (2018)" and the CSIR Guidelines for Ethics in Research and in Governance (2020)".*

c) that I would be solely held responsible if any plagiarised content in my thesis is detected,which is violative of the UGC regulations 2018.

Signature of the student

Date :18-06-2024

Place : Thiruvananthapuram

Acknowledgments

This thesis would not have been possible without the guidance and support of a remarkable number of individuals and institutions. I am deeply grateful to all of them.

I extend my deepest gratitude to my esteemed mentor, ***Dr. Ravi Shankar L.*** *His decision to welcome me into his lab not only provided me with the opportunity to embark on this research journey, but also opened the door to the fascinating world of synthetic organic chemistry. His knowledge in this field is truly vast and awe-inspiring. His expertise proved invaluable as I navigated the complexities of carbohydrate research, especially when confronting seemingly insurmountable challenges. His dedication to his students is evident in his preference for regular, in-depth discussions. He has a remarkable ability to motivate and inspire, patiently guiding me through every intricate detail of the subject, both research-specific and broader scientific concepts. I am particularly grateful for the intellectual freedom Dr. Ravi Shankar granted me. This allowed me to delve into areas that sparked my own scientific passions. His unwavering support was instrumental in keeping me afloat during challenging moments, and his constant encouragement has fuelled my desire to pursue a research career. Working under Dr. Ravi Shankar 's supervision undoubtedly ranks as one of the most pivotal experiences of my life.*

I am also incredibly grateful to the Directors of CSIR-NIIST, Dr. C. Anandharamakrishnan and Dr. A. Ajayaghosh (present and former), for allowing me to utilize the institute's infrastructure.

My sincere thanks go to the current and former Heads of the Chemical Sciences and Technology Division (CSTD), Dr. K. V. Radhakrishnan, Dr. Sujatha Devi, and Dr. Luxmi Varma. Their leadership and support within the CSTD fostered a nurturing environment for my research.

I would like to express my sincere gratitude to Dr. P. Jayamurthy, Dr. Karunakaran Venugopal, Dr. Suresh C. H., and Dr. Luxmi Varma, the present and former AcSIR program co-ordinators at CSIR-NIIST, for their invaluable help, support, and guidance with all the academic procedures of AcSIR. I am also grateful to Mr. Merin Santhosh and Ms. Aswathy for their kind support.

I would like to express my appreciation to the members of my Doctoral Advisory Committee (DAC): Dr. C. H. Suresh, Dr. B. S. Sasidhar, and Dr. B. S. Dileep Kumar. Their valuable suggestions and constructive criticism significantly enhanced the quality of my research.

Special thanks go to Dr. Joshy Joseph, Dr. Reshma M. V., and Dr. Jubi John for their unwavering motivation and support throughout my journey.

I am truly grateful to Mrs. Saumini, Mrs. Viji, and Mr. Pratheesh for their instrumental help. Their assistance with various tasks was invaluable.

I owe a debt of gratitude to my seniors, Dr. Jaggaiah, Dr. Chandrashekhar, Dr. Jamsheena, Dr. Veena K S, Dr. Arunkumar T, Dr. Jaice R., Dr. Jesmina. and Dr. Prabha their guidance and expertise in the lab were essential in my development as a researcher.

My lab mates, Sanjay, Naga, Abhi, Sorna, Aksa, Induja, Nirmal, Dr. Aiswarya, Sreedevi, Geethanjali, Vikas, Yadhu, Gayathri, Ameena, and Alna, made my days in the lab memorable with their friendship and camaraderie.

Outside the lab, I am grateful to my friends Billu Abraham, Dr. Saranya Giridharan, Dr. Rajimol, Akhil, and Lal for their unwavering belief in me.

I also want to acknowledge Sanjay Varma, Yadhukrishnan, Sangeeth, Shihas A, Dr. Prabha, and Dr. Shridevi D, who collaborated with me on the COVID-19 project.

Furthermore, thanks go to Dr. Aswathy, Venki, Theertha, Prasanna, Raveena, Kavya, and Abhijith for their support during my CSIR-800 project.

I am indebted to my teachers, Dr. Sadhasivan, Dr. Syamchand, and Mr. Jayachandran, who laid the foundation for my knowledge of chemistry.

I extend my gratitude to all the members of the RMV Group, KPS Group, DBS Group, and KVR Group for creating a collaborative research environment.

My thanks to the scientists and students of the CSTD who provided a supportive and stimulating atmosphere. I also thank all my friends in CSIR-NIIST who made my time there enjoyable.

Financial assistance from the UGC is gratefully acknowledged.

I would like to express my deepest gratitude to my family, especially my Amma, Achan, Chechi, and Aniyan, for their unwavering love and support. My heartfelt thanks go to my wife, Gayathri; your constant encouragement and motivation have been beyond words. I am profoundly grateful to all my family members who stood by me during my toughest times, offering both mental and financial support that was invaluable to my journey. If I haven't mentioned your name here, please know that you hold a special place in my heart. This thesis is dedicated to my entire family and friends, with my deepest appreciation.

Krishnakumar K A

CONTENTS

List of Figures

List of Schemes

List of Table

Abbreviations

$(Boc)_2O$	Di-tert-butyldicarbonate
$(CH_3CO)_2O$	Acetic anhydride
°C	Degree Celsius
µL	Microlitre
^1H NMR	Proton nuclear magnetic resonance
^{13}CNMR	Carbon-13 nuclear magnetic resonance
2,2 DMP	2-dimethoxy propane
Ac	Acetyl
ACN	Acetonitrile
AcOH	Acetic acid
aq	Aqueous solution
ATP	Adenosine triphosphate
$BF_3.Et_2O$	Boron trifluoride diethyl etherate
BH_3-DMS	Borane-dimethyl sulfide
Bn	Benzyl
Boc	T-Butoxycarbonyl
BOMCl	Benzylchloromethychloride

bs	Broad singlet
Bu_4NF	Tetrabutylammonium fluoride
CD_3OD	Methanol-d_4
$CDCl_3$	Deuterated chloroform
$CeCl_3$	Cerium(III) chloride
CH_3CN	Acetonitrile
CH_3COONH_4	Ammonium acetate
$CHCl_3$	Chloroform
COSY	Correlated spectroscopy
COVID-19	Coronavirus disease 2019
CRD	Carbohydrate recognition domain
CuI	Copper(I) iodide
d	Doublet
DCE	2-dichloroethane
DCM	Dichloromethane
dd	Doublet of doublet
DEAM	Diethyl aminomalonate
dGTP	Deoxyguanosine triphosphate
dGuo	Deoxyguanosine
DIPEA	N,N-diisopropylethylamine
DMAP	4-dimethylaminopyridine
DMF	Dimethylformamide
DMP	Dess-Martin periodinane
DMSO	Dimethyl sulfoxide
DMSO-d6	Dimethyl sulfoxide-d6
DRA	Double reductive amination
EDCI	(3-Dimethylamino-propyl)-ethyl-carbodiimide
equiv.	Equivalent
Et_2O	Diethyl ether
Et_3N	Triethylamine
Et_3SiH	Triethylsilane
EtOAc	Ethyl acetate
EtOH	Ethanol
Fmoc	Fluorenylmethyloxycarbonyl
g	Gram
GHs	Glycoside hydrolases
GSLs	Glycosphingolipids
GTs	Glycosyltransferases
Guo	Guanine
h	Hour
H_2	Hydrogen gas
H_2O	Water
HCl	Hydrochloric acid
HCOOH	Formic acid

$HCOONH_4$	Ammonium formate
HR-ESI-MS	High-resolution electrospray ionisation mass spectrometry
HRMS	High resolution mass spectrometry
HSCT	Hematopoietic stem cell transplantation
HWE	Horner–Wadsworth–Emmons
iNKT	Invariant natural killer T
*i*PrMgCl·LiCl	Isopropylmagnesium chloride- lithium chloride
KHSO4	Potassium hydrogen sulfate
K_i	Dissociation constants
KIE	Kinetic isotope effects
LCMS	Liquid chromatography–mass spectrometry
LiTMP	Lithium tetramethylpiperidide
m	Multiplet
M	Molar
m/z	Mass-to-charge ratio
Me_3SiN_3	Trimethylsilyl azide
MeOH	Methanol
MERS	Middle east respiratory syndrome
mg	Milligram
Mg	Magnesium
MHz	Megahertz
mins	Minute
mL	Millilitres
mmol	Millimoles
MTBE	Methyl tertiary butyl ether
N	Normal (Normality)
$Na(CH_3COO)_3BH$	Sodium triacetoxyborohydride
$Na(OAc)_3BH$	Sodium triacetoxyborohydride
$Na_2S_2O_3$	Sodium thiosulfate
Na_2SO_4	Sodium sulfate
$NaBH_3$	Sodium borohydride
$NaCNBH_3$	Sodium cyanoborohydride
NaH	Sodium hydride
NaH_2PO_4	Sodium dihydrogen phosphate
$NaHCO_3$	Sodium bicarbonate
NaHMDS	Sodium hexamethyldisilazide
NaN_3	Sodium azide
NaOH	Sodium hydroxide
NaOMe	Sodium methoxide
*n*BuLi	N-Butyllithium
NCS	N-chlorosuccinimid
NH_2OH	Hydroxylamine
NH_3	Ammonia
NH_4Cl	Ammonium chloride

NIS	N-iodosuccinimide
NMR	Nuclear magnetic resonance
nOe	Nuclear overhauser effect
$Pd(OH)_2$	Palladium hydroxide
Pd/C	Palladium on carbon
pM	Picomolar
PNP	Purine nucleoside phosphorylase
$POCl_3$	Phosphorus oxychloride
ppm	Parts per million
PPTS	Pyridinium p-toluenesulfonate
PTCL	Peripheral T-cell lymphoma
rt	Room temperature
s	Singlet
SARS	Severe acute respiratory syndrome
S_N2	Bimolecular nucleophilic substitution
t	Triplet
T-ALL	T-cell acute lymphoblastic leukemia
TBAF	Tetra-n-butylammonium fluoride
TBDMSCl	Tert-butydimethyllsilyl chloride
t-BuOK	Potassium *tert*-butoxide
Temp.	Temperature
tert	Tertiary
TFA	Trifluoroacetic acid
THF	Tetrahydrofuran
TLC	Thin layer chromatography
TMS	Trimethylsilyl
ZnCl2	Zinc chloride
β-C-GalCer	B-C-Galactosyl Ceramide
α	Alfa
β	Beta
γ	Gamma
δ	Delta

Preface

The realm of medicinal chemistry thrives on innovation, constantly seeking to unlock the potential of nature's building blocks for therapeutic benefit. This thesis delves into two captivating areas within this realm: glycomimetics and iminosugars.

Natural carbohydrates, the essential building blocks known as sugars, play a pivotal role in biological processes. However, their inherent limitations, such as instability and poor bioavailability, often hinder their therapeutic potential. This is where glycomimetics come into play. These meticulously crafted synthetic molecules mimic the structures and functions of natural carbohydrates, offering a powerful tool for influencing biological pathways. The ability of glycomimetics to bind to the same carbohydrate-binding proteins (lectins) as their natural counterparts presents a unique strategy for therapeutic intervention. Unlike natural sugars, glycomimetics can be engineered to possess superior stability, increased bioavailability, and tailored targeting towards specific lectins. These advantages pave the way for the development of more potent and specific drugs with fewer side effects. The potential applications of glycomimetics encompass a broad spectrum of diseases, including viral infections, cancer metastasis, and inflammatory disorders.

Within the fascinating world of glycomimetics lie iminosugars, a class of molecules with a unique structural twist. Iminosugars bear a striking resemblance to natural carbohydrates, but with a key distinction: a nitrogen atom replaces an endocyclic oxygen atom. This seemingly minor change significantly alters their biological properties. Iminosugars exhibit a remarkable range of bioactivities, including potent enzyme inhibition, immune modulation, and antiviral properties. The diverse therapeutic potential of iminosugars has fueled extensive research, leading to the development of several drugs that have progressed through clinical trials and even received regulatory approval. Some prominent examples include Miglustat, used to treat Niemann-Pick type C disease, Miglitol, an effective treatment for type 2 diabetes, and 1-Deoxynojirimycin, a naturally occurring iminosugar with promising applications against viral infections and cancer.

Immucilllins, a specific class of iminosugars, hold particular interest due to their diverse biological application. These molecules can interfere with the way certain organisms, like parasites, process essential molecules. Researchers are particularly interested in immucillin's ability to inhibit an enzyme called human purine nucleoside phosphorylase (PNP). Disrupting PNP function is a potential strategy for treating diseases like gout and some cancers. Nevertheless, research on immucillins continues to inform the development of new and improved medications.

Chapter 2 embarks on a captivating journey of organic synthesis, focusing on the creation of Immucillin-H, a fascinating molecule with potent anticancer properties. Building upon the groundwork laid in Chapter 1, this chapter delves into the intricacies of synthesizing Immucillin-H, a specific class of iminosugar known for its ability to influence the immune system. However, the story doesn't end there. Recognizing the importance of stereochemistry in biological activity, the chapter further explores the synthesis of stereochemical variants of Immucillin-H. These variants, with slightly altered spatial arrangements of atoms, can offer valuable insights into the structure-activity relationship of this immunomodulatory molecule.

Chapter 3 shifts the focus to another captivating member of the immucillin family - Immucillin-A. Building upon the knowledge gained in previous chapters, this chapter delves into the selective synthesis of Immucillin-A starting from a, D-ribonolactam. This strategic approach streamlines the synthetic process and offers a potentially efficient route to this valuable antiviral molecule. The chapter meticulously details the reaction steps involved, emphasizing the importance of achieving the desired stereochemistry and functional groups for Immucillin-A.

The final chapter of this thesis culminates in the development of novel iminosugar analogs inspired by the immunostimulatory molecule KRN-7000. This chapter leverages the knowledge gained in previous chapters on iminosugar synthesis and functionalization. Here, we design and synthesize a series of novel iminosugar analogs with structural similarities to KRN-7000. The focus lies on exploring the potential of these analogs to mimic or even surpass the immunostimulatory properties of KRN-7000. By strategically modifying the structure of the iminosugar core, we aim to create potent immunomodulatory agents with potential therapeutic applications.

This thesis offers a comprehensive exploration of glycomimetics, their synthesis, and their potential applications in the development of novel therapeutic agents. Each chapter builds upon the knowledge established in the previous one, providing a cohesive journey into this exciting area of research.

As you delve into this exploration, you will gain a deeper understanding of the potential of glycomimetics, particularly iminosugars and immucillins, in drug discovery. Their ability to mimic natural sugars while offering advantages in stability and targeting makes them valuable tools for developing novel therapeutics across a broad spectrum of diseases. The future of this field holds immense promise, as ongoing research continues to unlock the secrets of these fascinating molecules, paving the way for advancements in human healthcare.

Significance of Glycomimetics: Synthesis and Examples

1.1. Abstract

This study explores the significant roles of carbohydrates in energy metabolism, genetic material formation, and cellular processes. It highlights advancements in glycomimetics and iminosugars, synthetic analogs designed to mimic carbohydrates while overcoming natural limitations like metabolic instability. Due to their enhanced stability and specific binding capabilities, these compounds show promise in drug development, diagnostics, and materials science. The study also examines immucillins, particularly Immucillin-H and Immucillin-A, which inhibit purine nucleoside phosphorylase (PNP), effectively treating T-cell malignancies and various viral infections. This research underscores the diverse therapeutic applications of these compounds and the evolving landscape of drug design informed by enzymatic mechanisms and transition states.

1.2. Carbohydrates and their Profound Significance

Carbohydrates, Earth's most abundant organic compounds, transcend their role as mere energy sources.[1] Composed of carbon, hydrogen, and oxygen, with a typical 2:1 hydrogen-oxygen ratio, they encompass a diverse array of molecules classified as polyhydroxy aldehydes, ketones, or their derivatives. Beyond the fundamental definition, carbohydrates hold profound significance in the biological world.[2,3]

Firstly, they serve as the primary fuel for living organisms. Glucose, the simplest carbohydrate, is readily metabolized through glycolysis to generate adenosine triphosphate (ATP), the universal energy currency of cells. Furthermore, complex carbohydrates like starch and glycogen act as readily available energy reserves, ensuring the survival of organisms during periods of energy scarcity.[4,5]

The significance of carbohydrates extends far beyond energy provision. They constitute the structural backbone of genetic material, with the sugar molecules in DNA and RNA

forming athe foundation of the genetic code.[6] Moreover, all cells are enveloped by a complex coat of carbohydrates known as glycans. These glycans are not merely passive decorations; they function as intricate identification tags, mediating crucial cell-cell recognition and adhesion processes essential for tissue development and immune function.[7] Carbohydrates are found in different biological conjugates, such as glycoproteins, proteoglycans, and glycolipids. These conjugates play vital roles in numerous fundamental biological processes, including cell signalling, the intricate metabolic pathways of glycolysis and gluconeogenesis, and signal transduction cascades.[8]

The therapeutic potential of carbohydrates is immense. Their specific interactions with proteins and lipids make them ideal targets for drug development. However, inherent limitations, such as insufficient metabolic stability and poor permeation properties, often hinder their efficacy.[9] To address these challenges, scientists have developed chemically modified versions of carbohydrates known as Glycomimetics.[10]

In simple words, carbohydrates are not simply the fuel of life; they are the very building blocks of our existence. Their diverse functions span from energy provision and structural support to intricate communication and signalling within and between cells. While their limitations pose challenges for therapeutic applications, the development of Glycomimetics opens a new avenue for harnessing their immense potential in medicine. Understanding the profound significance of carbohydrates is crucial for appreciating the intricate web of life and the exciting possibilities they hold for the future of healthcare.[11–13]

1.3. Glycomimetics

Glycomimetics, a fascinating class of synthetic molecules, are designed to mimic carbohydrates' structural and functional properties.[14] These intricate molecules, meticulously crafted by synthetic chemists, offer immense potential in various fields, particularly in the realm of medicine. While carbohydrates, the most abundant organic compounds on Earth, play a fundamental role in life, their inherent limitations often hinder their therapeutic application.[15] This is where glycomimetics step in, offering a unique advantage – they possess the desired functionalities of carbohydrates without their inherent drawbacks.

The significance of glycomimetics lies in their ability to overcome the limitations of natural carbohydrates. Unlike their natural counterparts, glycomimetics can be meticulously designed to possess superior metabolic stability and improved permeation properties. This allows them to navigate the complex biological environment more effectively, reaching their target sites with greater potency and efficacy. Moreover, precise control over their chemical structure enables the creation of highly specific glycomimetics that can interact with specific proteins or lipids involved in various biological processes.[15–17] This specificity opens up exciting possibilities for targeted therapeutic interventions.

Furthermore, the field of glycomimetics presents a unique opportunity for scientific advancement. It serves as a bridge between the realms of chemistry and biology, allowing researchers to leverage the power of synthetic chemistry to understand and manipulate complex biological processes. The intricate interplay between the chemical structure and biological activity of these molecules allows for the creation of highly specific and functional mimics. Additionally, the vast amount of data available on carbohydrate-binding proteins provides valuable insights for the design and synthesis of precise glycomimetics with desired properties.[18] The combination of chemistry and biology has enormous potential for discovering new therapeutic options.

The applications of glycomimetics extend far beyond the realm of therapeutics. Their unique properties make them valuable tools in various fields, including:

- **Drug Development:** Glycomimetics can be designed to target specific disease pathways, offering novel therapeutic avenues for various ailments. Their ability to mimic the interactions of carbohydrates with key biological molecules makes them ideal candidates for drug discovery and development.
- **Diagnostics:** Glycomimetics can be utilized as highly specific probes to detect and identify disease biomarkers. Their ability to selectively bind to specific molecules makes them valuable tools for early diagnosis and disease monitoring.
- **Materials Science:** The unique properties of glycomimetics can be harnessed to create novel materials with specific functionalities. For instance, glycomimetics can be incorporated into biocompatible materials for tissue engineering or drug delivery applications.

A well-designed glycomimetic can provide the following benefits:

- ✓ Enhanced Stability
- ✓ Enhanced affinities
- ✓ Increased bioavailability
- ✓ longer serum half-lives
- ✓ Selective Binding
- ✓ Reduced Immunogenicity
- ✓ Improved Pharmacokinetics

Glycomimetics presents a unique and promising approach to leveraging the potential of carbohydrates for therapeutic and technological advancements. Their ability to overcome the limitations of natural carbohydrates creates a vast array of possibilities in various fields, paving the way for a future where these synthetic mimics play a crucial role in improving human health and well-being. Additionally, the continued development of glycomimetics serves as evidence of the power of interdisciplinary collaboration between chemistry and biology, offering exciting prospects for future scientific breakthroughs.[19–22]

1.3.1. Classification of glycomimetics

Glycomimetics are synthetic molecules designed to mimic the structural and functional properties of carbohydrates. This allows them to interact with target proteins, particularly lectins, in place of natural carbohydrates. The most effective lectin antagonists often incorporate a natural carbohydrate fragment or a carbohydrate-like scaffold to guide the molecule toward the lectin's carbohydrate recognition domain (CRD). One common and effective modification employed in these scaffolds is deoxygenation. This process strategically removes or replaces non-essential oxygen atoms or hydroxyl groups with different atoms or groups. These modifications alter the molecule's overall properties, including its polarity, stability, conformation, ring flexibility, and hydrogen bonding patterns. Notably, deoxygenation often decreases polar surface area, which can significantly increase binding affinity. This improvement arises from creating new hydrophobic interactions with the protein and reducing the energy required to remove water molecules from the ligand during binding (desolvation penalty). It's important to note that not all carbohydrate-based drugs currently in clinical use primarily interact with lectins.[14,23–25]

Glycomimetics typically possess a carbohydrate or carbohydrate-like core structure, often further decorated with non-carbohydrate components. These additional elements enhance the interaction between the glycomimetic and its target lectin, leading to stronger and more specific binding. Furthermore, incorporating non-carbohydrate moieties can significantly decrease the ligand's overall polarity, improving its drug-like properties. Another crucial aspect of glycomimetic design is conformational preorganization. This refers to the molecule's inherent shape, which is pre-configured to minimize the entropic penalty associated with ligand binding. The following section will delve deeper into the classification of glycomimetics based on their structural features and provide a brief overview of their general characteristics.[26,27]

1.3.1.1. Replacement of endocyclic oxygen

The modification of the endocyclic oxygen atom in a carbohydrate scaffold with different atoms or groups results in the creation of various glycomimetics. Depending on the substituent used, these glycomimetics can be further classified based on the nature of the atom that replaces the endocyclic oxygen atom. This substitution leads to distinct classes of glycomimetics (Figure 1.3.1.1).

- **Replacement with carbon:** Carbasugars (cyclitols) are a class of glycomimetics formed by replacing the endocyclic oxygen atom in a carbohydrate ring with a carbon atom. This structural modification eliminates the anomeric center, a key site for glycosidase and glycosyltransferase activity. Consequently, carbasugars exhibit enhanced metabolic stability against these enzymes, making them less susceptible to degradation. The absence of endocyclic oxygen also abolishes the anomeric effect, a phenomenon that influences the hydrogen bonding potential, ring flexibility, and overall conformation of the carbohydrate. This altered behaviour can be advantageous for designing carbasugars with specific binding properties tailored for target recognition.[28]
- **Replacement with nitrogen:** Replacing the endocyclic oxygen with nitrogen in a monosaccharide ring yields iminosugars, one of the most extensively studied classes of monosaccharide mimics.[29] These naturally occurring compounds are found in plants and microorganisms. The endocyclic nitrogen atom in iminosugars acquires a positive charge at physiological pH. This unique feature allows them to closely mimic the positively charged oxocarbenium ion transition state intermediate

formed during the activity of glycosyl-hydrolases and -transferases. This property has been harnessed for their development as potent inhibitors of these enzymes, leading to their clinical use in various therapeutic applications.[30]

- **Replacement with sulphur:** Replacing the endocyclic oxygen with sulphur in sugars results in the formation of thio-sugars, which are generally more hydrophobic compared to their oxygen counterparts. This increased hydrophobicity has the potential to enhance their binding affinity to proteins through stronger hydrophobic interactions.[31]
- **Replacement with phosphorus:** Phosphorus-based glycomimetics are a class of compounds where a phosphorus atom replaces either the anomeric carbon or the endocyclic oxygen atom in the sugar ring. These can be further categorized into three main groups. Phospha-sugars mimic the overall structure of carbohydrates but lack the endocyclic oxygen atom entirely. Phosphono-sugars (phostones): These possess a phosphorus atom linked to the anomeric carbon through a C-P bond. The phosphonolactone group (O–P=O) in phostones acts as a bioisostere of the hemiacetal group (O–C–OH) found in natural sugars. Phosphino-sugars (phostines, 1,2-oxaphosphinanes): These feature a phosphorus atom incorporated into a five-membered ring, mimicking carbohydrates' pyranose or furanose forms. The phosphinolactone group (O–P–O) present in phostines also serves as a bioisostere of the hemiacetal group.[32,33]

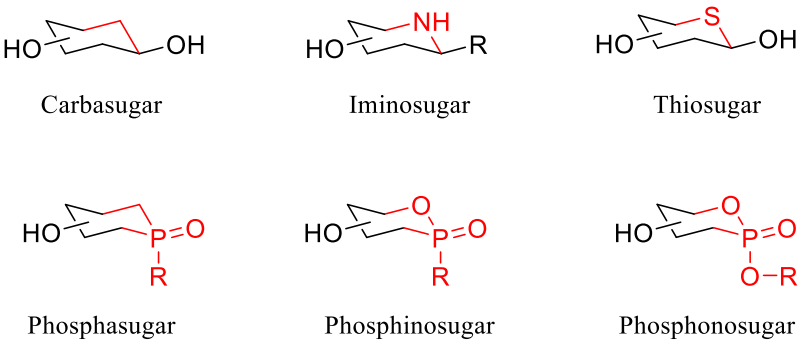

Figure 1.3.1.1: Endocyclic oxygen replacement

1.3.1.2. Alteration on the O-glycosidic linkage

Another key classification of glycomimetics hinges on the nature of the glycosidic linkage. In natural O-glycosides, the oxygen atom connecting the sugar units poses a challenge. This

linkage is susceptible to breakdown by both chemical reactions and enzymes within the body, limiting the drug's pharmacokinetic properties like bioavailability and half-life in the bloodstream. To overcome this hurdle, a common strategy involves replacing the oxygen atom in the glycosidic linkage with another atom that forms a more stable bond. Common alternatives include nitrogen, carbon, sulphur, or selenium, as illustrated in Figure 1.3.1.2.

- **C-glycosides and C-acylglycosides:** They boast remarkable resistance to hydrolysis but their inherent structural difference involving a carbon linkage can lead to unintended conformational changes. This occurs because they lack the stabilizing exo-anomeric effect present in traditional O-glycosides.[34]
- **N-glycosides:** N-glycosides are a type of glycomimetic where the glycosidic linkage involves an N-C bond. Acylated N-glycosides are commonly employed for the glycosylation of both synthetic and natural peptides. However, N-glycosidic bonds formed between two carbohydrate units through an N, O-acetal linkage are inherently unstable and rarely encountered in nature.[35]
- **Thioglycosides:** These analogs of O-glycosides offer enhanced stability due to sulphur's lower basicity compared to oxygen, making the S-glycosidic bond more resistant to hydrolysis. Thioglycosides not only exhibit diverse biological activities but also serve as valuable tools for studying carbohydrate-protein interactions through crystallographic techniques.[35]
- **Selenoglycosides:** Similar to thioglycosides, selenoglycosides are used as glycosyl donors in oligosaccharide synthesis and offer additional applications in crystallographic studies of carbohydrate-protein interactions.[36]

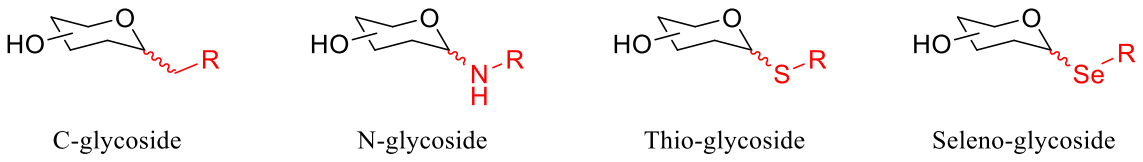

Figure 1.3.1.2: Alteration on the O-glycosidic linkage

1.3.1.3. Replacement of OH functional groups

Glycomimetics can also be classified based on modifications to their hydroxyl groups. Deoxygenation, the process of replacing a hydroxyl group with a hydrogen atom, leads to several beneficial effects. It reduces the molecule's overall polarity, making it easier for it

to exit the surrounding water molecules (desolvation) and potentially form new hydrophobic interactions with target proteins. Additionally, removing an electron-withdrawing hydroxyl group increases the electron density of the remaining scaffold. This can enhance the nucleophilicity (electron-donating ability) of other hydroxyl groups, potentially strengthening interactions like metal coordination or hydrogen bonding.[37]

Hydroxyl groups within glycomimetics can be further modified by replacing them with bioisosteres like fluorine (-F), methoxy (-OCH_3), thiol (-SH), selenol (-SeH), and amine (-NH_2). Each substitution offers unique advantages, Fluorine, with its high electronegativity, creates a highly polarized C-F bond. This leads to increased lipophilicity (fat solubility), decreased acidity (lower pKa) of neighbouring hydroxyl groups, and altered hydrogen bonding capabilities. Additionally, fluorine substitution can destabilize the oxocarbenium ion transition state involved in enzymatic glycosidic bond hydrolysis, potentially inhibiting the enzyme's activity.[37–41]

Etherification of hydroxyl groups is a common strategy in glycomimetic design to probe ligand binding requirements and can even be essential for recognition by specific lectins. Replacing oxygen with sulphur or selenium creates larger, more polarizable atoms. This leads to Increased lipophilicity, making the molecule more fat-soluble, Weaker hydrogen bond donor properties compared to hydroxyl groups Enhanced potential for π-interactions with target proteins. However, the synthesis of thioethers and selenoethers is often more challenging compared to ethers, and their redox instability limits their widespread use. Additionally, the amino group gains a positive charge at physiological pH, significantly altering its properties compared to the neutral hydroxyl group and diminishing its effectiveness as a mimic.[42]

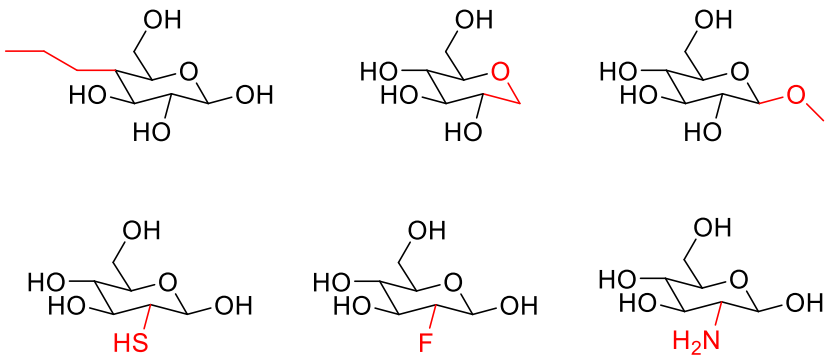

Figure 1.3.1.3: Replacement of OH functional groups

1.3.1.4. Replacement of H Atoms

Glycomimetic design can also involve the strategic substitution of hydrogen atoms within the carbohydrate scaffold. Due to its small size, chemical stability, and inherent hydrophobicity, Fluorine is often used as a bioisostere for hydrogen. While it shares similar steric properties, its strong electron-withdrawing effect can significantly influence the behaviour of neighbouring functional groups. Other small, hydrophobic groups like alkynes, fluoroalkyl chains, hydroxyls, and hydroxymethyls can also be employed for hydrogen replacement. Replacing hydrogen with an alkyne group has been proposed to enhance conformational preorganization due to stronger van der Waals interactions compared to hydrogen.[43–45]

Carboxylate groups are present in crucial glycan building blocks like neuraminic and uronic acids, yet their bioisosteric replacement in glycomimetic design remains uncommon. Traditional medicinal chemistry offers potential bioisosteres like amides, sulfonic acids, phosphonates, and tetrazoles. However, these alternatives are rarely employed in the development of glycan-based drugs, likely due to the critical role carboxylate interactions play in achieving effective binding with target molecules. This revised version provides a clearer structure and emphasizes the rationale behind hydrogen substitution in glycomimetics. It also highlights the specific properties of fluorine and other potential substitutes, while acknowledging the limited use of -CO_2^- bioisosteres in glycan-based drugs due to the importance of carboxylate interactions.[46,47]

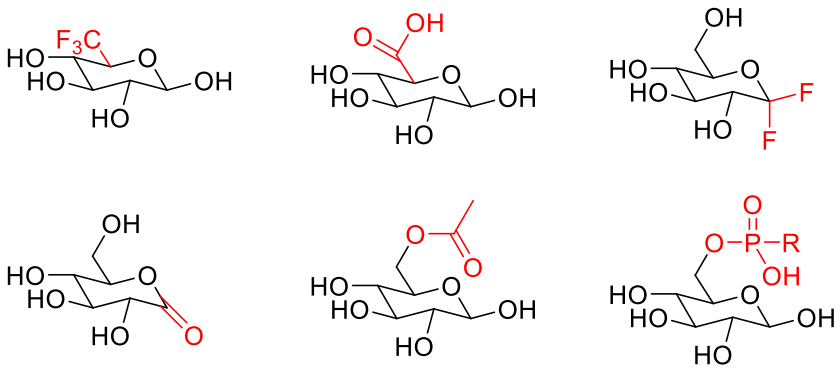

Figure 1.3.1.4: Replacement of OH functional groups

1.3.2. Importance of glycomimetic synthesis

Mimicking the intricate code of sugars within glycomimetics is a formidable task. Lectins, proteins that decipher this code through oligosaccharide binding, further complicate

matters. Their large, flat, solvent-exposed binding sites inherently limit binding affinity. Yet, recent clinical trial triumphs with the galectin modulator TD139 and selectin antagonists like rivipansel and uproleselan have ignited excitement in the pharmaceutical industry, demonstrating the potential to conquer these challenges.[48,49]

The most potent lectin antagonists leverage a natural sugar unit, usually a single sugar (monosaccharide), as an anchor. This anchor steers the molecule toward the lectin's carbohydrate recognition domain (CRD). It's then linked to scaffolds or extra fragments, allowing for additional interactions near the sugar-binding site on the target protein. Recent breakthroughs in carbohydrate chemistry have enabled a wider variety of structural tweaks, resulting in improved drug-like properties and better stability within the body (*in vivo*). Importantly, these modifications often aim to decrease the overall polarity of the ligand. This not only strengthens binding affinity but also improves how the drug travels passively through the body (passive permeation) and other pharmacokinetic parameters compared to the highly hydroxylated structures of natural carbohydrates.[24,50]

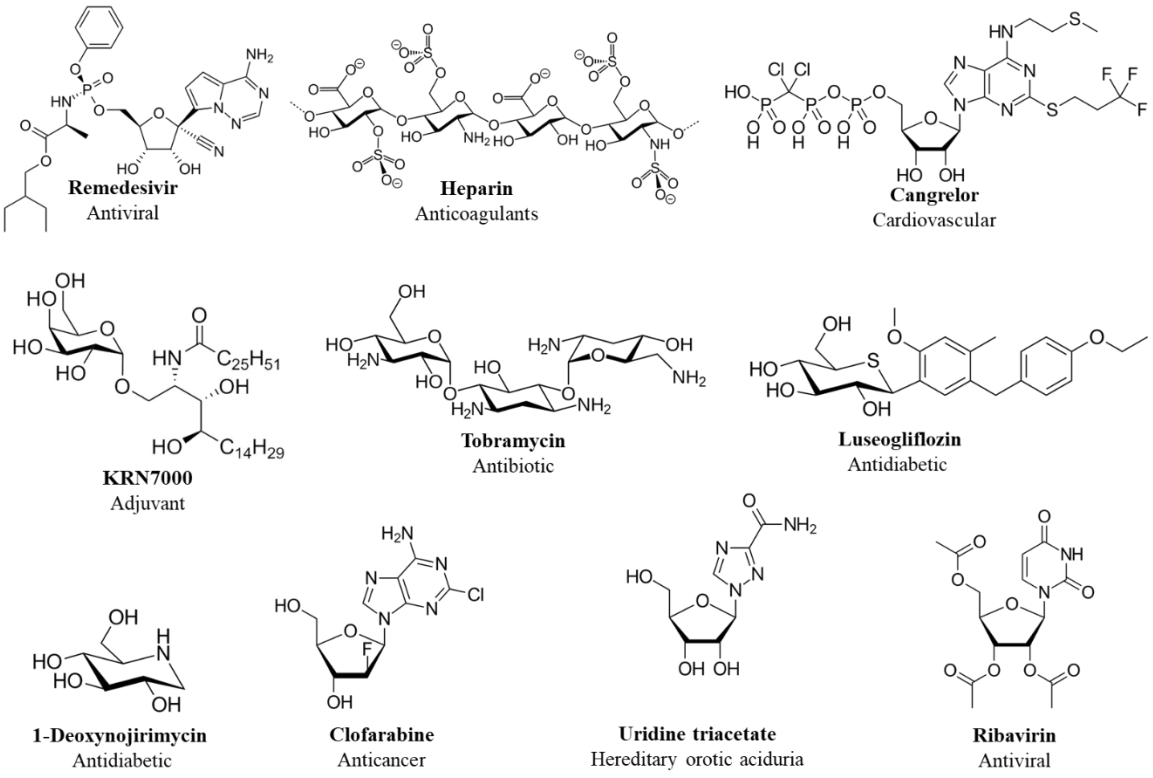

Figure 1.3.2: Some important glycomimetic drugs[55]

Glycomimetics as enzyme blockers hold promise for new treatments. Enzymes called glycoside hydrolases (GHs) and glycosyltransferases (GTs) help build sugar molecules

crucial for cell communication, immune response, inflammation, and even cancer spread. Changes in these sugar decorations, especially a type called sialylation, are linked to various diseases. Over 150 different GH and GT families exist, classified by their building block similarities. Many inhibitors for these enzymes have been discovered, aiding research into how they work and potentially leading to new drugs. Designing these successful blockers often involves mimicking a fleeting molecular shape, the transition state, formed during sugar breakdown. This state has a positive charge, which is mimicked in two ways: by flattening a sugar ring to match the transition state's shape or by adding groups that can become charged.[51–54]

In conclusion, while mimicking the intricate code of sugars within glycomimetics presents a challenge, recent advancements are opening doors for novel therapeutic strategies. Lectin antagonists, designed to target specific sugar-binding proteins, are being optimized for stronger binding and improved drug-like properties. Glycomimetics can also act as enzyme inhibitors, mimicking a fleeting molecular shape crucial for sugar breakdown and potentially disrupting processes linked to various diseases. Overall, the field of glycomimetic research holds immense promise for the future of medicine, offering exciting possibilities for new treatments that target cell communication, immune response, and even cancer progression.

1.4. Introduction to iminosugar

Iminosugars, natural or synthetic, are small organic molecules that mimic carbohydrates or the transition states formed during their breakdown. They achieve this mimicry by incorporating a nitrogen atom within their ring structure, replacing an oxygen atom. This substitution allows for not only single-ring (monocyclic) but also double-ring (bicyclic) scaffolds.[56] In bicyclic iminosugars, the nitrogen atom can be strategically placed at a junction shared by both rings. Hydroxyl groups are the most common substituents on these rings, but nature also offers iminosugars with carboxylic acids and amides. Synthetic analogs further expand the possibilities with a wider variety of functional groups.[57]

Natural iminosugars exhibit a remarkable diversity in structure, with five main classes identified (Figure 1.4): pyrrolidines, piperidines, indolizidines, pyrrolizidines, and nor-tropanes. These molecules share the defining feature of a nitrogen atom replacing oxygen within their cyclic framework, mimicking the structure of sugars but with a key variation.

Each class is distinguished by its ring size and configuration, resulting in a wide array of structural possibilities. Pyrrolidines and piperidines are characterized by simple five- and six-membered rings, respectively. Indolizidines exhibit a more complex bicyclic structure with fused rings, while pyrrolizidines possess a five-membered ring containing a distinctive nitrogen bridge. Finally, nor-tropanes represent the most intricate class, featuring a bridged bicyclic structure reminiscent of the tropane alkaloid cocaine. This remarkable structural diversity within natural iminosugars suggests a broad spectrum of potential biological functions and applications[58–61]

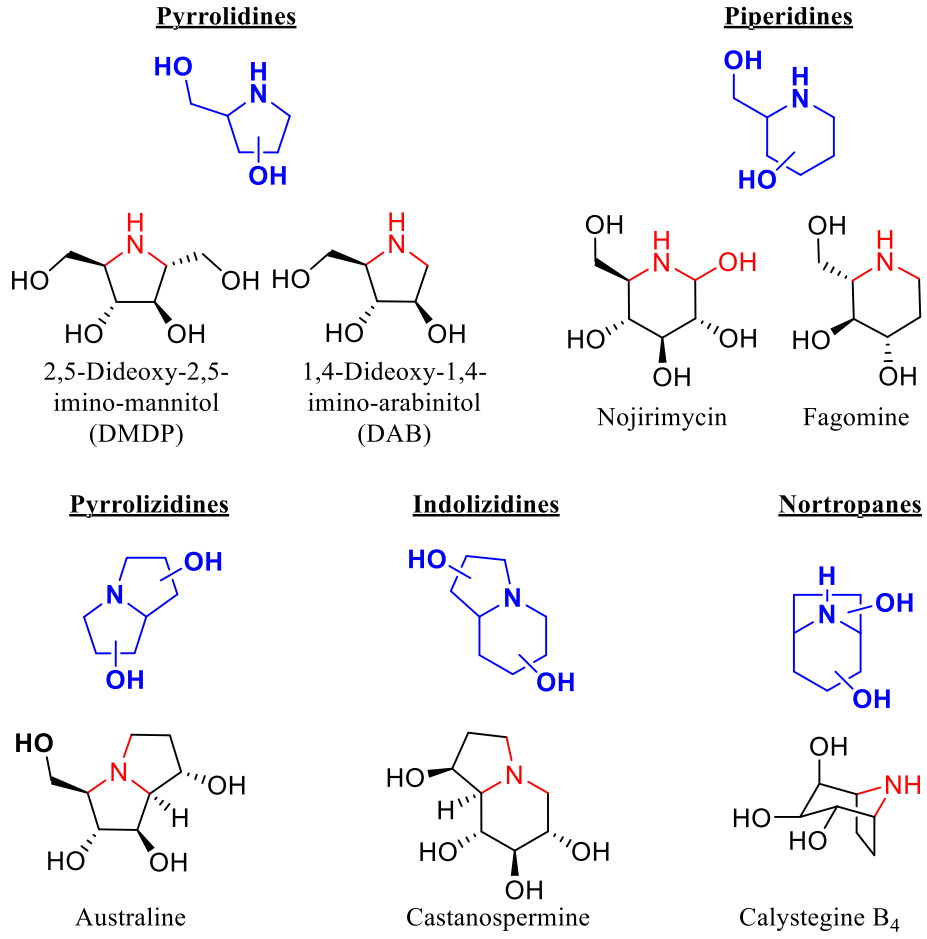

Figure 1.4: Classification of iminosugar with examples

Iminosugars emerged as a leading class of modulators for carbohydrate-processing enzymes. This pioneering role has allowed scientists to achieve remarkable feats, including altering the glycosylation patterns of human cells, disrupting the metabolism of sugars and sugar-containing molecules (glycoconjugates), and modifying the sugar-dependent functionalities of proteins.[62] Additionally, iminosugars have shown promise in blocking

interactions between host cells and infectious agents, offering a potential weapon against pathogens.[63] These fascinating biological properties have positioned iminosugars as a promising new frontier for therapeutic drug development, with the potential to address a wide range of diseases.

1.4.1. Significance of iminosugar C glycoside

The inhibitory potential of iminosugars has expanded beyond glycosidases to encompass a wider range of medicinally relevant enzymes, including glycosyltransferases, metalloproteinases, nucleoside-processing enzymes, and sugar nucleotide mutases. This broad enzymatic target profile is particularly attractive due to the involvement of these enzymes in numerous fundamental biological processes. Consequently, iminosugars offer promising leads for the development of novel therapeutics across various disease areas. However, the focus on synthetically accessible derivatives has resulted in a predominance of simple iminoalditols related to 1-deoxynojirimycin lacking substituents at the anomeric position. This structural limitation compromises the ability of these iminosugars to mimic the full complexity of oligosaccharides or glycoconjugates when targeting carbohydrate-processing enzymes.

Iminosugar-O-glycoside (unstable)

Iminosugar-C-glycoside (stable)

Figure 1.4.1.a: Representative structure of iminosugar

A major challenge in using imino sugar analogs of glycosides is their natural instability. This is due to the weakness of the aminal linkage, which makes them unsuitable as biological probes or drug candidates. To address this issue, scientists have often replaced the oxygen atom in the aminal function with a methylene group. This results in imino-C-glycosides, which offer significantly improved stability as glycoconjugate analogs. Since the groundbreaking synthesis of miglitol-hydroxylamine (also known as homonojirimycin), one of the simplest examples of this class, a considerable amount of synthetic effort has been focused on developing efficient and stereo chemically controlled methods for producing iminosugar C-glycosides.[64,65]

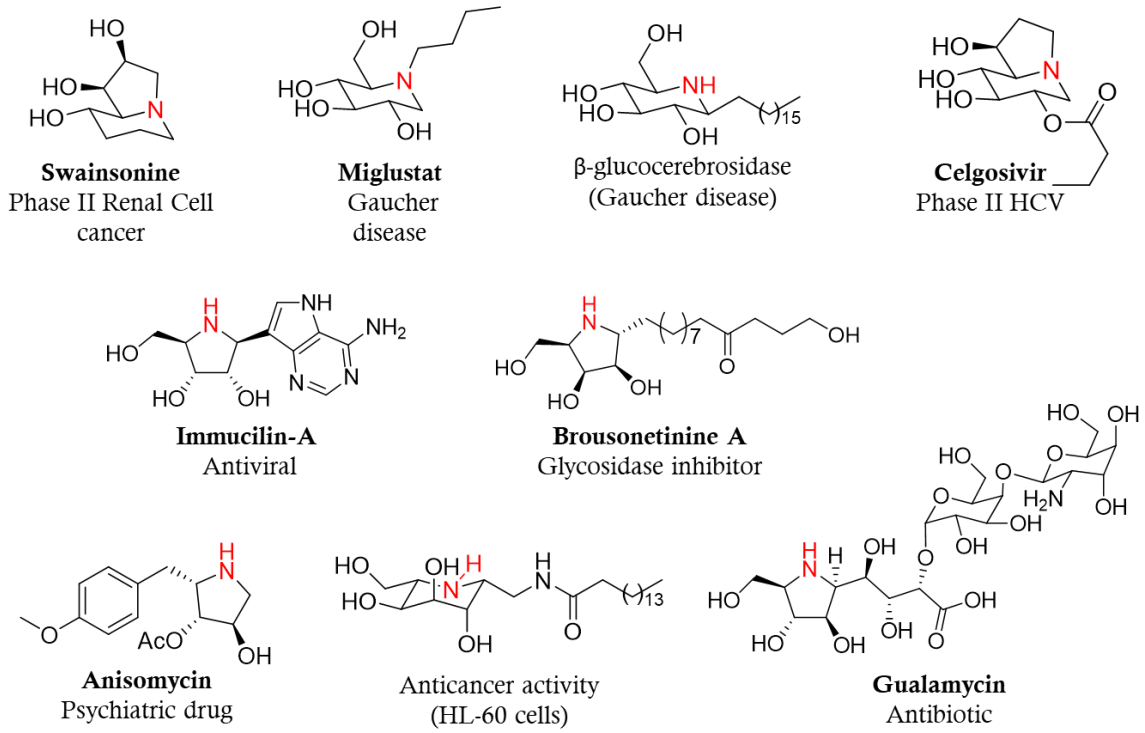

Figure 1.4.1.b: Potent molecules having iminosugar moiety[66]

1.4.2. Synthesis of iminosugar C glycoside

Iminosugar C-glycosides hold immense promise for drug discovery, but their synthesis presents significant hurdles. One major challenge lies in achieving precise control over the stereochemistry. These molecules often possess four or more contiguous stereocenters, meaning each carbon center can have two possible orientations. Precise control over these orientations is crucial for biological activity, requiring meticulous synthetic strategies.[67] Additionally, efficiently constructing the core piperidine or pyrrolidine ring, a key structural element, presents another obstacle. Finally, the high density of functional groups within iminosugar C-glycosides necessitates careful selection of protecting groups. These groups temporarily mask reactive sites during synthesis, preventing unwanted side reactions. Choosing the right protecting group, especially for the endocyclic amino group (an amine group within the ring), is critical for a successful synthesis.[67–70]

Synthetic approaches to iminosugar C-glycosides fall into two main categories:

1.4.2.1. Intramolecular Cyclization

This approach involves constructing the C-glycosidic bond (the link between the iminosugar and the sugar unit) through a clever internal ring closure. This strategy often

relies on "key disconnections," which are imaginary bond breaks that guide the synthetic plan. Here, common disconnections involve C5/C4–N or C1–N bonds, representing the points where the internal cyclization occurs.[71]

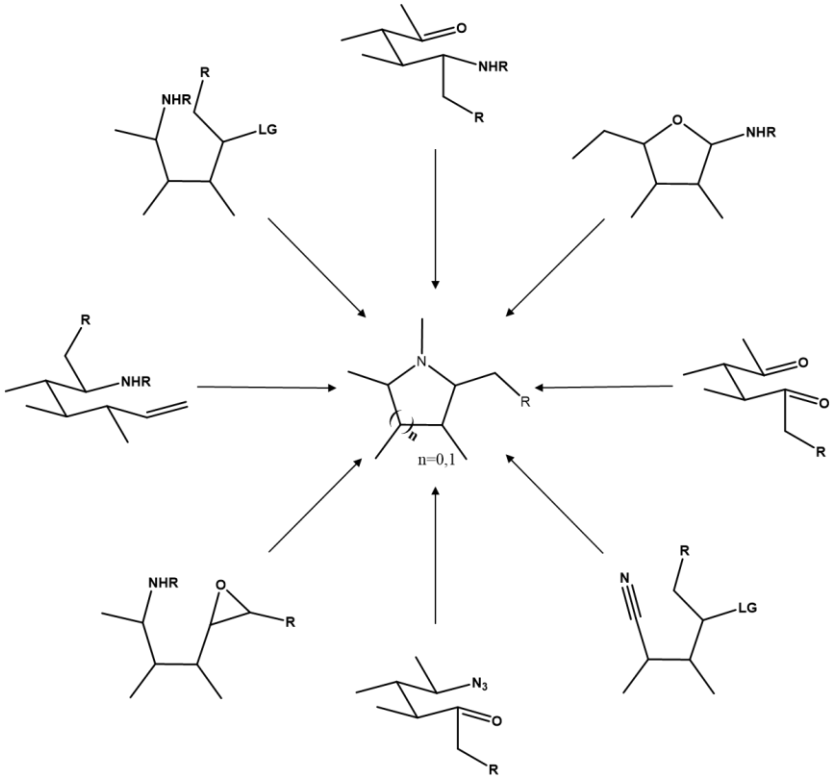

Figure 1.4.2.1: Intramolecular Cyclization approaches

1.4.2.1a. Intramolecular reductive amination

Reductive amination serves as a cornerstone reaction in organic synthesis for the preparation of iminosugar. This versatile transformation commences with a carbonyl group (C=O) of an aldehyde or ketone undergoing condensation with an amine to form an imine intermediate. The subsequent reduction of the imine furnishes the desired amine product.[72] The key advantage of reductive amination lies in its chemoselectivity, allowing for the targeted conversion of the carbonyl group while leaving other functional groups within the molecule intact.

La Ferla *et al*. (Scheme 1.4.2.1a.I)[73] presented a valuable strategy for synthesizing cyclic iminosugars. This approach begins with commercially available 2,3,4,6-tetra-*O*-benzyl-D-glucopyranose which was converted to *α, β*-unsaturated esters **1** and utilizes a Michael addition to introduce a desired amino group and form **2**. The resulting amine **2** then

undergoes intramolecular reductive amination to form the cyclic iminosugar structure. However, this cyclization requires prior oxidation of a secondary hydroxyl group (C7) to an electrophilic ketone. Nicotra *et al*. achieved this in four steps, converting compound **2** to **3**. Finally, Fmoc group removal and intramolecular reductive amination furnished the desired iminosugars **4** in good yield.

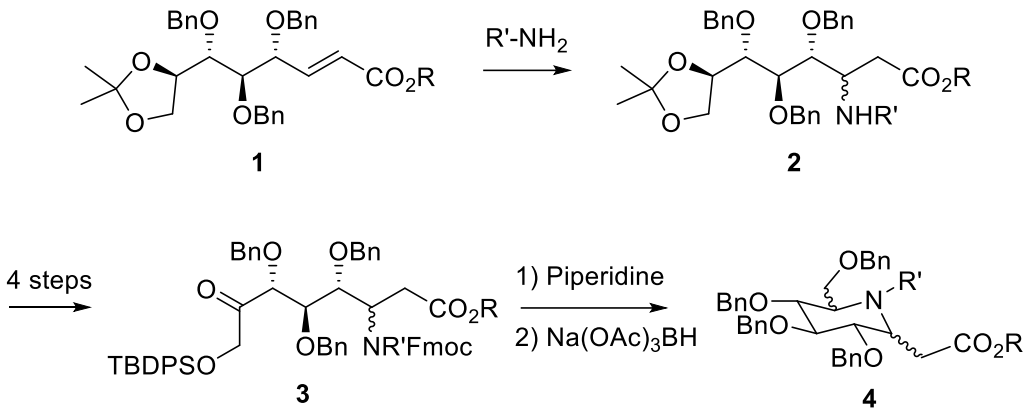

Scheme 1.4.2.1a.I: Intramolecular reductive amination

However, Cipolla *et al*. (2000)[74] showcased the versatility of reductive amination in creating nojirimycin C-glycosides (Scheme 1.4.2.1a.II). Their method for -1-C-allyl 1-deoxynojirimycin derivatives (**7**) leverages this chemoselectivity. The process starts with introducing an amine group onto a protected glucose derivative. Subsequent reaction with allyl magnesium bromide provides a stereoselective open-chain amino alcohol which on oxidation yielded **6**. Further steps involving oxidation, Fmoc group removal, and reductive amination with $Na(OAc)_3BH$ yield the desired C-glycosides (**7**). This approach allows for further modifications on the allylic appendage, highlighting the flexibility it offers.

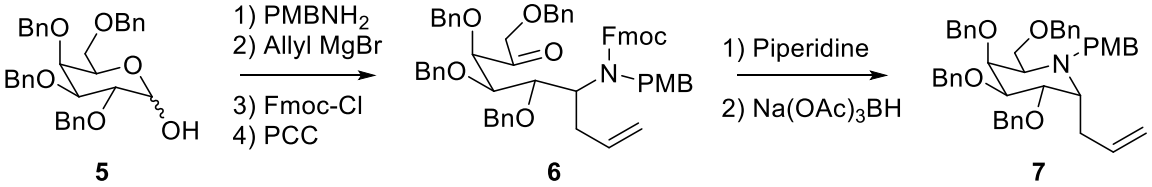

Scheme 1.4.2.1a.II: Intramolecular reductive amination

1.4.2.1b. Double reductive amination

Double reductive amination (DRA) has emerged as a powerful tool for constructing the core framework of pyrrolidine and piperidine iminosugars. This versatile strategy leverages

the ability of reductive amination to selectively form carbon-nitrogen bonds. The process typically involves two consecutive reductive amination steps. In the first step, a dicarbonyl compound reacts with an amine or hydroxylamine to form a key intermediate, often containing a protected amino group. The second reductive amination step involves internal cyclization, where the newly introduced amine group attacks an electrophilic center within the molecule, forming the desired pyrrolidine or piperidine ring. This cyclization can be achieved through various strategies, including intramolecular reductive amination with a reducing agent like sodium borohydride. The key advantage of DRA lies in its ability to efficiently introduce the nitrogen atom and construct the cyclic core structure in a single reaction sequence, offering a streamlined approach to synthesizing these valuable iminosugars.[67,69]

Jaggaiah *et al*. (2014)[75] showcased the efficiency of double reductive amination for synthesizing an aza analog of *β*-C-Galactosyl Ceramide (*β*-C-GalCer) (Scheme 1.4.2.1b.I). Their strategy began with the preparation of a key intermediate, *β*-keto phosphonate **8** (HWE precursor), derived from D-galactose in three steps. Diketone **9**, crucial for the subsequent cyclization, was then synthesized from **8** through a three-step process involving an HWE reaction with phytosphingosine aldehyde and consecutive oxidations. Finally, the desired aza-*β*-C-GalCer precursor **10** was achieved using standard DRA conditions commonly employed for piperidine aza-sugars (ammonium formate and sodium cyanoborohydride).

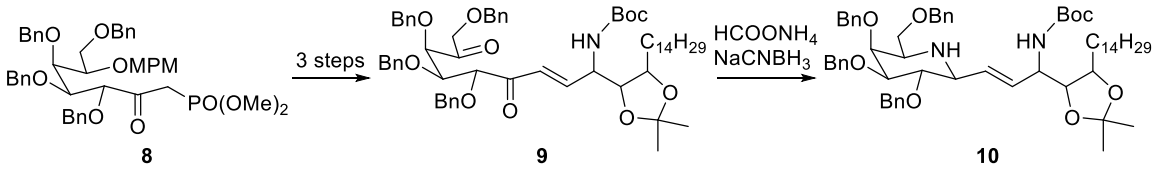

Scheme 1.4.2.1b.I: Intramolecular double reductive amination

A similar procedure was employed to create aza-C-nucleosides by Momotake *et al*. (1998),[76] which was shown in Scheme1.4.2.1b.II. Their method began with a protected hemiacetal **11** undergoing coupling with aryl lithium compounds, and the resulting intermediate will be subjected to subsequent oxidation, yielding the crucial diketone **13**. Finally, they implemented DRA on compound **13** to achieve the desired aza-C-nucleoside **14**. DRA can also done by using alkyl or aryl amines, giving diversity nitrogen substitution.

These examples emphasize DRA's effectiveness as a streamlined strategy for constructing cyclic amines.

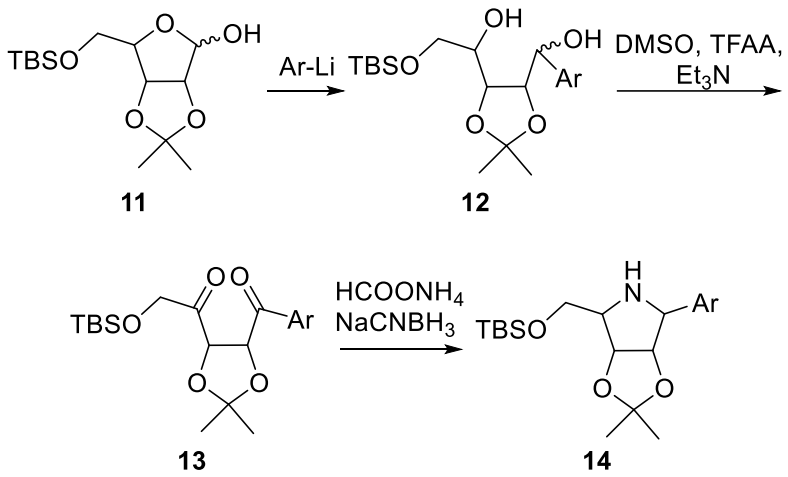

Scheme 1.4.2.1b.II: Intramolecular double reductive amination

1.4.2.1c. Intramolecular S_N2 cyclization

Classical methods for constructing piperidine and pyrrolidine rings in iminosugar C-glycosides rely on two main strategies: displacing a leaving group with an amine or ring-opening an epoxide. However, these approaches can lead to unintended products, hindering their broad applicability. Displacing a leaving group on a readily available D-sugar precursor, a common starting point, aims to establish the crucial C5-N bond. Unfortunately, this reaction often inverts the configuration at the C5 carbon atom. This inversion leads to the formation of an iminosugar belonging to the L-series, which is uncommon in nature and thus less desirable for mimicking natural sugar functions. Conversely, if the attack on the molecule comes from the nitrogen atom attached to C5 and targets a leaving group positioned at C1 (the other end of the sugar ring), the outcome is typically the formation of an α or β C-glycoside. While these C-glycosides are desirable, S_N2 cyclization plays a key role in synthesizing iminosugar C-glycosides.[67–69]

Radicamine B, a naturally occurring pyrrolidine-type iminosugar, has attracted interest due to its potential biological properties. Ribes *et al*. (2008)[77] achieved a concise synthesis of radicamine B by leveraging a strategic intramolecular S_N2 cyclization (Scheme 1.4.2.1c.I). Their approach began with Weinreb amide **15**, which was efficiently converted to alcohol **16** *via* a Grignard reaction and a stereoselective reduction with L-selectride. Subsequent

mesylation of **16** yielded compound **17**. The key step involved subjecting crude **17** to acidic conditions, aiming to achieve a cascade reaction: cleavage of the acetonide and Boc protecting groups, followed by cyclization through the nucleophilic displacement of the mesyl group by the internal amine, forming the desired pyrrolidine ring. However, this reaction yielded an unexpected outcome – a 2:1 mixture of stereoisomeric pyrrolidines **18**

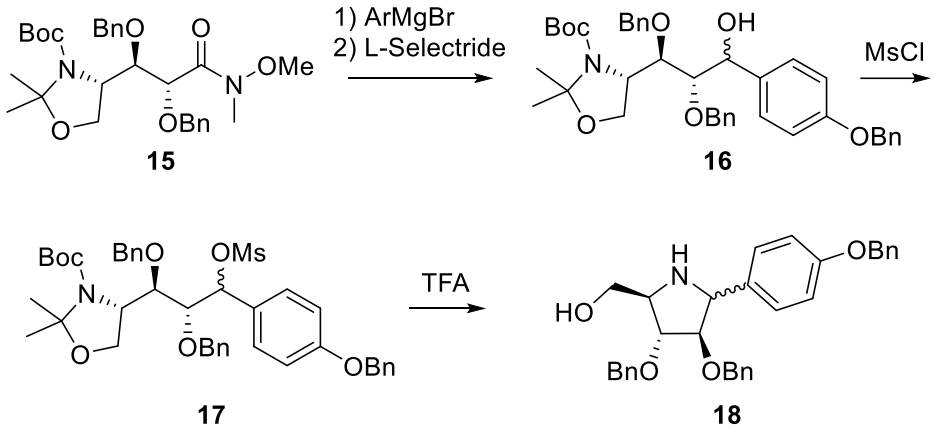

Scheme 1.4.2.1c.I: Intramolecular S_N2 cyclization

Moreno-Vargas *et al*. (2005)[78] further expanded the applicability of intramolecular S_N2 cyclization by employing a dual leaving group strategy with an external nitrogen source (Scheme 1.4.2.1c.II). Tetrabutylammonium azide (generated in situ from trimethylsilyl azide (Me_3SiN_3) and tetrabutylammonium fluoride (Bu_4NF) in DMF) served as the external nucleophile. This approach facilitated chemoselective S_N2 displacement of the mesyloxy groups at C-2 and C-5, leading to the formation of the pyrrolidine core.

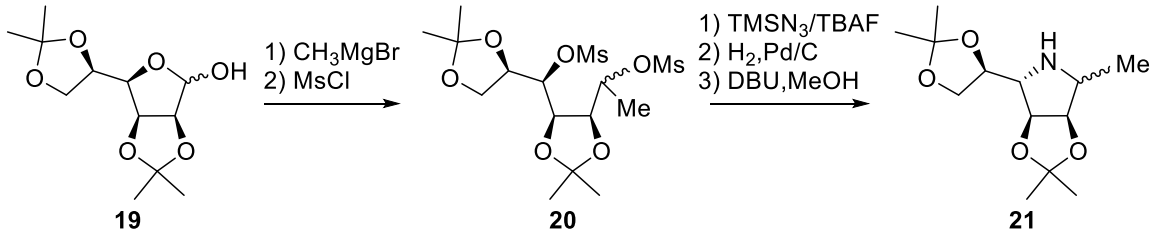

Scheme 1.4.2.1c.II: Double S_N2 cyclization

Beyond mesyl (Ms) groups, tosyl (Ts) groups can also serve as effective leaving groups in this intramolecular S_N2 cyclization. Notably, both Ms and Ts groups can facilitate the desired cyclization to form the pyrrolidine ring.

1.4.2.1d. Aminoalkene cyclization

The synthesis of C-glycosides from aminoalkene molecules can be achieved through amino alkenecyclization, also known as electrophile-induced cyclization. This technique involves the use of mercuric acetate or triflate and iodo-mediated cyclization procedures. In 1998, Bouix *et al.*[79] reported an iodine-mediated intramolecular cyclization approach for synthesizing iminosugar C-glycoside analogs derived from arabinose phosphonates. This method hinges on a key step: an intramolecular iodoamination-cyclization reaction utilizing N-iodosuccinimide (NIS) as the iodine source. This electrophile-induced cyclization approach remains a valuable method due to its relative ease in producing various iminosugar derivatives.

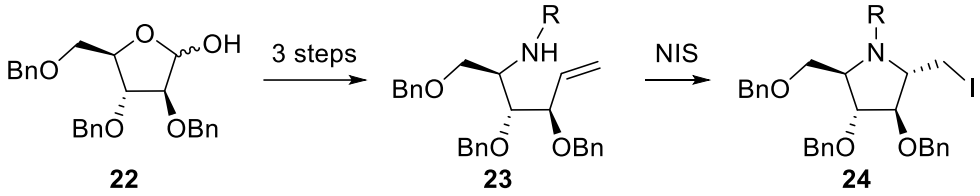

Scheme 1.4.2.1d: Intramolecular amino alkene cyclization

1.4.2.1e. Reductive cyclization

Reductive cyclization offers a versatile strategy for synthesizing C-glycosides. This method exploits the in-situ reduction of an azide moiety to an amine, which then undergoes intramolecular cyclization to form the C-glycoside core. This approach has gained significant traction in recent years, as evidenced by the numerous publications describing its application.

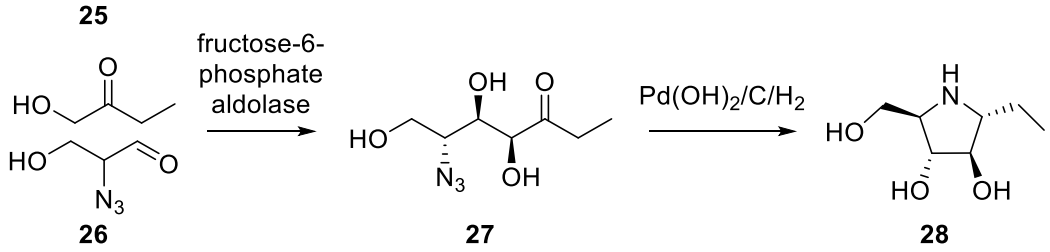

Scheme 1.4.2.1e: Reductive cyclization

Sugiyama *et al*. (2007)[80] presented a one-pot chemoenzymatic strategy for synthesizing diverse iminosugars from readily available, non-phosphorylated donor substrates. This method capitalizes on the reductive cyclization of an intermediate azide to directly furnish

the desired iminosugar products. Notably, this approach offers its own advantages: not only does it enable iminosugar synthesis from non-carbohydrate starting materials, expanding substrate scope, but it also eliminates the need for protecting groups, simplifying the overall process.

1.4.2.2 Electrophilic Iminosugar Donor

A longstanding challenge in sugar mimetic synthesis has been the early introduction of C1 substituents, hindering late-stage diversification essential for creating libraries for high-throughput screening. To address this, researchers aimed to develop a method for introducing these substituents at a late stage in the synthesis of aza-sugars. This method utilizes a pre-formed iminosugar fragment with an electrophilic (electron-loving) group attached at the C1 position (the carbon atom closest to the ring nitrogen). This electrophilic group then reacts with a suitable acceptor molecule, forming the C-glycosidic bond.[71]

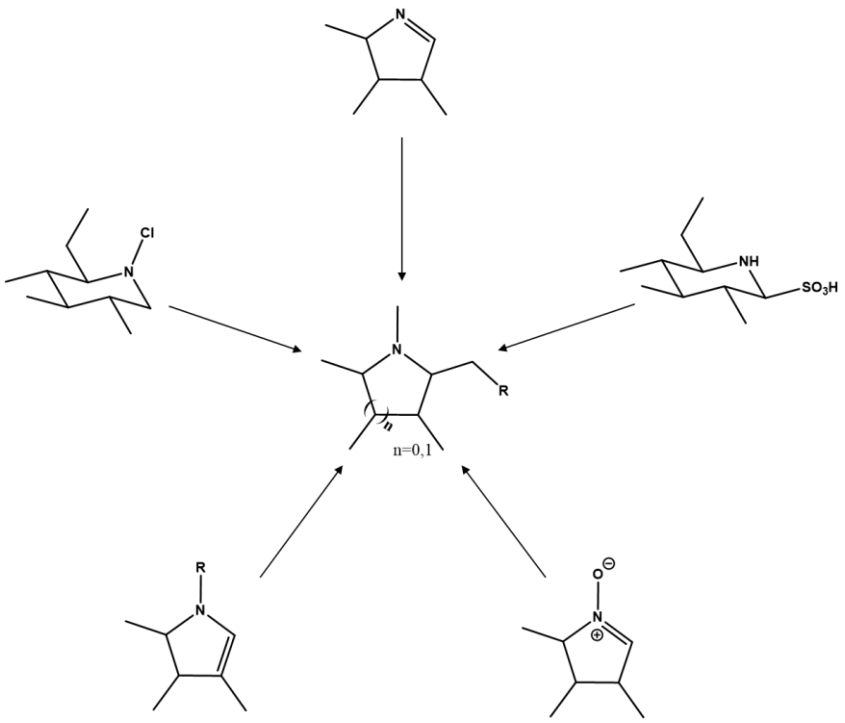

Figure 1.4.2.2: Intermolecular C glycosylation approaches

This approach, also known as intermolecular iminosugar C-glycoside synthesis, offers a distinct advantage over other methods. The key lies in utilizing an iminosugar derivative as the starting material, streamlining the overall synthetic process.

1.4.2.2a Iminosugar C-glycosides from imines

Imines are particularly valuable intermediates in intramolecular iminosugar C-glycoside synthesis owing to their inherent electrophilic character at the imine carbon. This electrophilic character makes them susceptible to nucleophilic attack by organometallic reagents, such as Grignard reagents or alkyllithium compounds. This nucleophilic attack initiates an irreversible coupling, ultimately leading to the formation of the desired C-glycoside product.

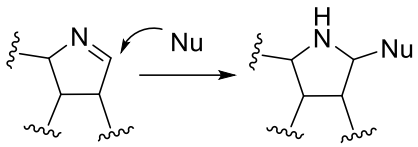

Figure 1.4.2.2a: Intermolecular C glycosylation of imins[71]

Horenstein *et al*. (1993)[81] pioneered the use of an imine intermediate for the synthesis of aza-C-nucleoside derivatives. Their approach involved sequential treatment of Iminoribitol with N-chlorosuccinimide (NCS) and lithium tetramethylpiperidide (LiTMP) to generate the desired imine. This intermediate then underwent a one-pot reaction with aryl Grignard reagents, furnishing the corresponding aza-C-nucleosides (Scheme 1.4.2.2a.II). In contrast, Bosco *et al*. (2001)[82] reported an alternative strategy for imine synthesis, employing lithium hydroxide instead of LiTMP.

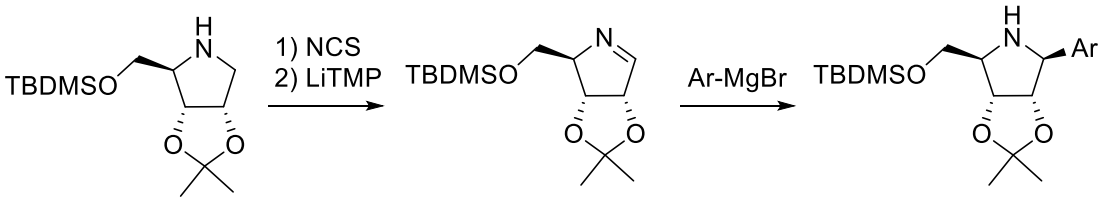

29 **30** **31**

Scheme 1.4.2.2a.I: Intermolecular iminosugar C glycosylation using imine

On the other hand, Szcześniak *et al*. (2014)[83] achieved a more streamlined approach for imine synthesis by employing the Schwartz reagent to directly convert lactam molecules into cyclic imine products in a single step (Scheme 1.4.2.2a.III). This one-pot strategy eliminates the need for isolating the often-unstable imine intermediates, facilitating their immediate utilization in subsequent reactions.

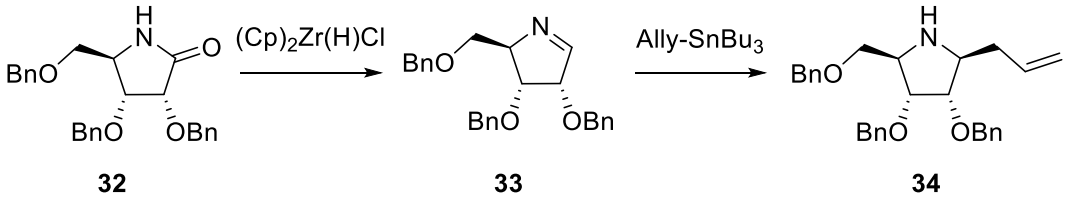

Scheme 1.4.2.2a.II: Intermolecular iminosugar C glycosylation using imine

1.4.2.2b Iminosugar C-glycosides from cyclic nitrones

Cyclic nitrones offer a distinct advantage over their cyclic imine counterparts due to their enhanced stability. Unlike imines, which can be quite reactive and challenging to isolate, cyclic nitrones often exhibit greater stability, allowing for their purification through techniques like column chromatography. This stability makes cyclic nitrones attractive alternatives as intermediates in glycosylation reactions, a key step in the synthesis of iminosugar analogs.

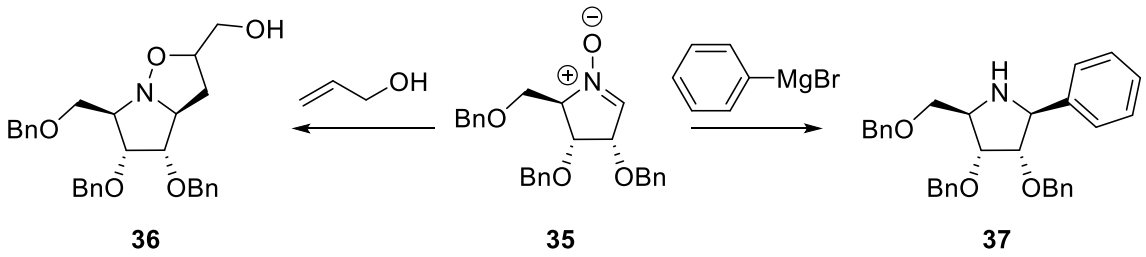

Scheme 1.4.2.2b: Iminosugar C glycosides from nitrones

Tsou *et al*. (2008)[84] capitalized on this advantage by employing a cyclic nitrone intermediate for the synthesis of aza-C-nucleoside derivatives. Their approach involved a Grignard reaction with aryl Grignard bromide, leveraging the nitrone's stability to facilitate isolation and subsequent transformation into the desired aza-C-nucleoside products. In contrast, Carmona *et al*. (2003)[85] explored a different strategy for iminosugar synthesis. Their work focused on a 1,3 dipolar cycloaddition approach, utilizing cyclic nitrone and allyl alcohol as key reactants. This approach offers a distinct pathway for the construction of bicyclic iminosugar structures.

1.4.2.2c. Iminosugar C-glycosides from iminoglycal

Imino-glycals, carbohydrates with a C=C double bond between C-1 and C-2, serve as versatile starting materials for diverse organic molecules.[86] Inspired by classical glycal

chemistry, Dransfield *et al*. (2003)[87] demonstrated that imino-glycals can undergo Lewis acid-mediated carbon-carbon bond formation (Scheme 1.4.2.2c.I). This approach leverages the allylic displacement of the C-3 acetate group, followed by stereospecific dihydroxylation, ultimately affording highly oxygenated iminosugar C-glycosides.

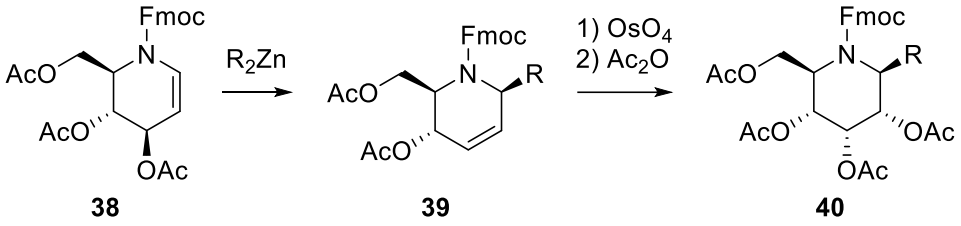

38 **39** **40**

Scheme 1.4.2.2c.I: Iminosugar C glycosides from imino glycal

Oliveira *et al*.[88] described a modified Heck reaction for the efficient synthesis of C-arylated azasugars (Scheme 1.4.2.2c.II). The Heck reaction, a powerful palladium-catalyzed method in organic synthesis, enables the controlled construction of carbon-carbon (C-C) bonds. In this approach, Correia *et al*. employed enecarbamates and aryl diazonium salts as coupling partners, achieving the desired C-arylation in a highly regio- and stereoselective manner. Notably, the reaction utilized 2,6-di-*t*-butylpyridine or 2,6-di-*t*-butyl-4-methylpyridine as bases. The resulting Heck product was then strategically converted to aza-C-glycosides through stereospecific hydroxylation.

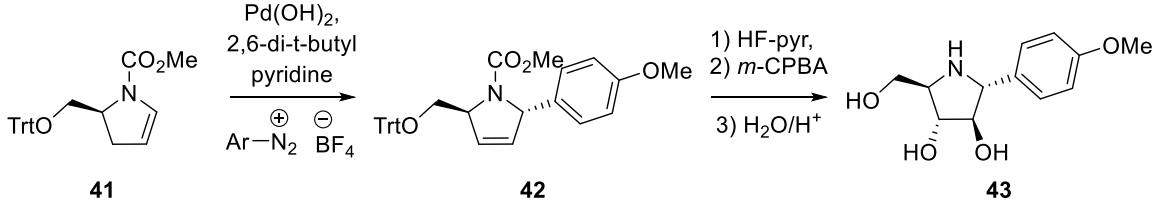

41 **42** **43**

Scheme 1.4.2.2c.II: Iminosugar C glycosides from imino-glycal

The synthesis and biological evaluation of natural and synthetic pyrrolidine and piperidine iminosugars have captivated researchers in both academic and industrial settings for decades. Initial efforts primarily focused on the development of efficient and stereoselective methods for synthesizing monovalent iminosugars with promising therapeutic activities, particularly those targeting diabetes. The success of iminosugars as a source of drug candidates has fuelled further research, with recent discoveries highlighting the potential of iminosugar C-glycosides in treating a wider range of diseases associated with carbohydrate transition state.

1.5. Immucillins

Aza-C-nucleosides and their derivatives, particularly polyhydroxylated pyrrolidines with aryl or heteroaryl groups at the C-1 position, have garnered significant interest from chemists and biochemists for their diverse pharmacological activities.[89] These activities include anticancer, antiviral, and antimicrobial properties.

Human PNP has emerged as a potential player in the development of T-cell-related cancers and autoimmune disorders.[90] This finding suggests that inhibiting PNP could offer a novel therapeutic strategy for treating these critical diseases. Understanding PNP's structure is crucial for developing such inhibitors.[91] Fortunately, X-ray crystallography studies at various resolutions have revealed the existence of several PNP families. These structural insights, combined with data from NMR techniques, kinetic isotopic effects, and theoretical calculations, have enabled researchers to delve into the intricate details of the transition state formed during the breakdown of purine nucleosides by PNP.[92–95] This detailed understanding of the enzyme's catalytic mechanism provides a blueprint for the development of specific PNP inhibitors.

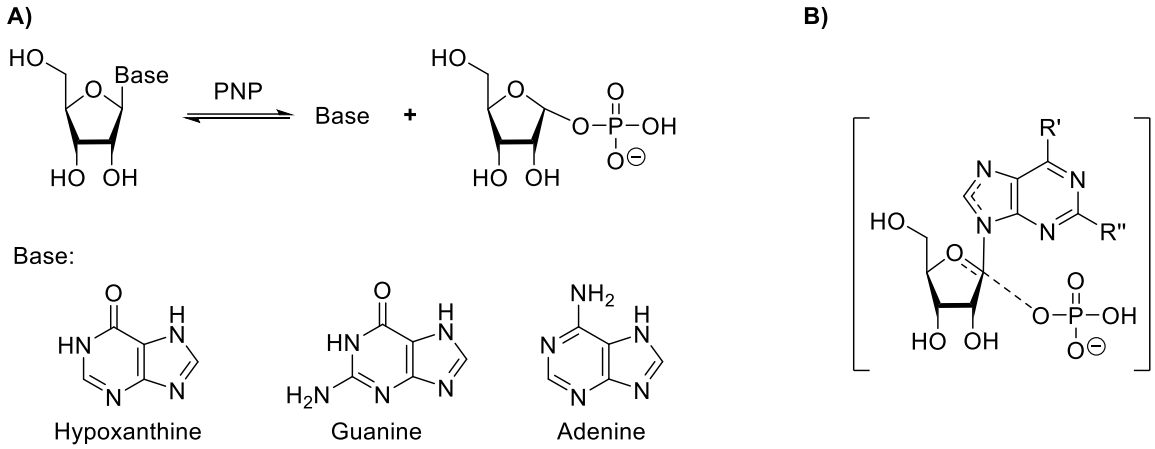

Figure 1.5a: A) PNP catalyzed Phosphorolysis of Purine Nucleosides; **B**) PNP catalyzed Transition State of Phosphorolysis of Purine Nucleosides [96]

Purine nucleoside phosphorylases (PNPs) are critical enzymes for processing purine molecules within cells. They act through a process called phosphorolysis (Figure 1.5a: A)[96], breaking down purine nucleosides into their building blocks: ribose or deoxyribose sugars and purine bases. Interestingly, a genetic deficiency in PNP leads to impaired T-cell function.[97] This is because PNP is essential for regulating deoxyguanosine triphosphate (dGTP) levels within T-cells. In healthy cells, PNP helps maintain a balanced pool of

deoxynucleotides, which are crucial for DNA synthesis. When PNP is absent, deoxyguanosine (dGuo) cannot be effectively broken down, leading to an accumulation of dGTP. This excess dGTP disrupts another enzyme, ribonucleotide reductase, which is vital for producing the building blocks of DNA.[98] The resulting imbalance in deoxynucleotide pools triggers a form of cell death (apoptosis) in T-cells. This newfound understanding of PNP's role in T-cell function has opened exciting possibilities for therapeutic development. By designing specific inhibitors of human PNP (hPNP), there is a hope to develop treatments for T-cell lymphomas and autoimmune disorders where abnormal T-cell activity is involved.[99]

Through a combination of kinetic isotope effects (KIE) and computational quantum chemistry, researchers have successfully proposed the mechanism by which PNP catalyzes phosphorolysis. Their work revealed a nucleophilic substitution reaction within the enzyme's active site (see Figure 1.5a: B).[96] In this process, a phosphate molecule serves as a nucleophile, attacking the anomeric carbon of the nucleoside substrate. This attack leads to the formation of a short-lived intermediate known as an oxocarbenium ion. This unstable ion then decomposes, releasing the nucleobase and sugar 1-phosphate as products. The detailed understanding of this enzymatic transition state has provided a valuable blueprint for the design of novel PNP inhibitors. By targeting this specific transition state, scientists can develop drugs that effectively block PNP activity.[100,101]

Armed with the detailed knowledge of the PNP transition state, researchers designed a new class of drugs called immucillins.[102] These molecules act as mimics of the natural substrates for PNP at the crucial transition state with greater binding affinity. The first generation of immucillins can be broadly categorized into three groups based on the nucleosides they mimic: inosine (Immucillin-H), guanosine (Immucillin-G), and adenosine (Immucillin-A). These mimics effectively disrupt PNP activity.[101] Following this success, scientists developed a second generation of immucillins with even more diverse pharmacological applications (Figure 1.5b).

The first generation of immucillins, like Immucillin-H and Immucillin-G, were built with an aza-ribose sugar backbone linked to a purine base *via* a carbon-carbon bond. These mimicked an early stage in the enzyme's reaction cycle. Notably, forodesine and Immucillin-G displayed impressive inhibitory power against human PNP, with dissociation constants (K_i) of 56 and 42 picomolar (pM), respectively.[100] Scientists further refined the

design with the second generation of immucillins. Ulodesine **47** and DADMe-immucillin-G **48** are prime examples. This approach led to even stronger inhibition, with K_i values of 8.5 pM and 7.0 pM for **47** and **48**, respectively.[103] This improvement highlights the importance of targeting the precise transition state for optimal enzyme inhibition. This finding paved the way for the development of next-generation immucillins with even more diverse acyclic (non-ringed) sugar backbones. Compounds like **49** (K_i= 3.4 pM) and **50** (K_i= 2.1 pM) achieved record-breaking inhibitory power, surpassing all previous generations.[104] These advancements demonstrate the ongoing efforts to refine immucillin design for maximum effectiveness.[105]

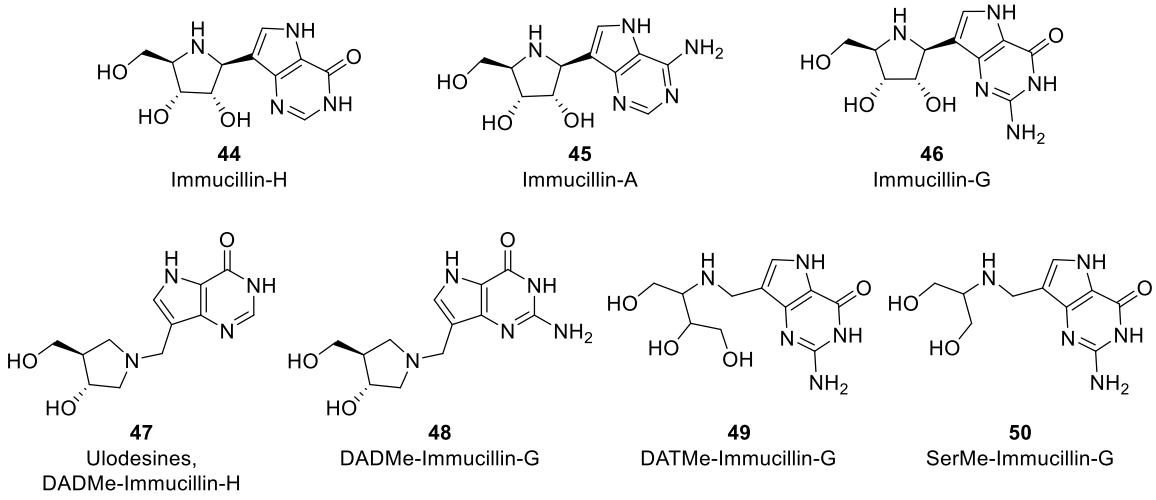

Figure 1.5b: Structures of some relevant immucillins[96]

The potential of immucillins goes beyond the lab. One success story is immucillin-H, which was approved in 2017 in Japan for treating a specific type of lymphoma called relapsed/refractory peripheral T-cell lymphoma (PTCL) after successful clinical trials.[106] This demonstrates the potential of immucillins in cancer treatment. Another promising candidate is immucillin-A, which has shown broad-spectrum antiviral activity in tests, effectively inhibiting over 20 viral species from ten different families. This suggests its potential use against various viral infections.[107] On a different note, Ulodesine **47** has completed phase II clinical trials for treating gout, a severe inflammatory condition caused by high uric acid levels. Ulodesine's mechanism involves inhibiting hPNP, which helps regulate the production of purine precursors, ultimately reducing uric acid formation.[108] These examples illustrate the diverse applications of immucillins, from combating viruses to managing complex diseases like gout.

The global rise of infectious diseases and cancers necessitates the development of novel therapeutic strategies. Immucillins, a class of antiviral and anticancer drugs, have emerged as promising candidates due to their unique mechanism of action. This thesis delves into the synthesis of two key immucillins, Immucillin-A and Immucillin-H, with the aim of contributing to the advancement of these potential drugs.

1.5.1. Immucillin-H

Immucillin-H also known as Forodesine, or BCX-1777, is a highly effective inhibitor of the enzyme purine nucleoside phosphorylase (PNP). Developed by BioCryst Pharmaceuticals, forodesine was designed based on the enzyme's transition state for optimal inhibition. This drug exhibits promising activity against T-cell malignancies like T-cell acute lymphoblastic leukemia (T-ALL) and cutaneous T-cell lymphoma.[109] Early studies also suggest its potential application in managing some B-cell cancers.[110,111]

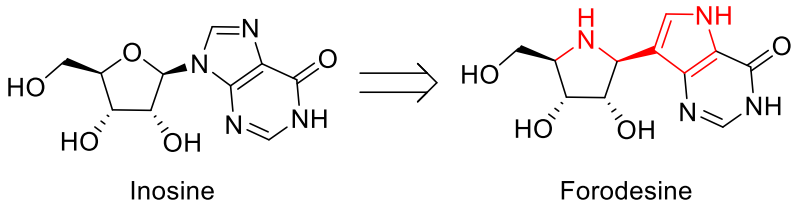

Figure 1.5.1: Structures of immucillin-H

Forodesine's effectiveness stems from its ability to disrupt the normal metabolism of purine nucleosides within T-cells.[112] In healthy cells, PNP plays a critical role in breaking down these molecules. However, forodesine inhibits PNP, leading to an accumulation of deoxyguanosine (dGuo) in the cell.[113] Since PNP is blocked, dGuo cannot be converted to guanine (Guo) for normal cell function. Instead, it gets converted to deoxyguanosine triphosphate (dGTP) through other pathways.[114] This elevated dGTP level disrupts DNA synthesis and repair, ultimately leading to DNA damage and cell death (apoptosis).[115]

Forodesine has demonstrated efficacy in treating relapsed and refractory T-cell leukemias, including T-ALL and cutaneous T-cell lymphoma.[116] Studies have shown promising results when used as a single agent in these conditions, with minimal side effects. Research by Furman *et al.*[117] suggests forodesine's effectiveness in treating relapsed T-cell leukemia after allogeneic hematopoietic stem cell transplantation (HSCT). Gore *et al.*[118] further revealed that forodesine not only has a direct cytotoxic effect on leukemia cells but also promotes an immune response against cancer cells. Additionally, preclinical and clinical data support forodesine's potential application in B-cell ALL.

Forodesine's journey from discovery to clinical use is a testament to its potential. Following successful clinical trials in Japan, forodesine received approval in 2017 for the treatment of relapsed/refractory peripheral T-cell lymphoma (PTCL).[106] This approval marks a significant step forward in the fight against T-cell cancers.

1.5.2. Immucillin-A

Immucillin A (aka galidesivir or BCX-4430) was originally developed as a potential treatment for trichomoniasis, a parasitic infection caused by *Trichomonas vaginalis*. This parasite exhibits purine auxotrophy, relying on the salvage pathway for essential purine building blocks. Notably, *T. vaginalis* expresses a unique purine nucleoside phosphorylase (TvPNP) with a preference for adenosine as a substrate.[119] This substrate specificity offered a window for selective targeting, and galidesivir demonstrated potent inhibition of TvPNP with a K_i of 87 pM. However, despite its high inhibitory activity, galidesivir displayed limited efficacy against trichomoniasis due to the presence of alternative purine salvage enzymes in the parasite.[120] The initial research on galidesivir, however, revealed an unexpected benefit. *In vitro* antiviral assays demonstrated broad-spectrum activity against over 20 viral species belonging to ten distinct families. This included filoviruses (Ebola, Marburg) and flaviviruses (West Nile, Zika, Yellow fever), for which effective therapeutic options are scarce.[107,121–124]

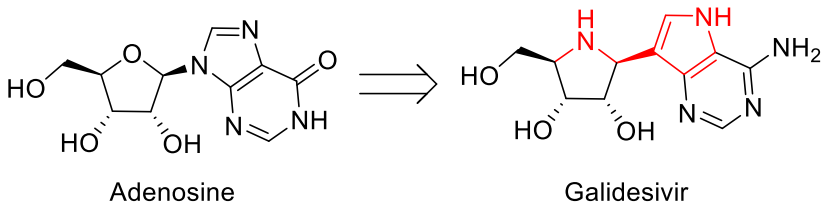

Figure 1.5.2: Structures of immucillin-A

Clinical trials have established galidesivir's safety and tolerability profile.[125] While initial studies explored its potential application for COVID-19 treatment due to activity against related coronaviruses (SARS, MERS),[126] Phase I trials, although demonstrating a dose-dependent reduction in viral load and good safety, ultimately did not lead to further development for COVID-19.[127] However, the broad-spectrum antiviral activity of galidesivir positions it as a promising candidate for treating other viral diseases. Currently, galidesivir is undergoing advanced clinical development for the treatment of Marburg virus disease, a highly lethal filovirus closely related to Ebola.[107] This highlights the potential of repurposing drugs with specific target mechanisms for broader therapeutic applications.

1.5.3. Synthesis of immucillin-H and immucillin-A

On the synthetic front, most of the reports for obtaining immucillin-H with the key step for C-nucleoside synthesis being C-C bond formation between iminoribitol and aglycon moieties. In a linear synthesis, an imine derived from an N-halo amine, obtained from D-gulono-1,4-lactone[128], by base-catalyzed elimination, was utilized in the addition reaction with excess lithiated acetonitrile to afford a cyanomethyl C-glycoside derivative (Scheme 1.5.3a), which culminated in forodesine with an overall yield of 3.7% in 20 steps.[129]

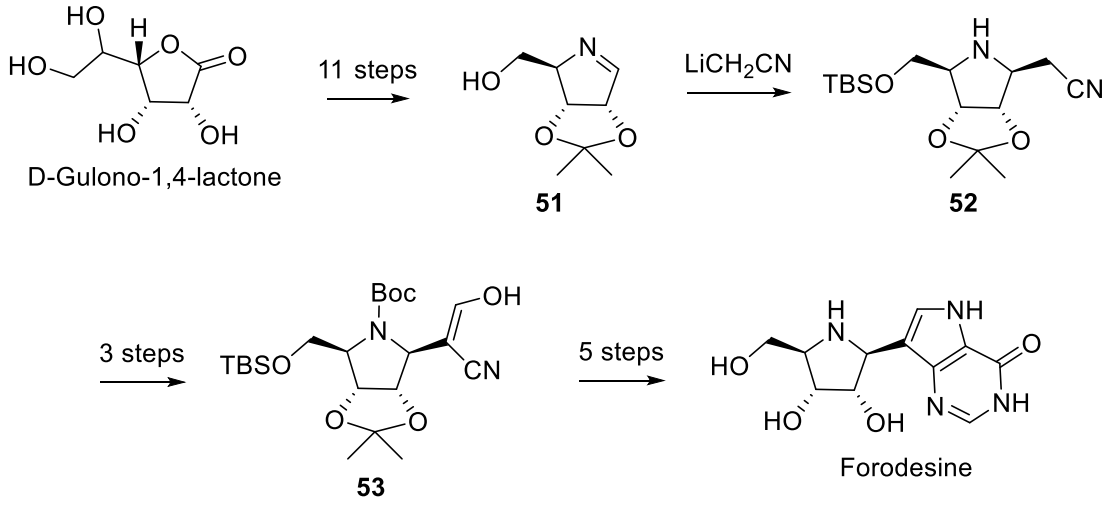

Scheme 1.5.3a: Linear synthesis of forodesine through imine

In a convergent route, adding a lithiated 9-deazahypoxanthine derivative, derived from isoxazole,[130] to an imine afforded *C*-nucleoside in the key step (Scheme 1.5.3b), providing forodesine in an overall yield of 19% in 14 steps.[131]

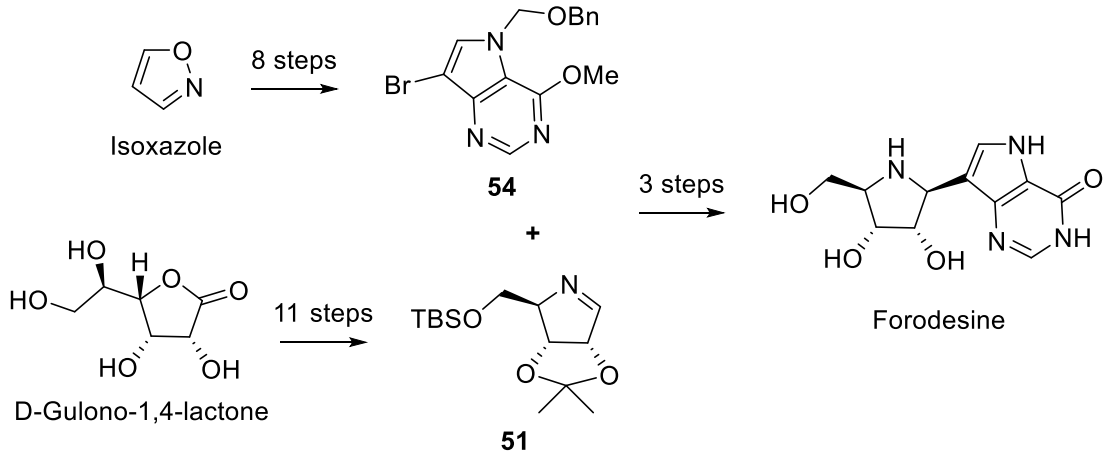

Scheme 1.5.3b: Convergent synthesis of forodesine through imine

Coupling the stable tri-*O*-benzyl cyclic nitrone, derived from D-ribose, with lithiated 9-deazahypoxanthine derivative furnished hydroxylamine as separable diastereoisomers of *β*:*α* (7:1) (Scheme 1.5.3c), which resulted in forodesine in an overall yield of 8% in 11 steps.[132]

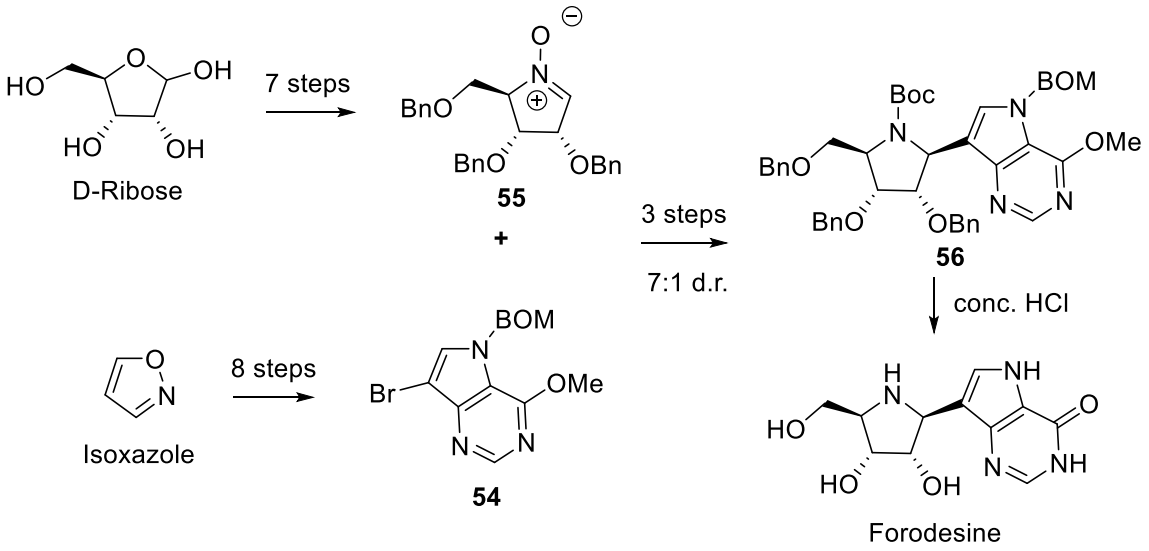

Scheme 1.5.3c: Convergent synthesis of forodesine through nitrone

Cross-coupling of a stable aza-sugar lactam (Scheme 1.5.3d), derived from L-pyroglutamic acid, with lithiated 9-deazahypoxanthine followed by reduction furnished a mixture of *β*:*α* (4:1) of forodesine in an overall yield of 14% from 10 steps.[133]

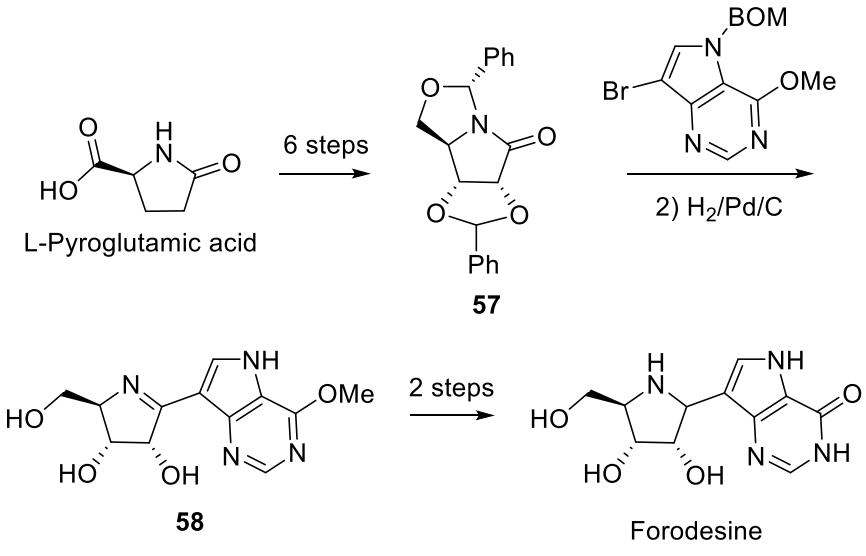

Scheme 1.5.3d: Convergent synthesis of forodesine through lactam

On the synthetic front, most of the reports for obtaining galidesivir rely on the intermediary of forodesine that involves seven linear steps, including the incorporation of amine in the C-6 position of the purine (Scheme 1.5.3e).[121]

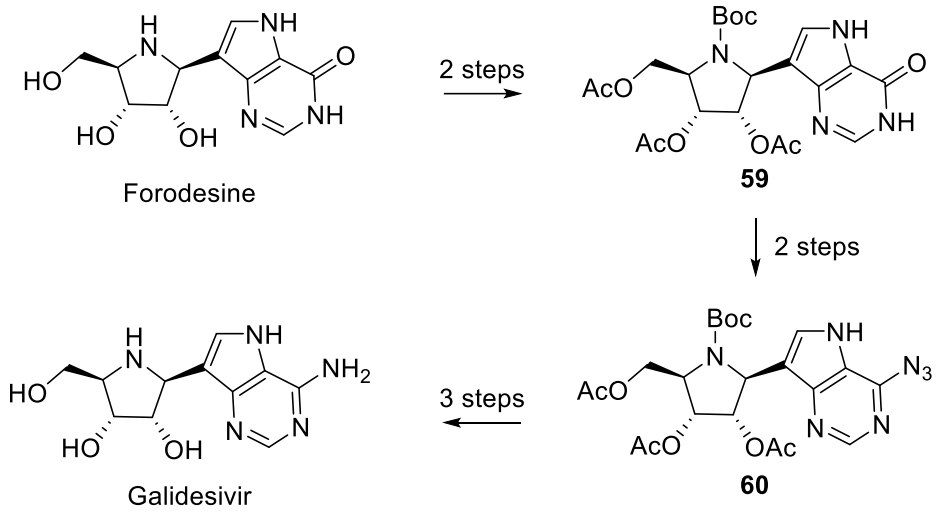

Scheme 1.5.3e: Synthesis of galidesivir from forodesine

However, Evans *et al*. synthesized ampicillin-A, with the key step for C-nucleoside synthesis being C-C bond formation between iminoribitol and aglycon moieties.[134] In a linear synthesis, an imine derived from an N-halo amine, obtained from D-Gulono-1,4-lactone, by base-catalyzed elimination, was utilized in the addition reaction with excess lithiated acetonitrile to afford a cyanomethyl C-glycoside derivative (Scheme 1.5.3f), which culminated in galidesivir with an overall yield of 1.5% in 19 steps.[129]

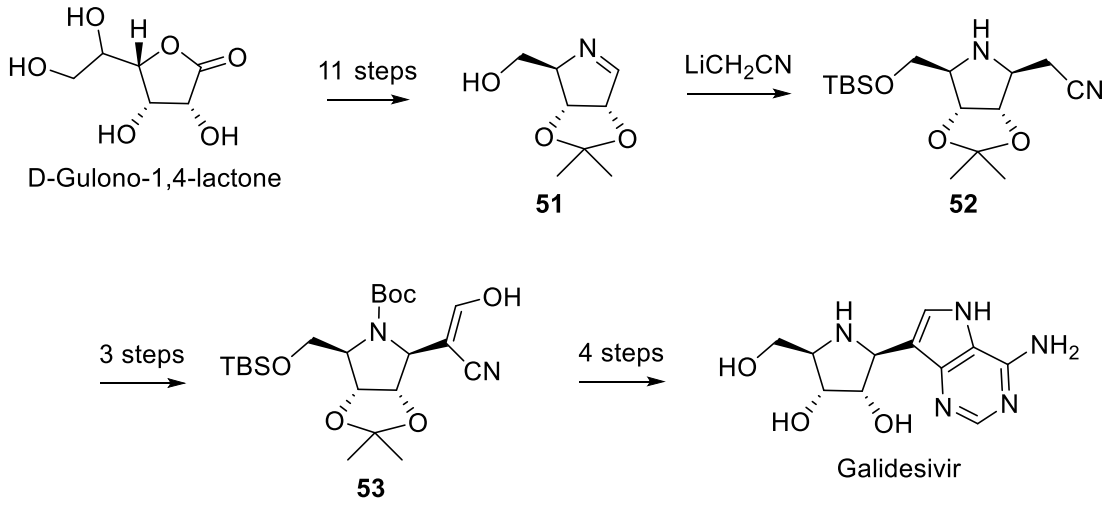

Scheme 1.5.3f: Linear synthesis of forodesine through imine

BioCryst Pharmaceuticals, the developer of galidesivir, has secured patents for various synthetic routes to this promising antiviral agent.[135] These patented methods demonstrate the flexibility in selecting starting materials for galidesivir synthesis. Notably, the

approaches encompass the utilization of both sugar-based and non-sugar-based precursors, highlighting the potential for diverse and potentially scalable synthetic strategies.[136]

1.6. Conclusions and present work

Glycomimetics, synthetic mimics of carbohydrates, overcome limitations like instability and poor absorption. These engineered molecules offer enhanced properties and targeted binding, making them valuable tools in drug development, diagnostics, and materials science.

Iminosugars are a class of glycomimetics, representing a significant leap forward. By mimicking a crucial enzymatic transition state, they potently inhibit glycosyltransferases and glycosylhydrolases, enzymes vital for various biological processes. This inhibition disrupts sugar metabolism, glycosylation patterns, and even pathogen-host interactions, offering promise for treating diverse diseases like viral infections and cancer.

Immucillins, a specific type of iminosugar, target purine nucleoside phosphorylase (PNP), an enzyme critical for purine metabolism in cells. Their design leverages a deep understanding of PNP's transition state, leading to highly specific and potent inhibitors. Forodesine (Immucillin-H) exemplifies this success. It disrupts purine nucleoside metabolism in T-cells, leading to DNA damage and cell death in T-cell malignancies. Forodesine's efficacy in treating these cancers has been clinically validated, paving the way for its approval in Japan. While forodesine tackles cancer, Immucillin-A showcases broad-spectrum antiviral activity. Additionally, Ulodesine, another immucillin derivative, shows promise in managing gout by regulating uric acid production.

These breakthroughs highlight the immense potential of glycomimetics, particularly iminosugars and immucillins. Their applications extend beyond cancer to viral infections, gout, and potentially more. As research refines these molecules, focusing on precise transition states and structural modifications, the impact of glycomimetic-based drug design on modern medicine is poised to grow significantly.

While existing methods for synthesizing immucillin-H (forodesine) and immucillin-A (galidesivir) have paved the way for their initial clinical applications, these methods may have limitations in terms of efficiency, scalability, or cost-effectiveness. In contrast, this thesis specifically focuses on developing novel synthetic strategies for these crucial immucillins. Additionally, the research will explore the synthesis of iminosugar analogs of

KRN-7000, a compound that has shown promising therapeutic applications. By developing new synthetic approaches, this thesis aims to address the potential limitations of current methods and unlock the full therapeutic potential of these promising molecules.

1.7. References

1. Kolb, H. C. & Ernst, B. Recent progresses in the glycodrug area. **69**, 1879–1884 (1997).
2. HENNING, R. & UHLENBRUCK, G. Detection of Carbohydrate Structures on Isolated Subcellular Organelles of Rat Liver by Heterophile Agglutinins. *Nat. New Biol.* **242**, 120–122 (1973).
3. Hanessian, S. *Preparative carbohydrate chemistry*. (CRC Press, 1997).
4. Shivatare, S. S. & Wong, C.-H. Synthetic Carbohydrate Chemistry and Translational Medicine. *J. Org. Chem.* **85**, 15780–15800 (2020).
5. Finkelstein, J. Glycochemistry & Glycobiology. *Nature* **446**, 999 (2007).
6. Bernardi, A. & Sattin, S. Interfering with the Sugar Code: Ten Years Later. *European J. Org. Chem.* **2020**, 4652–4663 (2020).
7. Fernández-Tejada, A., Cañada, F. J. & Jiménez-Barbero, J. Recent Developments in Synthetic Carbohydrate-Based Diagnostics, Vaccines, and Therapeutics. *Chem. – A Eur. J.* **21**, 10616–10628 (2015).
8. *Essentials of Glycobiology*. (2015).
9. Reily, C., Stewart, T. J., Renfrow, M. B. & Novak, J. Glycosylation in health and disease. *Nat. Rev. Nephrol.* **15**, 346–366 (2019).
10. Hudak, J. E. & Bertozzi, C. R. Glycotherapy: New Advances Inspire a Reemergence of Glycans in Medicine. *Chem. Biol.* **21**, 16–37 (2014).
11. Gabius, H. J. Biological information transfer beyond the genetic code: the sugar code. *Naturwissenschaften* **87**, 108–121 (2000).
12. Gabius, H.-J., Siebert, H.-C., André, S., Jiménez-Barbero, J. & Rüdiger, H. Chemical Biology of the Sugar Code. *ChemBioChem* **5**, 740–764 (2004).

13. Hirabayashi, J. & Kasai, K. Glycomics, coming of age! *Trends Glycosci. Glycotechnol.* **12**, 1–5 (2000).

14. Ernst, B. & Magnani, J. L. From carbohydrate leads to glycomimetic drugs. *Nat. Rev. Drug Discov.* **8**, 661–677 (2009).

15. Zhang, Y. & Wang, F. Carbohydrate drugs: current status and development prospect. *Drug Discov. Ther.* **9**, 79–87 (2015).

16. Patel, A. & Lindhorst, T. K. Synthesis of "Mixed Type" Oligosaccharide Mimetics Based on a Carbohydrate Scaffold. *European J. Org. Chem.* **2002**, 79–86 (2002).

17. Sears, P. & Wong, C.-H. Carbohydrate Mimetics: A New Strategy for Tackling the Problem of Carbohydrate-Mediated Biological Recognition. *Angew. Chemie Int. Ed.* **38**, 2300–2324 (1999).

18. Martínez, J. D. *et al.* The Interaction of Fluorinated Glycomimetics with DC-SIGN: Multiple Binding Modes Disentangled by the Combination of NMR Methods and MD Simulations. *Pharmaceuticals* vol. 13 at https://doi.org/10.3390/ph13080179 (2020).

19. He, X. M. & Liu, H. Formation of Unusual Sugars: Mechanistic Studies and Biosynthetic Applications. *Annu. Rev. Biochem.* **71**, 701–754 (2002).

20. McGeary, R. P., Jablonkai, I. & Toth, I. Carbohydrate-based templates for synthetic vaccines and drug delivery. *Tetrahedron* **57**, 8733–8742 (2001).

21. Lohof, E. *et al.* Carbohydrate Derivatives for Use in Drug Design: Cyclic alpha(v)-Selective RGD Peptides This work was supported by the Fonds der Chemischen Industrie, the Deutsche Forschungsgemeinschaft, and the Sanderstiftung. The authors thank M. Urzinger, B. Cordes, . *Angew. Chem. Int. Ed. Engl.* **39**, 2761–2764 (2000).

22. Marzabadi, C. H. & Talisman, I. J. Carbohydrate-based drugs in the treatment of epilepsy, depression and other affective disorders. *Curr. Top. Med. Chem.* **8**, 159–170 (2008).

23. Damalanka, V. C., Maddirala, A. R. & Janetka, J. W. Novel approaches to glycomimetic design: development of small molecular weight lectin antagonists. *Expert Opin. Drug Discov.* **16**, 513–536 (2021).

24. Hevey, R. Strategies for the Development of Glycomimetic Drug Candidates. *Pharmaceuticals* vol. 12 at https://doi.org/10.3390/ph12020055 (2019).

25. Wong, C.-H. *Carbohydrate-based drug discovery, 2 volume set*. vol. 1 (John Wiley & Sons, 2003).

26. Bordoni, V. *et al.* Stereoselective innovative synthesis and biological evaluation of new real carba analogues of minimal epitope Manα(1,2)Man as DC-SIGN inhibitors. *RSC Adv.* **6**, 89578–89584 (2016).

27. Tamburrini, A., Colombo, C. & Bernardi, A. Design and synthesis of glycomimetics: Recent advances. *Med. Res. Rev.* **40**, 495–531 (2020).

28. Arjona, O., Gómez, A. M., López, J. C. & Plumet, J. Synthesis and Conformational and Biological Aspects of Carbasugars. *Chem. Rev.* **107**, 1919–2036 (2007).

29. Compain, P. & Martin, O. R. *Iminosugars: From synthesis to therapeutic applications*. (John Wiley & Sons, 2007).

30. Horne, G. & Wilson, F. X. Therapeutic Applications of Iminosugars: Current Perspectives and Future Opportunities. in (eds. Lawton, G. & Witty, D. R. B. T.-P. in M. C.) vol. 50 135–176 (Elsevier, 2011).

31. He, P. *et al.* Synthesis of 5-Thio-α-GalCer Analogues with Fluorinated Acyl Chain on Lipid Residue and Their Biological Evaluation. *ACS Med. Chem. Lett.* **10**, 221–225 (2019).

32. Ferry, A., Guinchard, X., Retailleau, P. & Crich, D. Synthesis, Characterization, and Coupling Reactions of Six-Membered Cyclic P-Chiral Ammonium Phosphonite–Boranes; Reactive H-Phosphinate Equivalents for the Stereoselective Synthesis of Glycomimetics. *J. Am. Chem. Soc.* **134**, 12289–12301 (2012).

33. Dayde, B. *et al.* Synthesis of Unnatural Phosphonosugar Analogues. *European J. Org. Chem.* **2014**, 1333–1337 (2014).

34. Yang, Y. & Yu, B. Recent Advances in the Chemical Synthesis of C-Glycosides. *Chem. Rev.* **117**, 12281–12356 (2017).

35. Sánchez-Fernández, E. M. *et al.* sp2-Iminosugar O-, S-, and N-Glycosides as Conformational Mimics of α-Linked Disaccharides; Implications for Glycosidase

Inhibition. *Chem. – A Eur. J.* **18**, 8527–8539 (2012).

36. Zhu, F., O'Neill, S., Rodriguez, J. & Walczak, M. A. Stereoretentive Reactions at the Anomeric Position: Synthesis of Selenoglycosides. *Angew. Chemie Int. Ed.* **57**, 7091–7095 (2018).

37. Kerins, L., Byrne, S., Gabba, A. & Murphy, P. V. Anomer Preferences for Glucuronic and Galacturonic Acid and Derivatives and Influence of Electron-Withdrawing Substituents. *J. Org. Chem.* **83**, 7714–7729 (2018).

38. Biffinger, J. C., Kim, H. W. & DiMagno, S. G. The Polar Hydrophobicity of Fluorinated Compounds. *ChemBioChem* **5**, 622–627 (2004).

39. Ge, J.-T., Li, Y.-Y., Tian, J., Liao, R.-Z. & Dong, H. Synthesis of Deoxyglycosides by Desulfurization under UV Light. *J. Org. Chem.* **82**, 7008–7014 (2017).

40. Danac, R., Ball, L., Gurr, S. J. & Fairbanks, A. J. Synthesis of UDP-glucose derivatives modified at the 3-OH as potential chain terminators of *β*-glucan biosynthesis. *Carbohydr. Res.* **343**, 1012–1022 (2008).

41. Lin, C.-I., McCarty, R. M. & Liu, H. The biosynthesis of nitrogen-, sulfur-, and high-carbon chain-containing sugars. *Chem. Soc. Rev.* **42**, 4377–4407 (2013).

42. Pavashe, P., Elamparuthi, E., Hettrich, C., Möller, H. M. & Linker, T. Synthesis of 2-Thiocarbohydrates and Their Binding to Concanavalin A. *J. Org. Chem.* **81**, 8595–8603 (2016).

43. Büll, C. *et al.* Targeting Aberrant Sialylation in Cancer Cells Using a Fluorinated Sialic Acid Analog Impairs Adhesion, Migration, and In Vivo Tumor Growth. *Mol. Cancer Ther.* **12**, 1935–1946 (2013).

44. HANZAWA, Y. *et al.* TRIFLUOROMETHYLATION OF CHIRAL ALDEHYDE AND SYNTHESIS OF 6-DEOXY-6, 6, 6-TRIFLUOROHEXOSES. *Chem. Pharm. Bull. (Tokyo).* **39**, 2459–2461 (1991).

45. Soriano del Amo, D. *et al.* Chemoenzymatic synthesis of the sialyl Lewis X glycan and its derivatives. *Carbohydr. Res.* **345**, 1107–1113 (2010).

46. Hoos, R., Huixin, J., Vasella, A. & Weiss, P. Synthesis and Enzymatic Evaluation of Substrates and Inhibitors of *β*-Glucuronidases. *Helv. Chim. Acta* **79**, 1757–1784

(1996).

47. Zhang, Y., Liu, Y., Wang, Z., Wang, Z. & Huang, L. The Synthesis of a 2-Deoxy-2-Acetonyl Sugar from its Corresponding Natural Saccharide. *J. Chem. Res.* **36**, 244–246 (2012).

48. Aretz, J., Wamhoff, E.-C., Hanske, J., Heymann, D. & Rademacher, C. Computational and experimental prediction of human C-type lectin receptor druggability. *Front. Immunol.* **5**, 97274 (2014).

49. Cecioni, S., Imberty, A. & Vidal, S. Glycomimetics versus Multivalent Glycoconjugates for the Design of High Affinity Lectin Ligands. *Chem. Rev.* **115**, 525–561 (2015).

50. Queneau, Y., Rauter, A. P. & Lindhorst, T. *Carbohydrate chemistry: Chemical and biological approaches*. vol. 40 (Royal Society of Chemistry, 2014).

51. El Khadem, H. *Carbohydrate chemistry: monosaccharides and their oligomers*. (Elsevier, 2012).

52. Davies, G. J. & Williams, S. J. Carbohydrate-active enzymes: sequences, shapes, contortions and cells. *Biochem. Soc. Trans.* **44**, 79–87 (2016).

53. Glavey, S. V *et al.* The cancer glycome: carbohydrates as mediators of metastasis. *Blood Rev.* **29**, 269–279 (2015).

54. Gloster, T. M. & Davies, G. J. Glycosidase inhibition: assessing mimicry of the transition state. *Org. Biomol. Chem.* **8**, 305–320 (2010).

55. Cao, X. *et al.* Carbohydrate-based drugs launched during 2000−2021. *Acta Pharm. Sin. B* **12**, 3783–3821 (2022).

56. Asano, N. Naturally Occurring Iminosugars and Related Alkaloids: Structure, Activity and Applications. in *Iminosugars* 7–24 (2007). doi:https://doi.org/10.1002/9780470517437.ch2.

57. Conforti, I. & Marra, A. Iminosugars as glycosyltransferase inhibitors. *Org. Biomol. Chem.* **19**, 5439–5475 (2021).

58. Xavier, N. M. & Andreana, P. R. Glycomimetics and Glycoconjugates in Drug Discovery. *Pharmaceuticals* vol. 17 at https://doi.org/10.3390/ph17030323 (2024).

59. Horne, G., Wilson, F. X., Tinsley, J., Williams, D. H. & Storer, R. Iminosugars past, present and future: medicines for tomorrow. *Drug Discov. Today* **16**, 107–118 (2011).

60. Hensienne, R., Hazelard, D. & Compain, P. Conformationally constrained fused bicyclic iminosugars: synthetic challenges and opportunities. *ARKIVOC* **2019**, 4–43 (2019).

61. Rowicki, T. Iminosugars and related heterocycles with quaternary carbon adjacent to nitrogen: Synthesis and biological properties. *Targets Heterocycl. Syst.* **20**, 409–447 (2016).

62. Cox, T. M., Platt, F. M. & Aerts, J. M. F. G. Medicinal use of Iminosugars. in *Iminosugars* 295–326 (2007). doi:https://doi.org/10.1002/9780470517437.ch13.

63. Kurhekar, J. V. Antimicrobial lead compounds from marine plants. in *Phytochemicals as Lead Compounds for New Drug Discovery* 257–274 (Elsevier, 2020).

64. Zelli, R., Longevial, J.-F., Dumy, P. & Marra, A. Synthesis and biological properties of multivalent iminosugars. *New J. Chem.* **39**, 5050–5074 (2015).

65. Compain, P. Searching for Glycomimetics That Target Protein Misfolding in Rare Diseases: Successes, Failures, and Unexpected Progress Made in Organic Synthesis. *Synlett* **25**, 1215–1240 (2014).

66. Sánchez-Fernández, E. M., García-Moreno, M. I., García Fernández, J. M. & Mellet, C. O. Chapter 7 - sp2-Iminosugars as chemical mimics for glycodrug design. in (eds. Trabocchi, A. & Lenci, E. B. T.-S. M. D. D.) 197–224 (Elsevier, 2020). doi:https://doi.org/10.1016/B978-0-12-818349-6.00007-8.

67. Dhara, D., Dhara, A., Bennett, J. & Murphy, P. V. Cyclisations and strategies for stereoselective synthesis of piperidine iminosugars. *Chem. Rec.* **21**, 2958–2979 (2021).

68. Nicolas, C. & Martin, O. R. Glycoside Mimics from Glycosylamines: Recent Progress. *Molecules* vol. 23 at https://doi.org/10.3390/molecules23071612 (2018).

69. Dehoux-Baudoin, C. & Génisson, Y. C-Branched Imino Sugars: Synthesis and Biological Relevance. *European J. Org. Chem.* **2019**, 4765–4777 (2019).

70. Nishimura, Y. Gem-diamine 1-N-iminosugars as versatile glycomimetics: synthesis, biological activity and therapeutic potential. *J. Antibiot. (Tokyo).* **62**, 407–423 (2009).

71. Compain, P., Chagnault, V. & Martin, O. R. Tactics and strategies for the synthesis of iminosugar C-glycosides: a review. *Tetrahedron: Asymmetry* **20**, 672–711 (2009).

72. Clemente, F., Matassini, C. & Cardona, F. Reductive amination routes in the synthesis of piperidine iminosugars. *European J. Org. Chem.* **2020**, 4447–4462 (2020).

73. La Ferla, B., Bugada, P., Cipolla, L., Peri, F. & Nicotra, F. Synthesis of imino sugar scaffolds for the generation of glycosidase inhibitor libraries. *European J. Org. Chem.* 2451–2470 (2004) doi:10.1002/ejoc.200300805.

74. Cipolla, L., La Ferla, B., Peri, F. & Nicotra, F. A new procedure for the synthesis of -glycosides of nojirimycin. *Chem. Commun.* 1289–1290 (2000) doi:10.1039/B003877F.

75. Gorantla, J. N. & Lankalapalli, R. S. Synthesis of *β*-C-galactosyl ceramide and its new aza variant via the horner-wadsworth-emmons reaction. *J. Org. Chem.* **79**, 5193–5200 (2014).

76. Momotake, A., Mito, J. & Yamaguchi, K. Synthesis and Properties of C -Azalyxonucleosides. **3263**, 7207–7212 (1998).

77. Ribes, C. *et al.* Short , Stereoselective Synthesis of the Naturally Occurring Pyrrolidine Radicamine B and a Formal Synthesis of Nectrisine pyrrolidine radicamine B is reported . Garner ′ s (R) -aldehyde , prepared from D -serine , was the chiral starting material . The. 7779–7782 (2008).

78. Moreno-Vargas, A. J., Carmona, A. T., Mora, F., Vogel, P. & Robina, I. Stereoselective synthesis of (2S,3S,4R,5S)-5-methylpyrrolidine-3,4-diol derivatives that are highly selective α-L-fucosidase inhibitors. *Chem. Commun.* 4949–4951 (2005) doi:10.1039/b508855k.

79. Bouix, C., Bisseret, P. & Eustache, J. Stereoselective synthesis of arabinose-derived phosphonates. *Tetrahedron Lett.* **39**, 825–828 (1998).

80. Sugiyama, M. *et al.* D -Fructose-6-Phosphate Synthesis of Iminocyclitols. *J. Am.*

Chem. Soc. **129**, 14811–14817 (2007).

81. Horenstein, B. A., Zabinski, R. F. & Schramm, V. L. A new class of C-nucleoside analogues. 1-(S)-aryl-1,4-dideoxy-1,4-imino-D-ribitols, transition state analogue inhibitors of nucleoside hydrolase. *Tetrahedron Lett.* **34**, 7213–7216 (1993).

82. Bosco, M., Bisseret, P., Bouix-Peter, C. & Eustache, J. A new concise synthesis of nectrisine and its facile conversion to phosphonoazasugars. *Tetrahedron Lett.* **42**, 7949–7952 (2001).

83. Szcześniak, P., Stecko, S., Staszewska-Krajewska, O. & Furman, B. Sugar-derived cyclic imines: One-pot synthesis and direct functionalization. *Tetrahedron* **70**, 1880–1888 (2014).

84. Tsou, E. L. *et al.* Synthesis and biological evaluation of a 2-aryl polyhydroxylated pyrrolidine alkaloid-based library. *Bioorganic Med. Chem.* **16**, 10198–10204 (2008).

85. Carmona, A. T., Whigtman, R. H., Robina, I. & Vogel, P. Synthesis and glycosidase inhibitory activity of 7-deoxycasuarine. *Helv. Chim. Acta* **86**, 3066–3073 (2003).

86. Dransfield, P. J., Gore, P. M. & Slawin, A. M. Z. Divergent approach to imino sugar C -glycosides using imino glycals : application to the stereocontrolled synthesis of (+) -deoxoprosophylline Tri- O -acetyl imino glucal 2 is readily made and shown to bond forming reactions at C-1 of the piperidine nuc. 150–151 (2002).

87. Dransfield, P. J., Gore, P. M., Prokeš, I., Shipman, M. & Slawin, A. M. Z. Preparation and reactivity of imino glycals: Stereocontrolled, divergent approach to imino sugars. *Org. Biomol. Chem.* **1**, 2723–2733 (2003).

88. Oliveira, D. F., Severino, E. A. & Correia, C. R. D. Heck reaction of endocyclic enecarbemates with diazonium salts. Formal enantioselective syntheses of alkaloids (-)-codonopsine and (-)- codonopsinine, and the synthesis of a new C-aryl azasugar. *Tetrahedron Lett.* **40**, 2083–2086 (1999).

89. Asano, N. Glycosidase inhibitors: update and perspectives on practical use. *Glycobiology* **13**, 93R-104R (2003).

90. Giblett, E., Ammann, A., Sandman, R., Wara, D. & Diamond, L. NUCLEOSIDE-PHOSPHORYLASE DEFICIENCY IN A CHILD WITH SEVERELY

DEFECTIVE T-CELL IMMUNITY AND NORMAL B-CELL IMMUNITY. *Lancet* **305**, 1010–1013 (1975).

91. Canduri, F. *et al.* New catalytic mechanism for human purine nucleoside phosphorylase. *Biochem. Biophys. Res. Commun.* **327**, 646–649 (2005).

92. Birck, M. R. & Schramm, V. L. Nucleophilic Participation in the Transition State for Human Thymidine Phosphorylase. *J. Am. Chem. Soc.* **126**, 2447–2453 (2004).

93. Lewandowicz, A. & Schramm, V. L. Transition State Analysis for Human and Plasmodium falciparum Purine Nucleoside Phosphorylases. *Biochemistry* **43**, 1458–1468 (2004).

94. Deng, H. *et al.* Active Site Contacts in the Purine Nucleoside Phosphorylase−Hypoxanthine Complex by NMR and ab Initio Calculations. *Biochemistry* **43**, 15966–15974 (2004).

95. PUGMIRE, M. J. & EALICK, S. E. Structural analyses reveal two distinct families of nucleoside phosphorylases. *Biochem. J.* **361**, 1–25 (2001).

96. Zhang, Y., Geng, H., Zhang, J. & He, K. An Update Mini-Review on the Progress of Azanucleoside Analogues. *Chem. Pharm. Bull.* **70**, 469–476 (2022).

97. Bzowska, A., Kulikowska, E. & Shugar, D. Purine nucleoside phosphorylases: properties, functions, and clinical aspects. *Pharmacol. Ther.* **88**, 349–425 (2000).

98. ANDRICOPULO, A. D. & YUNES, R. A. Structure-Activity Relationships for a Collection of Structurally Diverse Inhibitors of Purine Nucleoside Phosphorylase. *Chem. Pharm. Bull.* **49**, 10–17 (2001).

99. Hernández, D. & Boto, A. Nucleoside Analogues: Synthesis and Biological Properties of Azanucleoside Derivatives. *European J. Org. Chem.* **2014**, 2201–2220 (2014).

100. Kicska, G. A. *et al.* Immucillin H, a powerful transition-state analog inhibitor of purine nucleoside phosphorylase, selectively inhibits human T lymphocytes. *Proc. Natl. Acad. Sci.* **98**, 4593–4598 (2001).

101. Evans, B. G., Schramm, L. V. & Tyler, C. P. The Immucillins: Design, Synthesis and Application of Transition- State Analogues. *Current Medicinal Chemistry* vol.

22 3897–3909 at https://doi.org/http://dx.doi.org/10.2174/092986732266615082110085 1 (2015).

102. Montgomery, J. A. Purine nucleoside phosphorylase: A target for drug design. *Med. Res. Rev.* **13**, 209–228 (1993).

103. Evans, G. B., Furneaux, R. H., Lewandowicz, A., Schramm, V. L. & Tyler, P. C. Synthesis of Second-Generation Transition State Analogues of Human Purine Nucleoside Phosphorylase. *J. Med. Chem.* **46**, 5271–5276 (2003).

104. Clinch, K. *et al.* Third-Generation Immucillins: Syntheses and Bioactivities of Acyclic Immucillin Inhibitors of Human Purine Nucleoside Phosphorylase. *J. Med. Chem.* **52**, 1126–1143 (2009).

105. Ho, M.-C. *et al.* Four generations of transition-state analogues for human purine nucleoside phosphorylase. *Proc. Natl. Acad. Sci.* **107**, 4805–4812 (2010).

106. Makita, S., Maeshima, A. M., Maruyama, D., Izutsu, K. & Tobinai, K. Forodesine in the treatment of relapsed / refractory peripheral T-cell lymphoma : an evidence-based review. 2287–2293 (2018).

107. Julander, J. G. *et al.* An update on the progress of galidesivir (BCX4430), a broad-spectrum antiviral. *Antiviral Res.* **195**, 105180 (2021).

108. Diaz-Torné, C., Perez-Herrero, N. & Perez-Ruiz, F. New medications in development for the treatment of hyperuricemia of gout. *Curr. Opin. Rheumatol.* **27**, (2015).

109. Al-Kali, A., Gandhi, V., Ayoubi, M., Keating, M. & Ravandi, F. Forodesine: Review of Preclinical and Clinical Data. *Futur. Oncol.* **6**, 1211–1217 (2010).

110. Furman, R. R. & Hoelzer, D. Purine Nucleoside Phosphorylase Inhibition as a Novel Therapeutic Approach for B-Cell Lymphoid Malignancies. *Semin. Oncol.* **34**, S29–S34 (2007).

111. Korycka, A., Blonski, J. & Robak, T. Forodesine (BCX-1777, Immucillin H) - A New Purine Nucleoside Analogue: Mechanism of Action and Potential Clinical Application. *Mini-Reviews Med. Chem.* **7**, 976–983 (2007).

112. Miles, R. W., Tyler, P. C., Furneaux, R. H., Bagdassarian, C. K. & Schramm, V. L.

One-Third-the-Sites Transition-State Inhibitors for Purine Nucleoside Phosphorylase. *Biochemistry* **37**, 8615–8621 (1998).

113. Bantia, S. *et al.* Purine nucleoside phosphorylase inhibitor BCX-1777 (Immucillin-H)—a novel potent and orally active immunosuppressive agent. *Int. Immunopharmacol.* **1**, 1199–1210 (2001).

114. Balakrishnan, K., Nimmanapalli, R., Ravandi, F., Keating, M. J. & Gandhi, V. Forodesine, an inhibitor of purine nucleoside phosphorylase, induces apoptosis in chronic lymphocytic leukemia cells. *Blood* **108**, 2392–2398 (2006).

115. Gandhi, V. *et al.* A proof-of-principle pharmacokinetic, pharmacodynamic, and clinical study with purine nucleoside phosphorylase inhibitor immucillin-H (BCX-1777, forodesine). *Blood* **106**, 4253–4260 (2005).

116. Ritchie, E. *et al.* Phase II Study of Forodesine, a PNP Inhibitor, in Patients with Relapsed or Refractory B-Lineage Acute Lymphoblastic Leukemia. *Blood* **108**, 1881 (2006).

117. Furman, R. R. *et al.* Forodesine (FodosineTM), a PNP Inhibitor Active in Relapsed or Refractory T-Cell Leukemia Patients (Phase II Study). *Blood* **106**, 881 (2005).

118. Gore, L., Stelljes, M. & Quinones, R. Forodesine Treatment and Post-Transplant Graft-Versus-Host Disease in Two Patients With Acute Leukemia: Facilitation of Graft-Versus-Leukemia Effect? *Semin. Oncol.* **34**, S35–S39 (2007).

119. Rinaldo-Matthis, A. *et al.* Inhibition and Structure of Trichomonas vaginalis Purine Nucleoside Phosphorylase with Picomolar Transition State Analogues. *Biochemistry* **46**, 659–668 (2007).

120. Evans, G. B., Tyler, P. C. & Schramm, V. L. Immucillins in Infectious Diseases. *ACS Infect. Dis.* **4**, 107–117 (2018).

121. Warren, T. K. *et al.* Protection against filovirus diseases by a novel broad-spectrum nucleoside analogue BCX4430. *Nature* **508**, 402–405 (2014).

122. Eyer, L. *et al.* Antiviral activity of the adenosine analogue BCX4430 against West Nile virus and tick-borne flaviviruses. *Antiviral Res.* **142**, 63–67 (2017).

123. Julander, J. G. *et al.* Efficacy of the broad-spectrum antiviral compound BCX4430

against Zika virus in cell culture and in a mouse model. *Antiviral Res.* **137**, 14–22 (2017).

124. Westover, J. B. *et al.* Galidesivir limits Rift Valley fever virus infection and disease in Syrian golden hamsters. *Antiviral Res.* **156**, 38–45 (2018).

125. Taylor, R. *et al.* BCX4430 – A broad-spectrum antiviral adenosine nucleoside analog under development for the treatment of Ebola virus disease. *J. Infect. Public Health* **9**, 220–226 (2016).

126. Li, G. & De Clercq, E. Therapeutic options for the 2019 novel coronavirus (2019-nCoV). *Nat. Rev. Drug Discov.* **19**, 149–150 (2020).

127. Taylor, R. *et al.* Activity of Galidesivir in a Hamster Model of SARS-CoV-2. *Viruses* vol. 14 at https://doi.org/10.3390/v14010008 (2022).

128. Fleet, G. W. J. & Son, J. C. Polyhydroxylated pyrrolidines from sugar lactomes: Synthesis of 1,4-dideoxy-1,4-imino-d-glucitol from d-galactonolactone and syntheses of 1,4-dideoxy-1,4-imino-d-allitol, 1,4-dideoxy-1,4-imino-d-ribitol, and (2s,3r,4s)-3,4-dihydroxyproline from d-gulonola. *Tetrahedron* **44**, 2637–2647 (1988).

129. Evans, G. B., Furneaux, R. H., Gainsford, G. J., Schramm, V. L. & Tyler, P. C. Synthesis of Transition State Analogue Inhibitors for Purine Nucleoside Phosphorylase and N-Riboside Hydrolases. *Tetrahedron* **56**, 3053–3062 (2000).

130. Furneaux, R. H. & Tyler, P. C. Improved Syntheses of 3H,5H-Pyrrolo[3,2-d]pyrimidines. *J. Org. Chem.* **64**, 8411–8412 (1999).

131. Evans, G. B. *et al.* Addition of Lithiated 9-Deazapurine Derivatives to a Carbohydrate Cyclic Imine: Convergent Synthesis of the Aza-C-nucleoside Immucillins. *J. Org. Chem.* **66**, 5723–5730 (2001).

132. Zhang, M. *et al.* Practical synthesis of immucillins BCX-1777 and BCX-4430. *Org. Chem. Front.* **7**, 3675–3680 (2020).

133. Kamath, V. P., Xue, J., Juarez-Brambila, J. J. & Morris, P. E. Alternative route towards the convergent synthesis of a human purine nucleoside phosphorylase inhibitor—forodesine HCl. *Tetrahedron Lett.* **50**, 5198–5200 (2009).

134. Horenstein, B. A., Zabinski, R. F. & Schramm, V. L. A new class of C-nucleoside analogues. 1-(S)-aryl-1,4-dideoxy-1,4-imino-D-ribitols, transition state analogue inhibitors of nucleoside hydrolase. *Tetrahedron Lett.* **34**, 7213–7216 (1993).

135. BIOCRYST PHARMACEUTICALS, I. COMPOSITIONS AND METHODS FOR INHIBITING VIRAL POLYMERASE. *WO 2013/158746 Al* (2013).

136. BABU, Yarlagadda, S. . 4836 S. P. *et al.* ANTIVIRAL AZASUGAR-CONTAINING NUCLEOSIDES. *WO 2014/078778 A2* (2014).

Chapter-2

Synthesis of Immucillin-H and its Stereochemical Variants

2.1. Abstract

The synthesis of forodesine, a potent iminosugar with significant immunosuppressive activity, involves the strategic assembly of its key subunits. The process begins with the functionalization of D-ribose to derive a lactam intermediate, followed by the construction of the pyrrolopyrimidine unit from readily available starting materials. Despite challenges in scaling and yields, optimizations in reductive amination and protection strategies have been pursued. The study also explores alternative routes to improve the efficiency and practicality of the synthesis, ultimately aiming to develop a viable method for producing forodesine and its analogs.

2.2. Introduction

Immucillins, a class of naturally occurring purine nucleoside analogs, have attracted considerable interest due to their diverse therapeutic potential.[1] These compounds exhibit promising immunomodulatory and antibacterial properties, making them attractive candidates for treating various T-cell proliferative disorders such as psoriasis, rheumatoid arthritis, and T-cell lymphomas.[2–4] Additionally, immucillins demonstrate activity against protozoan parasites responsible for malaria, trypanosomiasis, and sleeping sickness. This broad spectrum of bioactivity has spurred significant research efforts toward developing efficient and scalable synthetic methods for immucillins, particularly forodesine, a well-studied representative with potent immunosuppressive activity.[1,5,6]

Previous work by Evans *et al*. established a synthetic route for forodesine that relied on the key step of coupling an in situ generated imine derived from an aza-sugar intermediate with lithiated 9-deazahypoxanthine.[7] This approach was followed by deprotection to furnish the final product. However, this method presents limitations. The aza-sugar synthesis reported by Fleet *et al*., which utilized D-gulonolactone as the starting material,[8] is no longer readily applicable due to the limited commercial availability of D-gulonolactone. Additionally, while the reported imine and lithiated 9-deazahypoxanthine coupling delivered consistent

results,[9] the process involved cumbersome manipulations that significantly hindered its scalability for large-scale production.

These limitations in the existing synthetic routes for forodesine highlight the necessity for exploring alternative approaches. An ideal new method would address the challenges of precursor availability and scalability while offering a more efficient and streamlined synthesis of the aza-sugar intermediate and forodesine. This study aims to contribute to this ongoing research effort by investigating a novel synthetic route for forodesine, potentially paving the way for a more practical and commercially viable production method.

2.3. Result and discussions

The objective of this chapter is to develop novel routes for the synthesis of forodesine and its analogs.

2.3.1. Synthetic plan for forodesine (Immucillin-H)

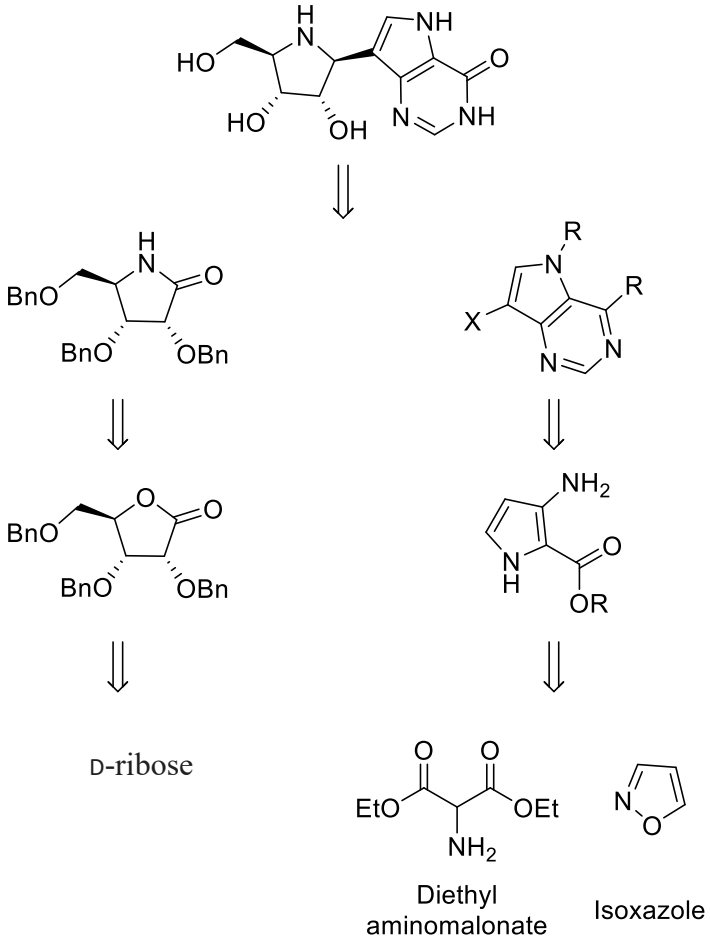

Figure 2.3.1: Synthetic plan for forodesine

We aim to leverage the advantages of convergent synthesis. This strategy involves assembling a molecule from independent subunits, often leading to higher yields and purer products compared to linear syntheses. Forodesine, an iminosugar derivative of D-ribose, features a lactam (cyclic amide) linked to a pyrrolopyrimidine unit. Our plan involves synthesizing these subunits independently and then coupling them in a key step. The lactam will be derived from D-ribose to ensure the correct sugar stereochemistry.[10] The pyrrolopyrimidine unit will be constructed from a substituted pyrrole, followed by a reaction with formamidine acetate. The pyrrole itself can be obtained from readily available diethyl aminomelanate and isoxazole.[11] The crux of the synthesis lies in the organometallic-assisted cross-coupling reaction between the synthesized lactam and the pyrrolopyrimidine unit. This reaction will forge the crucial bond that unites these subunits, ultimately leading to forodesine. Following forodesine's successful synthesis, we will then explore its conversion to the next target molecule, galidesivir.

2.3.1.1. Synthesis of the lactam *via* D-ribose functionalization

The synthesis commenced with selective protection of D-ribose's anomeric hydroxyl group as a methoxy ether (1-O-methyl-D-ribose) to control subsequent reactions (Scheme 2.3.1.1a). Subsequent benzylation using benzyl bromide and sodium hydride transformed the remaining hydroxyls into benzyl ethers, yielding compound **2**. The methoxy-protecting group was then strategically removed *via* cleavage with acid hydrolysis, generating hemiacetal intermediate **3**. Dess-Martin periodinane, a mild oxidant, facilitated the dehydrogenation of the hemiacetal to form γ-lactone **4** and δ-lactone **5**.[10,12]

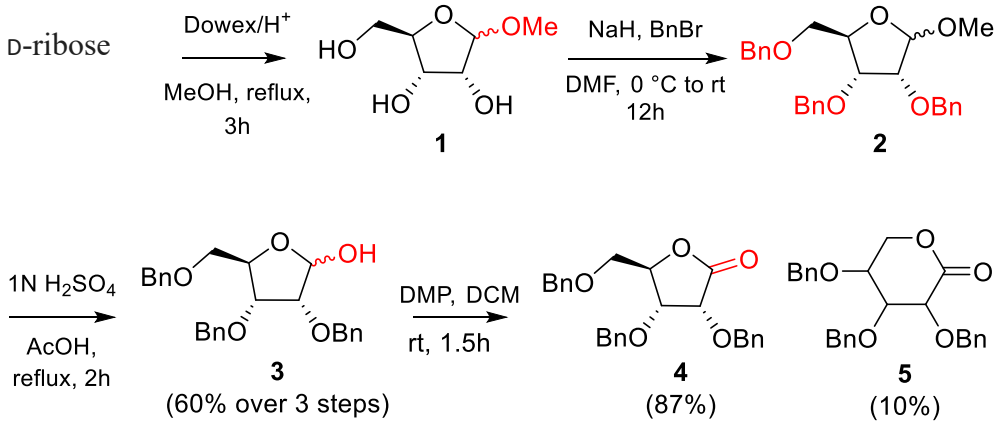

Scheme 2.3.1.1a: Synthesis of lactone form D-ribose

Our initial hypothesis suggested that *δ*-lactone **5** originated from the hemiacetal intermediate **3** derived from the anomeric methoxy ether (1-O-methyl-D-ribose). However, subsequent analysis revealed the *δ*-lactone likely formed directly from the cyclic pyranose form of D-ribose present in the starting material. D-ribose exists in equilibrium between its furanose and pyranose forms, and the reaction conditions might have favored the pyranose form to lead to the observed *δ*-lactone product **5**.

The *γ*-lactone **4,** on treatment with methanolic ammonia, converted the lactone to a hydroxy-carboxamide intermediate containing a secondary alcohol. Dess-Martin periodinane then mediated the oxidation of the alcohol to a ketone, generating a keto amide intermediate. This intermediate undergoes cyclization in the presence of methanolic ammonia, generating a mixture of lactam epimers (compound **8**).[10,12] Finally, reductive amination using the Kishi reduction selectively furnished the desired lactam **9**.

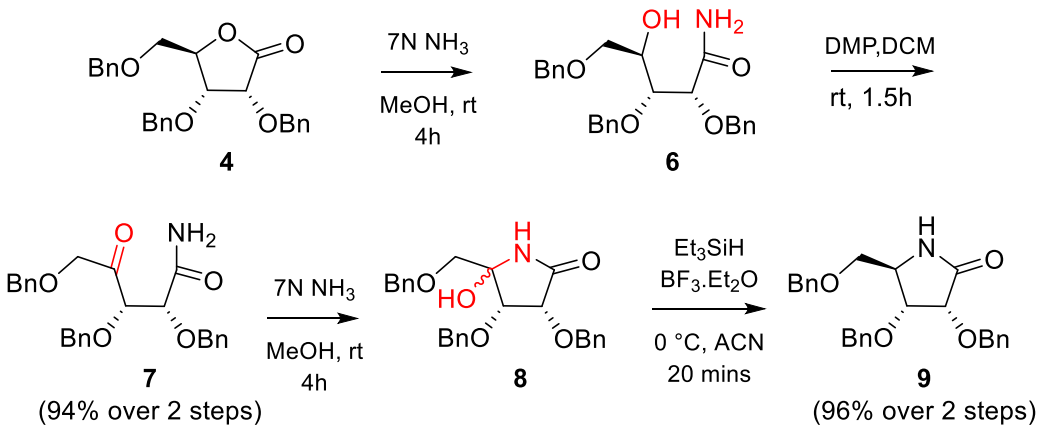

Scheme 2.3.1.1b: Synthesis of *γ*-lactone **9**

2.3.1.2. Synthesis of the pyrrolopiramidine partner

Pyrrolo[3,2-d]pyrimidines have garnered renewed interest due to their potential as synthetic precursors to the immucillins. However, the synthetic routes to access this ring system remain limited. Traditionally, these syntheses involve either functionalized pyrimidines[13] or the construction of the pyrimidine ring onto a substituted pyrrole.[14] Considering the readily available starting materials, we focused on the latter approach for pyrrolo[3,2-d]pyrimidine synthesis. A literature review identified two promising methods for this purpose.

Building upon the work of Furneaux *et al*. (1999),[15] who reported a convenient synthesis of a pyrrole derivative from isoxazole and diethyl aminomalonate in five days, we aimed to leverage this route. Their method offers a readily available starting material for the synthesis of 9-deazahypoxanthine through subsequent treatment with formamidine acetate, achieving an overall yield of 45% (Scheme 2.3.1.2a).

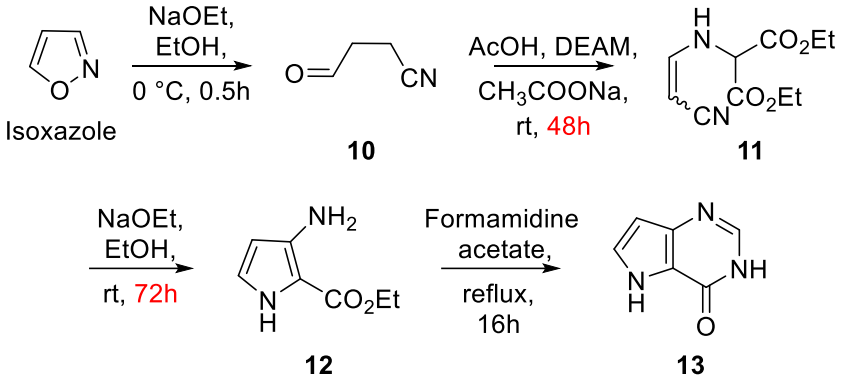

Scheme 2.3.1.2a: Synthesis of 9-deazahypoxanthine from isoxazole

However, when we tried this method, significant challenges emerged during scale-up, including efficient reaction monitoring, workup at a larger scale, ensuring intermediate stability, and achieving consistent reproducibility. These challenges prompted us to explore alternative routes for the synthesis of 9-deazahypoxanthine.

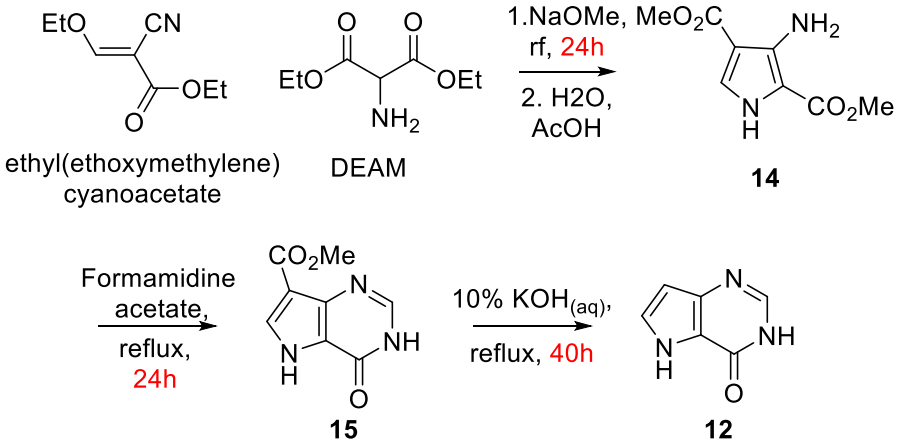

Scheme 2.3.1.2b: Synthesis of 9-deazahypoxanthine from ethyl(ethoxymethylene) cyanoacetate

Another report published in 2009 by V.P. Kamath *et al*.[16] offered a three-step route to 9-deazahypoxanthine, as illustrated in Scheme 2.3.1.2b. This method starts with the synthesis of a pyrrole derivative. The pyrrole is formed by refluxing ethyl

(ethoxymethylene)cyanoacetate, diethyl aminomalonate, and sodium methoxide in methanol. Subsequent condensation of the purified pyrrole with formamidine acetate in refluxing ethanol yields an intermediate product. Finally, base-catalyzed decarboxylation of this intermediate 9-deazahypoxanthine in a reported overall yield of 51%.

Unfortunately, replicating the reported yield and reaction times of this method proved challenging. Issues with reproducibility and long reaction times necessitated further optimization. In both cases, when we tried to reproduce the result, we got **13**, only a 9% overall yield. To address these limitations, we explored novel reaction conditions for the synthesis of the substituted pyrrole starting from isoxazole. As shown in Table 2.3.1.2, we systematically investigated the impact of various parameters on the pyrrole yield. These parameters included the addition and incubation time of reagents, the amount of sodium methoxide (NaOMe), and the reaction temperature.

Table 2.3.1.2: Optimization for compound **13**

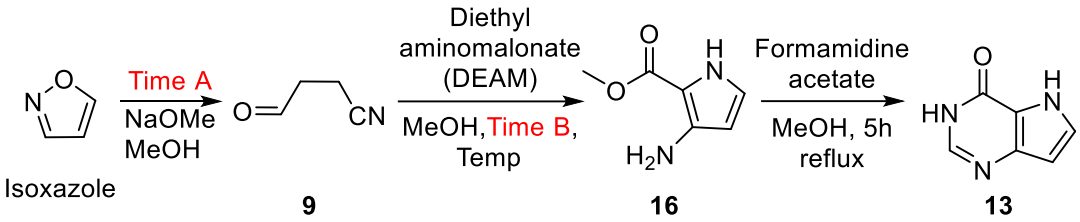

Sl. No.	Isoxazole (eq)	NaOMe (eq)	Time A (h)	DEAM (eq)	Temp (°C)	Time B (h)	Yield of 13 (%)
1	1	3	0.5	1	60	6	9
2	1	3	0.5	1	60	12	4
3	1	3	0.5	1	85	2	--
4	1	3	0.5	3	85	3	3.5
5	1	1	0.5	1.1	60	3	--
6	1	2	0.5	1.1	60	6	7
7	1	3	0.5	1.1	60	3	7
8	1	3	0.5	1.1	60	3	5
9	1	4	0.5	1.1	60	3	4
12	1	3	0.5	0.9	60	6	6
13	1	4	0.5	1.1	80	3	--
14	1	4	0.5	1.1	80	6	5

15	1	3	0.5	1.1	60	6	8
16	1	3	0.75	1	60	6	7
17	1	3	1	1	60	6	7
18	1	3	1.5	1	60	6	6

Our efforts culminated in the discovery of a novel route for synthesizing 9-deazahypoxanthine (**13**) with an overall yield of 9%. While the yield may be considered modest, this method offers a significant advantage in reaction time. Our approach requires only 12 hours of heating, compared to several days needed in the previously described methods.

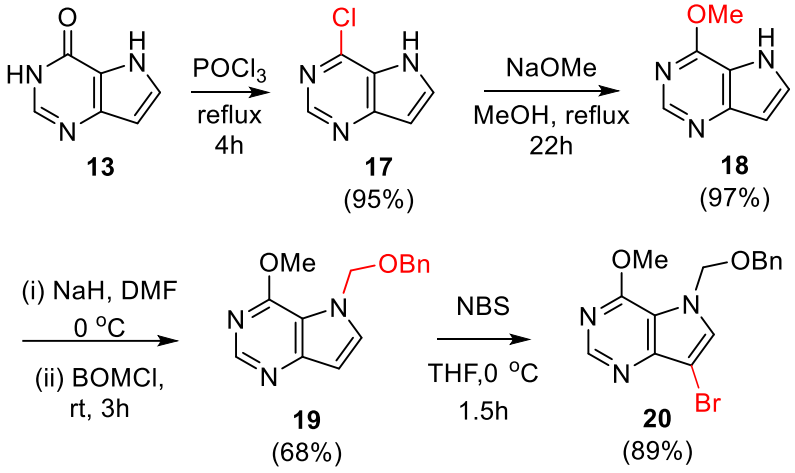

Scheme 2.3.1.2c: Synthesis of compound **20**

To generate a key precursor **20** (Scheme 2.3.1.2c) suitable for the subsequent cross-coupling reaction, compound **13** underwent a three-step functionalization process. The first step involved chlorination using phosphorus oxychloride under optimized conditions. This was followed by the selective replacement of the chlorine atom with a methoxy group *via* treatment with sodium methoxide, which yielded intermediate **18**. Finally, to prepare **18** for the cross-coupling reaction, the pyrrole NH group was protected as a benzyloxymethyl ether. N-bromosuccinimide then mediated the introduction of a bromine atom at the desired position, furnishing the key intermediate **20**. It is crucial to employ appropriate stoichiometry of NBS and portion-wise additions to prevent the formation of dibromo compounds.

2.3.1.3. The cross-coupling reaction of 16 with ribose partner

With both key starting materials (compounds **9** and **20**) prepared, we proceeded to the cross-coupling reaction utilizing organolithium chemistry. Compound 16, bearing a bromine atom, was subjected to lithium-halogen exchange using n-butyllithium in THF at -78 °C. The anticipated lithiated intermediate **20a** was then treated with *γ*-lactam **9**. Unfortunately, this attempt did not yield the desired cross-coupled product. In an effort to optimize the reaction, we explored alternative coupling partners. We replaced *γ*-lactam **9** with both *γ*-lactone **4** and *γ*-lactol **3**. However, none of these variations resulted in the formation of the targeted cross-coupled product. Notably, we were able to recover compound **19**, the dehalogenated derivative of **20**, from these reactions.

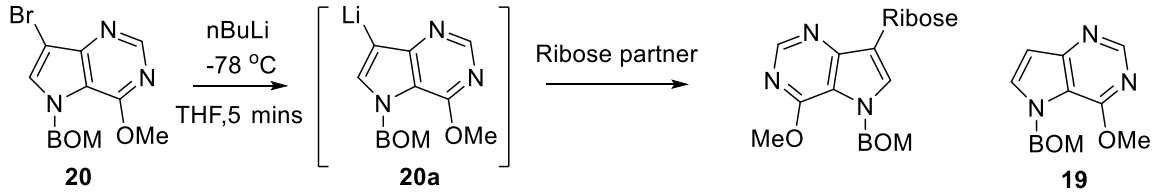

Scheme 2.3.1.3: Cross-coupling attempts with compound **20**

The recovery of compound **19** suggested successful lithium-halogen exchange, indicating the formation of the nucleophilic intermediate (**20a**). However, the lack of desired cross-coupling products in all attempts suggested that our sugar partners (lactam **9** and lactone **4**) might not possess sufficient electrophilicity to effectively react with the nucleophile. So, we hypothesized that the hemiacetal functionality in lactol **3**, acting as a masked aldehyde, could potentially offer some electrophilic character. However, this attempt was also unsuccessful. To address the apparent lack of electrophilicity, we opted to employ a stronger electrophile – ribose-aldehyde – as the next sugar partner in the cross-coupling reaction.

2.3.2.1. Synthesis of ribonaldehyde

Leveraging the inherent hemiacetal functionality in lactol **3**, we strategically targeted the carbonyl group for selective protection. Employing 1,3-propane-dithiol under triflic acid catalysis afforded the desired compound **21** as mentioned in Scheme 2.3.2.1a. Following the successful aldehyde protection, we focused on protecting the remaining secondary alcohol in compound **21**. Selective benzoylation using a suitable benzoylating agent (e.g., Benzoic acid, EDCI.HCl) yielded compound **22**. Triflic acid catalyzed protection strategy

offered an advantage over using other Brønsted acids, as attempts with those resulted in the formation of an undesired by-product (structure **22a**, see Figure 2.5.2.12) or a mixture of products. We suspected these issues might arise from competing reaction pathways with stronger Bronsted acids. Triflic acid, being a stronger Lewis acid, likely facilitated a more selective activation of the carbonyl group for the desired dithioacetal formation.

The intermediate compound 22 stood just one step away from the coveted aldehyde **23**. The cleavage of the 1,3-propanedithiol protecting group was efficiently achieved using N-bromosuccinimide in a mixture of acetonitrile and water. This deprotection reaction proceeded smoothly within a short reaction time of 10 minutes.

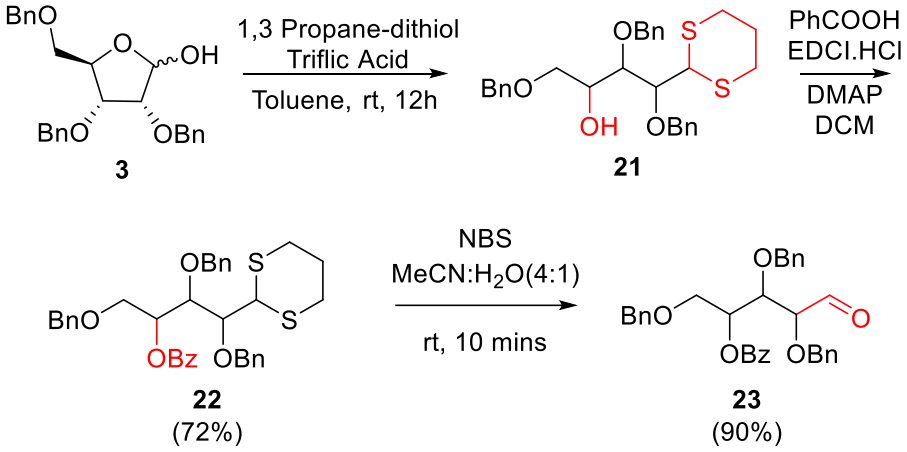

Scheme 2.3.2.1a: Synthesis of ribonaldehyde through aldehyde protection

While the reported synthesis of ribonaldehyde delivers a good yield, the utilization of 1,3-propanedithiol presents a significant health and safety concern. This compound is known to possess a potent and unpleasant odor, causing headaches and discomfort for researchers in close proximity. To mitigate these safety concerns and improve the overall laboratory experience, we sought an alternative route for the synthesis of target compound **23** (detailed in Scheme 2.3.2.1b).

This approach involved a reduction of the lactol functionality in compound **3** to a diol. Followed selective protection of the primary alcohol using *tert*-butyldimethylsilyl chloride facilitated the compound **24**. Following the successful primary alcohol protection, we focused on protecting the remaining secondary alcohol in compound **24**. Selective benzoylation using benzoic acid in the presence of EDCI.HCl strategy yielded intermediate **25**, where the secondary alcohol was protected as a benzoyl ester. Subsequent deprotection

of the primary alcohol was achieved under mild acidic conditions using 2% hydrochloric acid in ethanol. The liberated primary alcohol was then subjected to selective oxidation, furnishing the desired ribonaldehyde **23**.

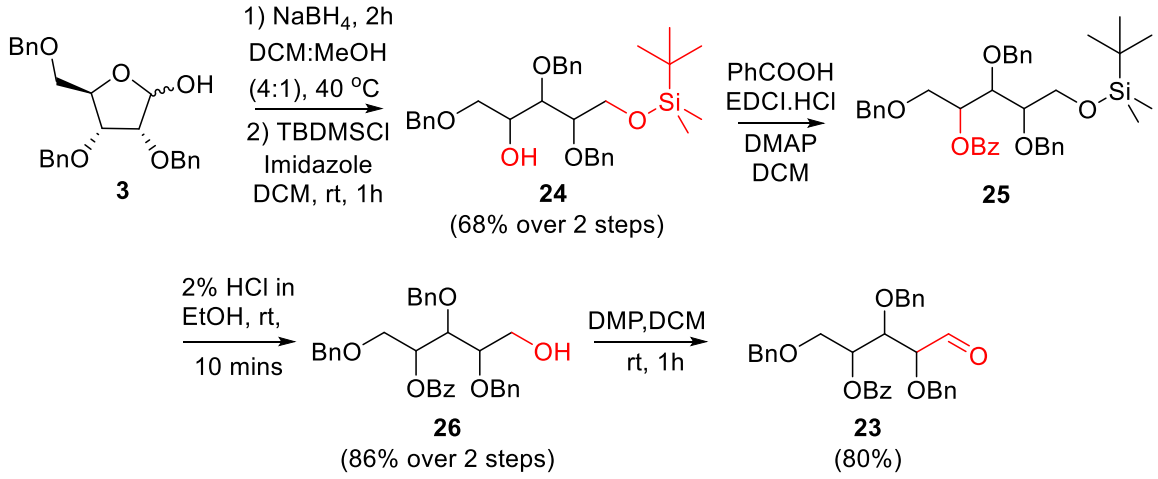

Scheme 2.3.2.1b: Synthesis of ribonaldehyde through aldehyde generation

A common approach for silyl deprotection involves tetrabutylammonium fluoride. While we initially attempted this method for the cleavage of the TBDMS group in compound **25**, we encountered an unexpected complication (Scheme 2.3.2.1c). TBAF is known to possess basic character, which can promote undesired side reactions under certain conditions.[17] In this case, TBAF treatment resulted in the migration of the benzoyl protecting group from the secondary alcohol to the newly deprotected primary alcohol in compound **25**. This yielded undesired product **26a**, characterized by a free secondary alcohol and a primary benzoyl ester. Confirmation of this rearrangement was achieved through subsequent oxidation of **26a** using Dess-Martin Periodinane reagent, which yielded ketone **23a** instead of the desired ribonaldehyde **23**.

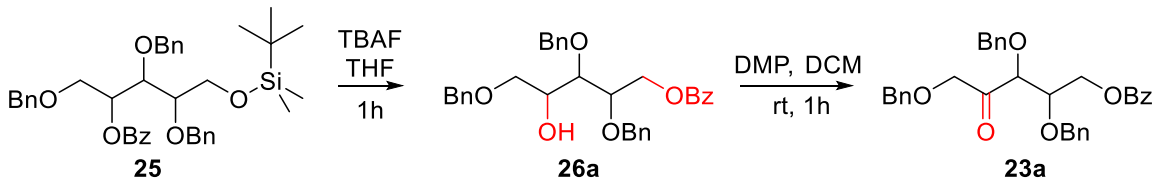

Scheme 2.3.2.1c: Undesired benzoyl migration

To circumvent this issue and achieve selective deprotection of the TBDMS group, we opted for a milder acidic approach. Treatment with 2% hydrochloric acid in ethanol effectively

cleaved the silyl ether while preserving the benzoyl ester at the secondary alcohol position. This strategy provided the desired intermediate with free primary alcohol ready for the subsequent oxidation step.

2.3.2.2. Cross-coupling with ribonaldehyde

With both the key coupling partners in hand (compound **20** and ribonaldehyde **23**), we revisited the cross-coupling reaction. Employing the established procedure, *n*BuLi was used to achieve lithium-halogen exchange on compound **20**, generating the anticipated lithiated intermediate **20a**. Subsequent treatment of **20a** with ribonaldehyde **23** was anticipated to yield the desired cross-coupled product. Unfortunately, this attempt, like the previous ones using different sugar partners, did not produce the targeted product. Recovery of the dehalogenated compound **19** from the reaction mixture indicated successful metal-halogen exchange. However, the absence of the desired cross-coupled product suggested potential incompatibility between the reaction intermediate (**20**) and the solvent. A review of the literature revealed that THF might not be an ideal solvent for this specific cross-coupling reaction. The basic nature of the lithiated intermediate (**20a**) could lead to proton abstraction from THF itself, resulting in the observed formation of the dehalogenated product **19**.[7]

Drawing on insights from the literature, we investigated the use of a solvent mixture for the cross-coupling reaction to address the incompatibility issues observed with THF. A combination of diethyl ether and anisole (4:1 ratio) was chosen based on its reported success in similar cross-coupling reactions. To achieve optimal reaction conditions, we further conducted an optimization process to maximize the yield of the cross-coupled product.

Table 2.3.2.2: Optimization for compound **27**

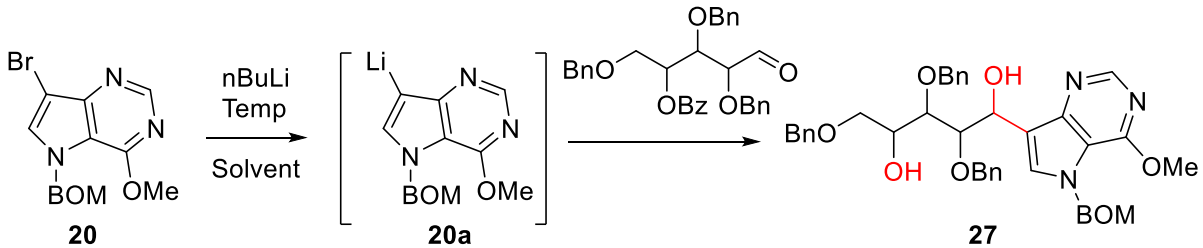

S.No	20 (eq)	23 (eq)	*n*BuLi (eq)	Solvent	Temperature (^{o}C)	27 (%)
1	1.5	1.0	2.25	THF	0	NR
2	1.5	1.0	2.25	THF	-78	Trace
3	1.5	1.0	3.0	Et_2O/Anisole(4:1)[7]	-78	25
4	1.5	1.0	2.25	Et_2O/Anisole(4:1)	-78	14
5	1.5	1.0	3	Et_2O/Anisole(4:1)	-40	Trace
6	1.5	1.0	3	Et_2O/Anisole(4:1)	0	NR
7	1.5	1.0	3	Anisole	-78	NR
8	1.5	1.0	3	Toluene	-78	NR

Further literature exploration identified another solvent system (methyl *tert*-butyl ether and anisole) reported for similar cross-coupling reactions.[18] We incorporated this solvent mixture into our optimized reaction conditions. Interestingly, this new solvent system yielded a distinct product compound **28** instead of compound **27** (Scheme 2.3.2.2).

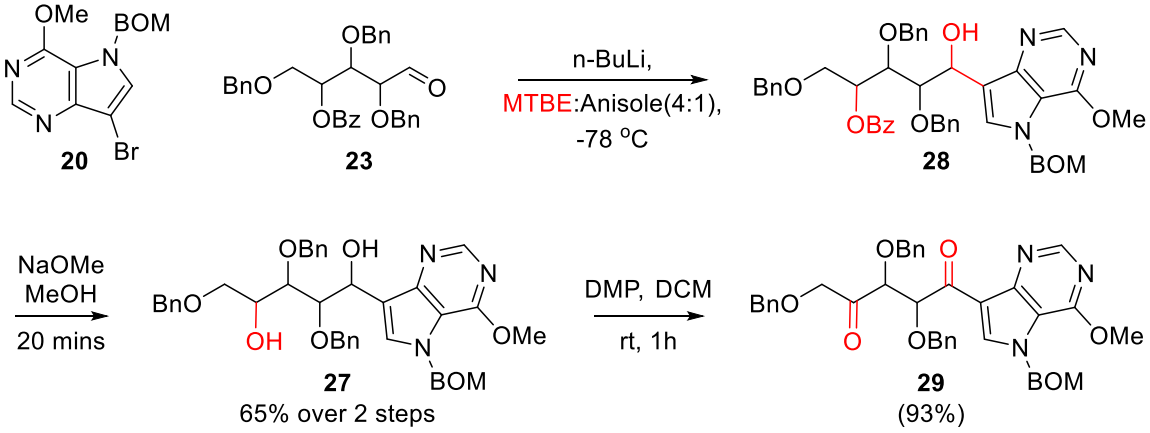

Scheme 2.3.2.2: Synthesis of diketone **29**

Subsequent analysis confirmed that compound **28** was indeed the cross-coupled product, but with the benzoyl protecting group (from compound **23**) remaining intact. This suggested selective cross-coupling at the desired position. To achieve the deprotected product (**27**), treatment with NaOMe effectively removed the benzoyl group under mild conditions. This two-step sequence provided the desired compound **27** in a respectable overall yield of 60%. The final step involved the conversion of compound **27** into the

corresponding diketone **29**. This oxidation step serves as a crucial precursor for the subsequent double reductive amination, a key reaction in the synthesis of the targeted iminosugar.

2.3.2.3. Double reductive amination using ammonia

Our initial attempt at the double reductive amination of diketone **29** employed ammonium formate as the nitrogen source and $NaCNBH_3$ as the reducing agent.[19] Unfortunately, this reaction yielded a complex mixture of products, as evidenced by thin-layer chromatography. While the starting material was fully consumed, isolation of any specific product proved challenging *via* silica gel column chromatography. Only trace amounts of the desired product compound **30** were isolable using preparative TLC.

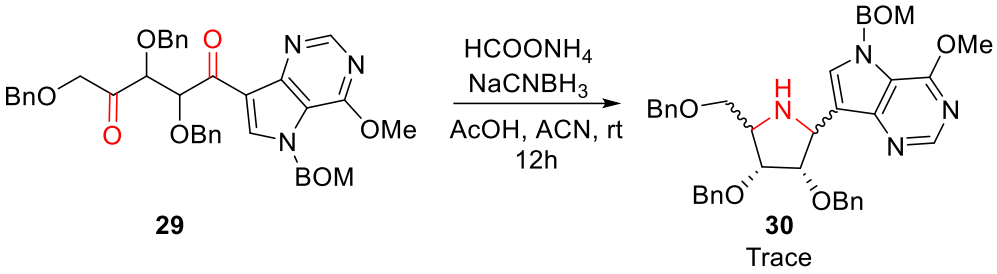

Scheme 2.3.2.3a: Double reductive amination

To optimize the reaction and achieve cleaner product formation, we embarked on a comprehensive optimization campaign. This involved systematically varying several reaction parameters:

- Nitrogen source: CH_3COONH_4, $HCOONH_4$, NH_3
- Reducing agent: $NaBH_4$, $Na(CH_3COO)_3BH$, Et_3SiH
- Promoter: HCOOH, CH_3COOH, BF_3-OEt, HCl
- Solvent: ACN, MeOH, DCM
- Temperature: -78 °C, 0 °C, room temperature, reflux

We explored various combinations of these parameters to identify a condition that would favor the selective formation of compound **30**. However, these efforts were unsuccessful in achieving a clean reaction. Lower reaction temperatures resulted in no observed

conversion, while reactions conducted at room temperature or higher yielded complex mixtures with complete consumption of the starting material.

The stereochemistry of compound **30** was elucidated using a combination of 1D and 2D NMR techniques. The 1D nOe spectrum (Figure 2.3.2.3) provided valuable insights into the spatial proximity of specific protons. The assignment of sugar protons was achieved through the analysis of 2D NMR data. Selective 1D nOe experiments were then performed, irradiating protons 3 and 4 individually. The absence of a nOe enhancement between protons 1 and 3 indicated an antiperiplanar relationship. Conversely, irradiation of proton 4 resulted in a nOe enhancement with proton 1, suggesting a synperiplanar arrangement. Additionally, the lack of nOe between protons 2 and 4 confirmed their antiperiplanar orientation.

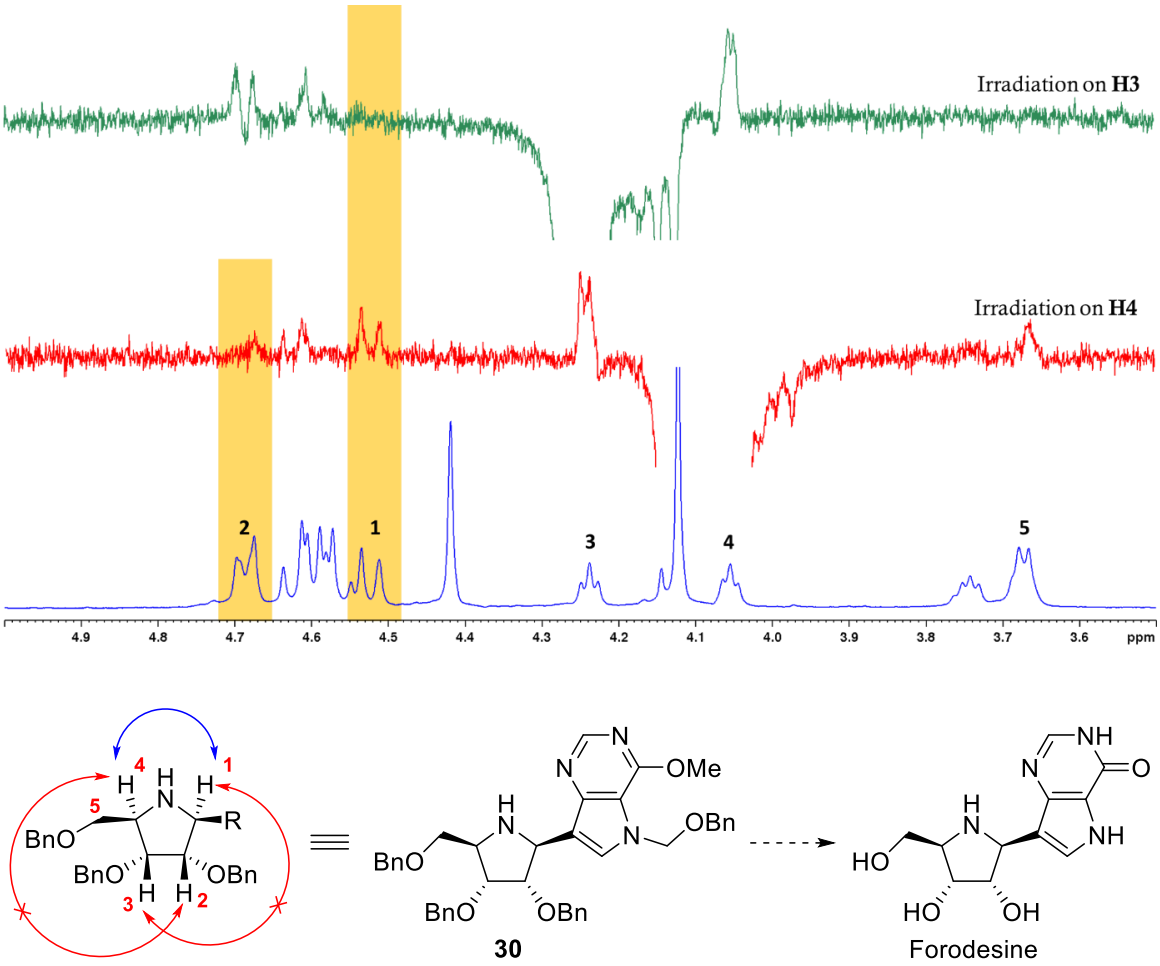

Figure 2.3.2.3: 1D nOe of compound **30**

Based on this comprehensive NOE analysis, the stereochemistry of compound **30** was assigned, confirming it as the desired forodesine precursor. Deprotection of all protecting groups in compound **30** would furnish the target molecule, forodesine. Unfortunately, the current method for synthesizing compound **30** suffers from limitations in scalability and yield. This scarcity of material has precluded further characterization, such as deprotection to obtain forodesine.

To rationalize the observed stereochemistry of compound **30**, a plausible mechanism for the double reductive amination reaction is proposed (Scheme 2.3.2.3b). This mechanism highlights the potential factors that might influence the selectivity of hydride attack during each reductive amination step.

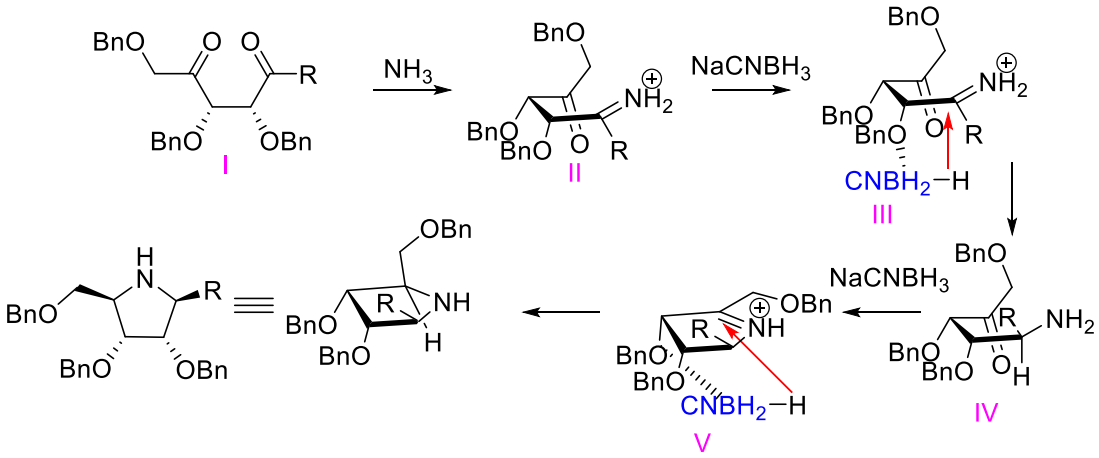

Scheme 2.3.2.3b: A plausible mechanism for the formation of compound **30**

The reaction sequence commences with the condensation of ammonia with the diketone **29** to form an iminium ion intermediate. Under the influence of the reduction condition, coordination of a borohydride moiety with the oxygen of the C-2' OBn group is envisioned. This chelation could potentially direct the delivery of the hydride from the *si*-face of the molecule, pushing the R group away from the OBn substituent.[20] The subsequent reduction of the iminium ion by the hydride would then establish the desired stereochemistry at the newly formed amine center.

Following this initial reduction, a second iminium ion is formed between the amine functionality and the remaining carbonyl. A similar chelation-assisted hydride delivery from the reducing agent, this time directed by the newly formed chiral center, would then lead to product **30** with the observed stereochemical configuration

2.3.2.4. Double reductive amination using ammine

Given the challenges encountered with simple nitrogen sources in the double reductive amination, we explored an alternative approach utilizing a primary amine. A literature review identified a novel protocol employing *para*-substituted benzylamine as the nitrogen source, $ZnCl_2$ as the promoter, $NaCNBH_3$ as the reducing agent, and methanol as the solvent at 65 °C.[21] We adapted these reaction conditions to our double reductive amination of diketone **29**. This modification resulted in the successful formation of the iminosugar, compound **31**.

To further improve the reaction efficiency and selectivity, we embarked on an optimization campaign. By systematically varying reaction parameters, we aimed to improve the yield of the products. During this optimization process, two additional products were identified: an aromatic compound **32** and an oxy-sugar product **33**.

Table 2.3.2.4: Optimization for double reductive amination

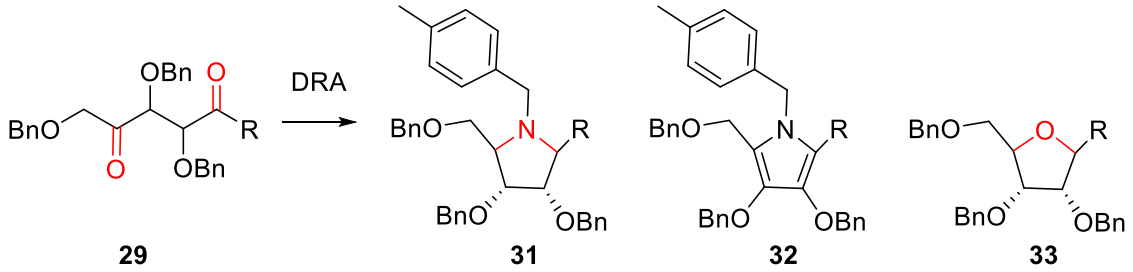

29 **31** **32** **33**

No.	Nitrogen Source	Reducing Agent	Promoter	Solvent	Temp. (°C)	Product
1	*p*-MeBnNH$_2$	NaCNBH$_3$	Zncl$_2$	MeOH	65	29 (65%)[21]
2	*p*-MeBnNH$_2$	NaCNBH$_3$	AcOH	MeOH	65	--
3	*p*-MeBnNH$_2$	NaCNBH$_3$	Zncl$_2$	AcOH	80	31 (18%)
4	NH$_2$OH	NaCNBH$_3$	Zncl$_2$	MeOH	65	--
5	NH$_3$	NaCNBH$_3$	Zncl$_2$	MeOH	65	--
6	BnNH$_2$	NaCNBH$_3$	HCOOH	MeOH	80	--
7	*p*-MeBnNH$_2$	NaCNBH$_3$	HCl	MeOH	65	--
8	*p*-MeBnNH$_2$	NaCNBH$_3$	MgSO$_4$	MeOH	65	--
9	*p*-MeBnNH$_2$	Na(AcO)$_3$BH	AcOH	DCE	27	30 (27%)
10	*p*-MeBnNH$_2$	NaCNBH$_3$	TFA	MeOH	65	--

11	CH_3COONH_4	$NaCNBH_3$	$Zncl_2$	MeOH	65	--
12	$HCOONH_4$	$NaCNBH_3$	$Zncl_2$	MeOH	65	--
13	CH_3COONH_4	$NaCNBH_3$	$Zncl_2$	MeOH	80	--
14	$HCOONH_4$	$NaCNBH_3$	$Zncl_2$	ACN	65	--
15	*p*-$MeBnNH_2$	$NaCNBH_3$	$Zncl_2$	ACN	65	--

The formation of compound **33** as an unexpected side product during the double reductive amination reaction was intriguing. While the desired outcome was iminosugar (compound **31**), the presence of an oxysugar product in a reaction mixture containing a nitrogen source was surprising. To elucidate the potential role of *para*-methylbenzylamine (the nitrogen source) in the formation of compound **33**, a control experiment was conducted. The double reductive amination reaction was repeated under identical conditions but excluding the nitrogen source (Scheme 2.3.2.4a). Notably, the reaction still yielded compound **33**, confirming that the nitrogen source was not directly involved in its formation.

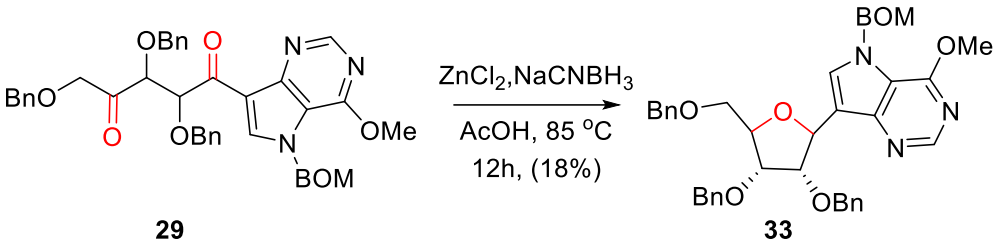

Scheme 2.3.2.4a: Synthesis of compound **33**

This observation suggests that the solvent, acetic acid, might be a contributing factor. The acidic nature of acetic acid could potentially promote intramolecular cyclization and subsequent reduction, leading to the formation of the oxy-sugar product.

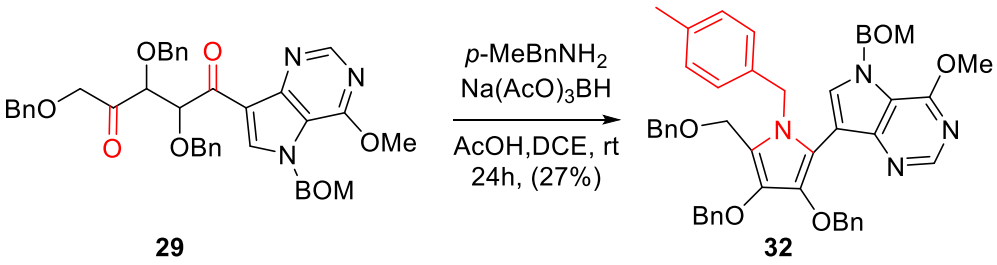

Scheme 2.3.2.4b: Synthesis of compound **32**

The isolation of compound **32** as another unexpected side product presented an interesting mechanistic inquiry. Unlike the desired iminosugar (compound **31**), this product possessed a substituted pyrrole ring. The reaction conditions employed a relatively nonpolar solvent (DCE) and stirred at room temperature for an extended period (24 hours) (Scheme 2.3.2.4b). These reaction parameters differed significantly from the standard protocol for double reductive amination, which typically involves polar solvents and elevated temperatures. We propose that the low polarity of DCE might have disfavored the intended reduction pathway. The lack of polarity could have limited the stabilizing interactions between the reaction intermediates and the solvent, potentially leading to an alternative reaction pathway favoring aromatization and pyrrole ring formation.

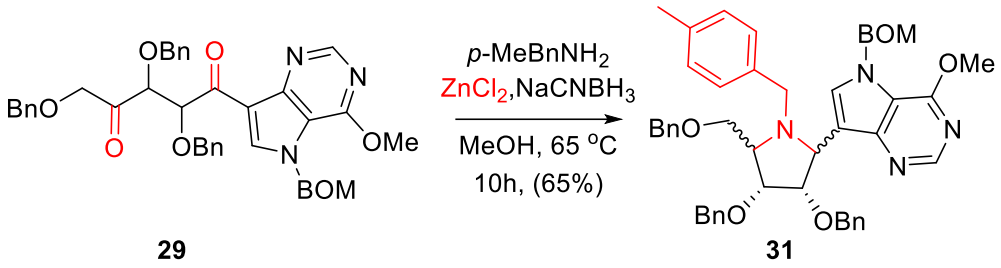

Scheme 2.3.2.4c: Synthesis of compound **31**[21]

Compound **31** exhibited all the spectral characteristics of our desired product (Scheme 2.3.2.4c). Analysis by NMR and HRMS confirmed the molecular formula and mass, consistent with an N-substituted iminosugar bearing a pyrrolopyrimidine moiety. To definitively assign the stereochemistry of compound **31**, a 1D nOe experiment was employed. The necessary sugar proton assignments were established using 2D NMR techniques. This information enabled the selective irradiation of protons 1 and 4 in the 1D nOe experiment

The 1D NOE experiment yielded valuable insights into the spatial arrangement of protons within compound **31**. Selective irradiation of proton 1 resulted in signal enhancements for both protons 4 and 3. This observation indicates that these three protons are coplanar within the molecule. Similarly, irradiation of proton 4 led to signal enhancements for protons 2 and 1, suggesting that all sugar ring protons share the same spatial orientation.

These nOe correlations are consistent with the proposed structure of compound **31** (Figure 2.3.2.4). However, it is important to note that this analysis reveals a stereochemical

configuration distinct from the desired forodesine precursor. While compound **31** possesses the correct N-substitution and pyrrolopyrimidine core, the relative stereochemistry at specific sugar ring positions differs from the target molecule.

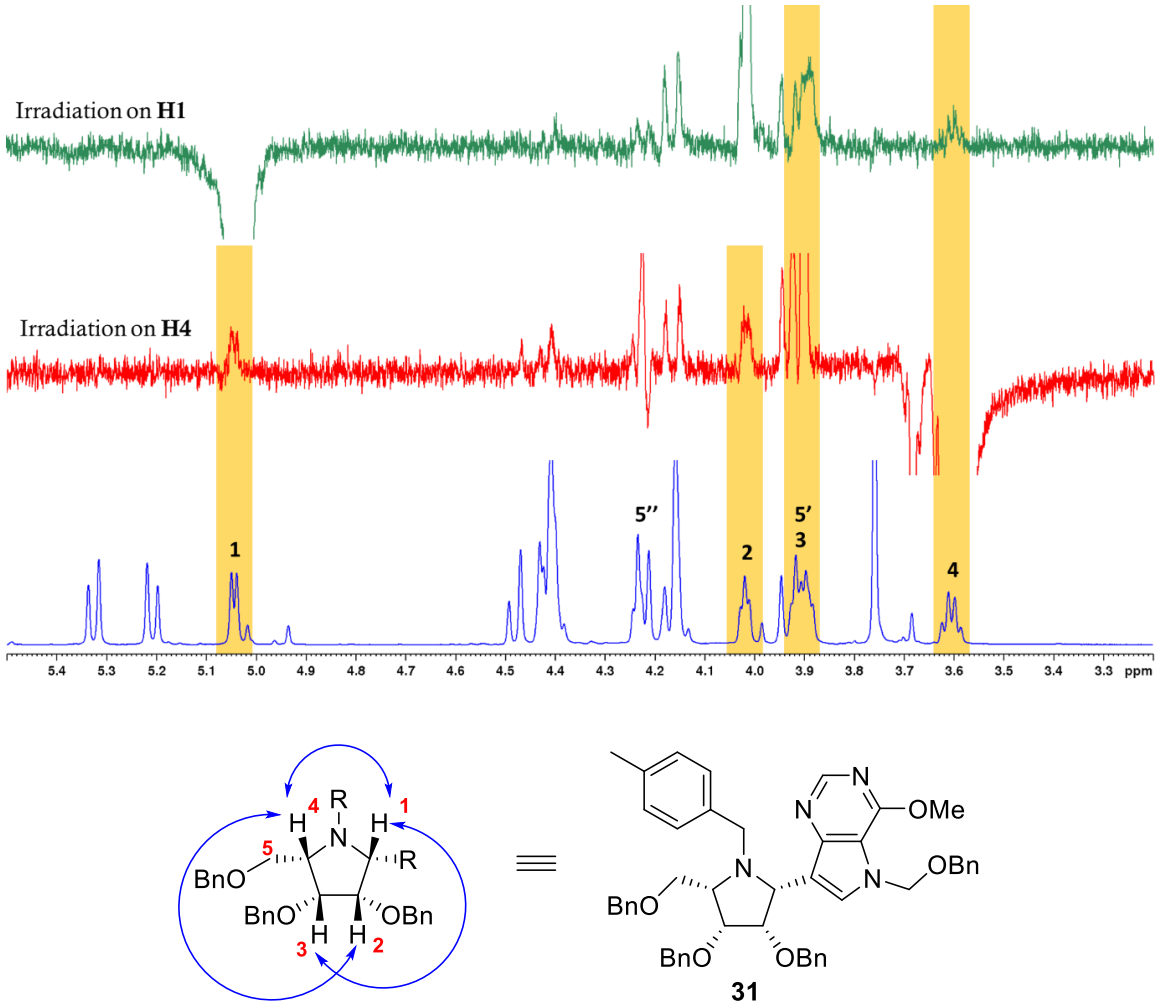

Figure 2.3.2.4: 1D nOe of compound **31**

Compounds **30** and **31**, both obtained through double reductive amination, exhibit distinct stereochemical configurations. To account for these diastereomeric outcomes, a plausible mechanistic rationale is proposed in Scheme 2.3.2.4d.[21,22]

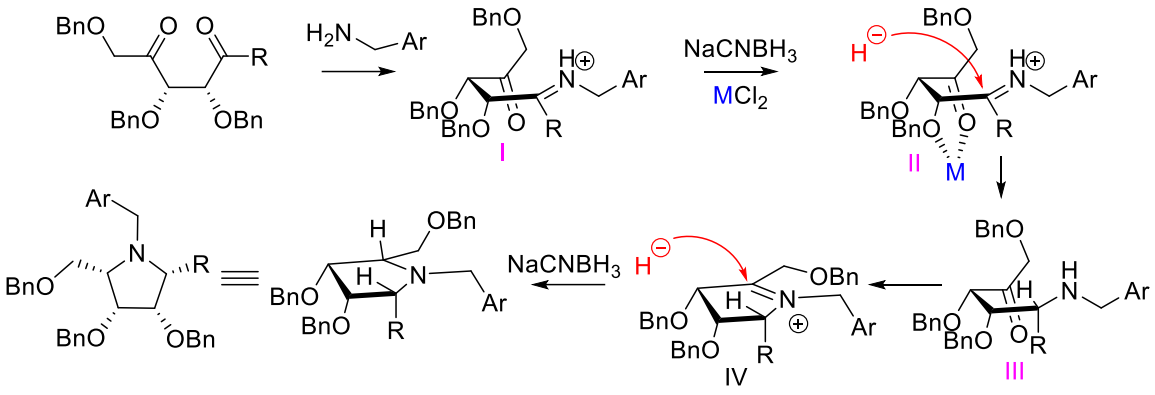

Scheme 2.3.2.4d: A plausible mechanism for the formation of **31**

The reaction sequence commences with the condensation of the amine with the diketone, forming an iminium ion intermediate. However, unlike the previously proposed mechanism (for compound **30**), chelation between the Lewis acidic metal center (Zn^{2+}) and both carbonyl oxygen and the oxygen atom of the C-2' OBn group on the *si*-face is envisioned. This chelation could sterically hinder hydride attack from the reducing agent on the *si*-face. Consequently, hydride delivery is favored from the *re*-face opposite the OBn substituent, establishing the stereochemistry at the newly formed amine center.

The subsequent reduction of the second imine functionality follows a similar logic. The newly formed chiral amine can adopt a conformation that positions the remaining ketone carbonyl group for hydride attack from the less hindered *re*-face. This diastereoselective reduction ultimately leads to the formation of compound **31**, where all sugar ring protons reside on the same side of the plane.

2.3.2.5. Synthesis of the stereochemical variant of forodesine

While compound **31** did not represent the desired forodesine precursor, it offered the potential to access a stereoisomer of forodesine. To achieve this conversion, a deprotection strategy was employed. Compound **31** was subjected to reflux conditions in a concentrated HCl-methanol solution (6:1) for 3 days. This treatment aimed to cleave all protecting groups, including benzyl ethers, the benzyloxymethyl (BOM) group, and the methyl ether, to furnish the corresponding deprotected product, a diastereomer of forodesine.

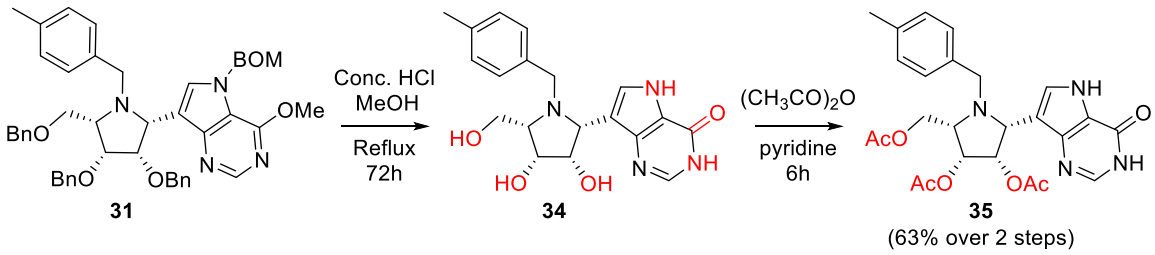

Scheme 2.3.2.5: Synthesis of stereoisomer of forodesine

Subsequent acetylation was performed for improved NMR analysis. The introduction of acetyl groups can simplify complex NMR spectra by shifting hydroxyl proton signals and enhancing the resolution of neighboring protons.

While the ultimate objective of directly synthesizing forodesine was not achieved in this study due to limitations in the yield of the key intermediate **30** (forodesine precursor), a significant outcome was the successful synthesis of a stereoisomer of the forodesine precursor through double reductive amination.

2.4. Conclusions

This study explored a novel synthetic route toward forodesine, starting with ribonaldehyde and culminating in a double reductive amination step. While the initial conditions employing a simple nitrogen source failed to yield the desired forodesine precursor, a literature-inspired modification using para-methylbenzylamine as the nitrogen source successfully delivered the iminosugar scaffold (compound **31**). However, detailed spectroscopic analysis, including 1D nOe experiments, revealed that compound **31** possessed a stereochemical configuration distinct from the targeted forodesine precursor. A plausible mechanism was proposed to explain the observed stereochemical divergence during the double reductive amination, highlighting the potential role of chelation-controlled hydride attack.

We halted the further deprotection steps for the synthesis of a forodesine stereo analog due to the poor yield of the forodesine precursor (compound **30**). Instead, we focused on studying the stereochemistry of the key intermediate (compound **31**). This helped us gain valuable insights into the reaction pathway and the factors that influenced the

stereoselectivity. Our future efforts will be based on these findings to optimize the double reductive amination step for the direct synthesis of the forodesine precursor.

2.5. Materials and methods

2.5.1. General experimental conditions

^{1}H and ^{13}C NMR spectra were obtained using a Bruker ASCEND^{TM}-500 spectrometer at 500 and 125 MHz, respectively. $CDCl_3$ and CD_3OD solvents were used to record the spectra. The NMR data is presented as chemical shifts in ppm (δ) along with integration, coupling constant in Hz, and multiplicity (s = singlet, bs= broad singlet, d = doublet, t = triplet, m = multiplet, dd = doublet of doublet, etc.). The HR-ESI-MS analysis was performed on a Thermo Scientific Exactive-LCMS instrument using the electrospray ionization method. The ions are reported in m/z using an Orbitrap analyzer. Optical rotation was measured on a JASCO P-2000 polarimeter. The reactions were monitored by silica gel G-60 F_{254} aluminum TLC plates, and the compounds were made visible by a short wavelength lamp; the TLC plate was charred after spraying with 15% sulfuric acid in ethanol. Chromatographic separations were carried out by conventional column chromatography on silica gel (100 - 200 mesh). The reagents were purchased at the highest commercial quality and used without further purification.

2.5.2. Other experimental procedures

2,3,5-tri-O-benzyl-D-ribonolactol (3): The hemiacetal compound **3** was synthesized using the Overkleeft protocol[10] and confirmed by comparison of the NMR data available in the literature; ^{1}H-NMR ($CDCl_3$): δ 7.40 (25 H, m), 5.52 (1H, m), 5.19 (1H, m), 4.93 (1H, m), 4.87 (2H, m), 4.78 (1Hm), 4.70 (2H, m), 4.58 (4H, m), 4.32 (1H, s), 4.17 (1H, s), 4.06 (1H, m), 3.92 (1H, m), 3.85 (1H, m), 3.71 (1H, m), 3.56 (2H, m), 3.40 (1H, s), 3.23 (1H, m) ppm; ^{13}C-NMR ($CDCl_3$): δ 138.99, 138.37, 138.10, 137.91, 137.84, 137.70, 128.55, 128.48, 128.43, 128.22, 128.18, 127.94, 127.89, 127.80, 127.75, 127.68, 127.51, 127.48, 127.43, 94.75, 92.00, 79.49, 75.30, 74.77, 74.54, 74.37, 74.04, 72.42, 71.43, 71.32, 70.60, 62.37, 56.25 ppm; HR-ESI-MS: $[M+Na]^+$ calculated for $C_{26}H_{28}O_5Na$ was m/z 443.1834, found 443.1837.

(3R,4R,5R)-3,4-bis(benzyloxy)-5-((benzyloxy)methyl)dihydrofuran-2(3H)-one (4): A solution of hemiacetal **3** (4.6 g, 10.92 mmol, 1 equiv.) was dissolved in DCM (200 mL),

followed by the addition of Dess-Martin periodinane (DMP) (6.95 g, 16.38 mmol, 1.5 equiv.). The reaction mixture was stirred for 2 h at room temperature under an argon atmosphere. After the reaction was complete, as indicated by TLC, the mixture was quenched with saturated $Na_2S_2O_3$(aq) (50 mL) and saturated $NaHCO_3$(aq) (50 mL), it was then extracted with DCM (2 x 100 mL). The combined organic extracts were dried over anhydrous Na_2SO_4 and concentrated. The resulting product was purified by column chromatography using hexane/EtOAc to afford **4** (3.98 g, 87% yield) and **5** (0.457 mg, 10% yield).; ^{1}H-NMR ($CDCl_3$): δ 7.34 (13H, m), 7.19 (2H, d, *J*=6.05 Hz), 4.97 (1H, d, *J* =11.96 Hz), 4.74 (2H, m), 4.54 (3H, m), 4.43 (2H, m), 4.12 (1H, m), 3.69 (1H, dd, *J*=2.25, 11.05 Hz), 3.58 (1H, dd, *J*=2.25, 11.00 Hz) ppm; ^{13}C-NMR ($CDCl_3$): δ 173.74, 137.24, 137.14, 136.96, 128.57, 128.54, 128.52, 128.29, 128.14, 128.09, 128.01, 127.62, 81.81, 75.38, 73.73, 73.67, 72.75, 72.42, 68.75 ppm; HR-ESI-MS: $[M+Na]^+$ calculated for $C_{26}H_{26}O_5Na$ was m/z 441.1678, found 441.1662.

3,4,5-tris(benzyloxy)tetrahydro-2H-pyran-2-one (5): formed along with **4** as a white solid (0.457 mg, 10% yield). ^{1}H-NMR ($CDCl_3$): δ 7.34 (15H, m), 5.11 (1H, d, *J* =12.16 Hz), 4.98 (1H, d, *J* =12.16 Hz), 4.90 (1H, d, *J* =12.16 Hz), 4.70 (1H, d, *J* =12.16 Hz), 4.55 (1H, d, *J* =11.96 Hz), 4.47 (2H, m), 4.30 (1H, dd, *J* =6.25, 10.55 Hz), 4.24 (1H, s), 3.86 (1H, d, *J* =2.05 Hz), 3.81 (1H, m) ppm; ^{13}C-NMR ($CDCl_3$): δ 169.83, 138.07, 137.38, 137.13, 128.62, 128.54, 128.27, 128.18, 128.09, 128.00, 127.88, 127.67, 127.59, 75.86, 74.01, 73.62, 73.23, 72.66, 71.56, 67.06 ppm; HR-ESI-MS: $[M+Na]^+$ calculated for $C_{26}H_{26}O_5Na$ was m/z 441.1678, found 441.1696.

(2R,3S)-2,3,5-tris(benzyloxy)-4-oxopentanamide (7): In compound **4** (4 g, 9.55 mmol) was added, 7 N ammonia in MeOH (10 mL) and stirred at room temperature for 1 hour. The reaction mixture was diluted with MeOH (50 mL), and concentrated under reduced pressure. The resulting yellow-colored oil was dissolved in DCM (150 mL), and Dess-Martin periodinane (6.08 g, 14.33 mmol, 1.5 equiv.) was added and stirred at room temperature for 90 mins. Upon completion of the reaction (from TLC analysis), saturated aqueous sodium thiosulphate (50 mL) was added and stirred vigorously until the reaction mixture became clear. The organic layer was then washed with saturated aqueous $NaHCO_3$ solution (3 x 100 mL), dried over anhydrous Na_2SO_4, concentrated, and purified using silica gel column chromatography (Hexane to 40% EtOAc in hexane) to afford compound **7** as a colorless viscous liquid (3.87 g, 94% yield over 2 steps). NMR spectral data of the open

chain product: ^{1}H-NMR (500 MHz, $CDCl_3$) δ 7.33 (15H, m), 6.61 (1H, s), 6.46 (1H, s), 4.63 (5H, m), 4.52 (2H, m), 4.45 (1H, s), 4.39 (2H, m) ppm; ^{13}C NMR (125 MHz, $CDCl_3$) δ 205.7, 171.5, 137.6, 136.9, 136.5, 128.7, 128.5, 128.43, 128.42, 128.1, 128.08, 128.01, 127.8, 83.3, 81.5, 74.2, 73.5, 73.3, 73.1 ppm; HR-ESI-MS: $[M+Na]^+$ calculated for $C_{26}H_{27}NO_5Na$ was m/z 456.1787, found 456.1792.

(3R,4R,5R)-3,4-bis(benzyloxy)-5-((benzyloxy)methyl)pyrrolidin-2-one (9): To compound **7** (3.87 g, 8.93 mmol), 7 N ammonia in MeOH (10 mL) was added and stirred at room temperature. After stirring the reaction mixture for 4 hours, diluted with MeOH (50 mL), and concentrated under reduced pressure. The resulting viscous liquid was dried thoroughly under a high vacuum and then dissolved in freshly distilled dry CH3CN (20 mL) under an argon atmosphere. The solution was then cooled to 0 °C using an ice-bath and Et_3SiH (14.19 mL, 89.45 mmol, 10 equiv.) and $BF_3.Et_2O$ (3.31 mL, 26.83 mmol, 3 equiv.) was added dropwise and stirred for 20 mins. The reaction mixture was quenched by adding saturated aqueous $NaHCO_3$ solution (50 mL), and extracted in EtOAc (150 mL). The organic layer was dried over anhydrous Na_2SO_4, and concentrated under reduced pressure to obtain an off-white flaky solid **9** (3.60 g 96% yield over 2 steps).; ^{1}H-NMR ($CDCl_3$) δ 7.23 (15H, m), 6.43 (1H, s), 4.82 (1H, d, J =11.93 Hz), 4.67 (1H, d, J =11.95 Hz), 4.53 (1H, d, J =11.81 Hz), 4.38 (3H, m), 3.98 (1H, d, J =5.50 Hz), 3.78 (2H, m), 3.44 (1H, dd, J =3.71, 9.79 Hz), 3.27 (1H, dd, J =5.98, 9.78 Hz) ppm; ^{13}C-NMR ($CDCl_3$): δ 173.47, 137.49, 137.47, 137.40, 128.54, 128.48, 128.42, 128.35, 128.10, 128.01, 127.94, 127.91, 127.69, 75.74, 74.33, 73.42, 72.20, 71.89, 70.40, 57.55 ppm; HR-ESI-MS: $[M+Na]^+$ calculated for $C_{26}H_{27}NO_4Na$ was m/z 440.1838, found 440.1824.

9-deazahypoxanthine (13): A 1.7 molar solution of NaOMe in methanol (127 mL, 217 mmol, 3 equiv.) was cooled to below 8 °C using an ice bath. Isoxazole (5 g, 72.4 mmol, 1 equiv.) was then added to the solution and stirred for 30 minutes. Subsequently, diethyl aminomalonate (15.3 g, 72.4 mmol, 1 equiv.) was added, and the mixture was gently heated to 60 °C and stirred for 6 hours under an argon atmosphere. After cooling the reaction mixture to room temperature, the methanol was removed using a rotary evaporator. The residue was quenched with water (200 mL) and extracted with $CHCl_3$ three times (200 mL each). The combined organic layers were washed with brine (100 mL), dried over anhydrous Na_2SO_4, and concentrated under reduced pressure to afford a yellow solid **16** (1.2 g, 8.56 mmol, 12% yield). This solid was then redissolved in methanol (20 mL), treated

with formamidine acetate (1.78 g, 17.13 mmol, 2 equiv.), and refluxed for 5 hours. The resulting precipitate was isolated by centrifugation, washed with cold methanol, and dried to obtain compound **13** as an off-white solid (889 mg, 9% yield over 2 steps).; ^{1}H-NMR (DMSO-d6) δ 8.49 (1H, s), 8.05 (1H, d, J =2.80 Hz), 7.06 (1H, d, J =2.76 Hz) ppm; ^{13}C-NMR (DMSO-d6) δ 154.21, 145.10, 142.01, 127.84, 118.26, 103.40 ppm; HR-ESI-MS: $[M+H]^+$ calculated for $C_6H_6ON_3$ was m/z 136.0505, found 136.0518.

4-chloro-5H-pyrrolo[3,2-d]pyrimidine (17): 9-Deazahypoxanthine **13** (1.06 g, 7.85 mmol) was heated under reflux in $POCl_3$ (7 mL, 74.87 mmol, 9.5 equiv.). After heating the reaction mixture for 5 hours, the resulting mixture was poured in ice and neutralized by adding cold aqueous NaOH solution (4.5 M, 100 mL). Extraction using EtOAc (3 x 100 mL) and subsequent evaporation of EtOAc afforded compound **17** as a pale yellow-colored solid (1.15 g, 95% yield). ^{1}H-NMR (500 MHz, DMSO-d6) δ 12.47 (1H, s, NH), 8.64 (2H, s), 7.99 (2H, s), 6.75 (2H, d, J =2.24 Hz) ppm; ^{13}C NMR (125 MHz, DMSO-d6) δ 151.4, 149.7, 142.2, 135.0, 124.4, 102.8 ppm; HR-ESI-MS: $[M+H]^+$ calculated for $C_6H_5ClN_3$ was m/z 154.0172, found 154.0167.

4-methoxy-5H-pyrrolo[3,2-d]pyrimidine (18): A solution of sodium methoxide (44 mg, 0.81 mmol, 2.5 equiv.) in methanol (4 mL) was treated with compound **17**. The reaction mixture was then refluxed for 22 hours. After cooling the reaction mixture to room temperature, it was quenched with distilled water (10 mL) and extracted with ethyl acetate (20 mL). The organic layer was dried over anhydrous Na_2SO_4, and concentrated under reduced pressure to afford an off-white solid identified as compound **18** (46 mg, 97% yield). ^{1}H-NMR ($CDCl_3$): δ 9.16 (1H, s), 8.51 (1H, s), 7.37 (1H, s), 6.62 (1H, s), 4.07 (3H, s) ppm; ^{13}C-NMR ($CDCl_3$): δ 155.97, 150.32, 150.23, 128.50, 115.20, 103.34, 53.50 ppm; HR-ESI-MS: $[M+Na]^+$ calculated for $C_7H_8N_3O$ was m/z 150.0662, found 150.0669.

5-((benzyloxy)methyl)-4-methoxy-5H-pyrrolo[3,2-d]pyrimidine (19): The solid **18** (108 mg, 0.72 mmol, 1 equiv.) was dissolved in anhydrous DMF (15 mL). The reaction mixture was cooled to 0 °C under an inert argon atmosphere, and then sodium hydride (60% suspension in mineral oil, 34 mg, 1.44 mmol, 2 equiv.) was added. After stirring for 15 minutes, benzylchloromethyl ether (0.11 mL, 0.79 mmol, 1.1 equiv.) was added dropwise to the reaction mixture. The mixture was then stirred at room temperature for 3 hours. The reaction was quenched by adding ice, and the product was extracted using ethyl acetate twice (50 mL each time). The organic layer was washed with distilled water (5 x 50 mL) to

remove DMF, then dried over anhydrous sodium sulfate, and concentrated under reduced pressure. Silica gel column chromatography (EtOAc/hexane) of the crude yellow syrup afforded compound **19** as a colorless solid (132 mg, 68% yield). ^{1}H-NMR ($CDCl_3$): δ 1H-NMR ($CDCl_3$): δ 8.47 (1H, s), 7.34 (1H, s), 7.22 (5H, m), 6.61 (1H, s), 5.67 (2H, s), 4.40 (2H, s), 4.04 (3H, s). ppm; ^{13}C-NMR ($CDCl_3$): δ 156.31, 151.53, 150.37, 136.87, 132.70, 128.49, 128.01, 127.72, 115.64, 104.10, 70.12, 53.50 ppm; HR-ESI-MS: $[M+H]^+$ calculated for $C_{15}H_{15}N_3O_2Na$ was m/z 270.1237, found 270.1259.

5-((benzyloxy)methyl)-7-bromo-4-methoxy-5H-pyrrolo[3,2-d]pyrimidine(20):
Compound **19** (525 mg, 1.95 mmol) was treated with anhydrous THF (5 mL) and N-bromosuccinimide (347 mg, 1.95 mmol, 1 equiv.). The NBS was added portion-wise (three portions of 116 mg each) with a 10-minute time interval between each addition. The reaction mixture was then stirred for 1.5 hours. After stirring, the reaction mixture was partitioned between EtOAc (25 mL) and distilled water (25 mL). The organic layer was washed with distilled water twice (25 mL each time) to remove any remaining water-soluble impurities. The organic layer was then dried over anhydrous Na_2SO_4 and concentrated under reduced pressure. Silica gel column chromatography (EtOAc/hexane) of the crude yilded white crystalline solid **20** (604 mg, 89% yield).; ^{1}H-NMR ($CDCl_3$): δ 8.63 (1H, s), 7.47 (1H, s), 7.25 (3H, m), 7.33 (2H, m), 5.74 (2H, s), 4.51 (2H, s), 4.14 (3H, s) ppm; ^{13}C-NMR ($CDCl_3$): δ 156.41, 151.03, 148.45, 136.50, 131.54, 128.53, 128.16, 127.70, 115.58, 92.44, 77.22, 70.43, 53.91 ppm; HR-ESI-MS: $[M+H]^+$ $C_{15}H_{15}BrN_3O_2$ calculated for m/z 348.0342, found 348.0365.

1,3,4-tris(benzyloxy)-4-(1,3-dithian-2-yl)butan-2-yl benzoate (22): Hemiacetal **3** (400 mg, 0.95 mmol, 1 equiv.) was dissolved in toluene (7 mL). Under an inert atmosphere, 1,3-propanedithiol (381 µL, 3.8 mmol, 4 equiv.) and a catalytic amount of triflic acid (8.3 µL, 0.1 mmol, 0.1 equiv.) were added to the solution. The mixture was then stirred for 3 hours. The reaction was quenched with 3 M NaOH solution (5 mL), and the product was extracted with DCM (50 mL). The organic layer was dried over anhydrous Na_2SO_4 and concentrated under reduced pressure.The residue was then redissolved in dry DCM (10 mL). Benzoic acid (174 mg, 1.4 mmol, 1.5 equiv.), EDCI.HCl (364 mg, 1.9 mmol, 2 equiv.), and 4-dimethylaminopyridine (12 mg, 0.1 mmol, 0.1 equiv.) were added, and the mixture was stirred for 12 hours under an inert atmosphere. The reaction was quenched with saturated $NaHCO_3$ solution (10 mL), and the product was extracted with DCM (2 x 30 mL). The

combined organic extracts were dried over anhydrous Na_2SO_4 and concentrated. Finally, purification by column chromatography using a mixture of hexane and EtOAc afforded compound **22** as a viscous liquid (391 mg, 67% yield over 2 steps).; ^{1}H-NMR ($CDCl_3$): δ 8.04 (2H, d, *J* =7.65 Hz), 7.58 (1H, t, *J*=7.35 Hz), 7.44 (4H, m), 7.30 (14H, m), 5.83 (1H, m), 5.00 (1H, d, *J* =11.21 Hz), 4.85 (1H, d, *J* =11.11 Hz), 4.69 (2H, dd, *J* =11.26, 17.16 Hz), 4.51 (2H, d, *J* =12.41 Hz), 4.42 (1H, d, *J* =12.21 Hz), 4.16 (1H, dd, J=2.48, 7.18 Hz), 3.91 (1H, dd, *J* =2.88, 7.18 Hz), 3.82 (2H, m), 2.83 (3H, m), 2.67 (1H, m), 2.07 (1H, m), 1.91 (1H, m) ppm; ^{13}C-NMR ($CDCl_3$): δ 165.62, 138.15, 138.02, 137.73, 132.99, 130.31, 129.76, 128.46, 128.41, 128.35, 128.29, 128.25, 128.11, 127.86, 127.66, 127.62, 127.49, 81.37, 79.22, 74.16, 74.06, 73.30, 72.96, 68.49, 50.44, 31.51, 30.11, 26.29 ppm; HR-ESI-MS: $[M+Na]^+$ calculated for $C_{36}H_{38}O_5S_2Na$ was m/z 637.2058, found 637.2034.

***S*-(3-(((3R,4R,5R)-3,4-bis(benzyloxy)-5-((benzyloxy)methyl)tetrahydrofuran-2-yl) thio)propyl) benzothioate (22a):** ^{1}H-NMR ($CDCl_3$): δ 7.88 (2H, d, *J*=7.80 Hz), 7.50 (2H, t, *J* =7.30 Hz), 7.23 (16H, m), 5.15 (1H, d, *J* =3.90 Hz), 4.57 (2H, m), 4.50 (2H, m), 4.43 (2H, m), 4.21 (1H, m), 3.95 (1H, m), 3.81 (1H, m), 3.50 (2H, m), 3.06 (2H, m), 2.66 (3H, m), 1.90 (2H, m) ppm; ^{13}C-NMR ($CDCl_3$): δ 191.73, 138.17, 137.68, 137.58, 137.06, 133.37, 128.62, 128.45, 128.41, 128.35, 128.13, 128.04, 127.93, 127.87, 127.66, 127.59, 127.23, 86.19, 81.74, 80.72, 78.08, 73.35, 72.29, 70.75, 29.84, 29.70, 27.78 ppm; HR-ESI-MS: $[M+Na]^+$ calculated for $C_{36}H_{38}O_5S_2Na$ was m/z 637.2058, found 637.2064.

1,3,4-tris(benzyloxy)-5-oxopentan-2-yl benzoate (23): N-bromosuccinimide (833 mg, 4.68 mmol, 8 equiv.) was dissolved in a mixture of acetonitrile and water (4:1 v/v). A solution of compound **22** (360 mg, 0.58 mmol, 1 equiv.) in pure acetonitrile (2 mL) was then added dropwise to the NBS solution while stirring. The reaction mixture was monitored by TLC and was completed within 10 minutes. The reaction was quenched with saturated $NaHCO_3$ solution (10 mL), and the product was extracted with DCM twice (30 mL each time). The combined organic extracts were dried over anhydrous Na_2SO_4 and concentrated under reduced pressure. Finally, purification by column chromatography (hexane/EtOAc) afforded compound **23** as a viscous liquid (274 mg, 90% yield).

A solution of compound **26** (390 mg, 0.74 mmol, 1 equiv.) was dissolved in DCM (25 mL). $NaHCO_3$ (280 mg, 3.33 mmol, 4.5 equiv.) was added, followed by Dess-Martin periodinane (471 mg, 1.11 mmol, 1.5 equiv.). The reaction mixture was stirred at room temperature for 2 hours. After monitoring by TLC to confirm completion, the reaction was quenched with

a saturated solution of $Na_2S_2O_3$ (20 mL). The product was then extracted with DCM (50 mL x 2). The combined organic extracts were dried over anhydrous Na_2SO_4 and concentrated under reduced pressure. Finally, purification by column chromatography using a mixture of hexane and EtOAc afforded compound **23** as a viscous liquid (310 mg, 80% yield); ^{1}H-NMR ($CDCl_3$) δ 9.45 (1H, d, J =1.17 Hz), 7.89 (2H, d, J =8.43 Hz), 7.49 (1H, m), 7.36 (2H, m), 7.19 (15H, m), 5.50 (1H, m), 4.61 (2H, m), 4.53 (2H, m), 4.45 (1H, d, J =12.12 Hz), 4.35 (1H, d, J =12.15 Hz), 4.25 (1H, dd, J =2.84, 8.03 Hz), 4.01 (1H, dd, J =1.12, 2.76 Hz), 3.75 (2H, m) ppm; ^{13}C-NMR ($CDCl_3$): δ 202.04, 165.09, 137.98, 137.35, 137.02, 133.27, 129.85, 129.66, 128.54, 128.53, 128.48, 128.37, 128.04, 128.03, 127.98, 127.65, 82.10, 79.08, 73.19, 73.18, 73.08, 71.40 ppm; HR-ESI-MS: $[M+Na]^+$ calculated for $C_{33}H_{32}O_6Na$ was m/z 547.2097, found 547.2124.

2,3,5-tris(benzyloxy)-4-oxopentyl benzoate (23a): A solution of compound **26a** (94 mg, 0.18 mmol, 1 equiv.) was dissolved in DCM (5 mL). Sodium bicarbonate (67.5 mg, 0.8 mmol, 4.5 equiv.) was added, followed by Dess-Martin periodinane (DMP) (151.5 mg, 0.36 mmol, 2 equiv.). The reaction mixture was stirred at room temperature for 2 hours. After monitoring by TLC to confirm completion, the reaction was quenched with a saturated solution of $Na_2S_2O_3$ (5 mL). The product was then extracted with DCM (10 mL x 2). The combined organic extracts were dried over anhydrous Na_2SO_4 and concentrated under reduced pressure. Purification by column chromatography using a mixture of hexane and EtOAc afforded compound **23a** as a viscous liquid (79 mg, 84% yield). ^{1}H-NMR ($CDCl_3$) δ 7.97 (2H, d, J =7.70 Hz), 7.59 (1H, t, J =7.38 Hz), 7.44 (2H, t, J =7.63 Hz), 7.30 (15H, m), 4.72 (1H, d, J =11.61 Hz), 4.61 (4H, m), 4.48 (3H, m), 4.36 (1H, m), 4.28 (2H, m), 4.20 (1H, m) ppm; ^{13}C-NMR ($CDCl_3$) δ 206.91, 166.18, 137.38, 137.23, 136.78, 133.15, 129.72, 128.57, 128.46, 128.43, 128.22, 127.96, 81.05, 77.89, 74.28, 73.29, 73.20, 72.64, 62.54 ppm; HR-ESI-MS: $[M+Na]^+$ calculated for $C_{33}H_{32}O_6Na$ was m/z 547.2097, found 547.2107.

1,3,4-tris(benzyloxy)-5-((*tert*-butyldimethylsilyl)oxy)pentan-2-ol (24): Ribonolactol **3** (2.2 g, 5.24 mmol, 1 equiv.) was dissolved in a mixture of DCM and methanol (4:1 v/v, 25 mL). Sodium borohydride (595 mg, 15.7 mmol, 3 equiv.) was then added, and the reaction mixture was stirred at 40 °C for 2 hours. The reaction was quenched with 1 M HCl (20 mL), and the product was extracted with DCM three times (50 mL each time). The combined organic layers were dried over anhydrous Na_2SO_4 and passed through a silica

plug to remove any unwanted polar impurities, affording the reduced products. The residue was then dissolved in a dry DCM solution (25 mL). *tert*-butydimethyllsilyl chloride (TBDMSCl) (1.18 g, 7.86 mmol, 1.5 equiv.) and imidazole (714 mg, 10.48 mmol, 2 equiv.) were added under an inert argon atmosphere. The reaction mixture was stirred for 1 hour. After stirring, the reaction was quenched with saturated ammonium chloride solution (50 mL), and the product was extracted with DCM three times (75 mL each time). The combined organic layers were dried over anhydrous Na_2SO_4 and purified by column chromatography using a mixture of hexane and EtOAc to afford the silylated products: compound **24** (1.9 g, 68% yield) and compound **24a** (196 mg, 7% yield); ^{1}H-NMR ($CDCl_3$) δ 7.23 (15H, m), 4.65 (2H, m), 4.53 (2H, m), 4.45 (2H, m), 3.95 (1H, m), 3.88 (1H, m), 3.72 (3H, m), 3.54 (2H, m), 2.90 (1H, d, J =3.83 Hz), 0.84 (9H, s), 0.00 (6H, s) ppm; HR-ESI-MS: $[M+Na]^+$ calculated for $C_{32}H_{44}O_5SiNa$ was m/z 559.2856, found 559.2848.

6,7,8-tris(benzyloxy)-2,2,3,3,11,11,12,12-octamethyl-4,10-dioxa-3,11-disilatridecane (24a): ^{1}H-NMR ($CDCl_3$) δ 7.27 (15H, m), 4.71 (2H, d, J =11.68 Hz), 4.65 (2H, s), 4.60 (2H, d, J =11.68 Hz), 3.88 (1H, m), 3.78 (5H, m), 0.87 (18H, s), 0.00 (12H, s) ppm; HR-ESI-MS: $[M+Na]^+$ calculated for $C_{38}H_{58}O_5Si_2Na$ was m/z 673.3720, found 673.3729.

1,3,4-tris(benzyloxy)-5-((*tert*-butyldimethylsilyl)oxy)pentan-2-yl benzoate (25): 2º alcohol **24** (1.4 g, 2.62 mmol, 2 equiv.) was dissolved in dry DCM (20 mL) under an inert argon atmosphere. Benzoic acid (480 mg, 3.93 mmol, 1.5 equiv.), 1-ethyl-3-(3-dimethylaminopropyl)carbodiimide hydrochloride (EDCI.HCl) (1.0 g, 5.24 mmol, 2 equiv.), and 4-dimethylaminopyridine (32 mg, 0.26 mmol, 0.1 equiv.) were then added to the reaction mixture. The mixture was stirred for 12 hours. The reaction was quenched with a saturated solution of $NaHCO_3$ (30 mL), and the product was extracted with DCM three times (30 mL each time). The combined organic extracts were dried over anhydrous Na_2SO_4 and concentrated under reduced pressure. Finally, purification by column chromatography using a mixture of hexane and EtOAc afforded compound **25** as a viscous liquid (1.54 g, 92% yield). ^{1}H-NMR ($CDCl_3$) δ 8.00 (2H, d, J =7.60 Hz), 7.54 (1H, t, J =7.38 Hz), 7.41 (2H, t, J =7.65 Hz), 7.28 (15H, m), 5.68 (1H, m), 4.73 (2H, m), 4.63 (2H, m), 4.51 (1H, d, J =12.16 Hz), 4.42 (1H, d, J =12.16 Hz), 4.03 (1H, t, J =4.98 Hz), 3.91 (1H, dd, J =3.34, 10.92 Hz), 3.82 (3H, m, J =5.93 Hz), 3.71 (1H, m), 0.85 (9H, s), 0.00 (6H, s) ppm; ^{13}C-NMR ($CDCl_3$) δ 165.64, 138.54, 138.30, 138.28, 132.94, 130.41, 129.78, 128.38, 128.33, 128.30, 127.98, 127.85, 127.70, 127.61, 127.49, 79.66, 78.21, 73.89, 73.21, 72.98, 72.51,

68.69, 62.79, 25.97, 18.33, -5.36 ppm; HR-ESI-MS: $[M+Na]^+$ calculated for $C_{39}H_{48}O_6SiNa$ was m/z 663.3118, found 663.3131.

1,3,4-tris(benzyloxy)-5-hydroxypentan-2-yl benzoate (26): Compound **25** (942 mg, 1.47 mmol, 1 equiv.) was desilylated by dissolving it in a solution of 2% hydrochloric acid in ethanol (EtOH) (20 mL) and stirring the mixture for 10 minutes. The reaction was quenched with a saturated $NaHCO_3$ solution (25 mL), and the product was extracted with DCM (50 mL x 2). The organic layer was then washed with distilled water (50 mL x 3) to remove any water-soluble impurities, followed by washing with brine (50 mL) to remove any remaining inorganic salts. Finally, the organic layer was concentrated under reduced pressure after drying over anhydrous Na_2SO_4. Purification of the residue by silica gel column chromatography using an EtOAc/Hexane afforded compound **26** as a colorless viscous liquid (728 mg, 94% yield). ^{1}H-NMR ($CDCl_3$): δ 7.95 (2H, d, J =7.78 Hz), 7.50 (1H, t, J =7.36 Hz), 7.37 (2H, t, J =7.57 Hz), 7.21 (15H, m), 5.61 (1H, m), 4.68 (1H, m), 4.58 (1H, m), 4.54 (2H, m), 4.46 (1H, m), 4.40 (1H, m), 4.01 (1H, m), 3.91 (1H, m), 3.74 (3H, m), 3.64 (1H, m) ppm; ^{13}C-NMR ($CDCl_3$): δ 165.87, 138.02, 137.78, 133.15, 130.08, 129.77, 129.68, 128.55, 128.50, 128.49, 128.46, 128.40, 128.37, 128.09, 128.00, 127.92, 127.69, 78.66, 78.51, 74.14, 73.16, 72.29, 72.16, 72.02, 68.39, 64.26, 61.20, 60.96, 29.72 ppm; HR-ESI-MS: $[M+Na]^+$ calculated for $C_{33}H_{34}O_6Na$ was m/z 549.2253, found 549.2266.

2,3,5-tris(benzyloxy)-4-hydroxypentyl benzoate (26a): A solution of compound **25** (188 mg, 0.3 mmol) in THF (5 mL) was stirred with a solution of tetrabutylammonium fluoride in THF (895 µL, 0.9 mmol, 3 equiv.) at room temperature for 4 hours. The reaction mixture was then quenched with 10 mL of saturated NH_4Cl solution and extracted with DCM (20 mL x 3). The combined organic extracts were dried over anhydrous Na_2SO_4 and concentrated under reduced pressure. Purification by column chromatography using a mixture of hexane and EtOAc afforded compound **26a** (148 mg, 94% yield) as a colorless viscous liquid. ^{1}H-NMR ($CDCl_3$) δ 7.94 (2H, d, J =7.82 Hz), 7.49 (1H, t, J =7.35 Hz), 7.36 (2H, t, J =7.63 Hz), 7.22 (15H, m), 4.68 (3H, d, J =11.51 Hz), 4.56 (2H, t, J =10.65 Hz), 4.43 (3H, m), 4.00 (2H, m), 3.75 (1H, m), 3.55 (2H, m), 2.64 (1H, m) ppm; ^{13}C-NMR ($CDCl_3$) δ 166.57, 137.95, 133.02, 130.12, 129.70, 128.47, 128.40, 128.12, 127.98, 127.90, 127.83, 127.80, 127.76, 78.84, 77.88, 73.93, 73.44, 72.40, 71.00, 70.69, 64.12 ppm; HR-ESI-MS: $[M+Na]^+$ calculated for $C_{33}H_{34}O_6Na$ was m/z 549.2253, found 549.2266.

2,3,5-tris(benzyloxy)-1-(5-((benzyloxy)methyl)-4-methoxy-5H-pyrrolo[3,2-d] pyrimidin-7-yl)pentane-1,4-diol (27): Thoroughly dried compound **20** (1.32 g, 3.8 mmol, 1 equiv.) was taken in a 100 mL round-bottomed flask and dissolved in dry MTBE: Anisole (4:1, 25 mL) under argon atmosphere. The solution was cooled to -78 °C, and 2 M *n*BuLi solution in cyclohexane (2.85 mL, 5.7 mmol, 1.5 equiv.) was transferred using a syringe. After 5 min, aldehyde **23** (2 g, 3.8 mmol, 1 equiv.) in 5 mL of MTBE: Anisole (4:1) was transferred *via* cannula and the stirring was continued at -78 °C. After 3 hours, the reaction mixture was quenched with 15 mL of saturated NH_4Cl solution and was allowed to warm to room temperature. The reaction mixture was partitioned between EtOAc (200 mL) and distilled water (200 mL). The aqueous layer was extracted with EtOAc (100 mL x 2) and the combined organic layers were dried over anhydrous Na_2SO_4, and concentrated under reduced pressure. The resulting crude syrup was dissolved in MeOH (30 mL), added 25% NaOMe in MeOH(w/v)(1.6 mL, 7.6 mmol, 2 equiv.) and stirred for 30 mins. after that the reaction mixture was diluted with cold water (50 mL) and extracted in EtOAc (100 mL x 2). Organic layers were dried over anhydrous Na_2SO_4, and concentrated under reduced pressure. Silica gel column purification using EtOAc/hexane of the crude afforded compound **27** (646 mg) as a colorless viscous liquid in 60% yield (Yield calculated on the basis of isolated compound **27** and recovered debrominated **19** (600 mg)). ^{1}H-NMR ($CDCl_3$) δ 8.38 (1H, s), 7.21 (10H, m), 7.13 (10H, m), 7.00 (2H, m), 5.55 (2H, m), 5.28 (1H, d, J =6.05 Hz), 4.63 (1H, d, J =11.71 Hz), 4.53 (1H, d, J =11.71 Hz), 4.47 (2H, d, J =11.96 Hz), 4.42 (2H, m), 4.33 (2H, s), 4.26 (2H, m), 4.20 (1H, m), 4.04 (3H, s), 3.76 (1H, dd, J =1.53, 7.73 Hz), 3.65 (1H, dd, J =2.45, 9.70 Hz), 3.57 (1H, dd, J =5.55, 9.65 Hz) ppm; ^{13}C-NMR ($CDCl_3$): δ 156.27, 149.65, 148.92, 138.25, 138.20, 138.07, 136.79, 131.24, 128.50, 128.36, 128.18, 128.15, 128.01, 127.89, 127.78, 127.73, 127.62, 127.51, 127.46, 117.54, 115.96, 81.72, 78.98, 76.85, 73.36, 73.08, 72.67, 71.51, 70.06, 69.84, 67.96, 53.62 ppm; HR-ESI-MS: $[M+Na]^+$ calculated for $C_{41}H_{43}N_3O_7Na$ was m/z 712.2993, found 712.3054.

2,3,5-tris(benzyloxy)-1-(5-((benzyloxy)methyl)-4-methoxy-5H-pyrrolo[3,2-d] pyrimidin-7-yl)pentane-1,4-dione (29): A solution of compound **27** (500 mg, 0.72 mmol, 1 equiv.) was dissolved in DCM (30 mL). Dess-Martin periodinane (768 mg, 1.81 mmol, 2.5 equiv.) was added and the reaction mixture was stirred at room temperature for 2 hours. After monitoring by TLC to confirm completion, the reaction was quenched with a saturated solution of $Na_2S_2O_3$ (30 mL). The product was then extracted with DCM (75 mL

x 2). The combined organic extracts were dried over anhydrous Na_2SO_4 and concentrated under reduced pressure. And purification by column chromatography using a mixture of hexane and EtOAc afforded compound **29** as a viscous liquid (462 mg, 93% yield). ^{1}H-NMR ($CDCl_3$): δ 8.53 (1H, s), 8.10 (1H, s), 7.20 (20H, m), 5.63 (1H, d, J =10.45 Hz), 5.53 (2H, q, J =8.32 Hz), 4.71 (1H, d, J =11.71 Hz), 4.61 (2H, q, J =10.04 Hz), 4.54 (1H, m), 4.51 (1H, m), 4.47 (1H, m), 4.42 (1H, s), 4.40 (3H, s), 4.36 (1H, m), 4.06 (3H, s) ppm; ^{13}C-NMR ($CDCl_3$): δ 206.05, 190.96, 156.72, 152.02, 148.69, 138.04, 137.70, 137.58, 137.46, 136.21, 128.56, 128.36, 128.32, 128.30, 128.21, 127.97, 127.83, 127.77, 127.75, 127.66, 116.64, 83.59, 83.55, 77.76, 74.26, 73.09, 72.78, 72.57, 70.75, 53.91 ppm; HR-ESI-MS: $[M+H]^+$ calculated for $C_{41}H_{40}N_3O_7$ was m/z 686.2861, found 686.2861.

5-((benzyloxy)methyl)-7-((2S,3S,4R,5R)-3,4-bis(benzyloxy)-5-((benzyloxy)methyl) pyrrolidin-2-yl)-4-methoxy-5H-pyrrolo[3,2-d]pyrimidine (30): To a solution of diketone **29** (81 mg, 0.12 mmol, 1 equiv.) in MeOH (6 mL) was added ammonium formate (37 mg, 0.9 mmol, 5 equiv.) and $NaCNBH_3$ (37 mg, 0.59 mmol, 5 equiv.), and then the reaction mixture was stirred overnight at room temperature under argon atmosphere. The reaction mixture was quenched with sat. aq. $NaHCO_3$ (20 mL), extracted with EtOAc (2×50 mL), dried over anhydrous Na_2SO_4 and concentrated. Purification preparative TLC method afforded compound **30** (trace). ^{1}H-NMR ($CDCl_3$): δ 8.40 (1H, s), 7.19 (20H, m), 5.51 (2H, m), 4.59 (2H, m), 4.53 (2H, m), 4.47 (2H, m), 4.43 (1H, d, J =11.92 Hz), 4.32 (2H, s), 4.14 (1H, t, J =5.61 Hz), 4.03 (3H, s), 3.96 (1H, t, J =5.23 Hz), 3.65 (1H, q, J =5.47 Hz), 3.58 (2H, m) ppm; HR-ESI-MS: $[M+H]^+$ calculated for $C_{41}H_{43}N_4O_5$ was m/z 671.3228, found 671.3250.

5-((benzyloxy)methyl)-7-((2R,3S,4R,5S)-3,4-bis(benzyloxy)-5-((benzyloxy)methyl)-1-(4-methylbenzyl)pyrrolidin-2-yl)-4-methoxy-5H-pyrrolo[3,2-d]pyrimidine (31): Diketone **29** (123 mg, 0.18 mmol, 1.0 equiv.) was dissolved in MeOH (3 mL). *p*-Methylbenzylamine (94 µL, 0.72 mmol, 4 equiv.), $NaBH_3CN$ (34 mg, 0.54 mmol, 3 equiv.), and $ZnCl_2$ (25 mg, 0.18 mmol, 1 equiv.) in MeOH (1.0 mL) were then successively added, and the mixture was stirred for 8 hours at 65 °C under condenser. After completion of the reaction as indicated by TLC, it was cooled to room temperature. The reaction mixture was then quenched with an aqueous $KHSO_4$ (10 mL) solution and extracted with EtOAc. The organic layer was dried over anhydrous Na_2SO_4, concentrated under reduced pressure, and purified by column chromatography using a mixture of hexane and EtOAc to afford

compound **31** as a sticky solid (91 mg, 65% yield). ^{1}H-NMR ($CDCl_3$) δ 8.42 (1H, s), 7.53 (1H, s), 7.21 (13H, m), 7.07 (3H, m), 7.00 (4H, m), 6.88 (4H, m), 5.49 (2H, s), 4.55 (3H, m), 4.37 (3H, m), 4.21 (2H, s), 4.09 (1H, d, J =11.96 Hz), 4.03 (5H, m), 3.92 (1H, dd, J=6.65, 9.20 Hz), 3.82 (1H, d, J =13.96 Hz), 3.67 (1H, t, J =10.96 Hz), 3.50 (1H, dd, J =5.10, 9.30 Hz), 3.33 (1H, dd, J =6.20, 11.81 Hz), 2.17 (1H, s) ppm; ^{13}C-NMR ($CDCl_3$): δ 156.03, 150.31, 149.66, 138.96, 138.84, 138.69, 137.03, 136.24, 134.87, 129.62, 128.61, 128.41, 128.23, 127.88, 127.85, 127.77, 127.57, 127.50, 127.36, 127.28, 127.16, 127.00, 115.53, 79.83, 79.66, 73.13, 72.92, 72.71, 72.01, 69.73, 61.89, 58.55, 56.97, 53.47, 21.06 ppm; HR-ESI-MS: $[M+H]^+$ calculated for $C_{49}H_{51}N_4O_5$ was m/z 775.3854, found 775.3874.

5-((benzyloxy)methyl)-7-(3,4-bis(benzyloxy)-5-((benzyloxy)methyl)-1-(4-methyl benzyl)-1H-pyrrol-2-yl)-4-methoxy-5H-pyrrolo[3,2-d]pyrimidine (32): Diketone **29** (84 mg, 0.12 mmol, 1.0 equiv.) was dissolved in DCE (3 mL). *p*-Methylbenzylamine (16 µL, 0.12 mmol, 1 equiv.), $Na(OAc)_3BH$ (37 mg, 0.30 mmol, 2.5 equiv.), and CH_3COOH (14 µL, 0.25 mmol, 2 equiv.) were then successively added, and the mixture was stirred for 24 hours. After completion of the starting material as indicated by TLC, it was cooled to room temperature. The reaction mixture was then quenched with a saturated solution of $NaHCO_3$ (10 mL) and extracted with EtOAc. The organic layer was dried over anhydrous Na_2SO_4, concentrated under reduced pressure, and purified by column chromatography using a mixture of hexane and EtOAc to afford compound **32** as a sticky solid (25 mg, 27% yield). ^{1}H-NMR ($CDCl_3$): δ 8.51 (1H, s), 7.33 (2H, d, J =7.38 Hz), 7.22 (9H, m), 7.13 (4H, m), 7.10 (3H, m), 7.02 (2H, m), 6.81 (2H, d, J =7.72 Hz), 6.77 (1H, s), 6.48 (2H, d, J =7.67 Hz), 5.46 (2H, s), 5.10 (2H, s), 5.04 (2H, s), 4.90 (2H, s), 4.33 (2H, s), 4.25 (2H, s), 4.09 (2H, s), 4.03 (3H, s), 2.09 (3H, s) ppm; ^{13}C-NMR ($CDCl_3$): δ 178.42, 156.69, 150.87, 148.97, 145.81, 138.73, 137.05, 136.41, 133.97, 128.51, 128.42, 128.27, 128.09, 127.94, 127.82, 127.55, 126.92, 126.25, 115.70, 105.67, 76.95, 73.44, 69.97, 53.83, 49.53, 29.72 ppm; HR-ESI-MS: $[M+Na]^+$ calculated for $C_{49}H_{46}N_4O_5Na$ was m/z 793.3366, found 793.3389.

5-((benzyloxy)methyl)-7-((3S,4R)-3,4-bis(benzyloxy)-5-((benzyloxy)methyl) tetrahydrofuran-2-yl)-4-methoxy-5H-pyrrolo[3,2-d]pyrimidine (33): Diketone **29** (100 mg, 0.15 mmol, 1.0 equiv.) was dissolved in CH_3COOH (3 mL). $NaBH_3CN$ (28 mg, 0.44 mmol, 3 equiv.), and $ZnCl_2$ (30 mg, 0.218 mmol, 1.5 equiv.) in MeOH (1.0 mL) were then successively added, and the mixture was refluxed for 12 hours at 80 °C. After completion

of the reaction as indicated by TLC, it was cooled to room temperature and diluted with EtOAc (25 mL). The reaction mixture was then quenched with saturated solution of $NaHCO_3$ (30 mL) solution and extracted with EtOAc. The organic layer was dried over anhydrous Na_2SO_4, concentrated under reduced pressure, and purified by column chromatography using a mixture of hexane and EtOAc to afford compound **33** as a sticky solid (17 mg, 18% yield). ^{1}H-NMR ($CDCl_3$): δ 8.46 (1H, s), 7.35 (1H, s), 7.19 (20H, m), 5.44 (2H, m), 5.30 (1H, d, J =10.56 Hz), 4.72 (2H, s), 4.48 (3H, m), 4.29 (5H, m), 4.10 (1H, t, J =5.73 Hz), 4.02 (3H, s), 3.81 (1H, dd, J =2.24, 10.46 Hz), 3.64 (1H, m) ppm; HR-ESI-MS: $[M+H]^+$ calculated for $C_{41}H_{42}N_3O_6$ was m/z 672.3068, found 672.3073.

(2S,3R,4S,5R)-2-(acetoxymethyl)-1-(4-methylbenzyl)-5-(4-oxo-4,5-dihydro-3H-pyrrolo[3,2-d]pyrimidin-7-yl)pyrrolidine-3,4-diyl diacetate (35): To a solution of compound **31** (52 mg, 0.067 mmol) in MeOH (0.5 mL), and added concentrated hydrochloric acid (3 mL). The resulting mixture was heated to boil, and after 72 hours, the solvent was removed under reduced pressure to afford a brownish-red solid, which was dissolved in MeOH (0.5 mL) and diluted with DCM until a white precipitate was obtained. It was dissolved in pyridine (1 mL), and then acetic anhydride (0.5 mL) was added at room temperature and stirred. After 6 h, the reaction mixture was neutralized with excess saturated $NaHCO_3$(aq) solution and extracted with EtOAc (20 mL x 2). The organic layer was washed with distilled water and dried with anhydrous Na_2SO_4. The resulting mixture was concentrated, and the residue was purified using hexane: EtOAc by silica gel column chromatography to obtain the triacetylated product **35** (21 mg, 63% yield). ^{1}H-NMR ($CDCl_3$): δ 10.58 (1H, s), 10.47 (1H, s), 7.84 (1H, s), 7.48 (1H, s), 6.99 (4H, s), 5.42 (1H, s), 5.32 (1H, s), 4.61 (1H, s), 4.07 (2H, m), 3.79 (1H, d, J=14.12 Hz), 3.60 (1H, d, J =14.15 Hz), 3.47 (1H, m), 2.22 (3H, s), 1.95 (3H, s), 1.91 (3H, s), 1.89 (3H, s) ppm; ^{13}C-NMR ($CDCl_3$): δ 169.75, 140.40, 129.49, 128.99, 128.53, 72.99, 71.28, 64.40, 59.04, 58.01, 55.85, 21.05, 20.79, 20.56 ppm; HR-ESI-MS: $[M+H]^+$ calculated for $C_{25}H_{29}N_4O_7$ was m/z 497.2031, found 497.2052.

Figure 2.5.2.1: NMR spectra of α,β mixture of compound **3**

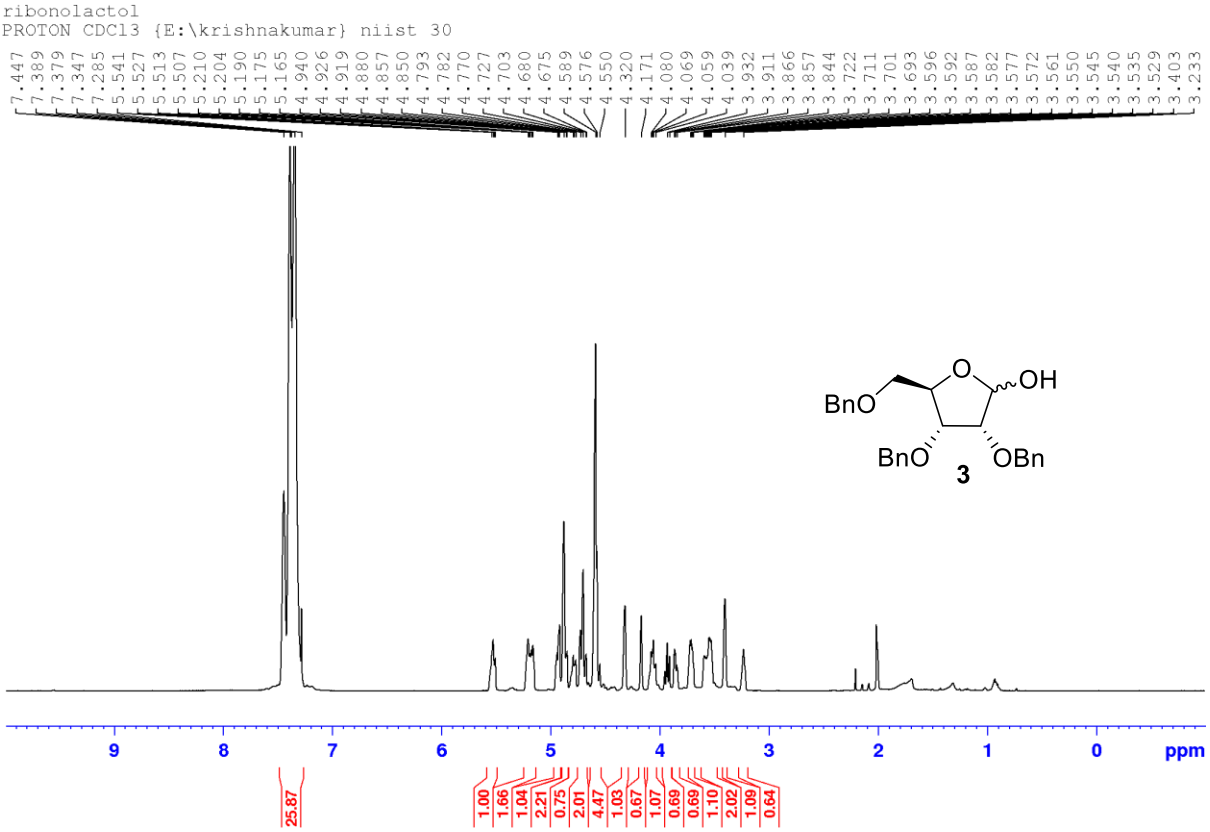

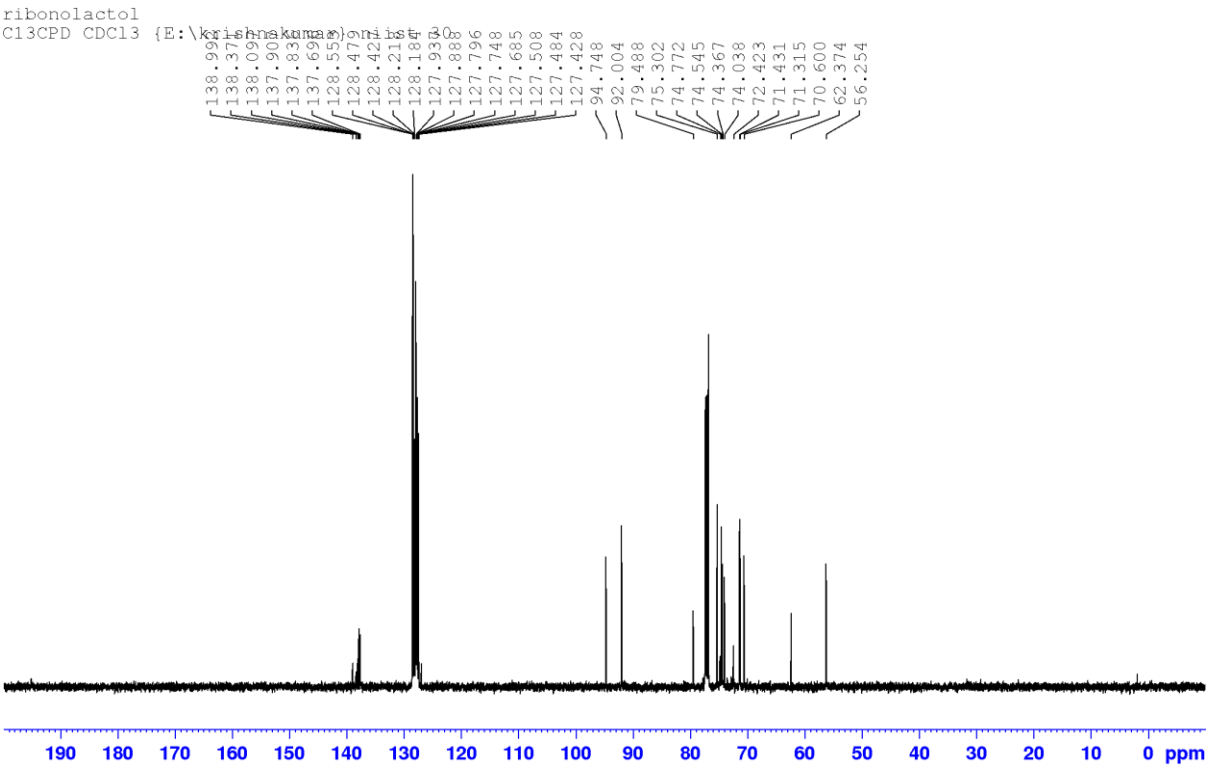

Figure 2.5.2.2: NMR spectra of compound **4**

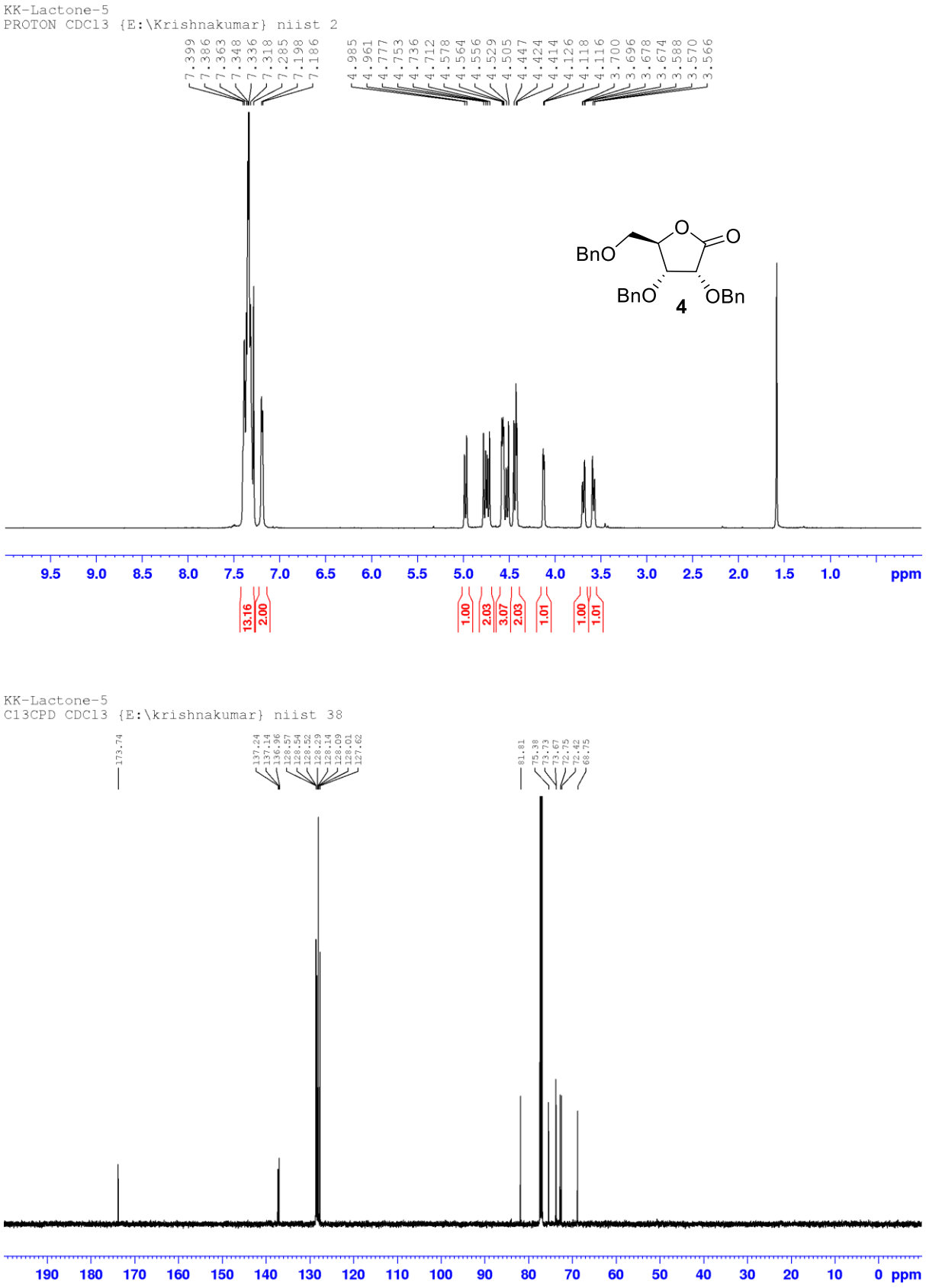

Figure 2.5.2.3: NMR spectra of compound **5**

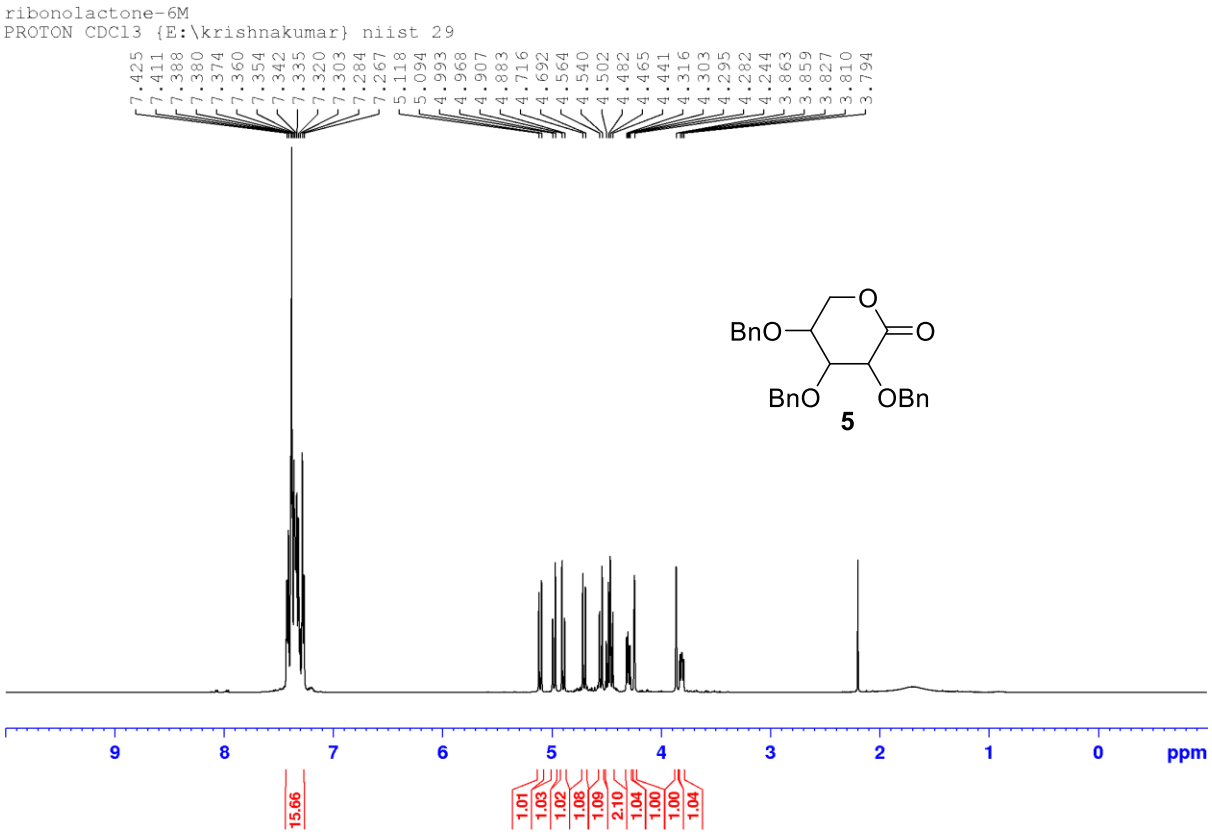

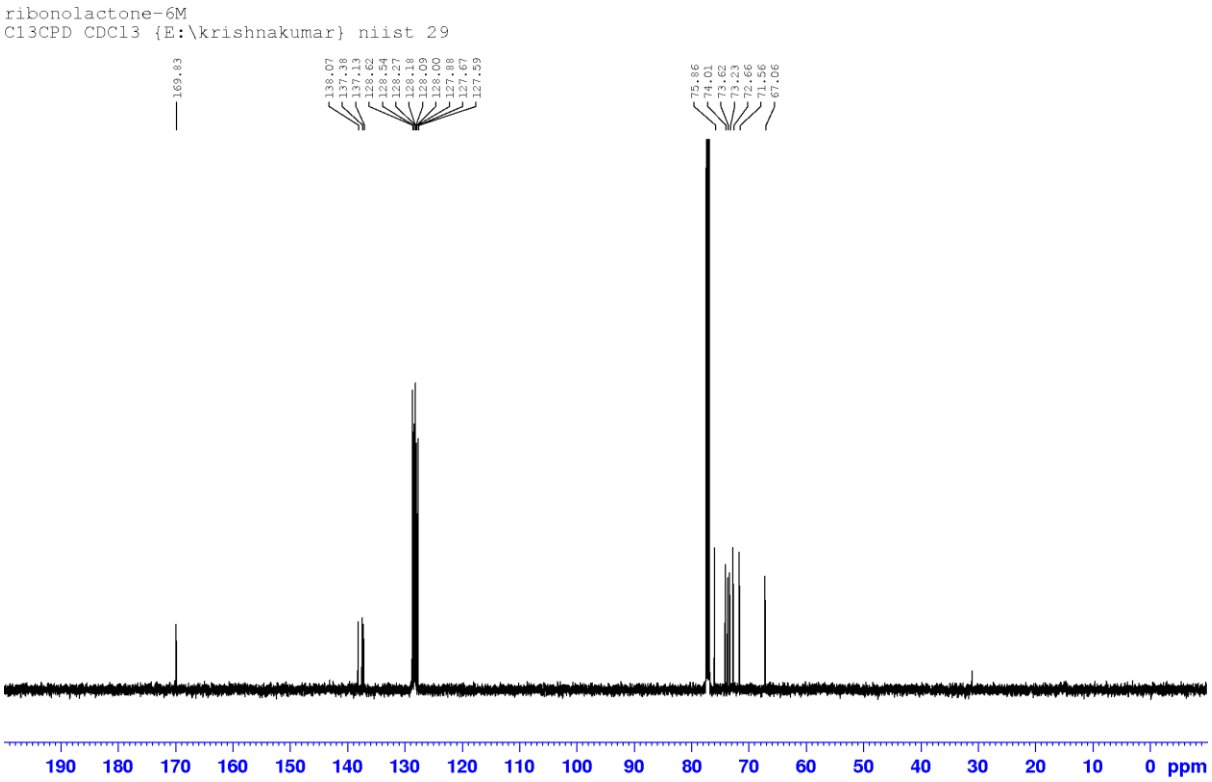

Figure 2.5.2.4: NMR spectra of compound **7**

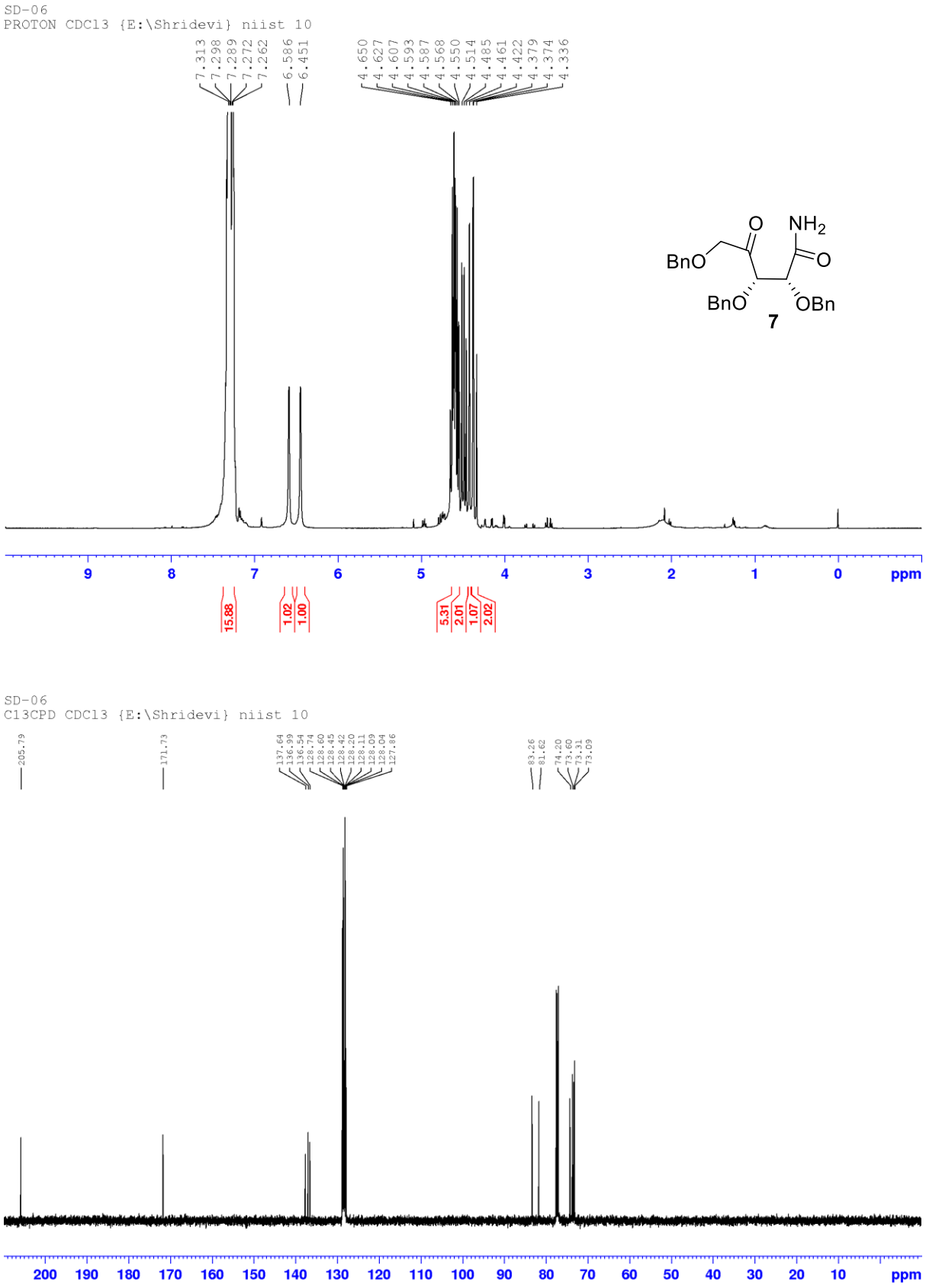

Figure 2.5.2.5: NMR spectra of compound **9**

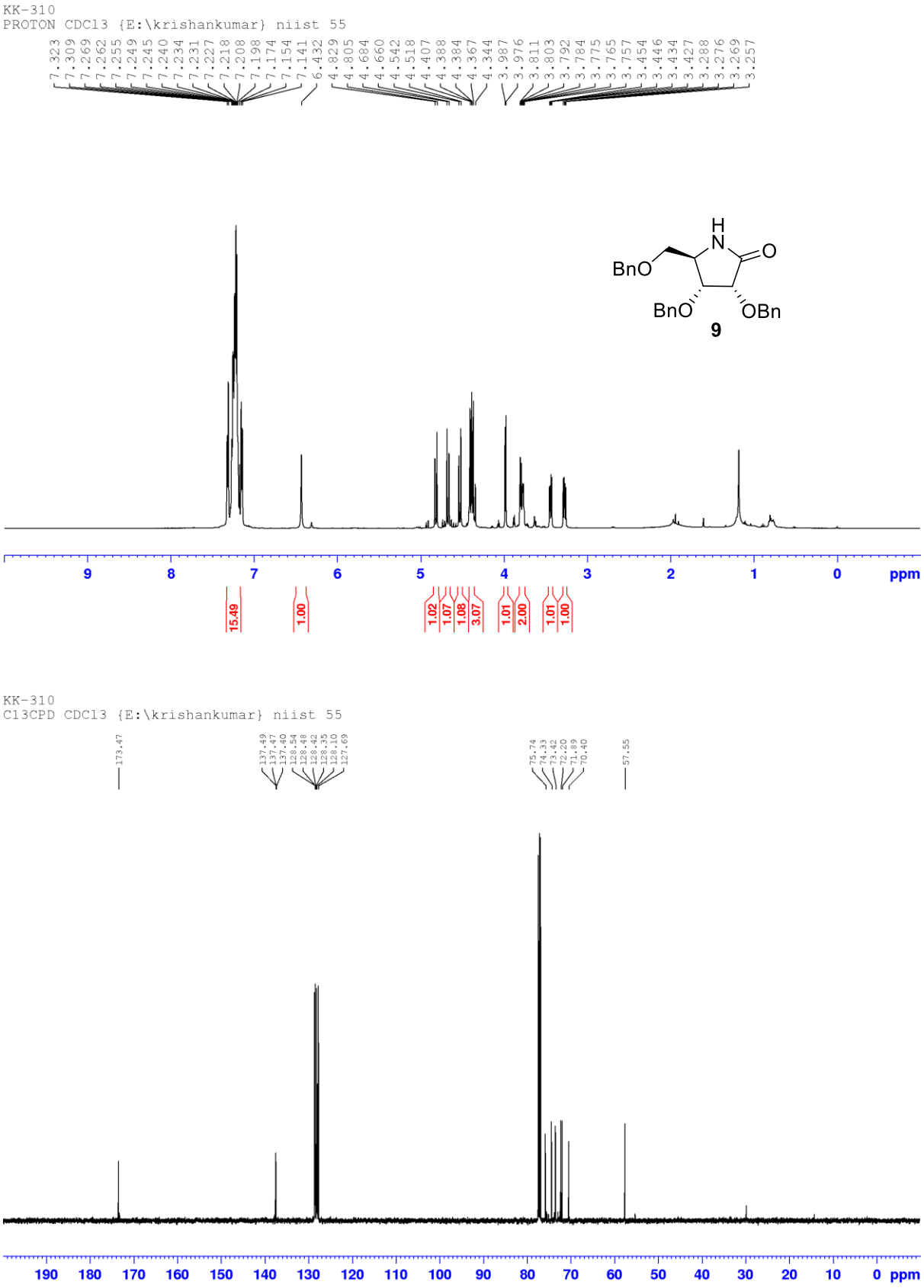

Figure 2.5.2.6: NMR spectra of compound **13**

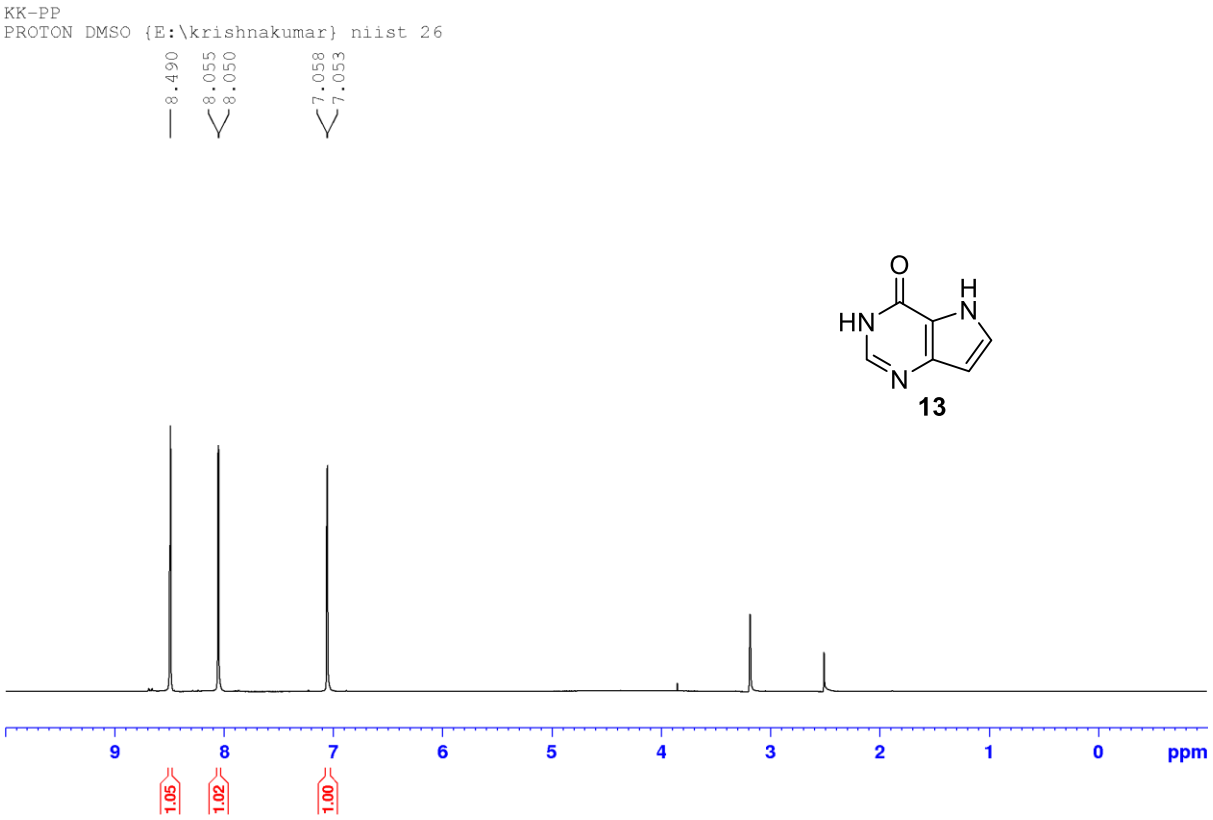

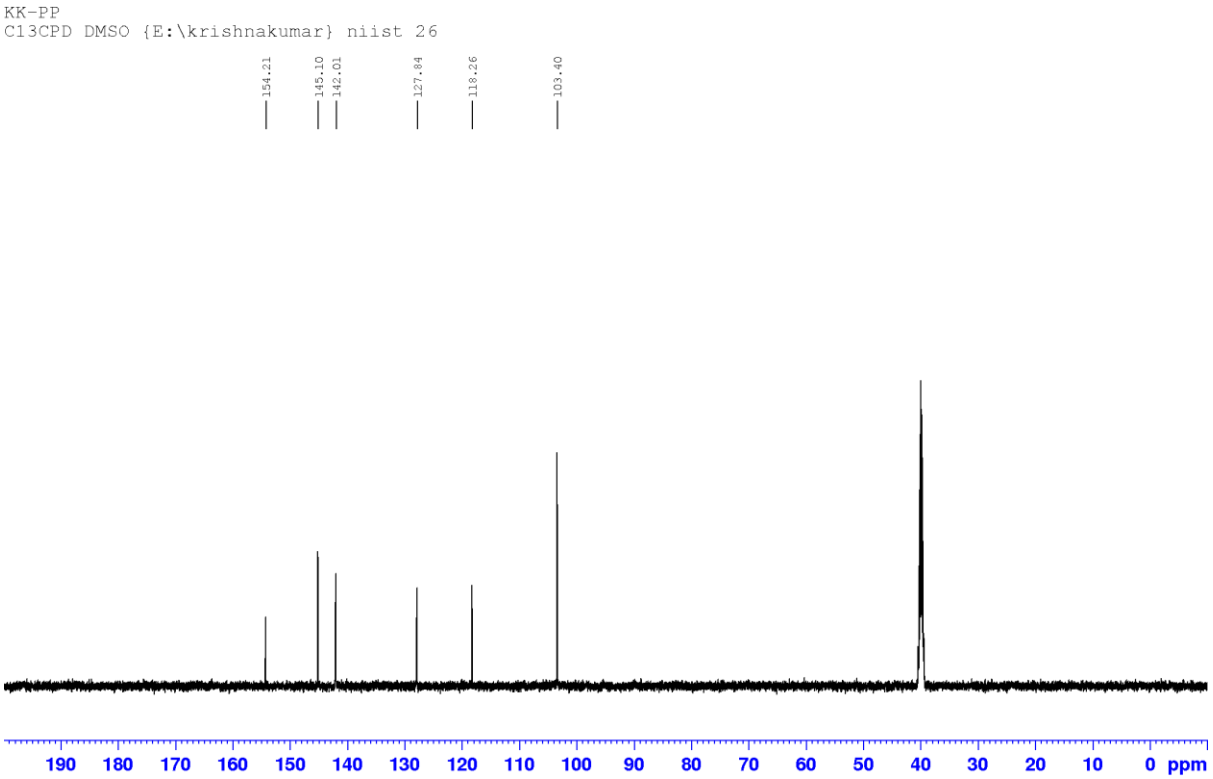

Figure 2.5.2.7: NMR spectra of compound **17**

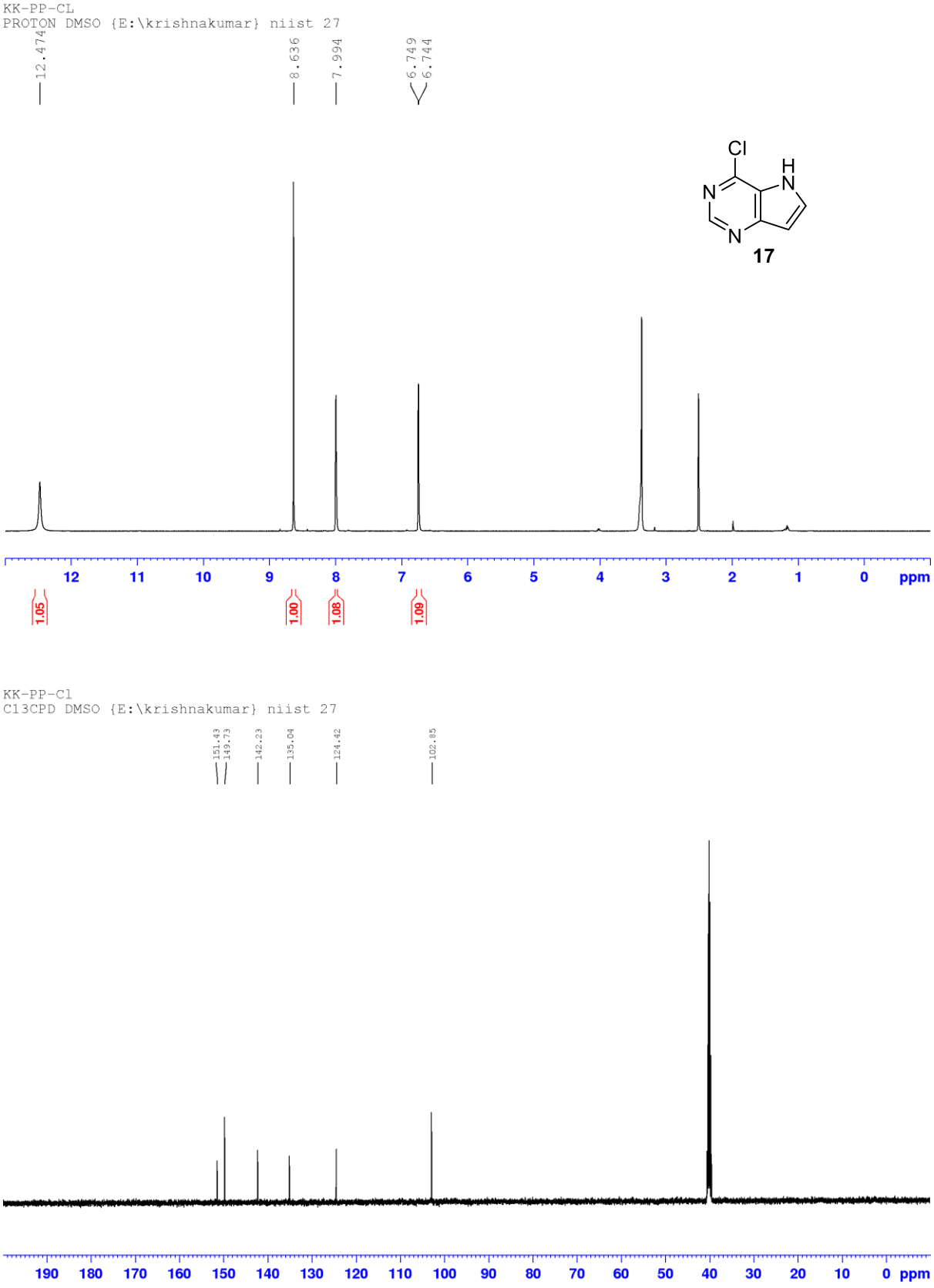

Figure 2.5.2.8: NMR spectra of compound **18**

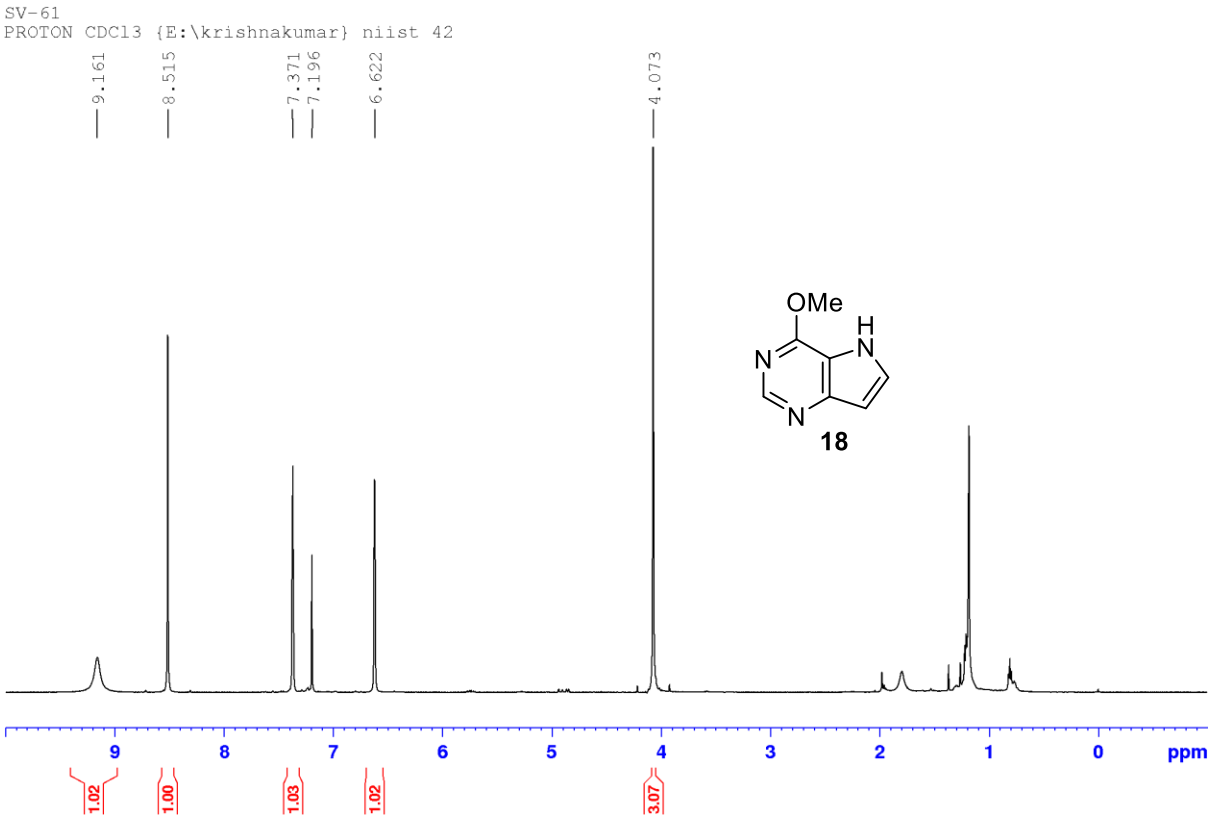

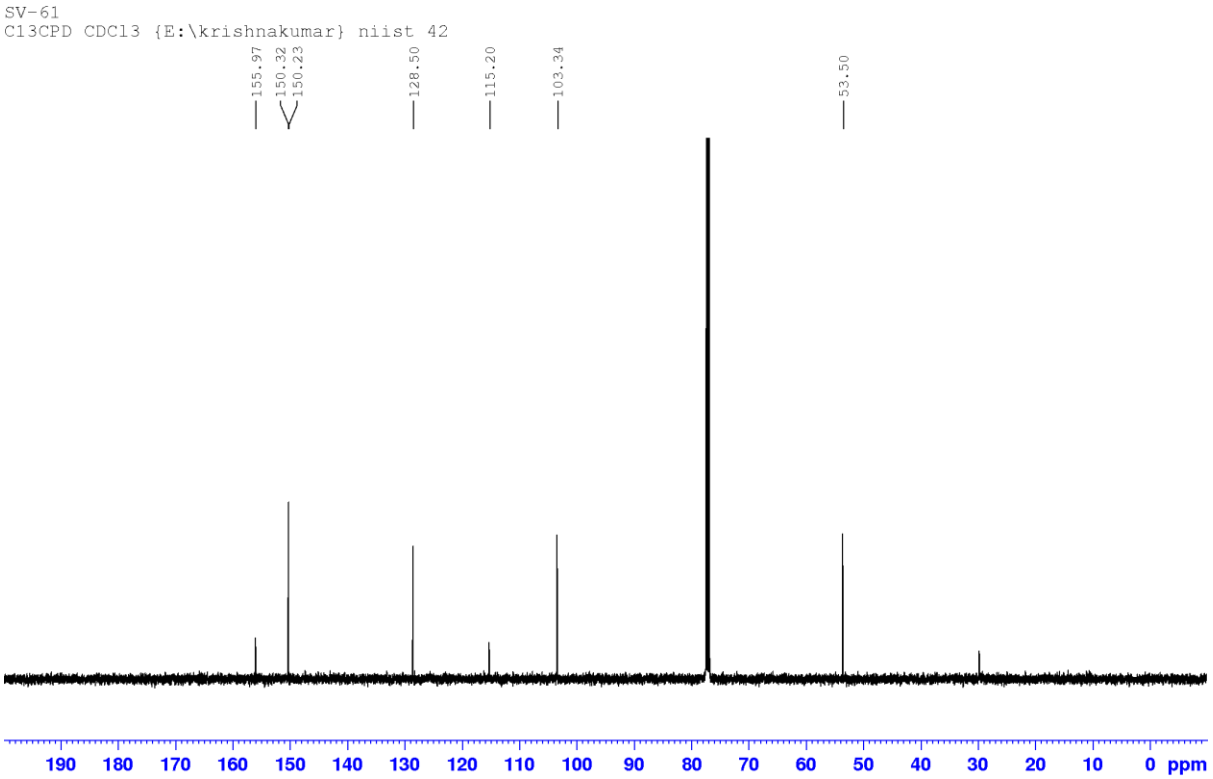

Figure 2.5.2.9: NMR spectra of compound **19**

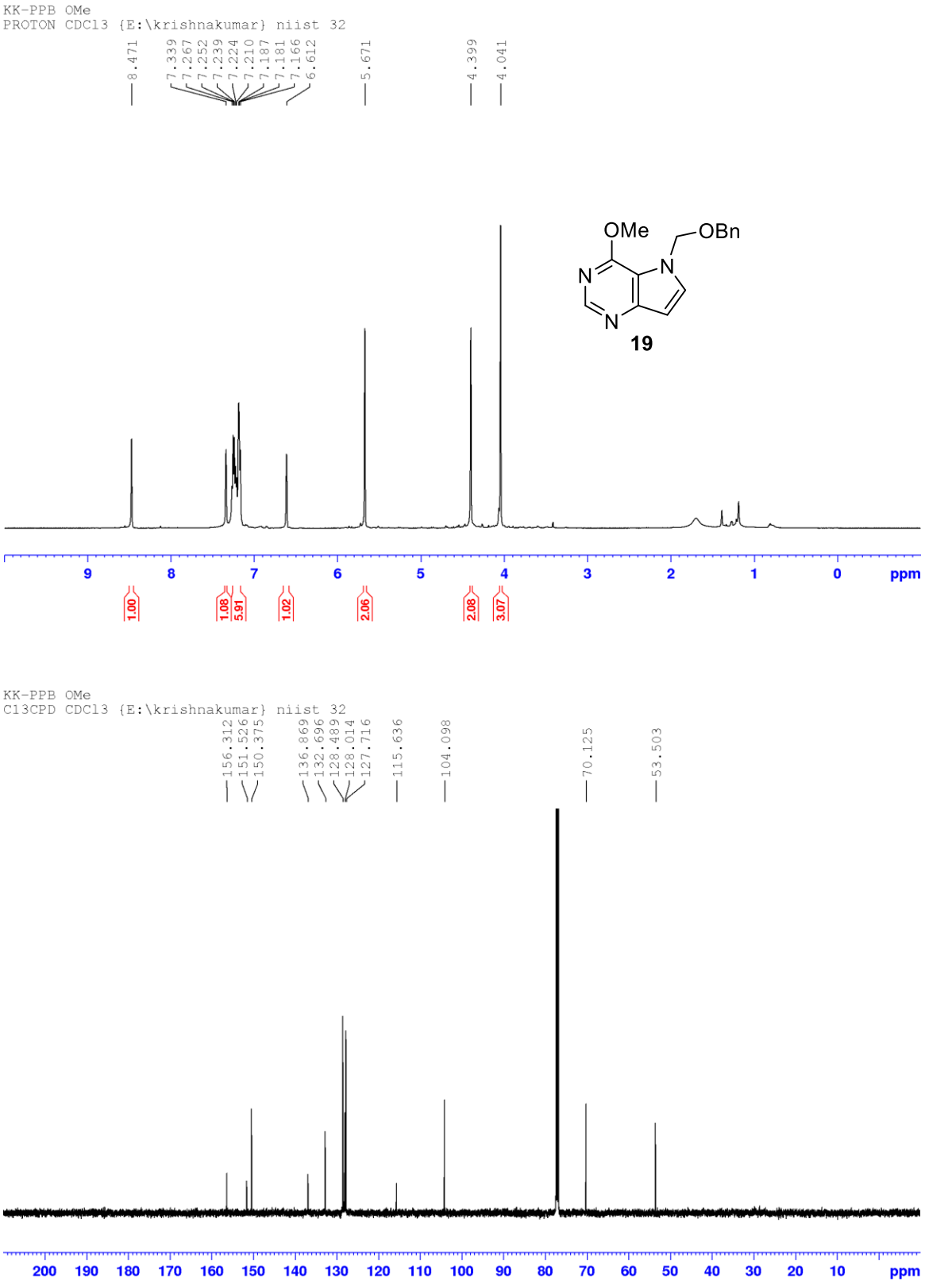

Figure 2.5.2.10: NMR spectra of compound **20**

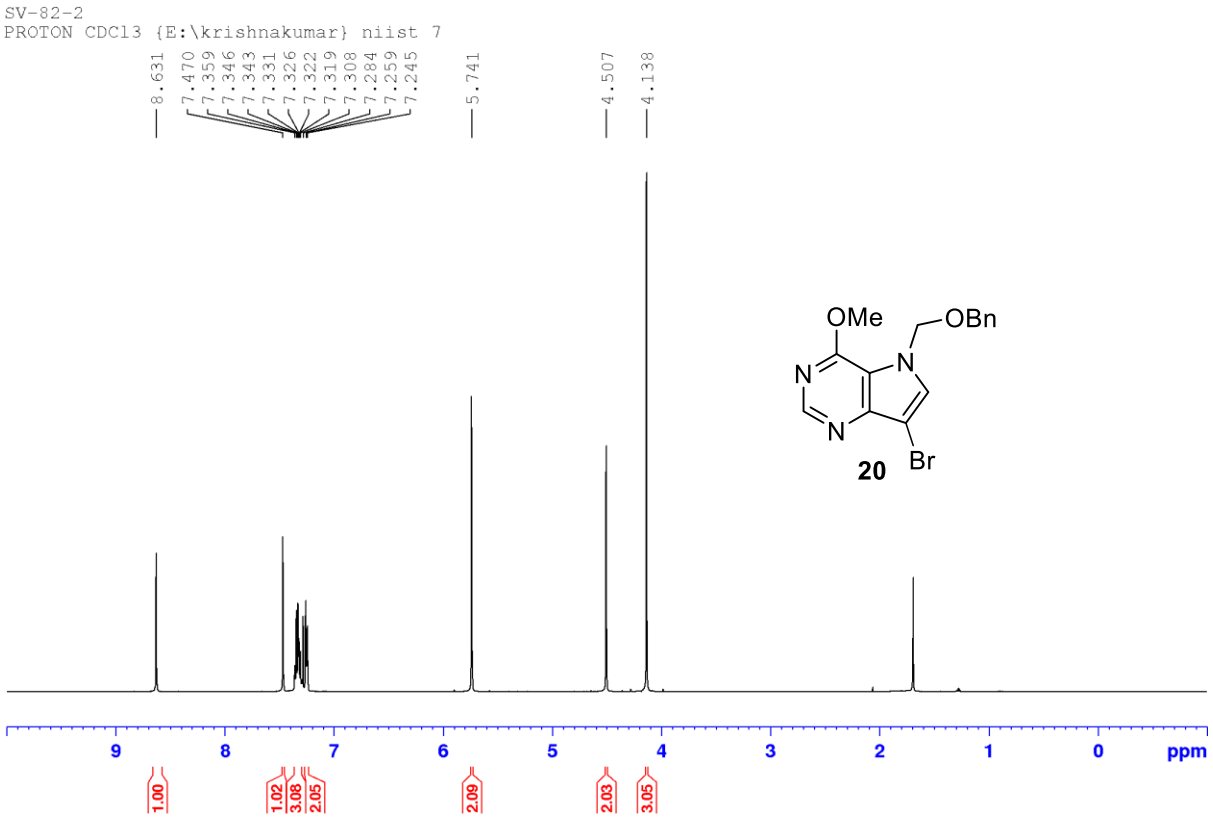

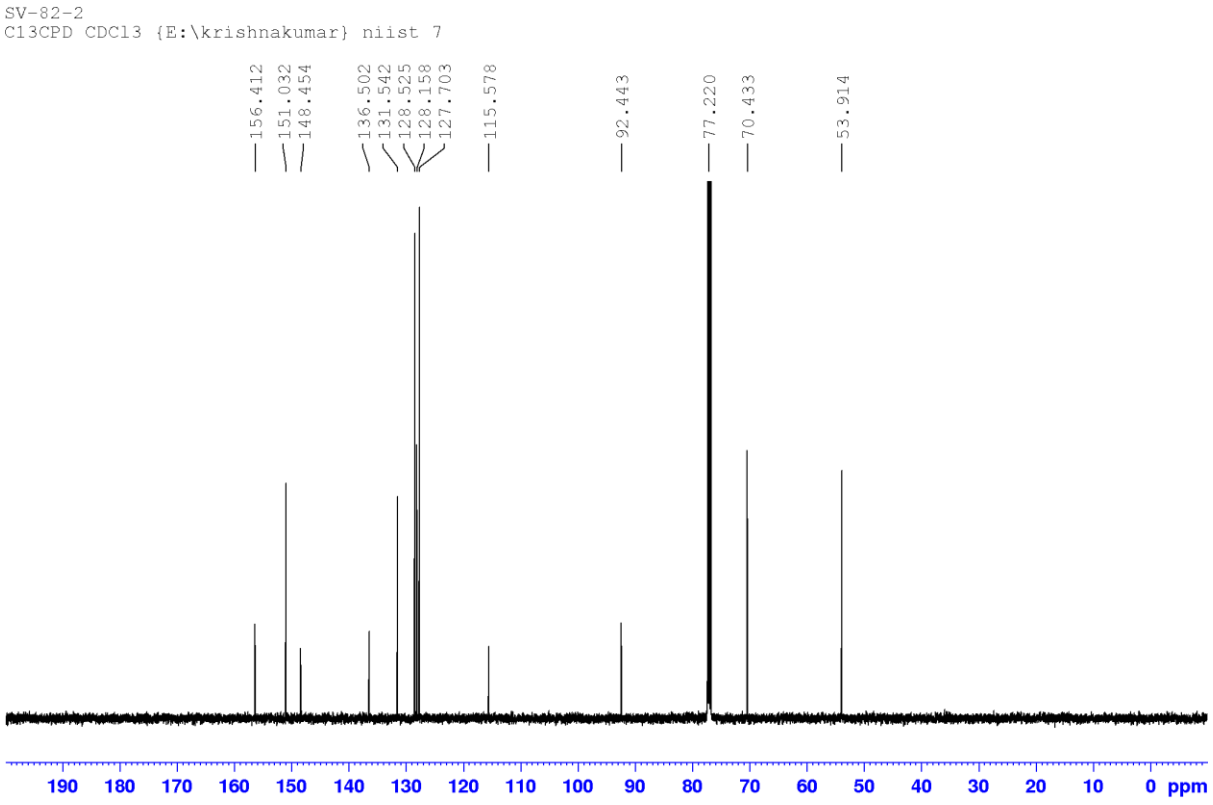

Figure 2.5.2.11: NMR spectra of compound **22**

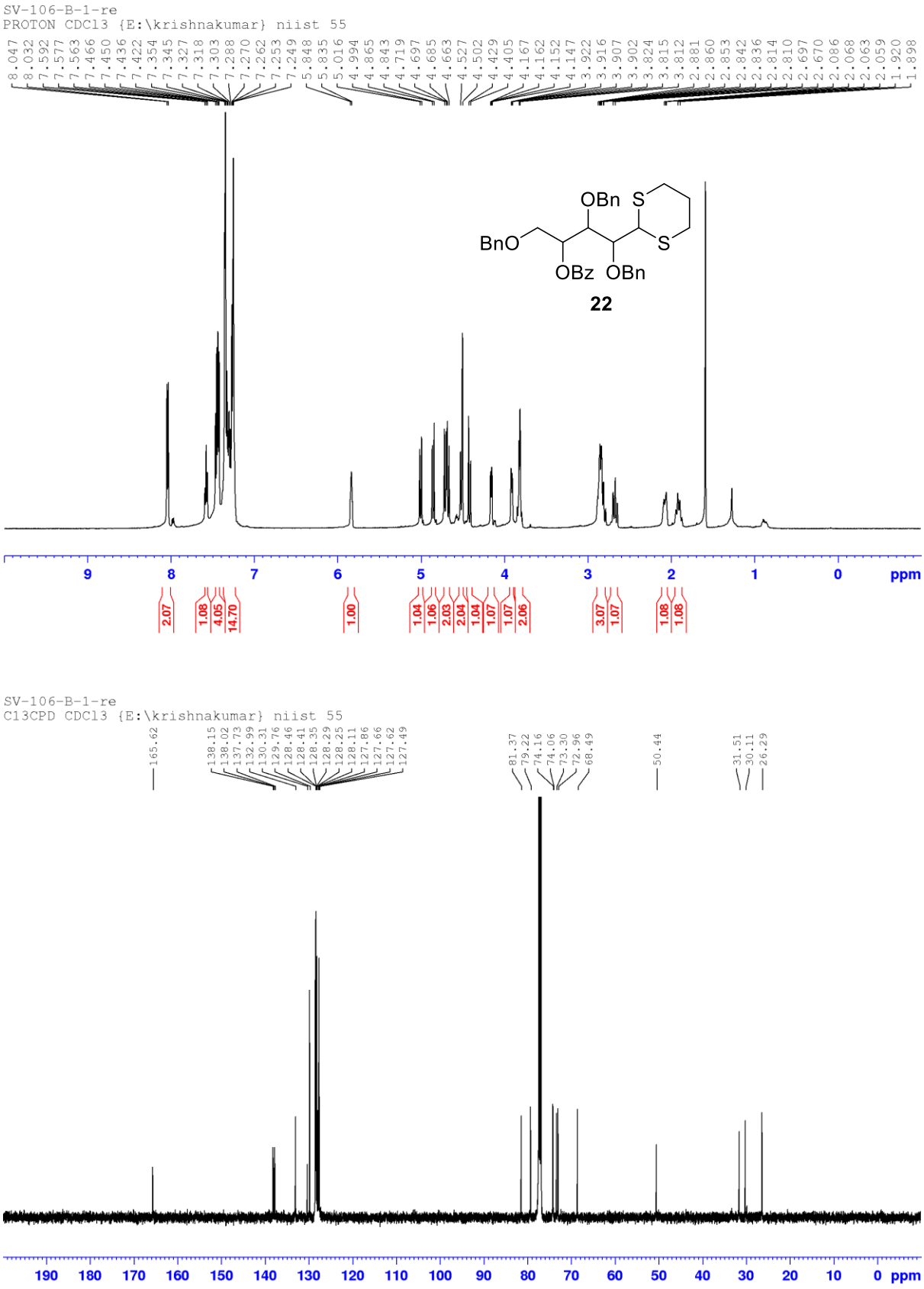

Figure 2.5.2.12: NMR spectra of compound **22a**

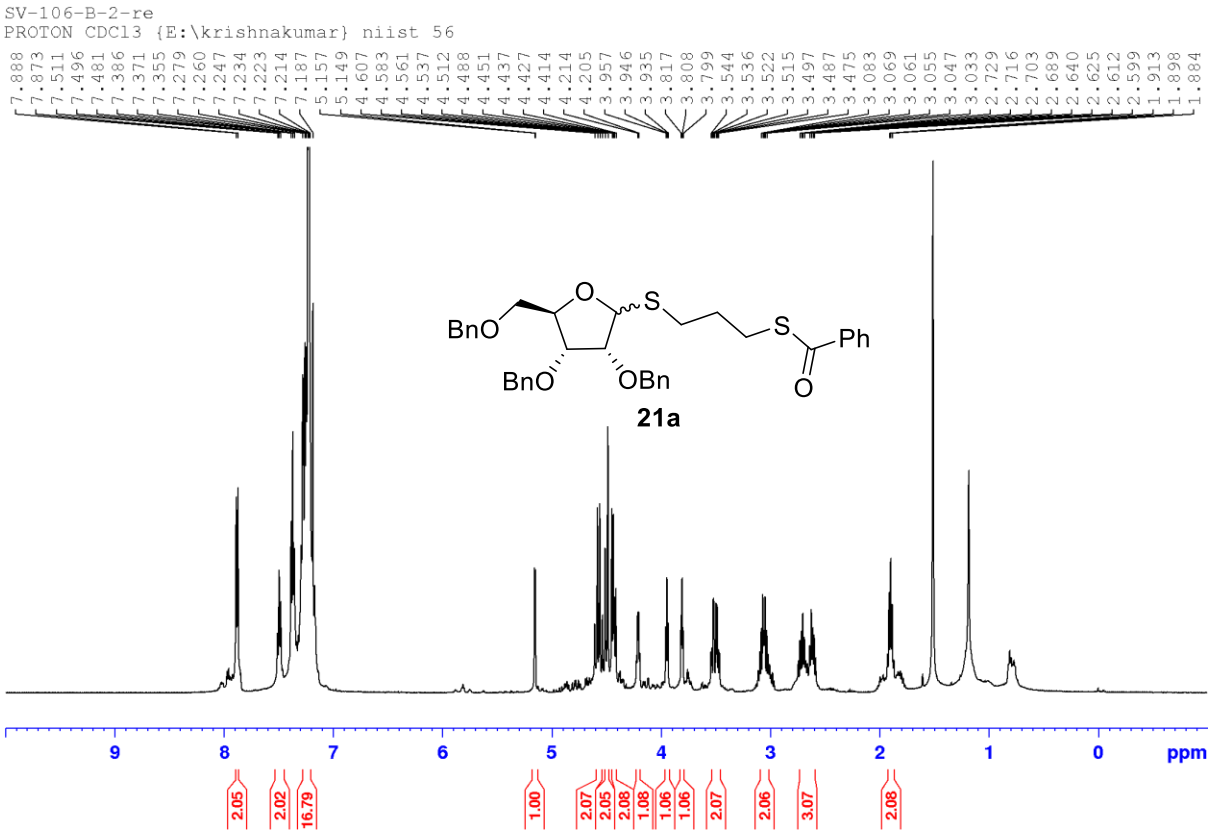

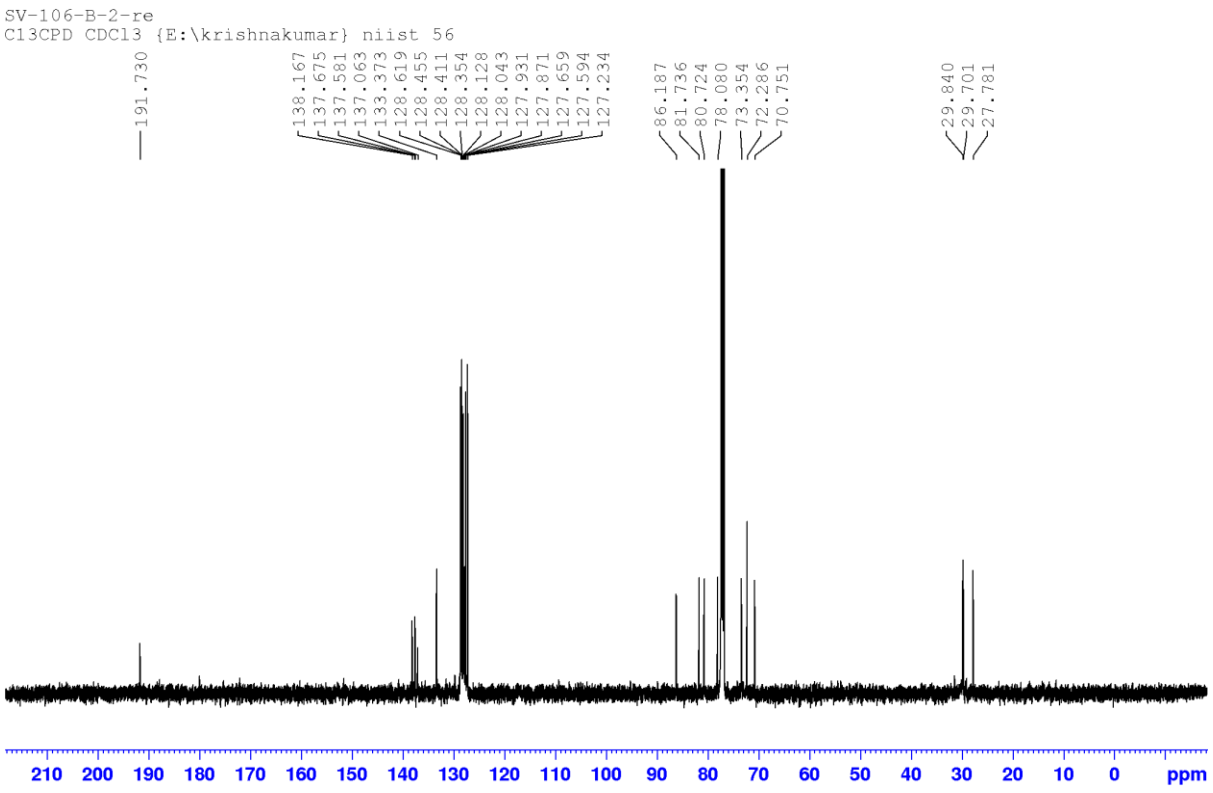

Figure 2.5.2.13: NMR spectra of compound **23**

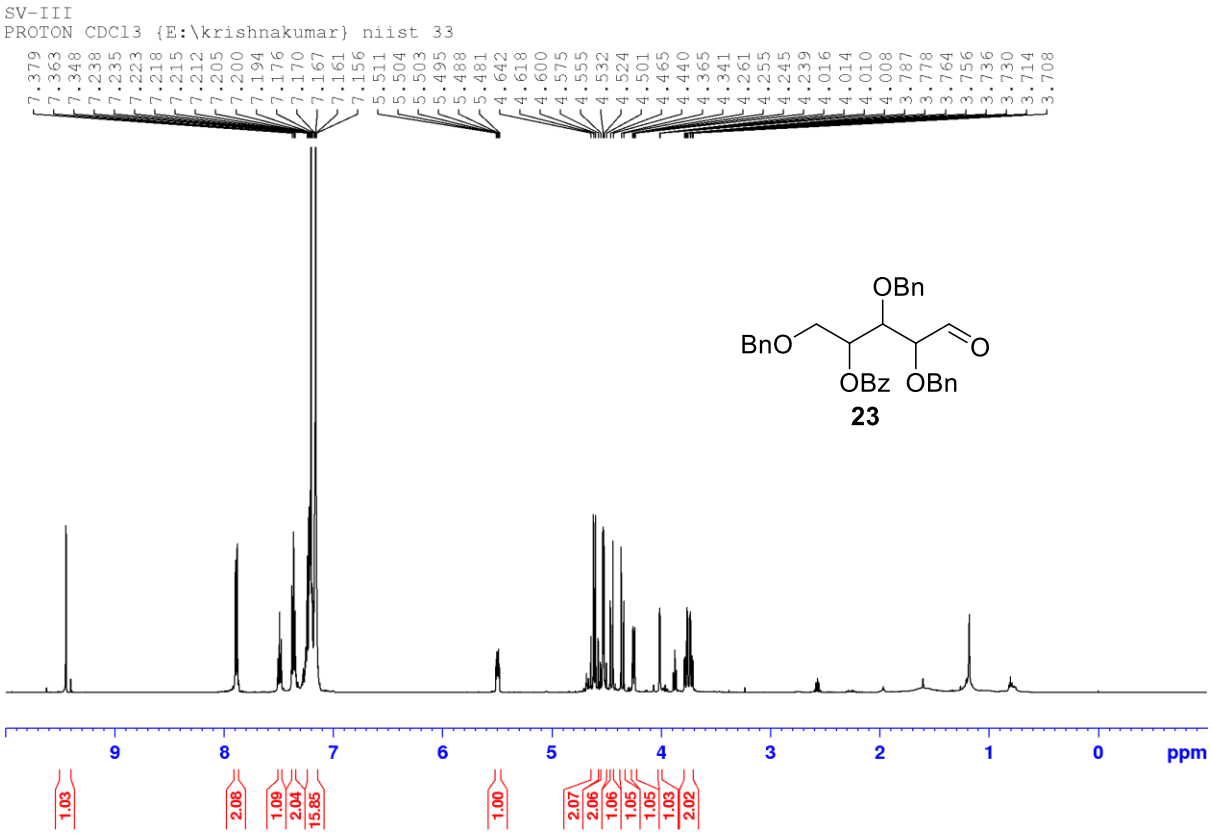

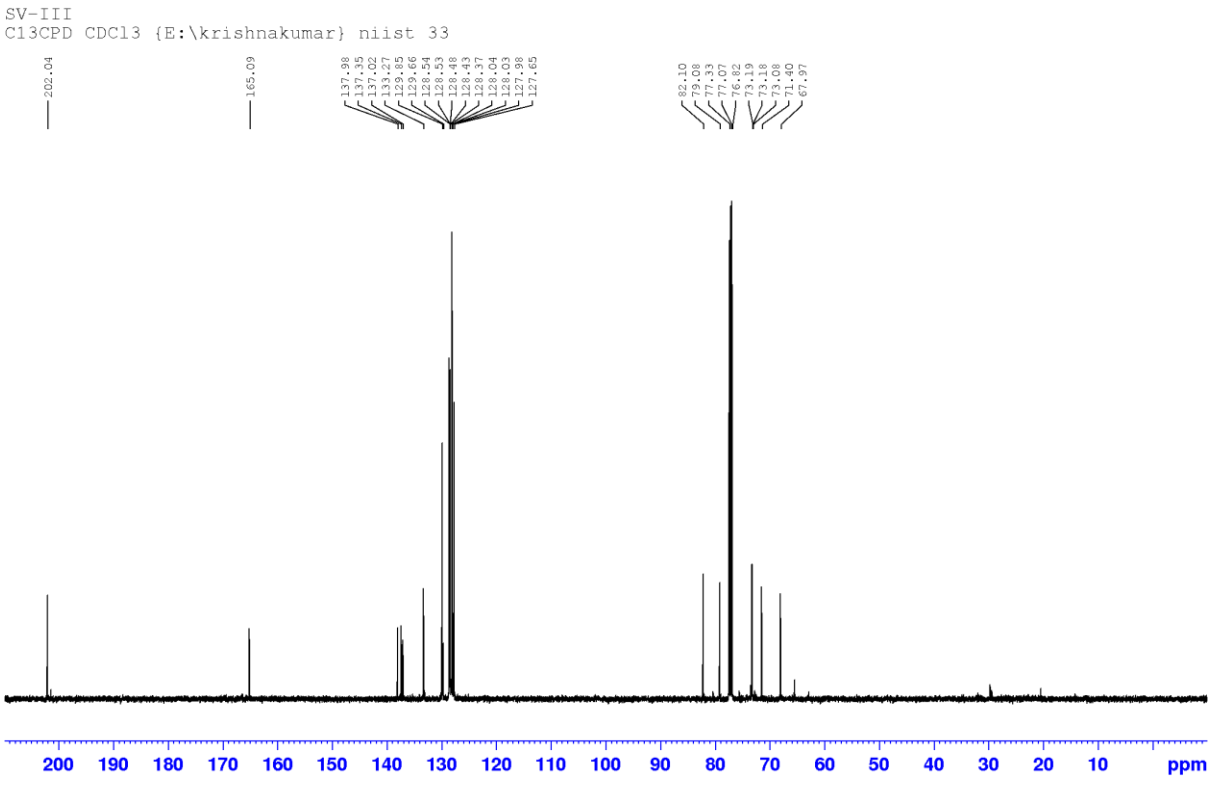

Figure 2.5.2.14: NMR spectra of compound **23a**

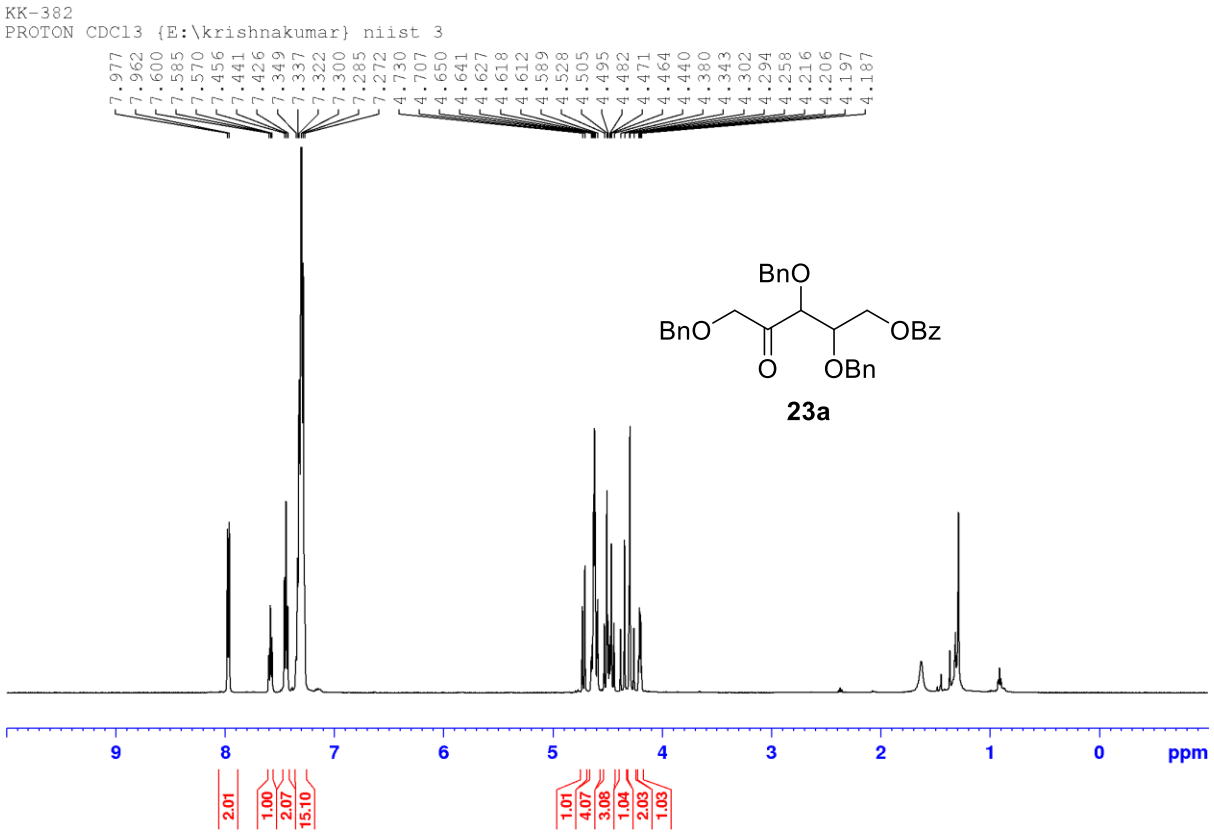

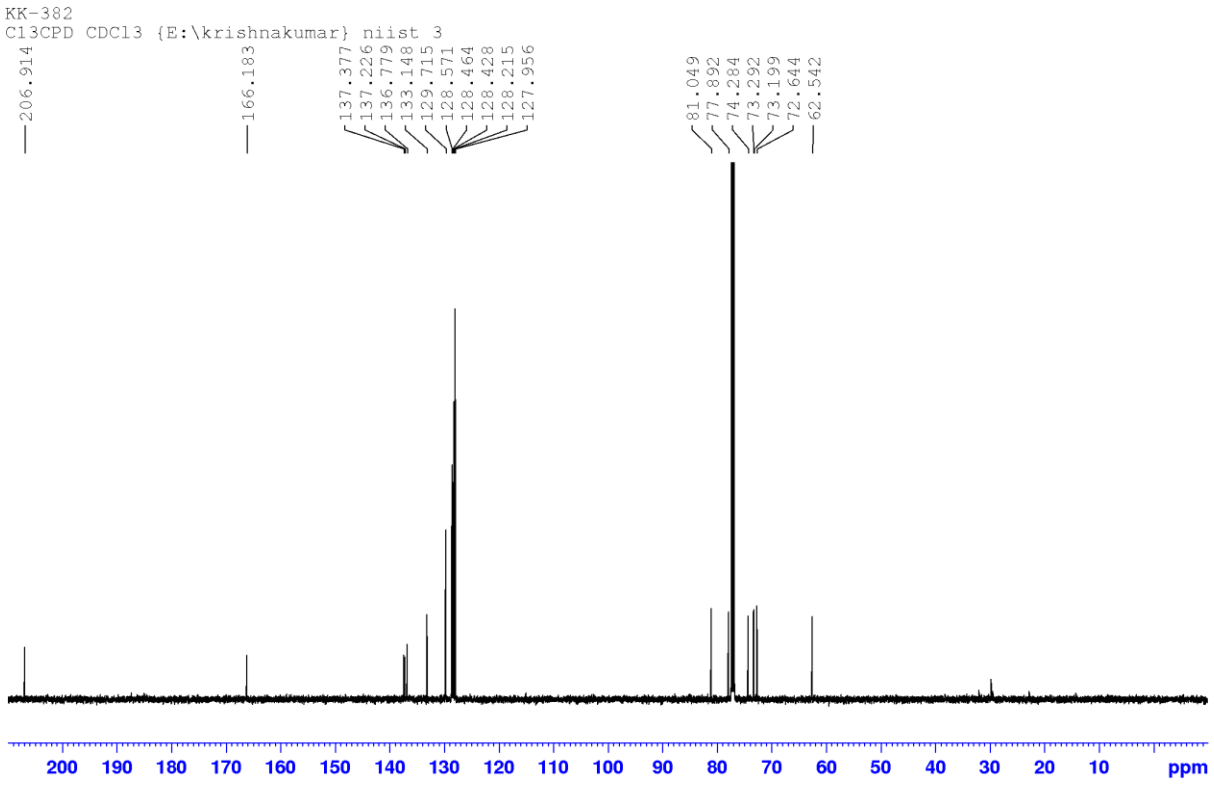

Figure 2.5.2.15: NMR spectra of compound **24**

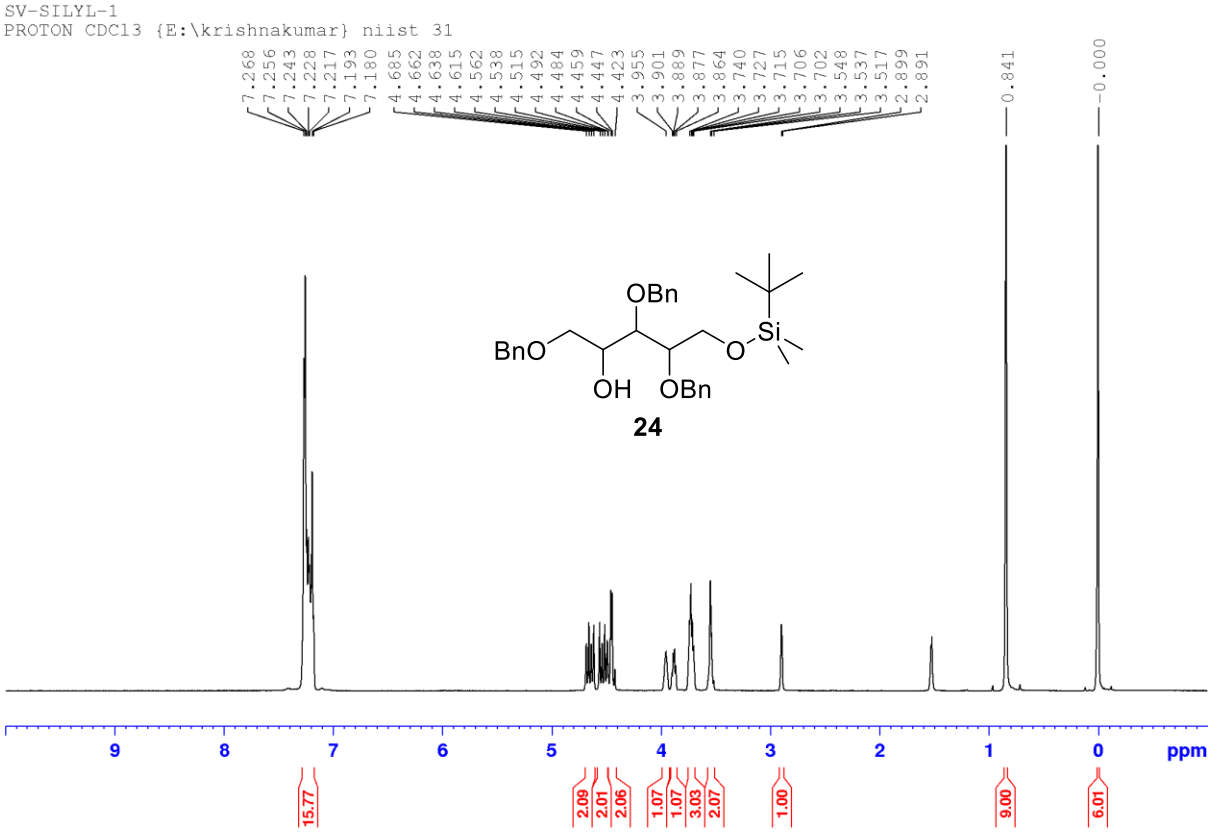

Figure 2.5.2.16: NMR spectra of compound **24a**

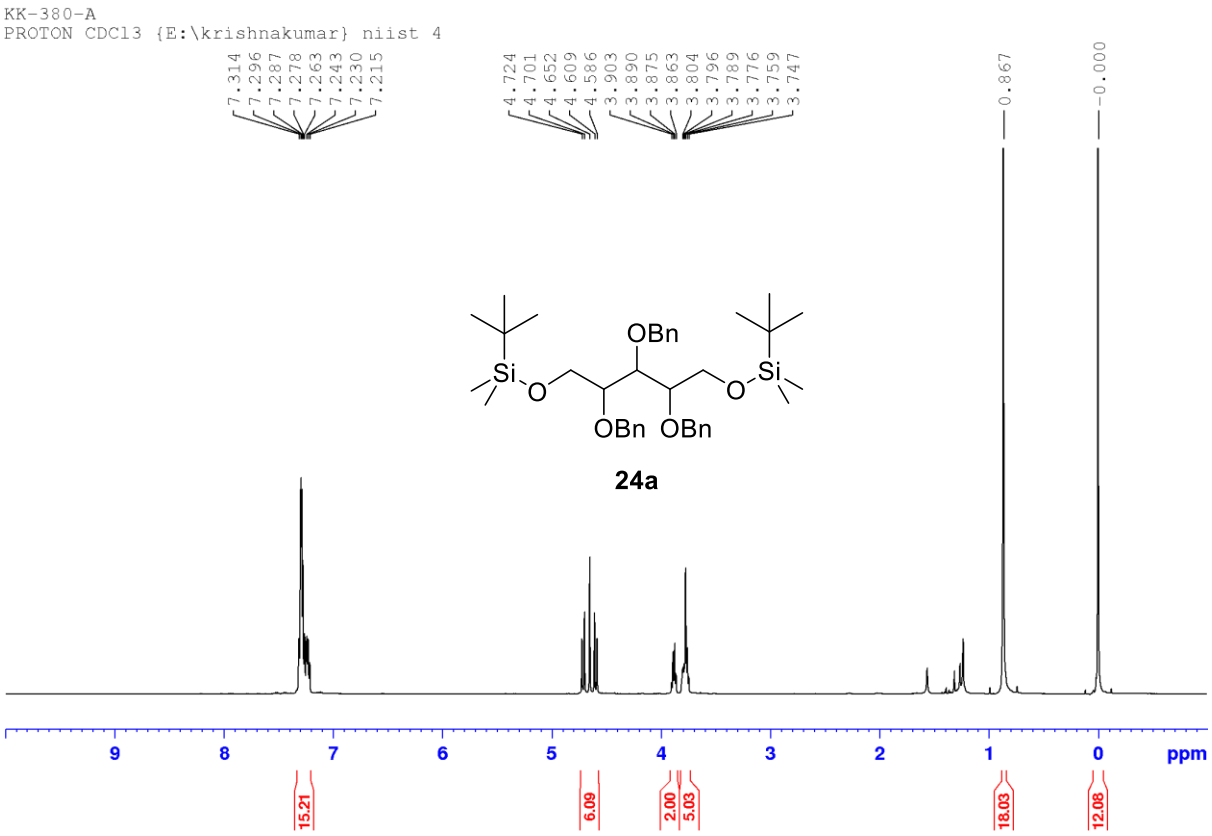

Figure 2.5.2.17: NMR spectra of compound **25**

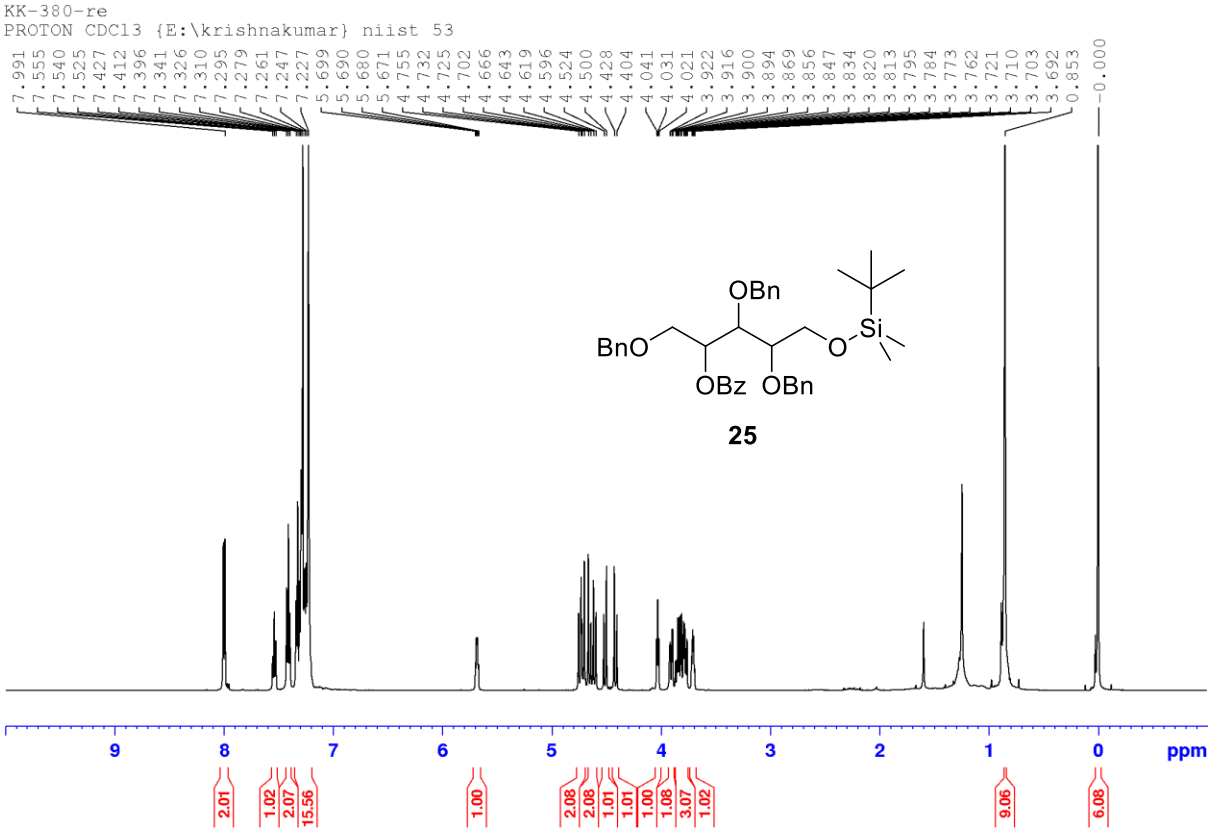

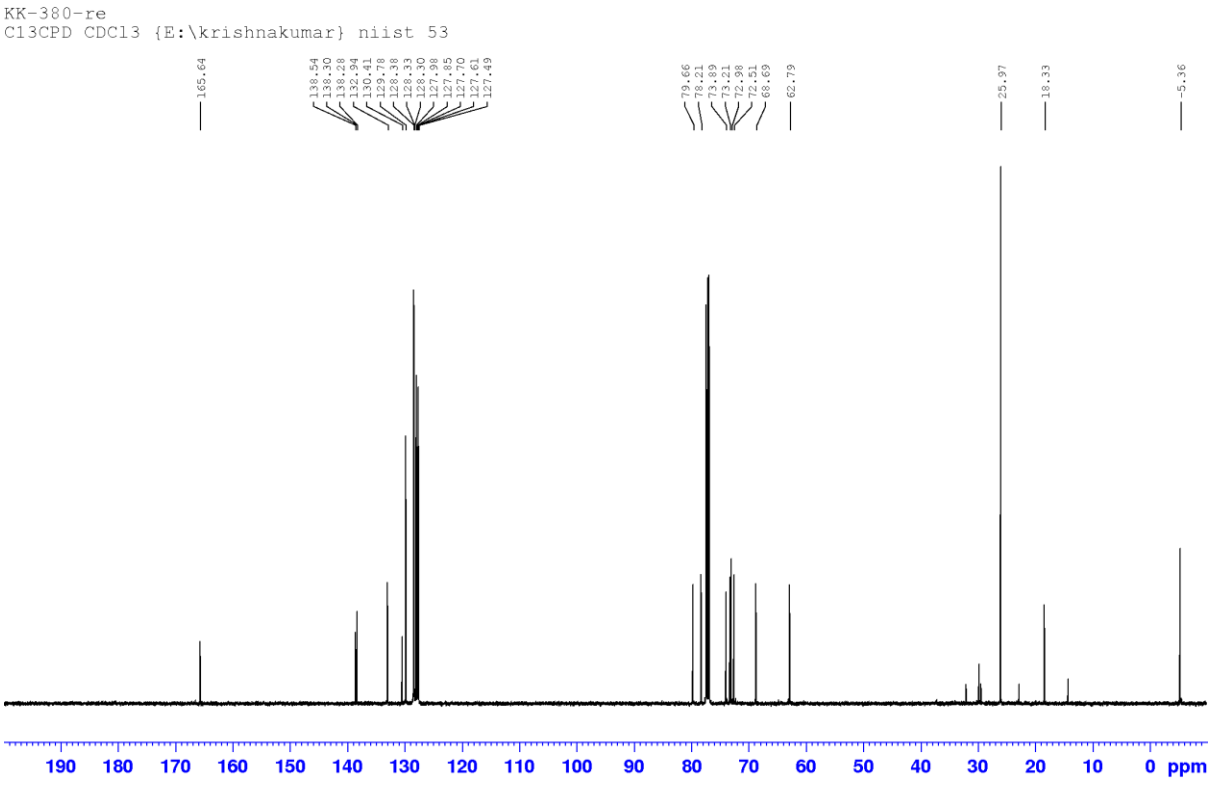

Figure 2.5.2.18: NMR spectra of compound **26**

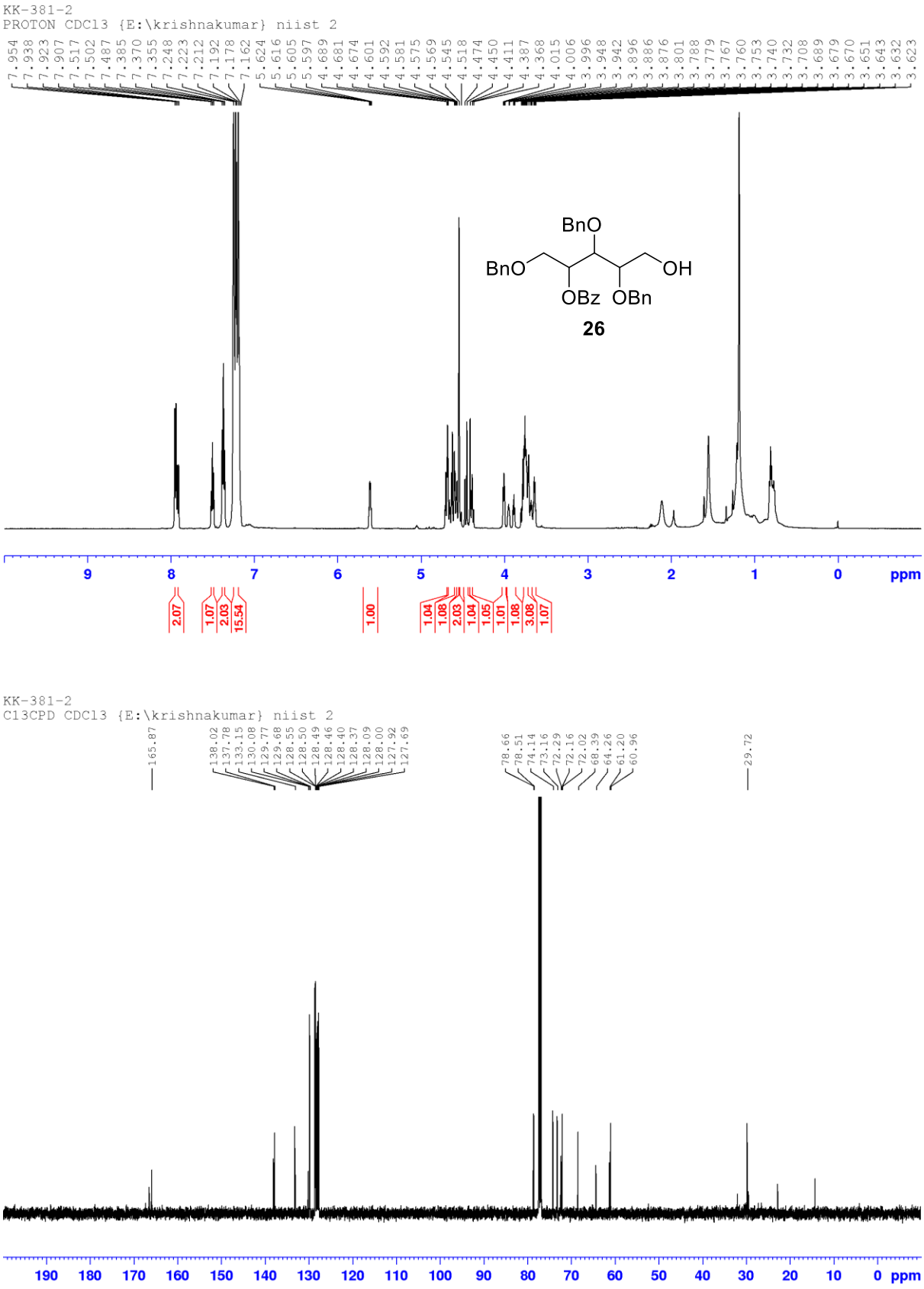

Figure 2.5.2.19: NMR spectra of compound **26a**

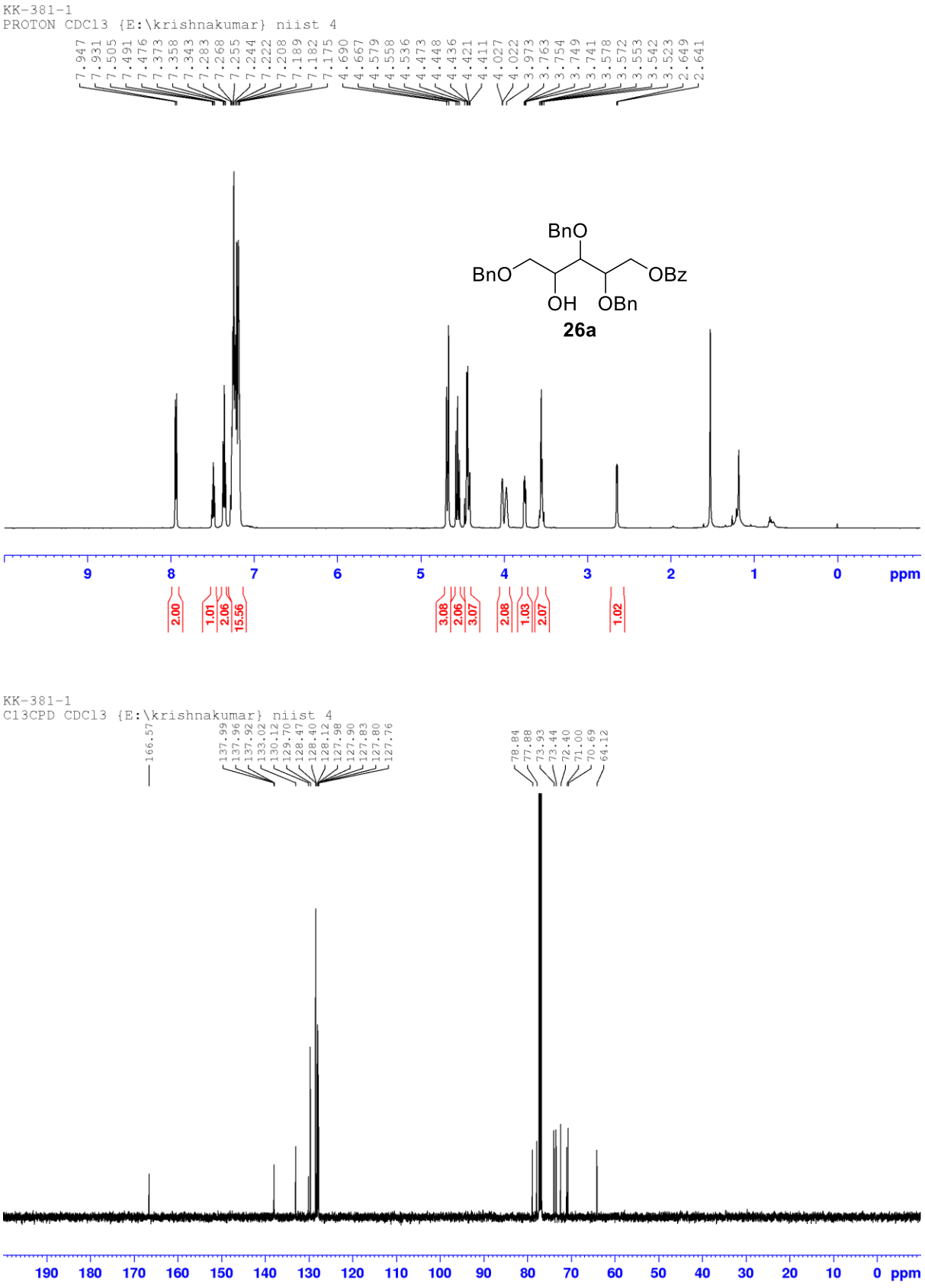

Figure 2.5.2.20: NMR spectra of compound **27**

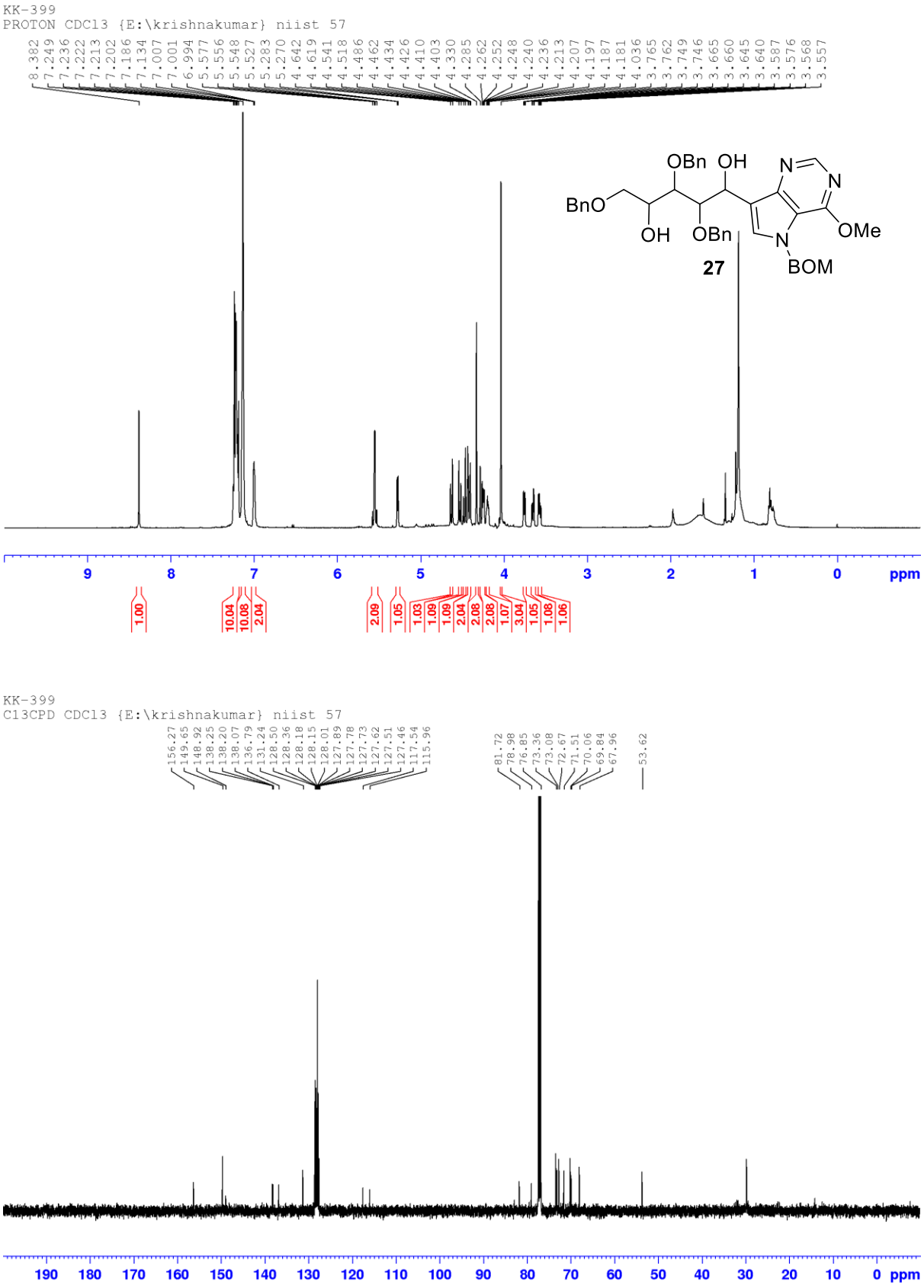

Figure 2.5.2.21: NMR spectra of compound **29**

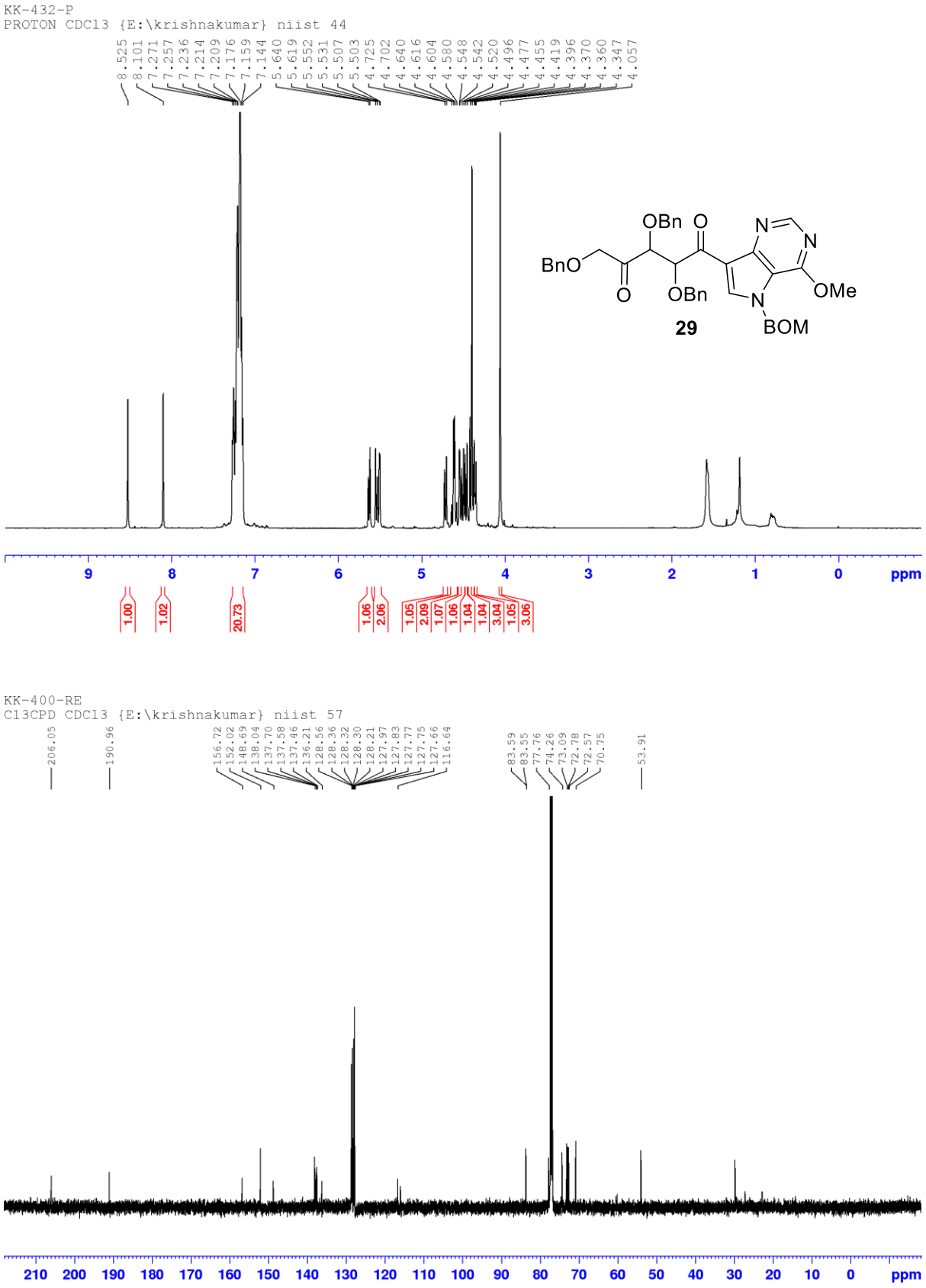

Figure 2.5.2.22: NMR spectra of compound **30**

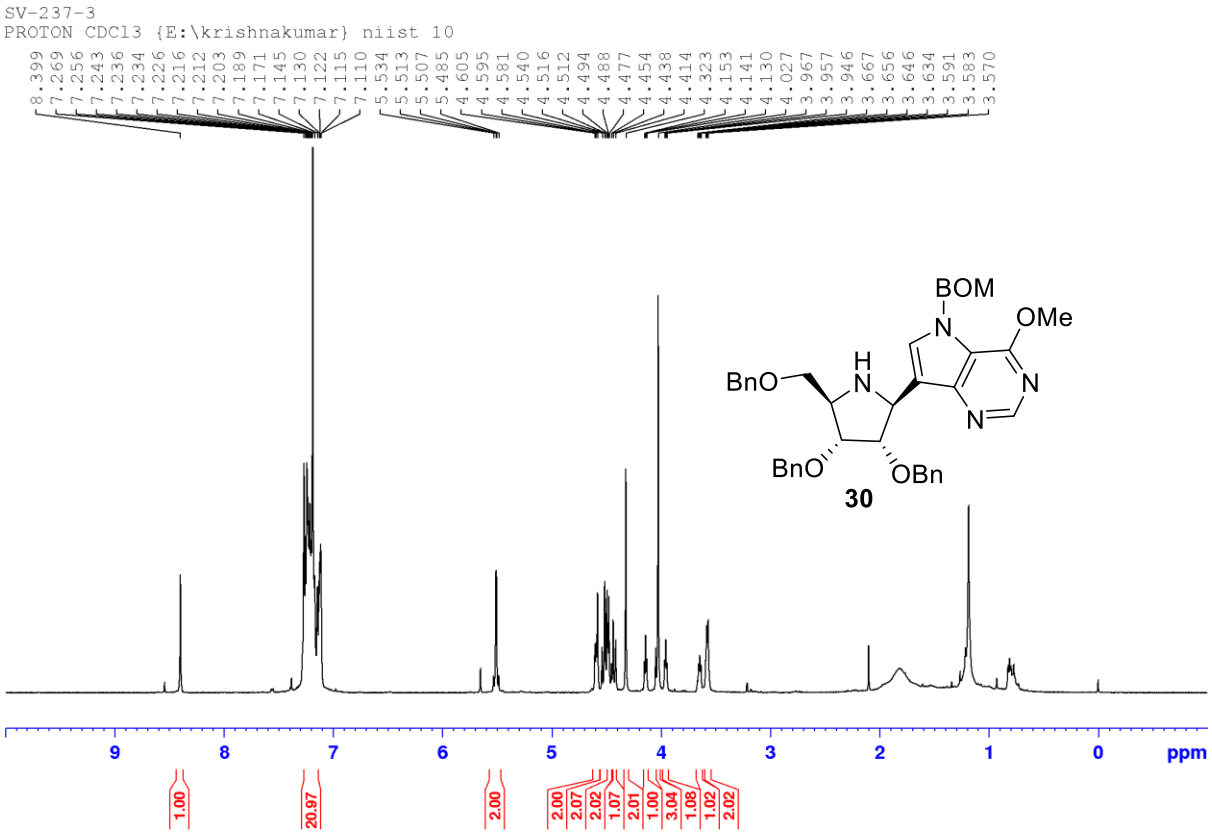

Figure 2.5.2.23: NMR spectra of compound **33**

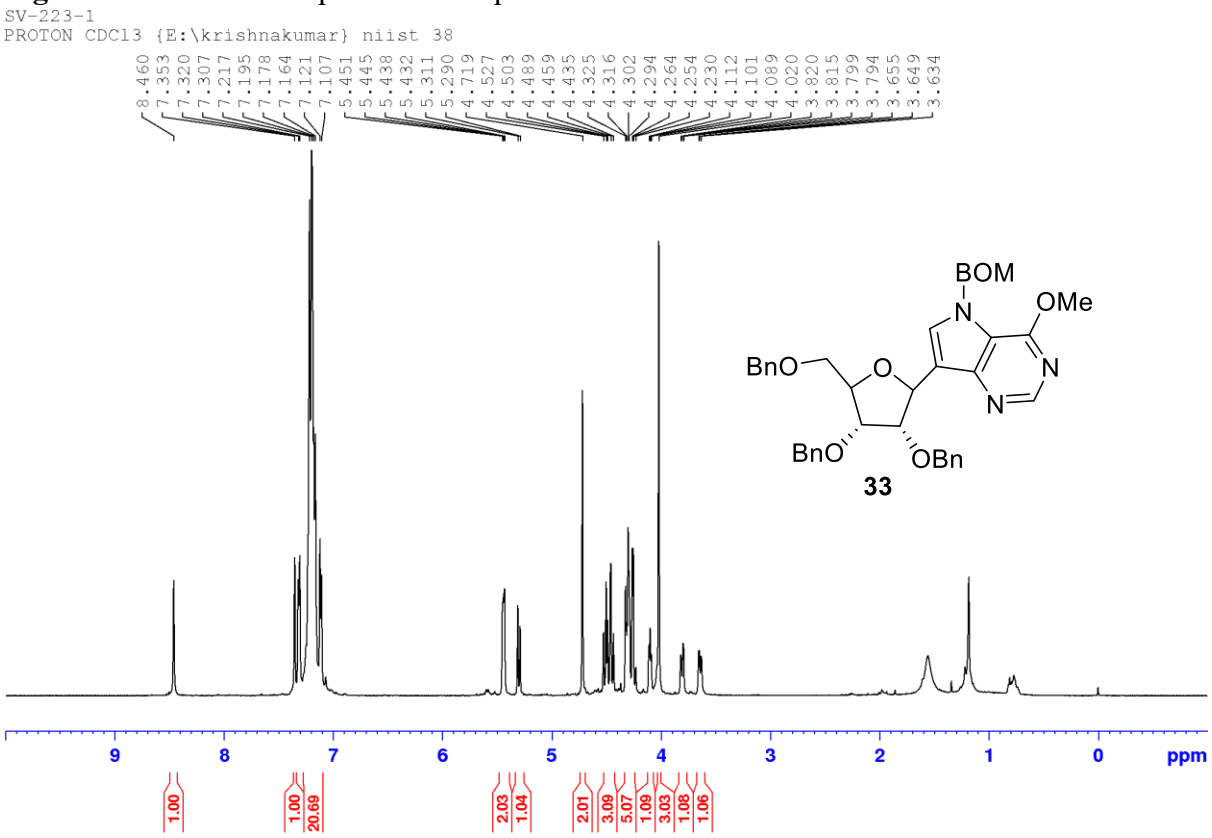

Figure 2.5.2.24: NMR spectra of compound **31**

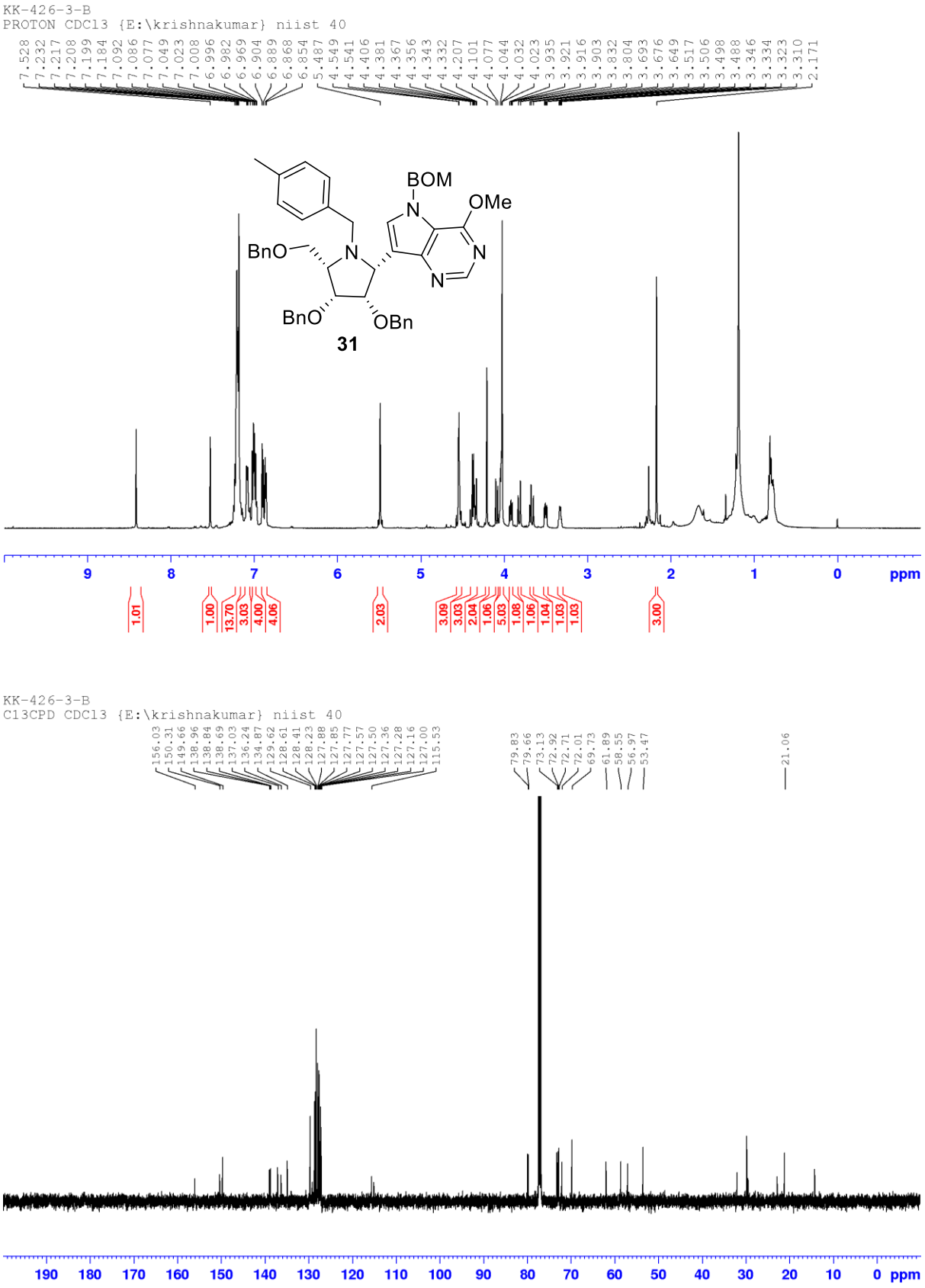

Figure 2.5.2.25: NMR spectra of compound **32**

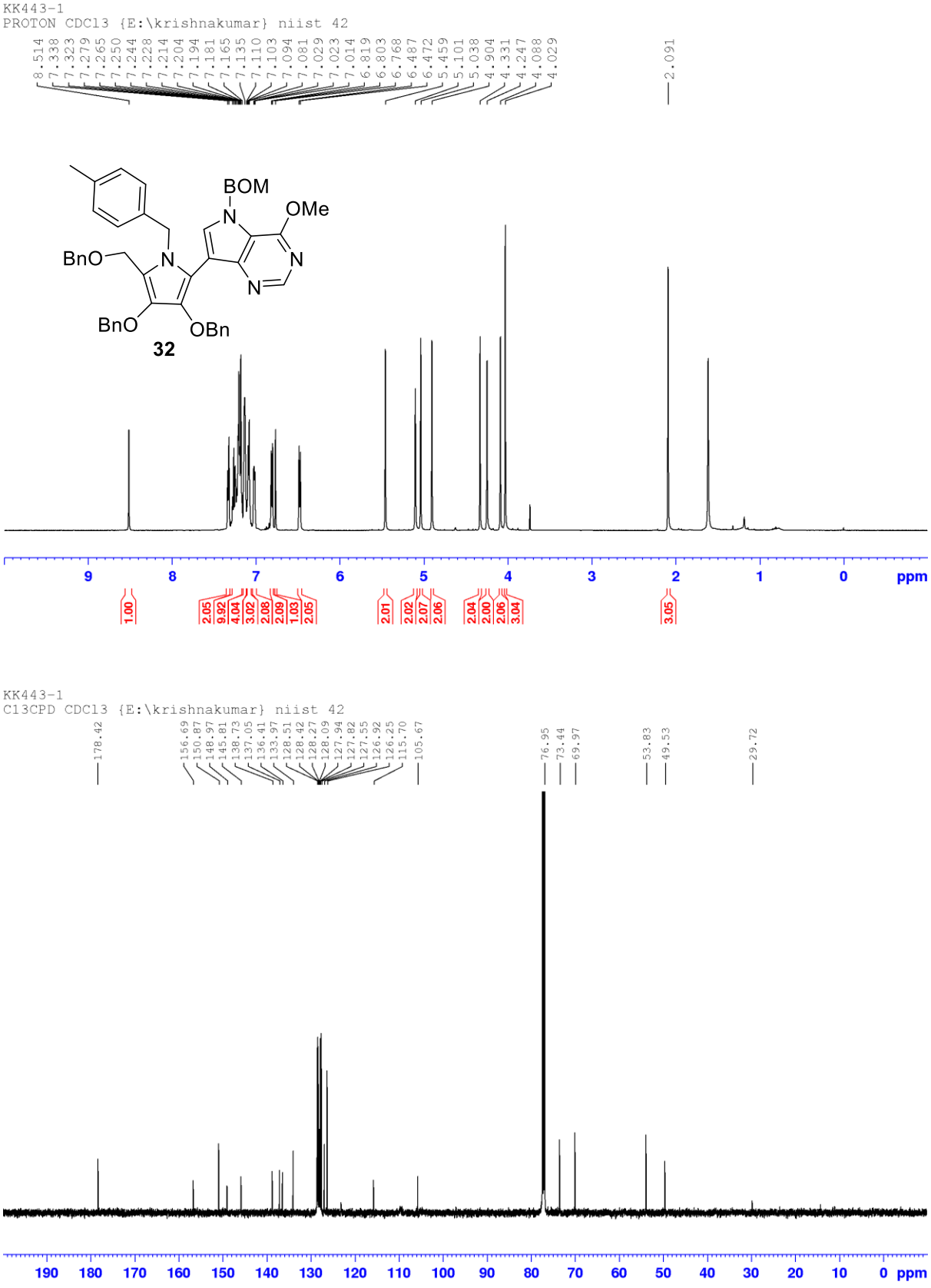

Figure 2.5.2.26: NMR spectra of compound **35**

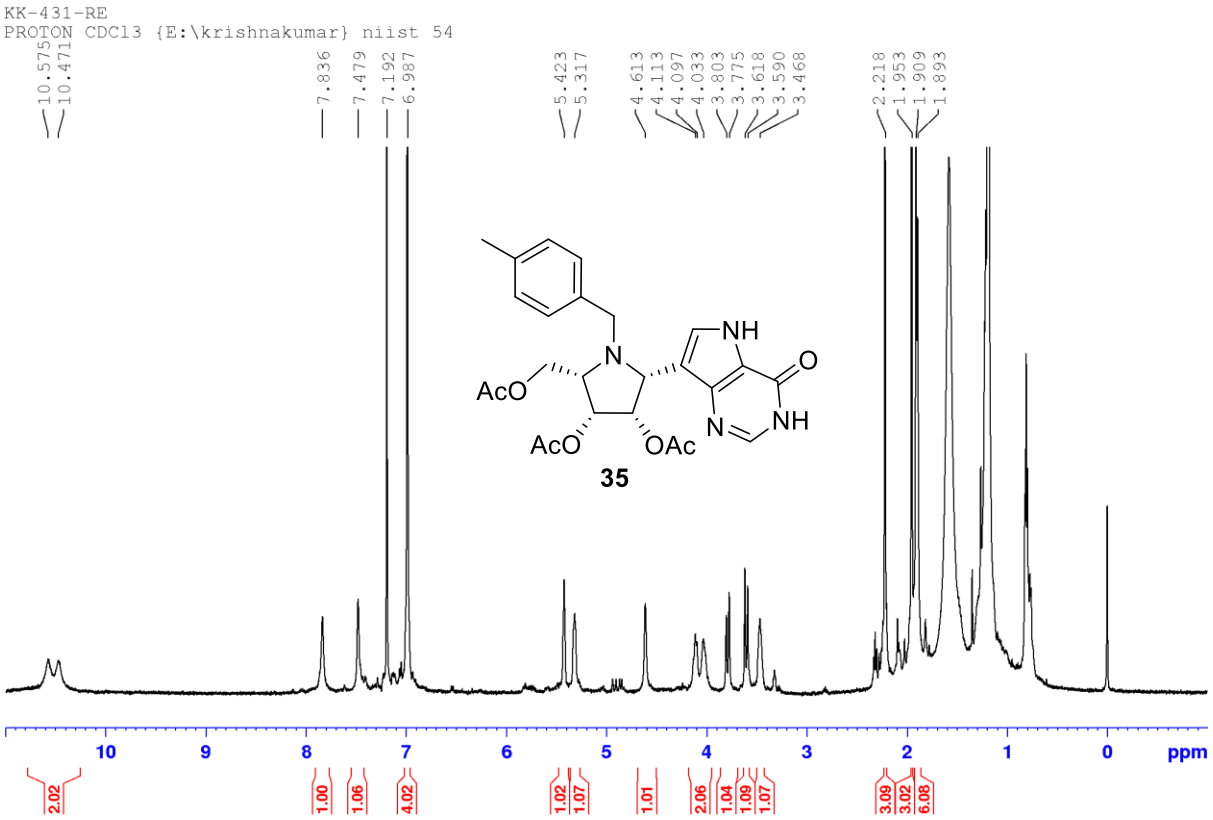

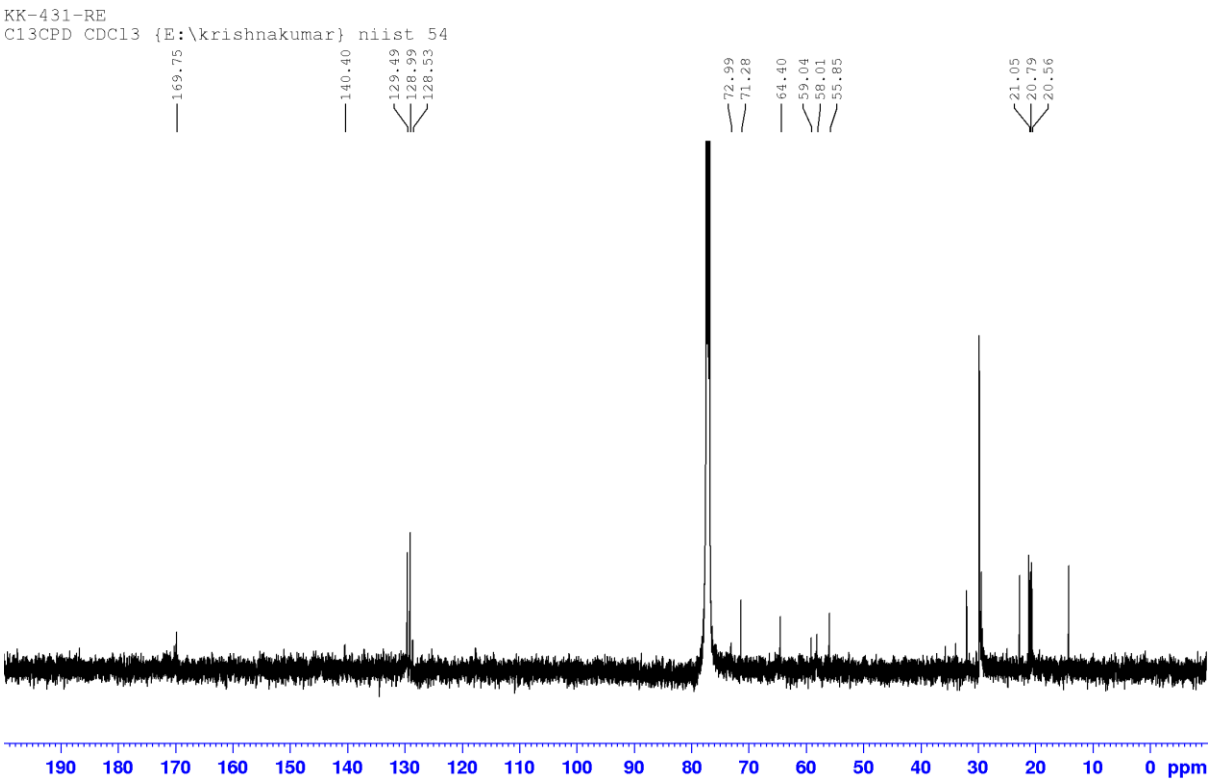

2.6. References

1. Evans, B. G., Schramm, L. V. & Tyler, C. P. The Immucillins: Design, Synthesis and Application of Transition- State Analogues. *Current Medicinal Chemistry* vol. 22 3897–3909 at https://doi.org/http://dx.doi.org/10.2174/0929867322666150821100851 (2015).
2. Evans, G. B., Tyler, P. C. & Schramm, V. L. Immucillins in Infectious Diseases. *ACS Infect. Dis.* **4**, 107–117 (2018).
3. Miles, R. W., Tyler, P. C., Furneaux, R. H., Bagdassarian, C. K. & Schramm, V. L. One-Third-the-Sites Transition-State Inhibitors for Purine Nucleoside Phosphorylase. *Biochemistry* **37**, 8615–8621 (1998).
4. Ritchie, E. *et al.* Phase II Study of Forodesine, a PNP Inhibitor, in Patients with Relapsed or Refractory B-Lineage Acute Lymphoblastic Leukemia. *Blood* **108**, 1881 (2006).
5. Kicska, G. A. *et al.* Immucillin H, a powerful transition-state analog inhibitor of purine nucleoside phosphorylase, selectively inhibits human T lymphocytes. *Proc. Natl. Acad. Sci.* **98**, 4593–4598 (2001).
6. Gore, L., Stelljes, M. & Quinones, R. Forodesine Treatment and Post-Transplant Graft-Versus-Host Disease in Two Patients With Acute Leukemia: Facilitation of Graft-Versus-Leukemia Effect? *Semin. Oncol.* **34**, S35–S39 (2007).
7. Evans, G. B. *et al.* Addition of Lithiated 9-Deazapurine Derivatives to a Carbohydrate Cyclic Imine: Convergent Synthesis of the Aza-C-nucleoside Immucillins. *J. Org. Chem.* **66**, 5723–5730 (2001).
8. Fleet, G. W. J. & Son, J. C. Polyhydroxylated pyrrolidines from sugar lactomes: Synthesis of 1,4-dideoxy-1,4-imino-d-glucitol from d-galactonolactone and syntheses of 1,4-dideoxy-1,4-imino-d-allitol, 1,4-dideoxy-1,4-imino-d-ribitol, and (2s,3r,4s)-3,4-dihydroxyproline from d-gulonola. *Tetrahedron* **44**, 2637–2647 (1988).
9. Evans, G. B., Furneaux, R. H., Lewandowicz, A., Schramm, V. L. & Tyler, P. C. Synthesis of Second-Generation Transition State Analogues of Human Purine Nucleoside Phosphorylase. *J. Med. Chem.* **46**, 5271–5276 (2003).
10. Overkleeft, H. S., van Wiltenburg, J. & Pandit, U. K. A facile transformation of sugar lactones to azasugars. *Tetrahedron* **50**, 4215–4224 (1994).
11. Gangjee, A., Li, W., Yang, J. & Kisliuk, R. L. Design, synthesis, and biological evaluation of classical and nonclassical 2-amino-4-oxo-5-substituted-6-methylpyrrolo [3, 2-d] pyrimidines as dual thymidylate synthase and dihydrofolate reductase inhibitors. *J. Med. Chem.* **51**, 68–76 (2008).
12. Gorantla, J. N., Faseela, A. & Lankalapalli, R. S. Design and synthesis of a novel glycosphingolipid derived from polyhydroxy 2-pyrrolidinone and phytoceramide appended by a 1,2,3-triazole linker. *Chem. Phys. Lipids* **194**, 158–164 (2016).

13. Brakta, M. & Daves, G. D. Efficient synthesis of 3H,5H-pyrrolo[3,2-d]pyrimidin-4-one. *J. Chem. Soc. Perkin Trans. 1* 1883–1884 (1992) doi:10.1039/P19920001883.

14. Elliott, A. J., Montgomery, J. A. & Walsh, D. A. A Short, Facile Synthesis of 2-Amino-l,5-dihydro-4H-pyrrolo[3,2-d]- pyrimidin-4-one (9-Deazaguanine). *Tetrahedron Lett.* **37**, 4339–4340 (1996).

15. Furneaux, R. H. & Tyler, P. C. Improved Syntheses of 3H,5H-Pyrrolo[3,2-d]pyrimidines. *J. Org. Chem.* **64**, 8411–8412 (1999).

16. Kamath, V. P., Juarez-Brambila, J. J., Morris, C. B., Winslow, C. D. & Morris, P. E. Development of a practical synthesis of a purine nucleoside phosphorylase inhibitor: BCX-4208. *Org. Process Res. Dev.* **13**, 928–932 (2009).

17. Graziani, A., Passacantilli, P., Piancatelli, G. & Tani, S. A mild and efficient approach for the regioselective silyl-mediated protection-deprotection of C-4 hydroxyl group on carbohydrates. *Tetrahedron Lett.* **42**, 3857–3860 (2001).

18. Zhang, M. *et al.* Practical synthesis of immucillins BCX-1777 and BCX-4430. *Org. Chem. Front.* **7**, 3675–3680 (2020).

19. Gorantla, J. N. & Lankalapalli, R. S. Synthesis of *β*-C-galactosyl ceramide and its new aza variant *via* the horner-wadsworth-emmons reaction. *J. Org. Chem.* **79**, 5193–5200 (2014).

20. Yokoyama, M., Ikenogami, T. & Togo, H. Stereoselective synthesis of C-4′-aminouridines (uracil C-4-amino-D-ribonucleosides). *J. Chem. Soc. Perkin Trans. 1* 2067–2071 (2000) doi:10.1039/B002063J.

21. Verma, A. K., Dubbu, S., Chennaiah, A. & Vankar, Y. D. Synthesis of di- and trihydroxy proline derivatives from D-glycals: Application in the synthesis of polysubstituted pyrrolizidines and bioactive 1C-aryl/alkyl pyrrolidines. *Carbohydr. Res.* **475**, 48–55 (2019).

22. Yoda, H., Nakajima, T. & Takabe, K. Total synthesis of natural (−)-codonopsinine employing stereoselective reduction of quaternary *α*-hydroxypyrrolidine. *Tetrahedron Lett.* **37**, 5531–5534 (1996).

Synthesis of Immucillin-A from D-Ribonolactam

3.1. Abstract

The synthesis of galidesivir, a novel adenosine analog with broad-spectrum antiviral activity, is detailed, emphasizing its efficacy against various RNA viruses such as Ebola, Zika, and SARS-CoV-2. The process involves creating a forodesine precursor through an optimized synthetic route, addressing previous challenges in cross-coupling reactions. Utilizing a Grignard reaction for a key intermediate step, the synthesis is streamlined to improve yield and scalability. This method provides an efficient pathway to produce galidesivir, facilitating its potential therapeutic application in combating significant viral infections.

3.2. Introduction

Immucillin-A, also known as BCX4430 and Galidesivir, is a novel adenosine analog exhibiting a remarkably broad-spectrum antiviral profile.[1] This characteristic stems from unique structural features (Figure 3.2).[2] This feature disrupts viral replication, making galidesivir effective against a wide range of RNA viruses, including members of nine distinct families such as flavivirus, togavirus, bunyavirus, arenavirus, paramyxovirus, coronavirus, filovirus, orthomyxovirus, and picornavirus.[3–6] *In vitro* and *in vivo* studies have demonstrated promising efficacy against various clinically significant viruses, including Ebola virus, yellow fever virus, Zika virus, and tick-borne flaviviruses. Notably, galidesivir is currently undergoing clinical investigation for the treatment of Ebola virus disease and yellow fever.[7,8] Furthermore, preliminary phase 1 data suggests good tolerability and potential antiviral activity against SARS-CoV-2, the virus responsible for COVID-19.[9] These findings highlight galidesivir's potential as a broad-spectrum antiviral therapeutic, warranting further clinical trials to confirm its safety and efficacy for specific viral diseases.[10]

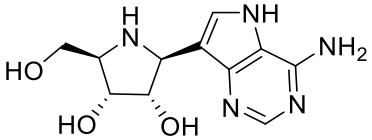

Figure 3.2: structure of Immucillin-A

Given galidesivir's promising pre-clinical and clinical data, its synthesis has become a scientific priority. Efficient and scalable synthetic methods are crucial to ensure the availability of sufficient quantities for ongoing clinical trials and, potentially, future therapeutic applications.

3.3. Result and discussions

The aim of this chapter is to discover novel methods for the synthesis of galidesivir.

3.3.1. Synthetic plan for galidesivir (Immucillin-A)

Building upon the findings of the previous chapter, this chapter explores an alternative synthetic route towards forodesine, a key precursor for the synthesis of galidesivir.[3] In the previous chapter, the double reductive amination approach encountered challenges after the cross-coupling step, ultimately leading to a product distinct from the desired forodesine precursor. Therefore, this chapter presents a revised strategy that utilizes lactam as the coupling partner for a more controlled and efficient synthesis of the forodesine precursor. This approach aims to overcome the limitations encountered previously and ultimately facilitate the large-scale production of forodesine, which can then be readily converted to galidesivir. The overall synthetic strategy for galidesivir hinges on its precursor, forodesine. Forodesine itself can be divergently synthesized from a lactam derived from D-ribose. This lactam intermediate can then be coupled with a suitably substituted pyrrolopyrimidine, which can be ultimately obtained from 9-deazahypoxanthine.

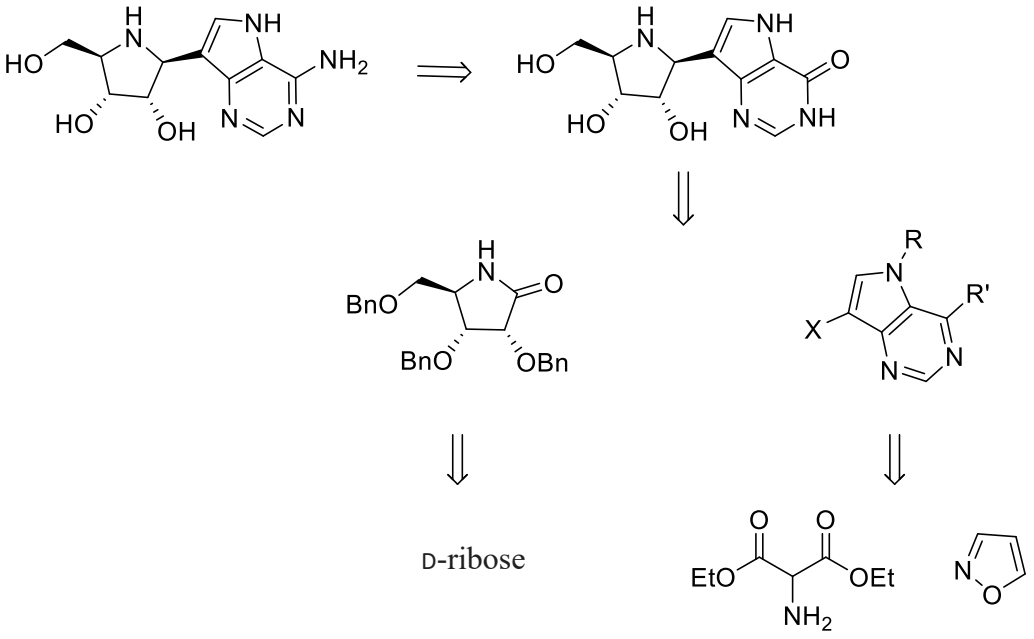

Figure 3.3.1: Synthetic plan for galidesivir

3.3.1.1. Synthesis of coupling partners

In accordance with the outlined synthetic plan, a convergent coupling strategy was adopted for the synthesis of forodesine, a key precursor for galidesivir. As previously described, the sugar moiety was envisioned as a *γ*-lactam (compound **2**).[11,12] This *γ*-lactam was successfully synthesized from D-ribose through an eight-step sequence, detailed in the previous chapter.

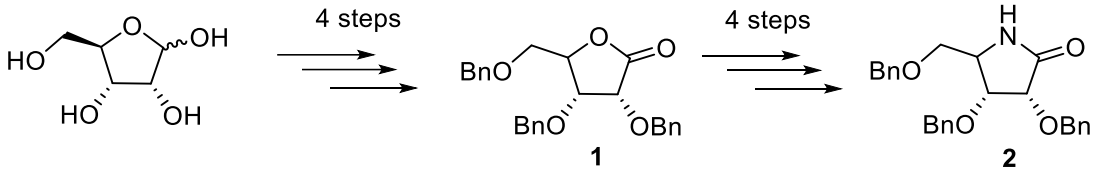

Scheme 3.3.1.1a: Synthesis of *γ*-lactam **2**

The convergent coupling strategy for forodesine synthesis necessitated a suitably substituted pyrrolopyrimidine as the second coupling partner. To achieve this, compound **5** was prepared, from 9-deazahypoxanthine.[13,14] The synthesis of 9-deazahypoxanthine, as detailed in the previous chapter, involved the condensation of isoxazole and diethyl aminomalonate followed by a formamidine acetate reaction.

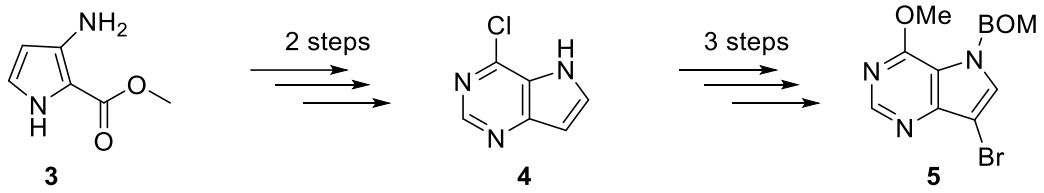

Scheme 3.3.1.1b: Synthesis of compound **5**

3.3.1.2. The cross-coupling reaction of pyrrolopyrimidine 5 with *γ*-lactam 2

Building upon the findings from the previous chapter, this chapter applies the optimized cross-coupling conditions to the *γ*-lactam **2**. As previously described, the prior chapter identified a superior solvent system for this type of reaction[15] compared to the butyllithium chemistry employed in THF. Therefore, we will utilize the same optimized conditions for the cross-coupling step involving *γ*-lactam **2**.

Compound **5** was subjected to lithium-halogen exchange using n-butyllithium in a pre-cooled mixture of MTBE and anisole (Scheme 3.3.1.2a). The reaction was monitored, and the formation of the lithiated intermediate **5a** was expected to occur within 5 minutes. Subsequent treatment with *γ*-lactam **2** aimed to achieve the desired cross-coupling product

(**6**). However, analysis of the reaction mixture revealed the absence of **6** and the sole presence of the dehalogenated product **7**.

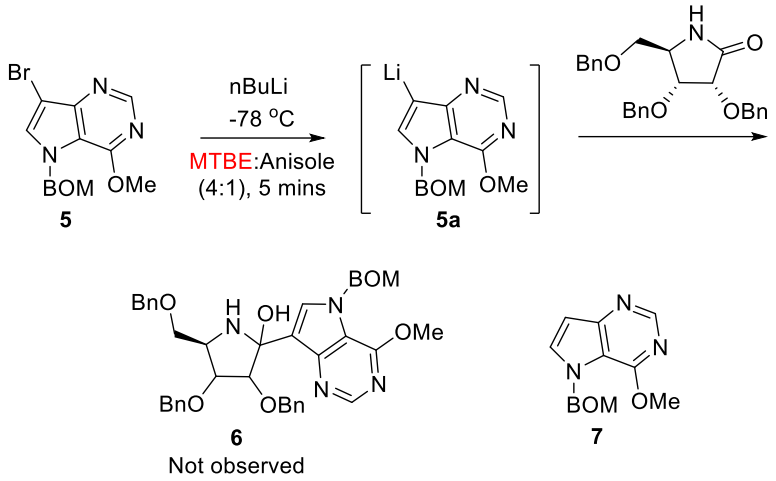

Scheme 3.3.1.2a: Cross-coupling reaction of **5** with *γ*-lactam **2**

These observations suggested potential challenges with the cross-coupling step even under the optimized solvent system (MTBE:anisole) identified in the previous chapter. To elucidate the reasons behind the unsuccessful coupling, a closer examination of the reaction mechanism was undertaken.

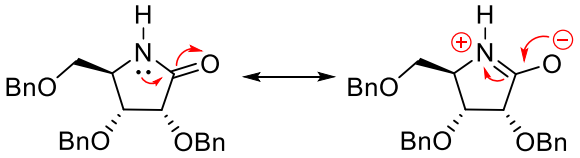

Figure 3.3.1.2a: resonance in *γ*-lactam **2**

It was hypothesized that the lone pair on the lactam nitrogen atom might be participating in conjugation with the carbonyl carbon, thereby reducing its electrophilic character and hindering the desired reactivity (Figure 3.3.1.2a). To address this possibility, strategies to divert the lone pair away from the conjugation and enhance the electrophilic character of the carbonyl group were explored.

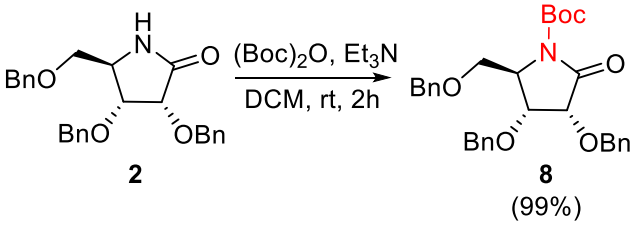

Scheme 3.3.1.2b: Synthesis of compound **8**

To address the potential influence of the lactam nitrogen lone pair on electrophilicity, N-protection of γ-lactam **2** was undertaken. Treatment with di-*tert*-butyl dicarbonate in the presence of triethylamine successfully afforded N-Boc-protected lactam **8** in excellent yield (99%) (Scheme 3.3.1.2b).

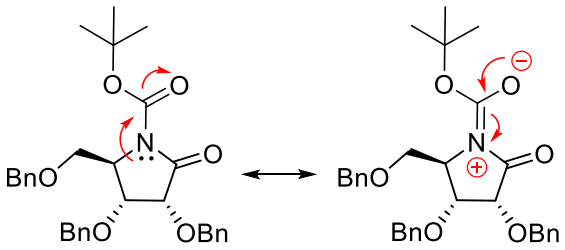

Figure 3.3.1.2b: Resonance in N-Boc-γ-lactam **8**

The introduced Boc group is anticipated to function beyond a simple protecting group. Its electron-withdrawing nature may act to delocalize the lone pair on the lactam nitrogen, reducing its conjugation with the carbonyl carbon (Figure 3.3.1.2b). This effect could potentially enhance the electrophilic character of the carbonyl group, facilitating the desired cross-coupling reaction with the lithiated intermediate **5**.

3.3.1.3. The cross-coupling reaction of pyrrolopyrimidine 5 with γ-lactam 8

Encouraged by the successful N-protection of γ-lactam **2** (compound **8**), the cross-coupling reaction with lithiated intermediate **5a** was revisited (Scheme 3.3.1.3). While the reaction proceeded smoothly, analysis of the product revealed the formation of an unexpected open-chain product **9** instead of the desired hemiaminal product **6**. This structural assignment was confirmed by the presence of a characteristic signal at δ 193 ppm in the ^{13}C NMR spectrum, indicative of a ketone group.

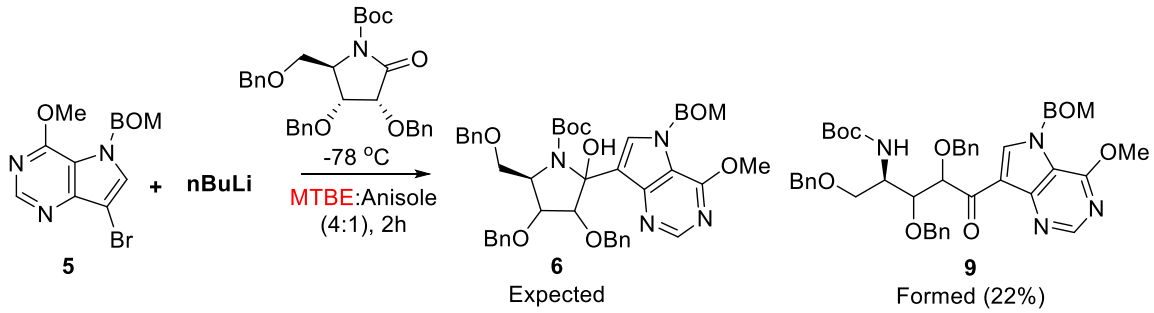

Scheme 3.3.1.3: Cross-coupling with N-Boc lactam

The cross-coupling reaction presented an unexpected hurdle. Instead of the desired cyclic hemiaminal intermediate **6**, the reaction yielded open-chain intermediate **9**. This

necessitated a significant change in our synthetic strategy to achieve the targeted forodesine precursor. Ideally, a simple reduction of hemiaminal **6** would have provided a readily transformable intermediate. Consequently, we explored various reduction conditions, as detailed in Table 3.3.1.3, with the aim of promoting the cyclization of intermediate **9** into the desired hemiaminal form. Unfortunately, none of these attempts proved successful. Neither the desired cyclization nor a tractable product mixture suitable for further purification could be obtained. Notably, the triethylsilane reduction conducted at -78 °C in dichloromethane, while resulting in a clean reaction mixture, offered no solace. Analysis revealed only recovered starting material (compound **9**) with no evidence of the desired product formation. This unexpected outcome necessitated a critical evaluation of the reaction pathway and the development of an alternative strategy to access the desired intermediate.

Table 3.3.1.3: Reduction conditions tried on compound **9**

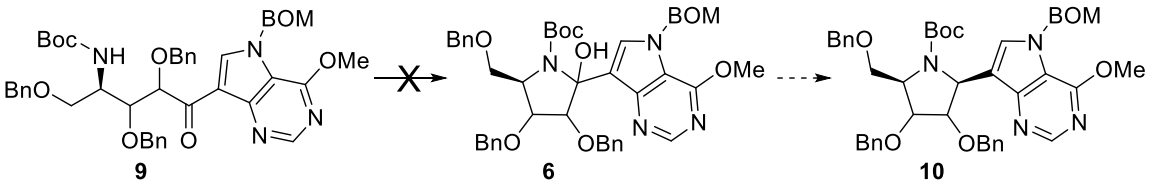

Reducing Agent	Promoter	Solvent	Temperature (^{o}C)
$NaCNBH_3$	TFA	MeOH	rt
$NaCNBH_3$	HCOOH	MeOH	rt
$Pd/C/H_2$	--	MeOH	rt
Et_3SiH	$BF_3.OEt_2$	ACN	0
Et_3SiH	$BF_3.OEt_2$	DCM	-78

3.3.2. The turbo Grignard reagent

Knochel *et al*. (2004)[16] described a novel approach for the preparation of functionalized aryl magnesium compounds (Scheme 3.3.2) employing *i*PrMgCl·LiCl as the key reagent. This reagent was conveniently synthesized through the addition of *i*PrCl to a mixture of magnesium turnings and LiCl in a 1:1.1:1 ratio (*i*PrCl/Mg/LiCl) within THF. Notably, *i*PrMgCl·LiCl functions as a superior metal halogen exchange reagent. In simpler terms, this Grignard reagent itself can promote metal halogen exchange in another aryl halide,

converting it into the corresponding aryl Grignard reagent. The resulting functionalized aryl magnesium compounds can then participate in reactions with electrophiles, ultimately affording Grignard addition products.[17]

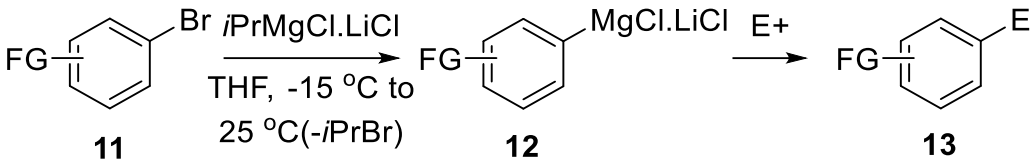

Scheme 3.3.2a: Functionalization to aryl bromide using *i*PrMgCl·LiCl

Building upon their previous work, the same research group subsequently published a follow-up study in the same year demonstrating the applicability of *i*PrMgCl·LiCl for metal halogen exchange in vinyl iodides (Scheme 3.3.2b).[18] This expanded the scope of the reaction beyond aryl halides. A significant advantage of this reagent is its compatibility with various functional groups, including ester and alkene functionalities, which remain intact under the reaction conditions

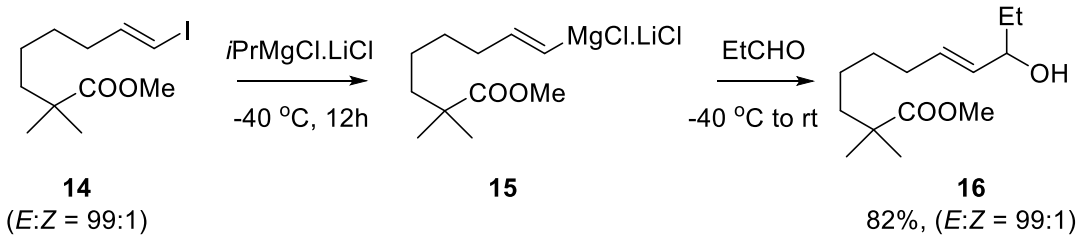

Scheme 3.3.2b: Functionalization to vinyl iodide using *i*PrMgCl·LiCl

The demonstrated advantages of *i*PrMgCl·LiCl in metal halogen exchange, particularly its functional group tolerance, have propelled its adoption within the organic synthesis community. Consequently, it has garnered the popular moniker "turbo-Grignard reagent" due to its enhanced reactivity compared to traditional Grignard reagents. This widespread recognition has led to its commercial availability, facilitating its use in various synthetic endeavors.[19]

3.3.2.1. The cross-coupling reaction using turbo Grignard reagent

In light of the challenges encountered with the organolithium-mediated cross-coupling, the synthetic strategy was revised to explore Grignard reaction chemistry. Notably, the study by Knochel *et al.*, 2004[16] demonstrated a remarkable rate acceleration for Br/Mg exchange in the presence of LiCl additives, particularly for functionalized heteroaryl magnesium

compounds. This approach was successfully applied in the key cross-coupling step for nucleoside synthesis of remdesivir. Inspired by these findings, we adopted similar reaction conditions for our cross-coupling reaction (Scheme 3.3.2.1).

While the formation of the Grignard reagent intermediate **5b** from compound **5** *via* Br/Mg exchange using the *i*PrMgCl·LiCl complex solution (1.3 M in THF) required a longer reaction time (12 hours), immediate subsequent treatment with lactam **8** furnished the desired hemiaminal product **22** in a satisfactory yield of 51%. This turbo-Grignard reagent-mediated cross-coupling offers several advantages compared to the previously attempted *n*BuLi-mediated reaction. The Grignard approach utilizes a higher reaction temperature (-20 °C) compared to the *n*BuLi reaction (-78 °C), potentially improving reaction efficiency. Most importantly, this method exhibits excellent compatibility with THF as the solvent. In contrast, the *n*BuLi reaction necessitated a mixture of MTBE and anisole, which can present challenges during isolation due to the high boiling point and poor water solubility of anisole.

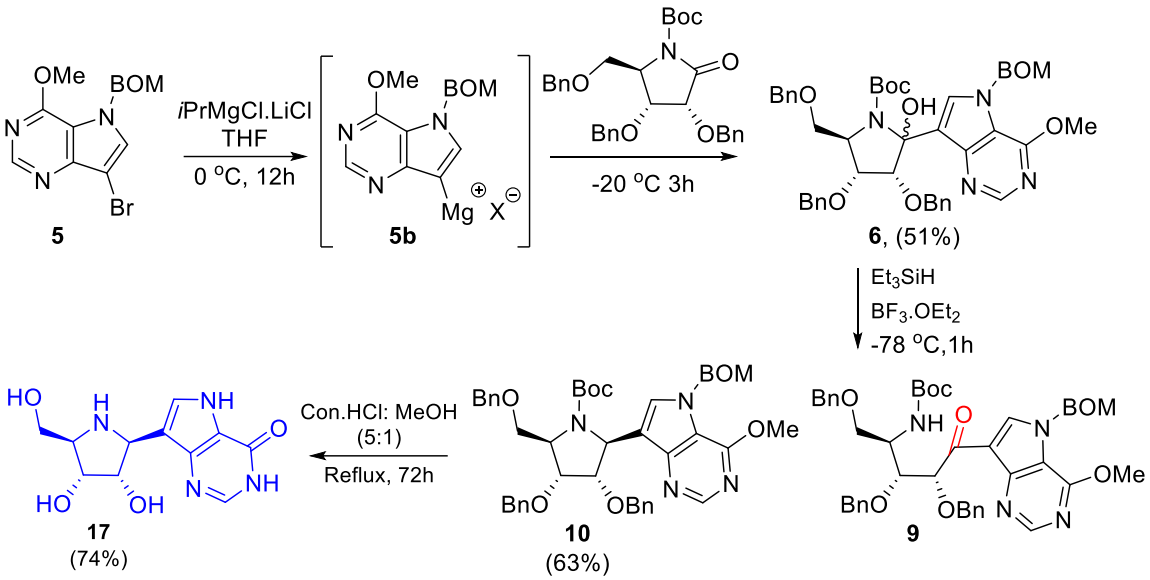

Scheme 3.3.2.1: Cross-coupling using turbo Grignard reagent

Following the successful cross-coupling reaction that delivered the desired hemiaminal intermediate **6**, the application of Kishi reduction conditions using dichloromethane as the solvent at -78 °C afforded the targeted forodesine precursor **10**. This specific condition was chosen based on our previous exploration (Table 3.3.1.3), where it was the only one that preserved the starting material degradation (compound **9**) during attempted cyclization. It is noteworthy that some starting material converted to compound **9** was also observed as a minor byproduct during this reduction step. Finally, global deprotection of compound **10**

was achieved under concentrated hydrochloric acid, furnishing forodesine **17** as the final product in a commendable yield of 74%.

Our method successfully established a novel and efficient synthetic route for forodesine **17**, a key precursor for the antiviral agent galidesivir. The optimized strategy employed a Grignard reaction mediated cross-coupling step, followed by Kishi reduction and global deprotection, ultimately affording forodesine in a good yield. This approach effectively addressed the limitations encountered in previous attempts, offering a more scalable and potentially cost-effective method for forodesine production.

3.3.2.2. Road map to galidesivir

Building upon the successful synthesis of forodesine, further exploration can focus on the conversion of it into galidesivir, the target antiviral agent. Literature reports suggest a potential seven-step route for this transformation as explained in Scheme 3.3.2.2. This approach involves selective protection of the iminosugar nitrogen and hydroxyl functionality with Boc and acetyl groups, respectively. Subsequent chlorination using phosphoryl chloride would furnish intermediate **19**. Finally, a sequence involving azide substitution for the chlorine atom using sodium azide, followed by reduction and global deprotection, could potentially yield galidesivir in a reported overall yield of 25% from forodesine.[3]

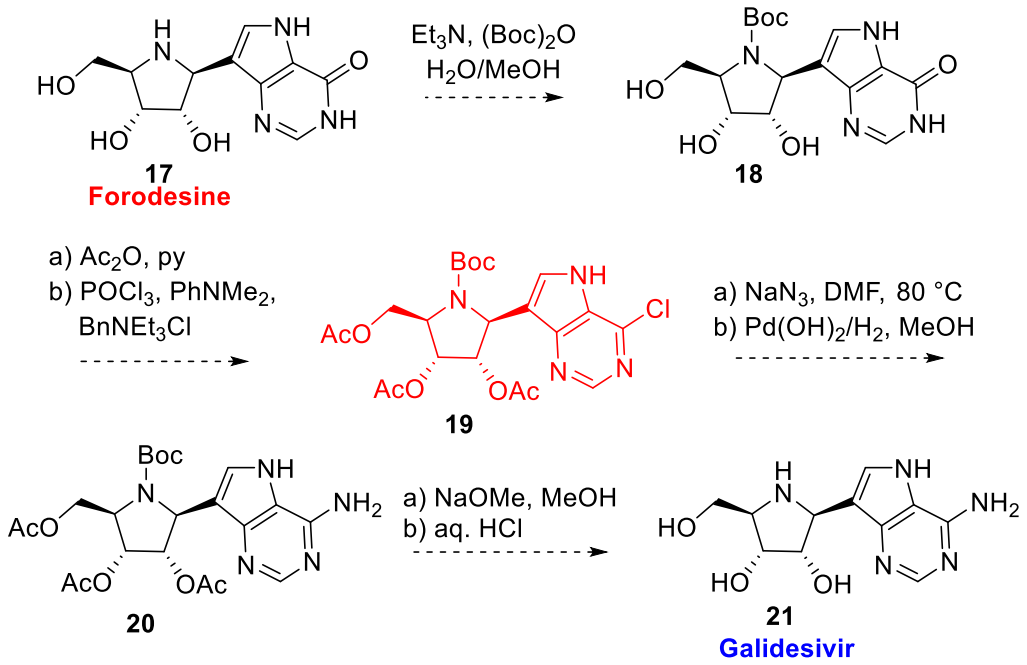

Scheme 3.3.2.2: Synthetic route to galidesivir from forodesine

Intriguingly, upon closer examination of the reported synthetic scheme for galidesivir, a structural similarity was observed between intermediate **19** and our synthesized forodesine precursor (compound **10**). This observation suggests potential opportunities for streamlining the overall synthetic strategy towards galidesivir in future endeavors.

3.3.3. Concept of an advanced intermediate

A comparative analysis of the structural features of forodesine precursor (compound **10**) and intermediate **19** (identified in the galidesivir synthesis pathway) revealed a key difference beyond the protecting groups. While both compounds share identical functional groups and overall framework, compound **19** possesses a chlorine atom on the pyrrolopirimidine ring, whereas compound **10** features a methoxy group at the same position.

Inspired by this observation, we envisioned the potential for a convergent synthetic strategy. By synthesizing a novel intermediate (compound **22**) harboring a chlorine substituent on the pyrrolopirimidine ring similar to compound **19**, we could potentially leverage this intermediate for the synthesis of both forodesine and galidesivir. This advanced intermediate could be obtained through a cross-coupling reaction using a chloro-substituted pyrrolopirimidine coupling partner instead of the methoxy-substituted version employed in the current forodesine synthesis.

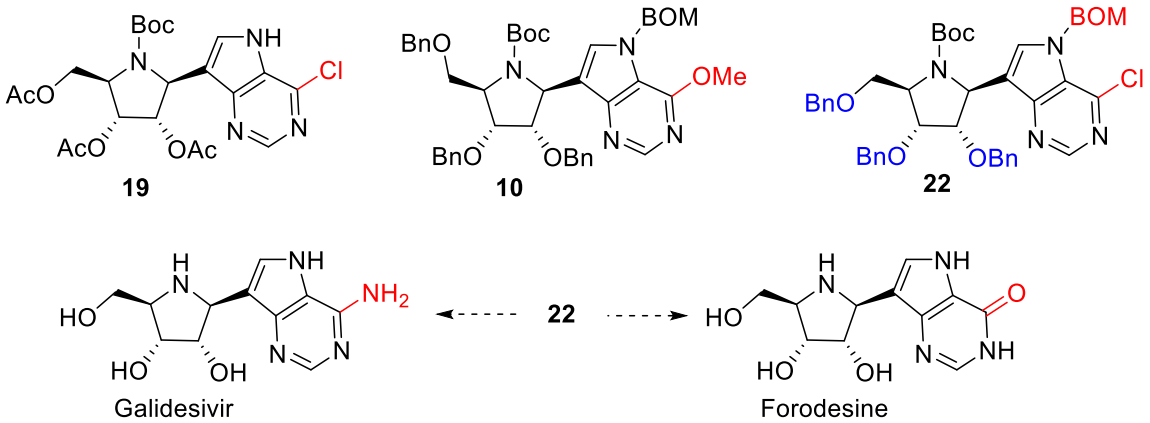

Scheme 3.3.3: Concept of an advanced intermediate **22**

3.3.3.1. Synthesis of pyrrolopirimidine partner for advanced intermediate

To achieve the synthesis of the proposed advanced intermediate **22**, a modified pyrrolopirimidine precursor containing a chlorine substituent in place of the methoxy group is required. To address chemoselectivity concerns during subsequent cross-coupling

reactions, a strategic halogen exchange is planned. Bromine substitution with iodine is envisioned, as iodine undergoes magnesium-halogen exchange more readily compared to chlorine. This selective exchange will ensure that the desired chlorine group on the pyrrolopirimidine ring remains intact for the cross-coupling step.

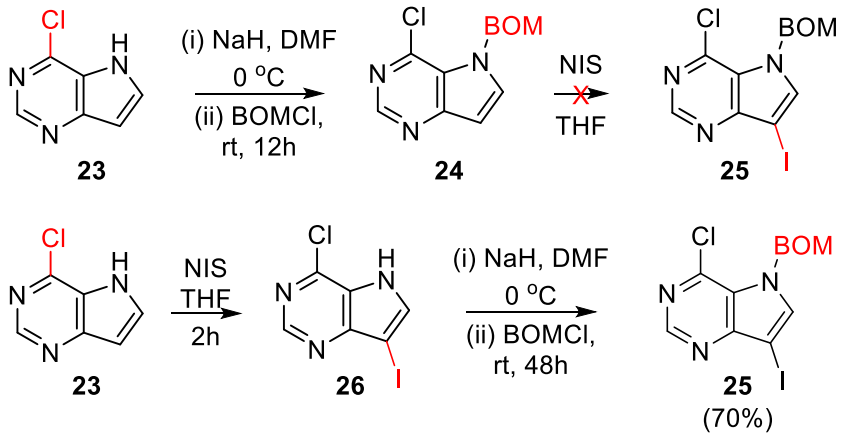

Scheme 3.3.3.1: synthesis of compound **25**

Building upon the pyrrolopirimidine synthesis strategy from the previous chapter, initial attempts focused on protecting the pyrrole nitrogen of compound **23** using BOM chloride to afford intermediate **24**. However, the subsequent reaction of **24** with N-iodosuccinimide failed to yield the desired product (compound **25**). Fortunately, an alternative reaction sequence proved successful. Treatment of compound **23** with NIS resulted in the formation of dihalo intermediate **26**. Subsequent selective BOM protection of the pyrimidine nitrogen in compound **26** furnished the desired compound **25** with a commendable yield of 70%.[20]

3.3.3.2. Synthesis advanced intermediate

Leveraging the successful synthesis of the chlorinated pyrrolopirimidine intermediate **25**, the cross-coupling reaction was explored. Employing the turbo-Grignard reagent (*i*PrMgCl·LiCl solution) at -50 °C facilitated chemoselective metal-halogen exchange at the iodine atom, leaving the chlorine intact. This exchange was significantly faster (5 minutes) compared to the 12-hour reaction time observed for bromine exchange. The resultant Grignard intermediate **25a** was immediately treated with lactam **8** at the same temperature, affording hemiaminal intermediate **27** (Scheme 3.3.3.2a). However, purification of **27** yielded a mixture of separable open-chain and closed-chain products (**28** and **27**, respectively).

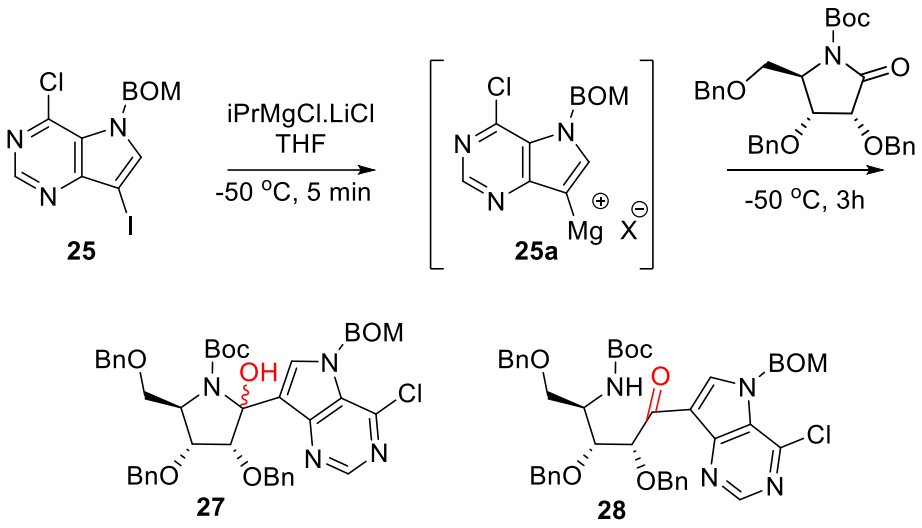

Scheme 3.3.3.2a: Utilisation of compound **25** in cross-coupling

Intriguingly, the closed-chain hemiaminal **27** underwent a stereoselective reaction under Kishi reduction conditions using triethylsilane to furnish the desired pyrrolidine intermediate **22** (advanced intermediate). Unfortunately, this reduction also resulted in the undesired formation of open-chain byproduct **28**. Subsequent attempts to convert the open-chain intermediate **28** into the pyrrolidine product **22** using various reaction conditions, including repeated Kishi reduction attempts and Boc deprotection with trifluoroacetic acid followed by reduction of the resulting imine, were unsuccessful.

Further investigation revealed the inherent instability of hemiaminal **27**, leading to rearrangement into the more stable open-chain product **28** over time. This posed a significant challenge, as our initial strategy relied on the reduction of a stable hemiaminal intermediate. To overcome this obstacle, an alternative approach was devised to achieve the advanced intermediate using the open-chain product **28**. Hence, mesylation of the 2° alcohol, by reduction of ketone for ring-closing to afford pyrrolidine was envisaged. To achieve this, the mixture containing hemiaminal **27** was treated with catalytic $BF_3 \cdot Et_2O$, promoting complete conversion to the open-chain isomer **28**, as confirmed by ^{13}C NMR spectroscopy. Subsequently, Luche reduction conditions were successfully applied to convert the ketone functionality in compound **28** to a secondary alcohol. Treatment of this alcohol with mesyl chloride then facilitated a cyclization reaction, furnishing the desired advanced intermediate **22** along with its C-1' epimer **22a** in a combined yield of 87% (**34**: 77%, **34a**: 10%) over two steps.

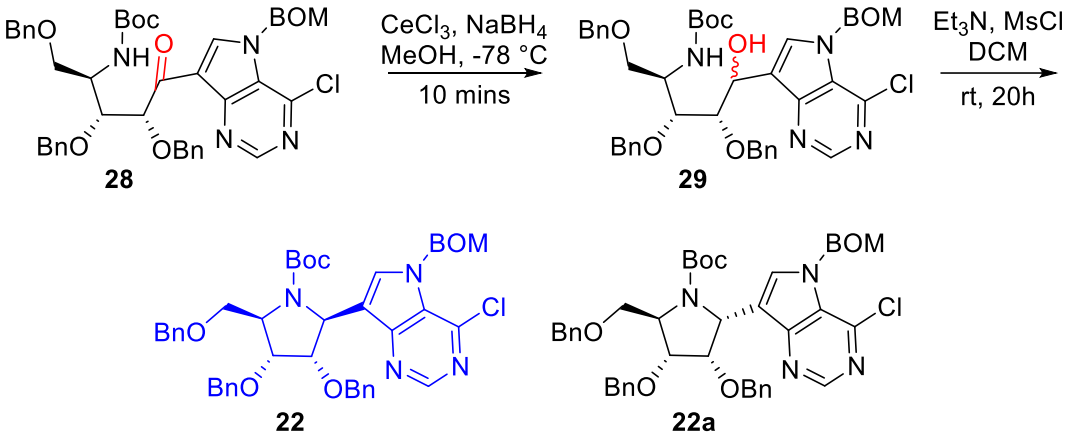

Scheme 3.3.3.2b: Synthesis of advanced intermediate

To determine the stereochemistry at C-1' position, compounds **22** and **22a** were treated with sodium methoxide, and the resulting C-6 methoxy substituted product (**10**) exhibited a specific optical rotation of +56.7°, which was in agreement with the reported value of +56.2°,[15] with the desired '*S*' configuration at C-1' position. The undesired '*R*' configuration at C-1' position (**10a** structure mentioned in Figure 3.5.13) exhibited a specific optical rotation of +20.4°, which was in agreement with the reported value of +21.7°.[15]

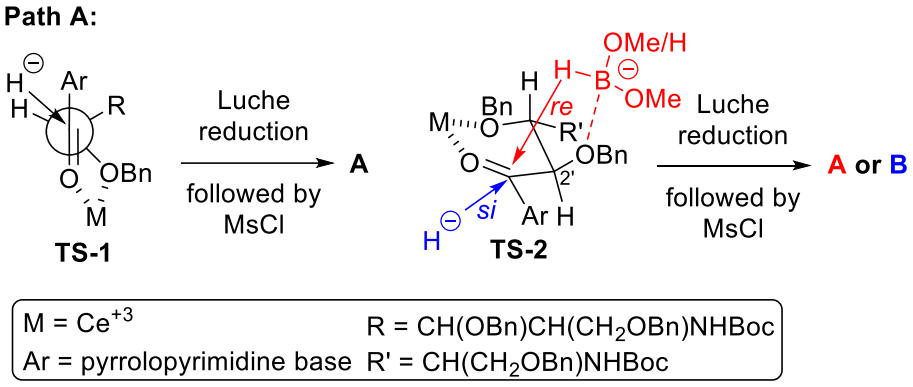

Figure 3.3.3.2a: Plausible pathways for stereoselective formation of compound **29**

Based on the overall addition-reduction-cyclization synthetic strategy for the synthesis of pyrrolidine in literature, *vide supra*, the reduction of ketone by $NaBH_4$ is considered as the stereoselective step, which was explained by transition state models.[21,22] Accordingly, Cram's non-chelation or five-membered or Ce^{3+} chelation model (TS-1, Path A, Figure 3.3.3.2a) favors the formation of mesylate A that leads to undesirable C-1' epimer compound **22a**. In a six-membered Ce^{3+} chelation model (TS-2, Path A, Figure 3.3.3.2a),

hydride attack from *si*-face delivers the formation of desired mesylate B, and subsequent cyclization affords desired compound **22**. However, under Luche reduction conditions, possible coordination of methoxyborohydride with the oxygen atom of C-2' OBn group next to the reaction site to deliver hydride from *re*-face to afford the undesired mesylate A cannot be ruled out, a rationale disregarded in reports involving addition-reduction-cyclization synthetic strategy.

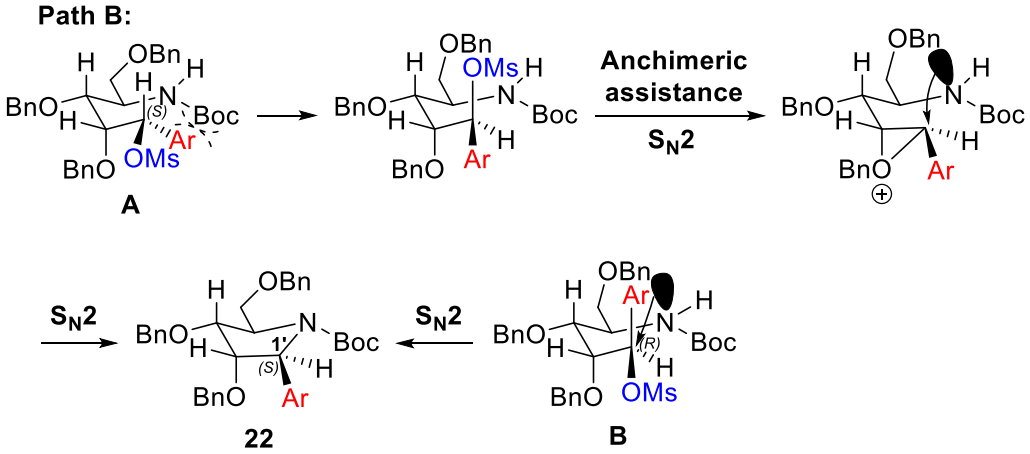

Figure 3.3.3.2b: Plausible pathways for stereoselective formation of compound **22**

Cyclization of mesylate A is hindered by the steric factor, which prompts the positioning of mesylate group (I) to facilitate S_N2 attack by C-2' OBn group by anchimeric assistance (II) and subsequent unhindered and facile S_N2 attack by NHBoc group affords the desired compound **22** (Path B, Figure 3.3.3.2b). On the other hand, an apparent S_N2 attack by NHBoc with mesylate B affords compound **22**.

3.3.3.3. Utilization of advanced intermediate

Building upon the successful synthesis of the key intermediate **22**, further derivatization yielded the target compounds forodesine (Immucillin-H) and galidesivir (Immucillin-A).

Treatment of compound **22** with methoxide afforded a C-6 methoxy substitution product in 70% yield over two steps. Global deprotection was then achieved under concentrated hydrochloric acid, furnishing forodesine (Immucillin-H) (Scheme 3.3.3.3). Alternatively, compound **22** was subjected to C-6 substitution with sodium azide. Subsequent reduction using palladium hydroxide under a hydrogen atmosphere ($Pd(OH)_2/H_2$) in methanol for three days facilitated global deprotection. Finally, treatment with 5N hydrochloric acid yielded galidesivir (Immucillin-A) in an overall yield of 59% over three steps.

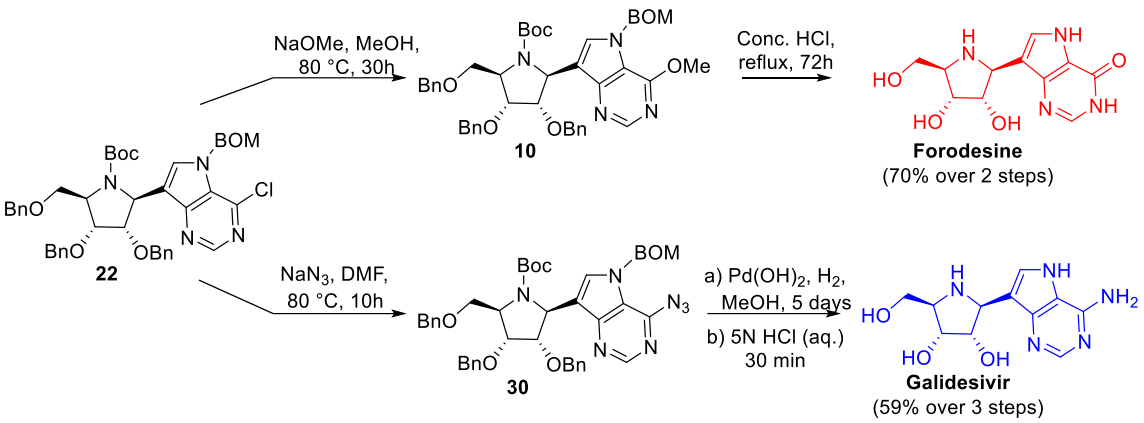

Scheme 3.3.3.3: Utilization of advanced intermediate **22**

Finally, a standalone process for synthesizing Immucillin-H and Immucillin-A from a common intermediate is described against the existing routes that rely on Immucillin-H as the starting material for the synthesis of Immucillin-A. An addition-reduction-cyclization synthetic strategy was undertaken to afford the common intermediate, with chemoselective and stereoselective steps. We proposed the role of anchimeric assistance for stereoselectivity that facilitates even the undesired mesylate to afford the desired configuration of compound **22** at the C-1' position. The advanced common intermediate offers an opportunity to vary the chloro substituent in the C-6 position with other nucleophiles to afford novel immucillin derivatives.

3.4. Conclusions

This chapter describes a novel and efficient synthetic route for forodesine (Immucillin-H) and the antiviral agents galidesivir (Immucillin-A). The approach leverages a convergent strategy utilizing a γ-lactam for cross-coupling. A key innovation involved overcoming the challenges associated with the electrophilic nature of the lactam carbonyl group. This hurdle was addressed by employing a Boc protecting group on the lactam nitrogen, which doesn't serve as a mere protecting group but as an activating group to promote cross-coupling. Furthermore, the study demonstrates the advantages of the turbo-Grignard reagent over conventional *n*BuLi for this reaction, offering chemoselectivity and compatibility with THF as a solvent.

The most significant contribution lies in the development of a unified intermediate (advanced intermediate **22**) for the synthesis of both forodesine and galidesivir. Existing

methods rely on forodesine as the starting material for galidesivir production. This work establishes a streamlined process bypassing this limitation. The unified intermediate is efficiently obtained through a chemoselective and stereoselective addition-reduction-cyclization strategy. Notably, the proposed role of anchimeric assistance in this strategy offers a potential explanation for the observed stereoselectivity, even when an undesired intermediate forms.

Finally, the presence of a strategically placed chlorine group in the advanced intermediate allows for further derivatization using various nucleophiles. This opens exciting avenues for the exploration of novel immucillin derivatives with potential therapeutic applications.

3.5. Materials and methods

3.5.1. General experimental conditions

^{1}H and ^{13}C NMR spectra were obtained using a Bruker ASCEND^{TM}-500 spectrometer at 500 and 125 MHz, respectively. $CDCl_3$, CD_3OD, D_2O and DMSO-D6 solvents were used to record the spectra. The NMR data is presented as chemical shifts in ppm (δ) along with integration, coupling constant in Hz, and multiplicity (s = singlet, bs= broad singlet, d = doublet, t = triplet, m = multiplet, dd = doublet of doublet, etc.). The HR-ESI-MS analysis was performed on a Thermo Scientific Exactive-LCMS instrument using the electrospray ionization method. The ions are reported in m/z using an Orbitrap analyzer. Optical rotation was measured on a JASCO P-2000 polarimeter. The reactions were monitored by silica gel G-60 F_{254} aluminum TLC plates, and the compounds were made visible by a short wavelength lamp; the TLC plate was charred after spraying with 15% sulfuric acid in ethanol. Chromatographic separations were carried out by conventional column chromatography on silica gel (100 - 200 mesh) and C-18 column. The reagents were purchased at the highest commercial quality and used without further purification.

3.5.2. Other experimental procedures

***tert*-butyl(3R,4R,5R)-3,4-bis(benzyloxy)-5-((benzyloxy)methyl)-2-(5-((benzyloxy) methyl)-4-methoxy-5H-pyrrolo[3,2-d]pyrimidin-7-yl)-2-hydroxypyrrolidine-1-carboxylate (6):** Thoroughly dried compound **5** (2.8 g, 8.05 mmol, 1.5 equiv.) was taken in a 100 mL round-bottomed flask and dissolved in dry THF (25 mL) under argon atmosphere. The solution was cooled to 0 °C and 1.3 M *i*PrMgCl·LiCl solution in THF (9.3

mL, 12.08 mmol, 2.25 equiv.) was transferred using a cannula and stirred for 12 hours. After metal halogen exchange, the solution was cooled to -20 °C then the lactam **8** (2.78 g, 5.37 mmol, 1 equiv.) in 8 mL of THF was transferred *via* cannula and the stirring was continued at -20 °C. After 3 hours, the reaction mixture was quenched with 5 mL of MeOH and was allowed to warm to room temperature. The reaction mixture was partitioned between EtOAc (150 mL) and distilled water (150 mL). The aqueous layer was extracted with EtOAc (100 mL x 2) and the combined organic layers were dried over anhydrous Na_2SO_4, and concentrated under reduced pressure. The resulting crude pale yellow colored syrup was purified using silica gel column chromatography (EtOAc/hexane) to obtain compound **6** as a colorless viscous liquid (2.15 g, 51% yield). ^{1}H-NMR ($CDCl_3$) δ 8.54 (1H, s), 7.27 (20H, m), 5.64 (2H, s), 5.18 (1H, m), 4.80 (2H, m), 4.39 (5H, m), 4.18 (3H, m), 4.02 (6H, m), 3.63 (1H, m), 1.38 (4H, s), 1.17 (5H, s) ppm; ^{13}C NMR ($CDCl_3$) δ 156.43, 151.04, 148.48, 138.32, 138.05, 136.51, 131.55, 128.53, 128.38, 128.23, 128.14, 128.02, 127.71, 127.59, 115.60, 92.46, 76.91, 71.41, 70.44, 69.73, 60.71, 53.91, 53.42, 28.48, 28.31 ppm; HR-ESI-MS: $[M+H]^+$ calculated for $C_{46}H_{51}N_4O_8$ was m/z 787.3701, found 787.3693

***tert*-butyl(2R,3R,4R)-3,4-bis(benzyloxy)-2-((benzyloxy)methyl)-5-oxopyrrolidine-1-carboxylate (8):** The compound **2** (3.60 g, 8.83 mmol, 1 equiv.) was dissolved in DCM (50 mL), added $(Boc)_2O$ (3.85 g, 17.65 mmol, 2 equiv.), Et_3N (2.7 mL, 19.41 mmol, 2.2 equiv.) and DMAP (0.11 g, 0.88 mmol, 0.1 equiv.), and stirred at room temperature. The reaction mixture was quenched with water (50 mL), and the product was extracted in DCM (250 mL). The organic layer was dried using anhydrous Na_2SO_4, concentrated under reduced pressure, and purified using silica gel column chromatography (10% EtOAc in hexane to 30% EtOAc in hexane) to obtain compound **8** as a colorless viscous liquid (4.46 g, 99% yield). ^{1}H-NMR (500 MHz, $CDCl_3$) δ 7.42 (2H, d, *J*=7.34 Hz), 7.35 (11H, m), 7.17 (2H, d, *J*=6.97 Hz), 5.05 (1H, d, *J*=12.16 Hz), 4.81 (2H, m), 4.67 (1H, d, *J*=12.07 Hz), 4.52 (1H, d, J=4.93 Hz), 4.45 (2H, s), 4.23 (1H, s), 4.09 (1H, d, *J*=5.05 Hz), 3.68 (1H, dd, *J*=3.68, 10.00 Hz), 3.57 (1H, d, *J*=9.97 Hz), 1.55 (9H, s) ppm; ^{13}C NMR (125 MHz, $CDCl_3$) δ 171.5, 149.9, 137.7, 137.6, 137.3, 128.5, 128.49, 128.45, 128.0, 127.93, 127.90, 127.5, 83.3, 76.88, 74.8, 73.4, 72.8, 72.3, 68.0, 60.9, 28.0 ppm; HR-ESI-MS: $[M+Na]^+$ calculated for $C_{31}H_{35}NO_6Na$ was m/z 540.2362, found 540.2377.

***tert*-butyl((2R)-1,3,4-tris(benzyloxy)-5-(5-((benzyloxy)methyl)-4-methoxy-5H pyrrolo [3,2-d]pyrimidin-7-yl)-5-oxopentan-2-yl)carbamate (9):** Thoroughly dried compound **5** (1.21 g, 3.48 mmol, 1.5 equiv.) was taken in a 100 mL round-bottomed flask and dissolved

in dry MTBE: Anisole (4:1, 20 mL) under argon atmosphere. The solution was cooled to -78 °C, and 2 M *n*BuLi solution in cyclohexane (2.6 mL, 5.22 mmol, 2.25 equiv.) was transferred using a cannula. After 5 min, lactam **8** (1.2 g, 2.32 mmol, 1 equiv.) in 5 mL of MTBE: Anizole(4:1) was transferred *via* cannula and the stirring was continued at -78 °C. After 3 hours, the reaction mixture was quenched with 15 mL of saturated NH_4Cl solution and was allowed to warm to room temperature. The reaction mixture was partitioned between EtOAc (100 mL) and distilled water (100 mL). The aqueous layer was extracted with EtOAc (100 mL x 2) and the combined organic layers were dried over anhydrous Na_2SO_4, and concentrated under reduced pressure. The resulting crude pale yellow colored syrup was purified using silica gel column chromatography (EtOAc/hexane) to obtain compound **9** as a colorless viscous liquid (401 mg, 22% yield). ^{1}H-NMR ($CDCl_3$) δ 8.61 (1H, s), 8.03 (1H, s), 7.18 (20H, m), 5.56 (2H, d, *J*=9.95 Hz), 5.37 (2H, d, *J*=10.10 Hz), 4.62 (1H, d, *J*=11.41 Hz), 4.46 (3H, m), 4.31 (5H, m), 4.19 (1H, s), 4.05 (3H, s), 3.59 (2H, m), 1.27 (9H, s) ppm; ^{13}C NMR ($CDCl_3$) δ 193.74, 156.66, 152.11, 138.45, 138.23, 137.71, 136.27, 128.55, 128.31, 128.18, 128.14, 128.06, 127.75, 127.72, 127.65, 127.37, 127.31, 115.88, 83.42, 79.39, 78.92, 77.61, 72.62, 70.54, 69.29, 53.91, 51.24, 28.37, 27.44 ppm; HR-ESI-MS: $[M+H]^+$ calculated for $C_{46}H_{51}N_4O_8$ was m/z 787.3701, found 787.3693.

***tert*-butyl(2R,3R,4S,5S)-3,4-bis(benzyloxy)-2-((benzyloxy)methyl)-5-(5-((benzyloxy) methyl)-4-methoxy-5H-pyrrolo[3,2-d]pyrimidin-7-yl)pyrrolidine-1-carboxylate (10):** Compound **6** (200 mg, 0.25 mmol) dissolved in freshly distilled dry DCM (5 mL) under argon atmosphere. The solution was then cooled to -78 °C using an ice bath and Et_3SiH (121 µL, 0.76 mmol, 3 equiv.) and $BF_3.Et_2O$ (47 µL, 0.38 mmol, 1.5 equiv.) was added dropwise and stirred for 20 mins. The reaction mixture was quenched by adding saturated aqueous $NaHCO_3$ solution (10 mL), and extracted in EtOAc (50 mL). The organic layer was dried over anhydrous Na_2SO_4, and concentrated under reduced pressure to obtain an off-white flaky solid **10** (123 mg 63% yield); ^{1}H-NMR ($CDCl_3$) δ 8.44 (1H, s), 7.39 (3H, m), 7.14 (17H, m), 5.28 (3H, m), 4.78 (2H, m), 4.36 (4H, m), 4.11 (9H, m), 3.63 (1H, m), 1.38 (4H, s), 1.17 (5H, s) ppm; ^{13}C NMR ($CDCl_3$) δ 156.07, 155.39, 155.02, 149.65, 149.60, 148.95, 138.59, 138.28, 138.01, 137.15, 137.00, 132.36, 132.23, 128.69, 128.39, 128.26, 128.17, 128.08, 128.01, 127.91, 127.75, 127.62, 117.05, 116.08, 115.71, 115.50, 80.04, 79.54, 78.90, 77.54, 76.89, 76.17, 73.37, 73.28, 71.36, 71.24, 71.03, 69.73, 67.97, 67.60, 60.67, 58.24, 58.13, 53.48, 28.49, 28.32 ppm; HR-ESI-MS: $[M+H]^+$ calculated for $C_{46}H_{51}N_4O_7$ was m/z 771.3752, found 771.3786.

Synthesis of compound 10/10a: To a solution of compound **22** or C1' epimer **22a** (0.2 g, 0.26 mmol) in MeOH (3 mL) was added NaOMe (0.07 g, 1.29 mmol, 5 equiv.) and heated under reflux. After 30 hours, the solvent was completely evaporated and the residue was partitioned between DCM (25 mL) and distilled water (25 mL). The organic layer was washed with brine (25 mL) and dried over anhydrous Na_2SO_4, concentrated and purified by silica gel column chromatography (40% EtOAc in hexane to 50% EtOAc in hexane) to afford compound **10** or **10a** as a colorless viscous liquid.

***tert*-butyl(2R,3R,4S,5R)-3,4-bis(benzyloxy)-2-((benzyloxy)methyl)-5-(5-((benzyloxy) methyl)-4-methoxy-5H-pyrrolo[3,2-d]pyrimidin-7-yl)pyrrolidine-1-carboxylate(10a):** ^{1}H-NMR ($CDCl_3$) δ 8.54 (1H, s), 7.24 (20H, m), 5.68 (2H, m), 5.27 (1H, m), 4.88 (2H, m), 4.71 (1H, m), 4.58 (3H, m), 4.45 (3H, m), 4.32 (2H, m), 4.11 (3H, m), 3.97 (1H, d, *J*=7.86 Hz), 3.76 (1H, d, *J*=9.05 Hz), 1.28 (5H, s), 1.14 (4H, s) ppm; ^{13}C NMR ($CDCl_3$) δ 156.07, 154.13, 149.89, 149.65, 138.79, 138.67, 138.56, 136.80, 130.32, 129.51, 128.43, 128.18, 128.16, 128.10, 127.79, 127.73, 127.49, 127.35, 118.39, 116.39, 116.06, 82.80, 81.88, 79.87, 77.46, 73.18, 72.85, 72.47, 72.20, 72.02, 70.65, 70.21, 69.23, 58.30, 57.87, 53.46, 29.70, 28.43, 28.16 ppm; HR-ESI-MS: $[M+H]^+$ calculated for $C_{46}H_{51}N_4O_7$ was m/z 771.3752, found 771.3786.

***tert*-butyl(2R,3R,4S,5S)-3,4-bis(benzyloxy)-2-((benzyloxy)methyl)-5-(5-((benzyloxy) methyl)-4-chloro-5H-pyrrolo[3,2-d]pyrimidin-7-yl)pyrrolidine-1-carboxylate (22):** To compound **28** (1.45 g, 1.83 mmol, 1 equiv.) in MeOH (25 mL), $CeCl_3$ (0.68 g, 2.74 mmol, 1.5 equiv.) was added and cooled to -78 °C, and sodium borohydride (0.17 g, 4.58 mmol, 2.5 equiv.) was added and stirred for 10 mins. The reaction mixture was quenched with 1 M NaH_2PO_4 (20 mL) and extracted in DCM (100 mL x 3). The organic layer was dried over anhydrous Na_2SO_4, and passed through a silica plug to yield 1.4 g (96.3%) of the reduced product as a colorless viscous liquid. The reduced product was dissolved in dry DCM (30 mL) and cooled to 0 °C, and added triethylamine (1.72 mL, 12.35 mmol, 7 equiv.), mesyl chloride (0.82 mL, 10.58 mmol, 6 equiv.) was added dropwise into the reaction mixture by maintaining an inert argon atmosphere. The reaction mixture was allowed to warm to room temperature and stirred. After 20 hours, the reaction mixture was quenched with saturated aqueous NH_4Cl (100 mL), and extracted in DCM (100 mL x 3). The organic layer was washed with distilled water (2 x 50 mL), and brine (50 mL). Concentration of organic layer and purification by silica gel column chromatography (20% EtOAc in hexane to 30% EtOAc in hexane) afforded a separable mixture of compound **22** as a colorless viscous

liquid (1.09 g, 76.8% yield over 2 steps), and C1' epimer **22a**. as a colorless viscous liquid (0.14 g, 9.9% yield over 2 steps), culminating in an 8:1 ratio of compound **22** and its C1' epimer **22a**. ^{1}H-NMR (500 MHz, $CDCl_3$) δ 8.73 (1H, d, *J*=9.41 Hz). 7.69-7.60 (1H, m), 7.48-7.43 (2H, m), 7.28-7.19 (18H, m), 5.56 (1H, s), 5.38 (1H, d, *J*=10.67 Hz), 5.10-5.27(1H, m), 4.94-4.78 (2H, m), 4.42-4.52 (3H, m), 4.31-4.03 (7H, m), 3.70-3.76 (1H, m), 1.50 (5H, s), 1.26 (4H, s) ppm; ^{13}C NMR (125 MHz, $CDCl_3$) δ 155.3, 154.8, 150.5, 149.8, 149.7, 142.2, 138.4, 138.1, 138.0, 137.9, 136.6, 136.4, 136.2, 128.4, 128.2, 128.19, 128.12, 127.98, 127.92, 127.76, 127.70, 127.5, 124.2, 124.0, 116.9, 115.9, 80.2, 79.7, 78.7, 76.5, 76.3, 76.0, 73.5, 73.3, 71.4, 71.3, 71.1, 69.8, 68.0, 67.6, 60.7, 57.8, 28.4, 28.3 ppm; HR-ESI-MS: $[M+H]^+$ calculated for $C_{45}H_{48}ClN_4O_6$ was m/z 775.3262, found 775.3269.

5-((benzyloxy)methyl)-4-chloro-7-iodo-5H-pyrrolo[3,2-d]pyrimidine (25): To compound **23** (1.15 g, 7.46 mmol), anhydrous THF (25 mL) and *N*-Iodosuccinimide (1.68 g, 7.46 mmol, 1 equiv.) were added and stirred the reaction mixture by protection from light. After 2 hours, the reaction mixture was partitioned between EtOAc (50 mL) and distilled water (50 mL). The organic layer was washed with distilled water (2 x 30 mL) and finally with brine (50 mL). The organic layer was dried over anhydrous Na_2SO_4, and concentrated under reduced pressure to yield pale yellow colored solid **26** which was directly used for the next step considering 100% yield. The solid was dissolved in anhydrous DMF (30mL), cooled to 0 °C and NaH (60% suspension in mineral oil, 0.45 g, 11.17 mmol, 1.5 equiv.) was added to the stirring reaction mixture by maintaining an inert argon atmosphere. After one hour, benzylchloromethyl ether (1.56 mL, 11.17 mmol, 1.5 equiv) was added to the reaction mixture dropwise, and allowed to stir for 48 hours at room temperature. The reaction mixture was quenched by adding ice, and the product was extracted using EtOAc (100 mL). The organic layer was washed with distilled water (5 x 50 mL) to remove DMF, and dried over anhydrous Na_2SO_4, and concentrated under reduced pressure. Silica gel column purification (20% EtOAc in hexane to 30% EtOAc in hexane) of the crude yellow syrup afforded the compound **25** as a white crystalline solid (2.1 g, 70% yield over 2 steps), and 67% overall yield over 3 steps from 9-deazahypoxanthine. ^{1}H-NMR (500 MHz, $CDCl_3$) δ 8.85 (1H, s), 7.66 (1H, s), 7.28-7.32 (3H, m), 7.25 (2H, d, *J*=7.46 Hz), 5.86 (2H, s), 4.57 (2H, s) ppm; ^{13}C NMR (125 MHz, $CDCl_3$) δ 153.1, 151.0, 142.9, 140.1, 135.9, 128.5, 128.3, 127.6, 124.2, 76.9, 70.8, 59.4 ppm; HR-ESI-MS: $[M+H]^+$ calculated for $C_{14}H_{12}ClIN_3O$ was m/z 399.9714, found 399.9717.

5-((benzyloxy)methyl)-4-chloro-5H-pyrrolo[3,2-d]pyrimidine (deiodo-25): ^{1}H-NMR ($CDCl_3$) δ 8.67 (1H, s), 7.49 (1H, d, *J*=3.11 Hz), 7.22 (5H, m), 6.68 (1H, d, *J*=3.10 Hz), 5.77 (2H, s), 4.44 (2H, s) ppm; ^{13}C NMR ($CDCl_3$) δ 153.31, 150.44, 142.65, 136.86, 136.27, 128.59, 128.22, 127.73, 124.02, 103.86, 76.58, 70.36 ppm; HR-ESI-MS: $[M+H]^+$ calculated for $C_{14}H_{13}ClN_3O$ was m/z 274.0742, found 274.0755.

***tert*-butyl((2R,3R,4R)-1,3,4-tris(benzyloxy)-5-(5-((benzyloxy)methyl)-4-chloro-5H-pyrrolo[3,2-d]pyrimidin-7-yl)-5-oxopentan-2-yl)carbamate (28):** Thoroughly dried compound **25** (1.9 g, 4.78 mmol, 1.5 equiv.) was taken in a 100 mL round-bottomed flask and dissolved in dry THF (20 mL) under argon atmosphere. The solution was cooled to -50 °C and 1.3 M *i*PrMgCl·LiCl solution in THF (3.67 mL, 4.78 mmol, 1.5 equiv.) was transferred using a cannula. After 10 min, lactam **5** (1.65 g, 3.18 mmol, 1 equiv.) in 5 mL of THF was transferred *via* cannula and the stirring was continued at -50 °C. After 3 hours, the reaction mixture was quenched with 2 mL of MeOH and was allowed to warm to room temperature. The reaction mixture was partitioned between EtOAc (200 mL) and distilled water (200 mL). The aqueous layer was extracted with EtOAc (100 mL x 3) and the combined organic layers were dried over anhydrous Na_2SO_4, and concentrated under reduced pressure. The resulting crude pale yellow colored syrup was dried under vacuum, dissolved in DCM (25 mL), and cooled to -20 °C under argon atmosphere. Catalytic amount of $BF_3.OEt_2$ was added, after 30 min, the reaction mixture was quenched by adding saturated aqueous $NaHCO_3$ solution (10 mL), and extracted in EtOAc (150 mL). Organic layers were dried over anhydrous Na_2SO_4, and concentrated under reduced pressure. Silica gel column purification (30% EtOAc in hexane to 40% EtOAc in hexane) of the crude pale yellow colored syrup afforded 1.63 g of compound **28** as a colorless viscous liquid in 79% yield (yield calculated on the basis of isolated compound **28** and recovered lactam **5** (0.29 g). ^{1}H-NMR (500 MHz, $CDCl_3$) δ 8.90 (1H, s), 8.28 (1H, s), 7.39 (2H, d, *J*=7.01 Hz), 7.32-7.26 (10H, m,), 7.21-7.18 (7H, m), 7.12 (2H, br s), 5.76 (1H, d, *J*=10.68 Hz), 5.47 (1H, d, *J*=10.70 Hz). 5.43 (1H, d, *J*=8.45 Hz), 5.35 (1H, br s), 4.71 (1H, d, *J*=11.37 Hz), 4.61-4.54 (1H, m), 4.46-4.39 (5H, m), 4.27 (1H, s), 3.73-3.70 (1H, m), 3.67-3.64 (1H, t, *J*=7.48 Hz), 1.34 (9H, s) ppm; ^{13}C NMR (125 MHz, $CDCl_3$) δ 193.2, 155.7, 152.0, 150.5, 143.7, 141.7, 138.2, 137.9, 137.5, 135.8, 128.6, 128.4, 128.3, 128.2, 128.15, 128.12, 127.9, 127.7, 127.6, 127.48, 127.45, 127.3, 124.3, 116.2, 83.7, 79.5, 79.1, 77.3, 72.9, 72.7, 72.6, 70.7, 69.1, 51.1, 28.3 ppm; HR-ESI-MS: $[M+Na]^+$ calculated for $C_{45}H_{47}ClN_4O_7Na$ was m/z 813.3031, found 813.3027.

***tert*-butyl(2S,3S,4R,5R)-2-(4-azido-5-((benzyloxy)methyl)-5H-pyrrolo[3,2-d]pyrimidin-7-yl)-3,4-bis(benzyloxy)-5-((benzyloxy)methyl)pyrrolidine-1-carboxylate (30):** ^{1}H-NMR ($CDCl_3$) δ 9.34 (1H, s), 7.23 (20H, m), 5.64 (2H, m), 5.35 (2H, m), 4.83 (3H, m), 4.50 (5H, m), 4.39 (2H, m), 4.25 (4H, m), 4.05 (1H, m), 3.74 (1H, m), 1.49 (5H, s), 1.25 (4H, s) ppm; ^{13}C NMR ($CDCl_3$) δ 155.36, 141.72, 138.37, 138.05, 137.93, 137.84, 137.27, 136.60, 130.86, 130.67, 130.48, 128.53, 128.46, 128.35, 128.26, 128.15, 128.09, 127.96, 127.87, 127.79, 127.73, 127.66, 127.52, 119.51, 80.41, 79.85, 79.73, 78.00, 77.78, 76.56, 73.51, 73.37, 71.57, 71.11, 67.89, 60.85, 57.87, 28.48, 28.30 ppm; HR-ESI-MS: $[M+H]^+$ $C_{45}H_{48}N_7O_6$ calculated for m/z 782.3661, found 782.3671.

Forodesine/Immucillin-H: To a solution of compound **22** (0.2 g, 0.26 mmol) in MeOH (3 mL) was added NaOMe (0.07 g, 1.29 mmol, 5 equiv.) and heated under reflux. After 30 hours, the solvent was completely evaporated and the residue was partitioned between DCM (25 mL) and distilled water (25 mL). The organic layer was washed with brine (25 mL) and dried over anhydrous Na_2SO_4, and passed through a small plug of silica to remove polar impurities. The resulting filtrate was concentrated to afford a colorless viscous liquid (0.19 g), dissolved in MeOH (0.5 mL), and added concentrated hydrochloric acid (3 mL). The resulting mixture was heated to boil, after 72 hours, the solvent was removed under reduced pressure to afford a brownish red colored solid, which was dissolved in MeOH (0.5 mL) and diluted with DCM until a white precipitate was obtained. The precipitate was filtered and washed with DCM, and dried to afford 0.055 g of BCX-1777 (70% yield over 2 steps) as a white powder, and an overall yield of 38% from 2,3,5-tri-*O*-benzyl-D-ribonolactone over 10 steps. ^{1}H-NMR (500 MHz, DMSO-d6) δ 12.41 (s, 1H, NH-5), 12.16 (s, 1H, NH-3), 10.30 (s, 1H, NH-1'), 8.35 (s, 1H, NH-1'), 7.93 (s, 1H, H-2), 7.63 (d, *J*=3.10 Hz, 1H, H-6), 5.43 (brs, 3H, 3 x OH), 4.64 (d, *J*=6.90 Hz, 1H, H-2'), 4.47 – 4.44 (m, 1H, H-3'), 4.18 (t, *J*=4.42 Hz, 1H, H-4'), 3.73 (d, *J*=4.90 Hz, 2H, H-6'), 3.48 (q, *J*=4.92 Hz, 1H, H-5') ppm; ^{13}C NMR (125 MHz, DMSO-d6) δ 153.5, 142.8, 142.2, 127.3, 118.1, 109.2, 73.9, 70.4, 65.0, 58.5, 56.5 ppm; HR-ESI-MS: $[M+Na]^+$ calculated for $C_{11}H_{14}N_4O_4Na$ was m/z 289.0913, found 289.0908.

Galidesivir/Immucillin-A: To compound **22** (0.2 g, 0.26 mmol, 1 equiv.) in DMF (3 mL), NaN_3 (0.08 g, 1.29 mmol, 5 equiv.) was added and stirred at 80 °C. After 10 hours, the reaction mixture was cooled to room temperature and poured into ice, and the product was extracted using DCM (3 x 20 mL). The organic layer was washed with distilled water (5 x 60 mL) to remove DMF, and dried over anhydrous Na_2SO_4, and passed through a small

plug of silica to remove polar impurities to afford a colorless viscous liquid (0.18 g), which was dissolved in MeOH (3 mL) and $Pd(OH)_2/C$ (20% w/w) was added (0.2 g). H_2 gas was purged through the reaction mixture for 5 mins and the suspension was stirred for 5 days under H_2 atmosphere. The reaction mixture was filtered through celite (2 g) and the solvent was completely evaporated. To the resulting mixture aqueous 5N HCl (3 mL) was added and stirred at room temperature. After 30 mins, the solvent was evaporated to afford a brown colored solid, which was purified by C18 column chromatography (0.001 M HCl (aq.)) to afford 0.046 g of BCX-4430 (59 % yield over 3 steps) as a white powder, and an overall yield of 32% from 2,3,5-tri-*O*-benzyl-D-ribonolactone over 11 steps. ^{1}H NMR (500 MHz, D_2O) δ 8.32 (s, 1H, H-2), 7.94 (s, 1H, H-8), 4.90 (d, *J*=8.90 Hz, 1H, H-1'), 4.69 (m, 1H, H-2'), 4.37 (dd, *J*=3.57, 4.67 Hz, 1H, H-3'), 3.88 (d, *J*=4.65 Hz, 2H, H-5'), 3.81 (q, *J*=4.24 Hz, 1H, H-4') ppm; ^{13}C NMR (125 MHz, D_2O) δ 149.4, 143.4, 138.1, 132.4, 112.7, 105.0, 73.3, 70.4, 65.6, 58.5, 55.5 ppm; HR-ESI-MS: $[M+H]^+$ calculated for $C_{11}H_{16}N_5O_3$ was m/z 266.1253, found 266.1248.

Figure 3.5.3: NMR spectra of compound **6**

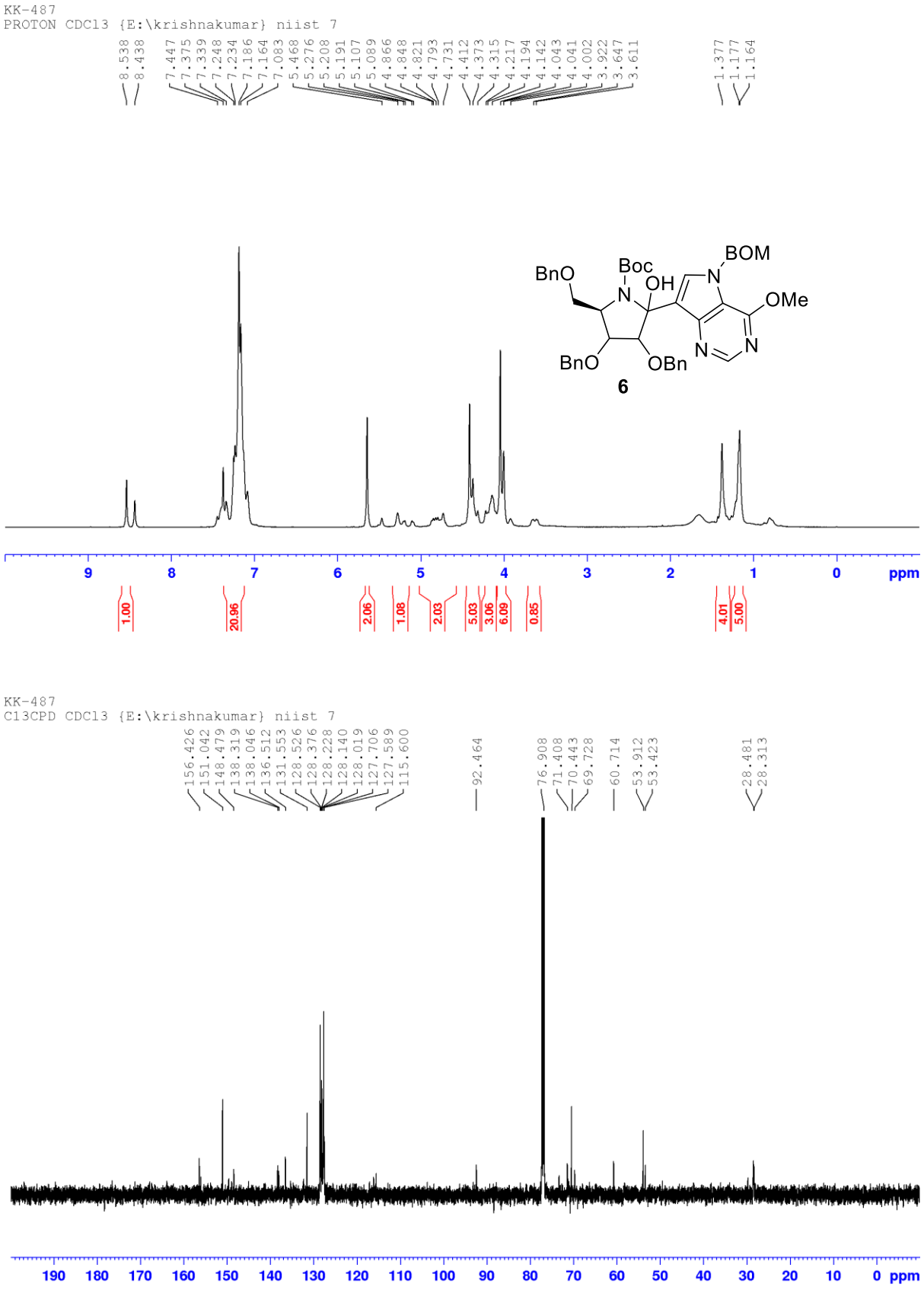

Figure 3.5.4: NMR spectra of compound **8**

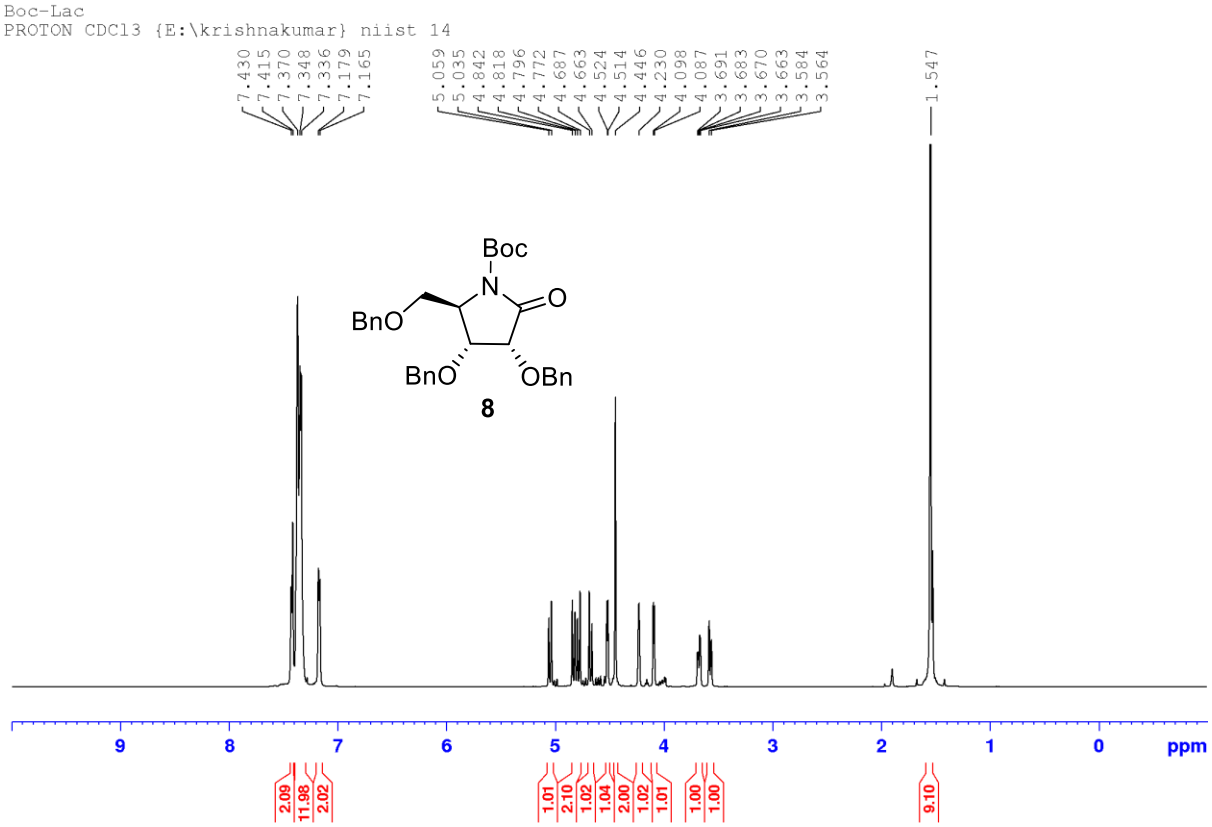

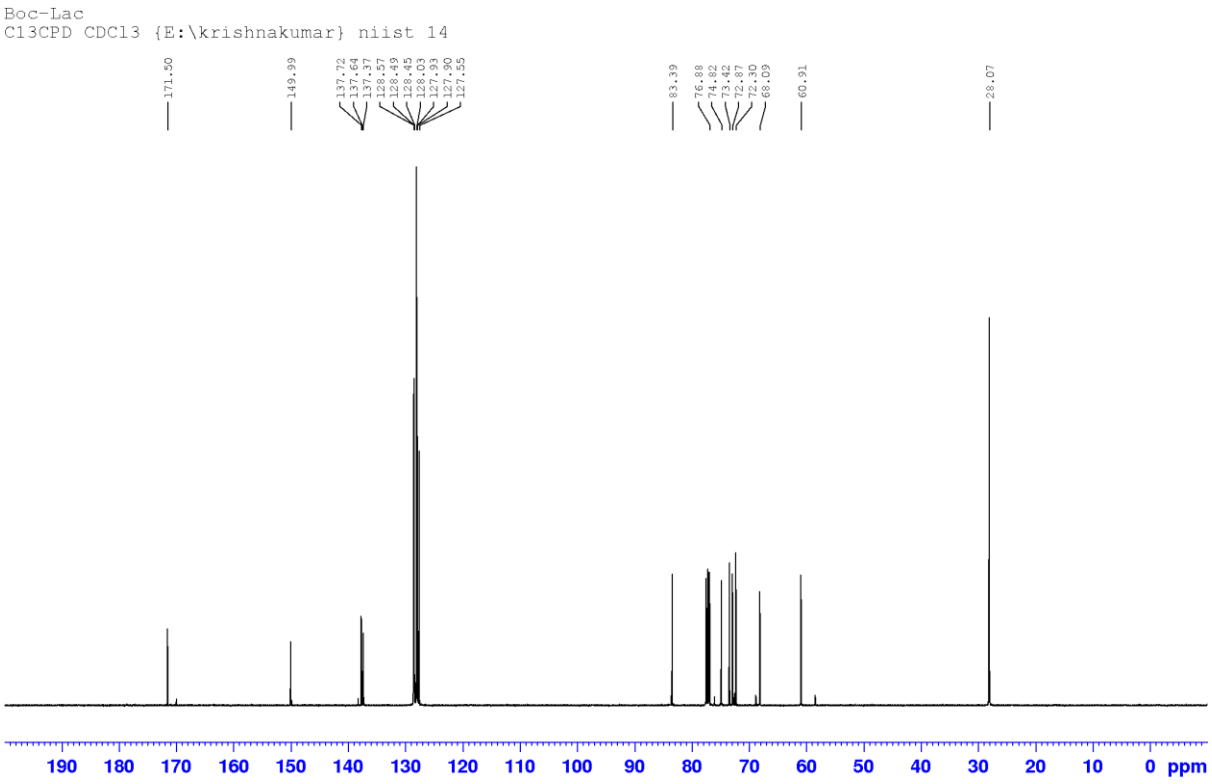

Figure 3.5.5: NMR spectra of compound **9**

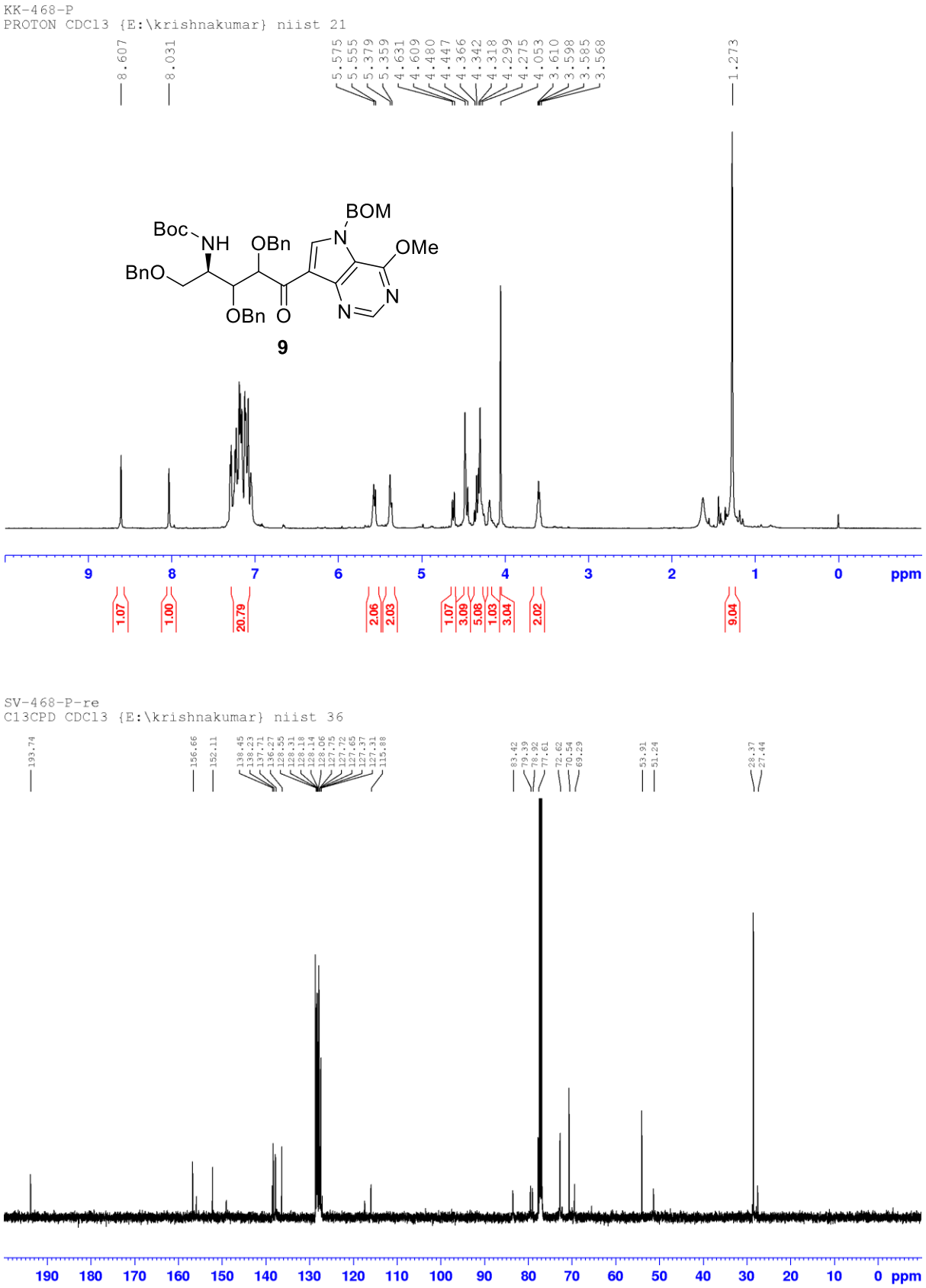

Figure 3.5.6: NMR spectra of compound **10**

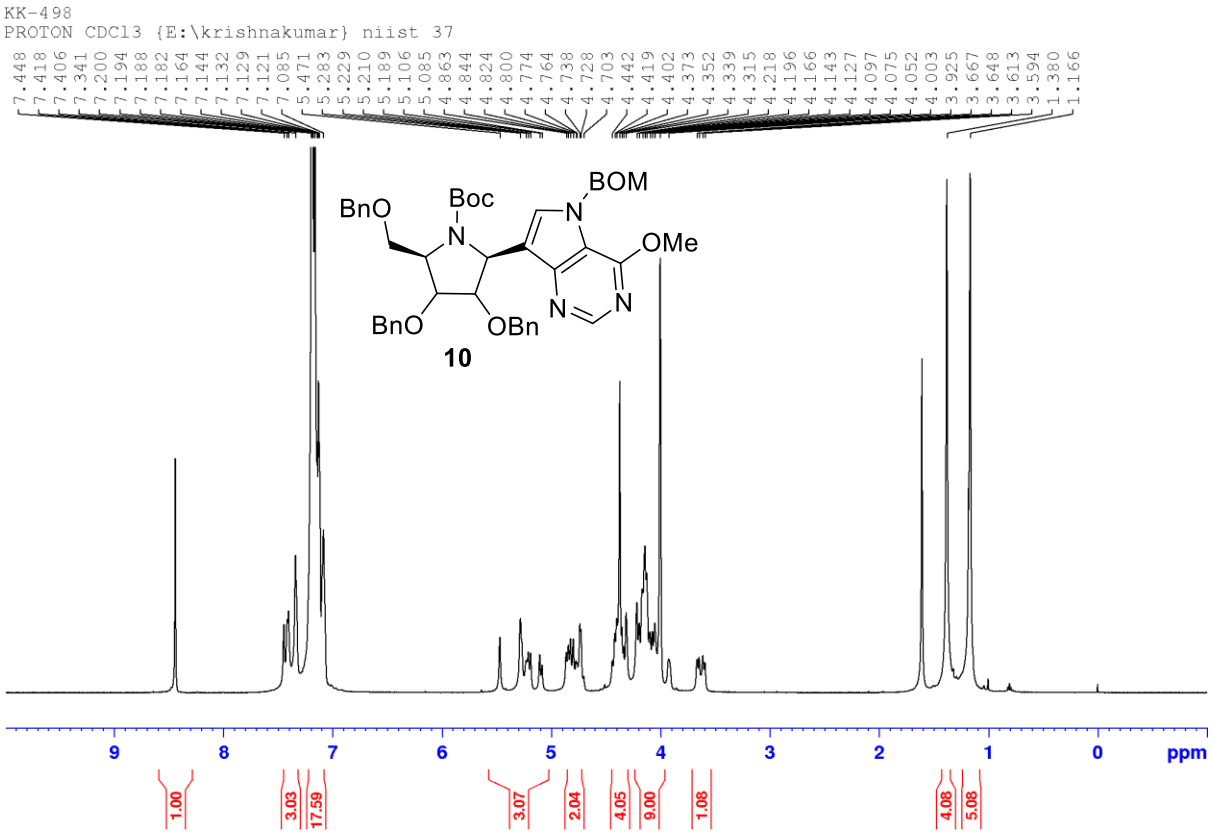

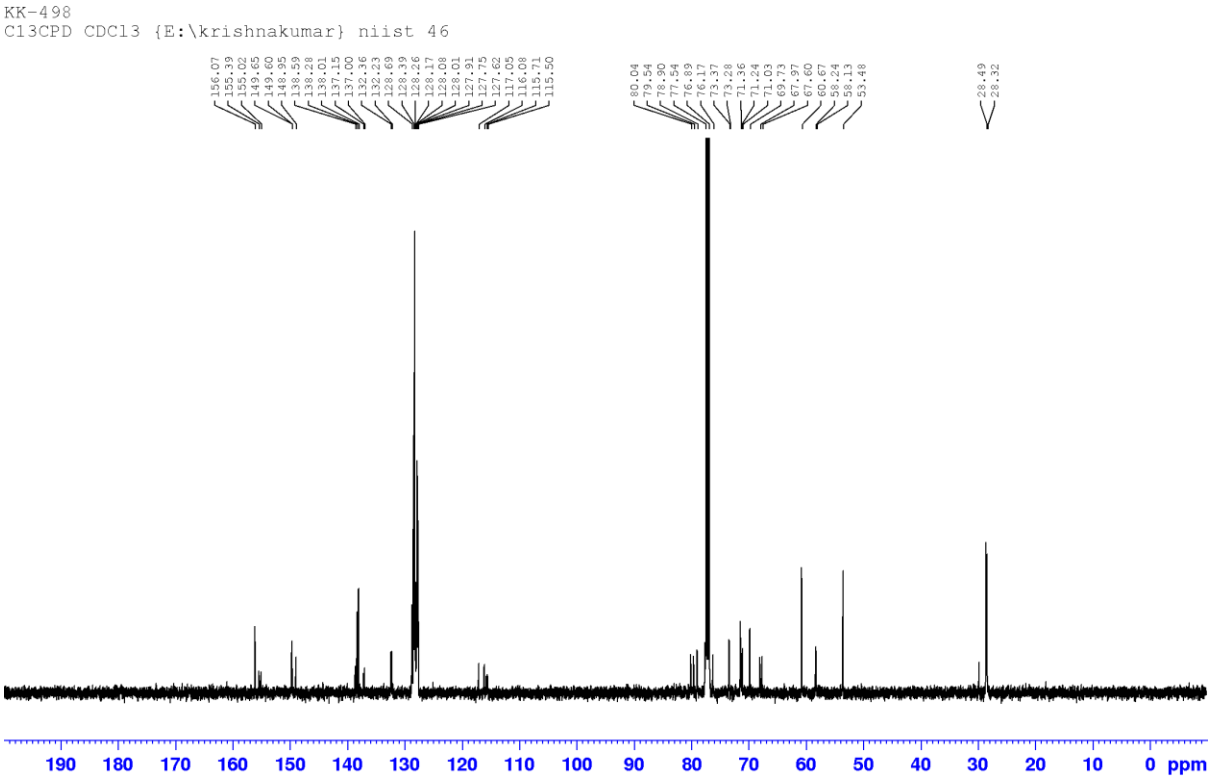

Figure 3.5.7: NMR spectra of compound **10a**

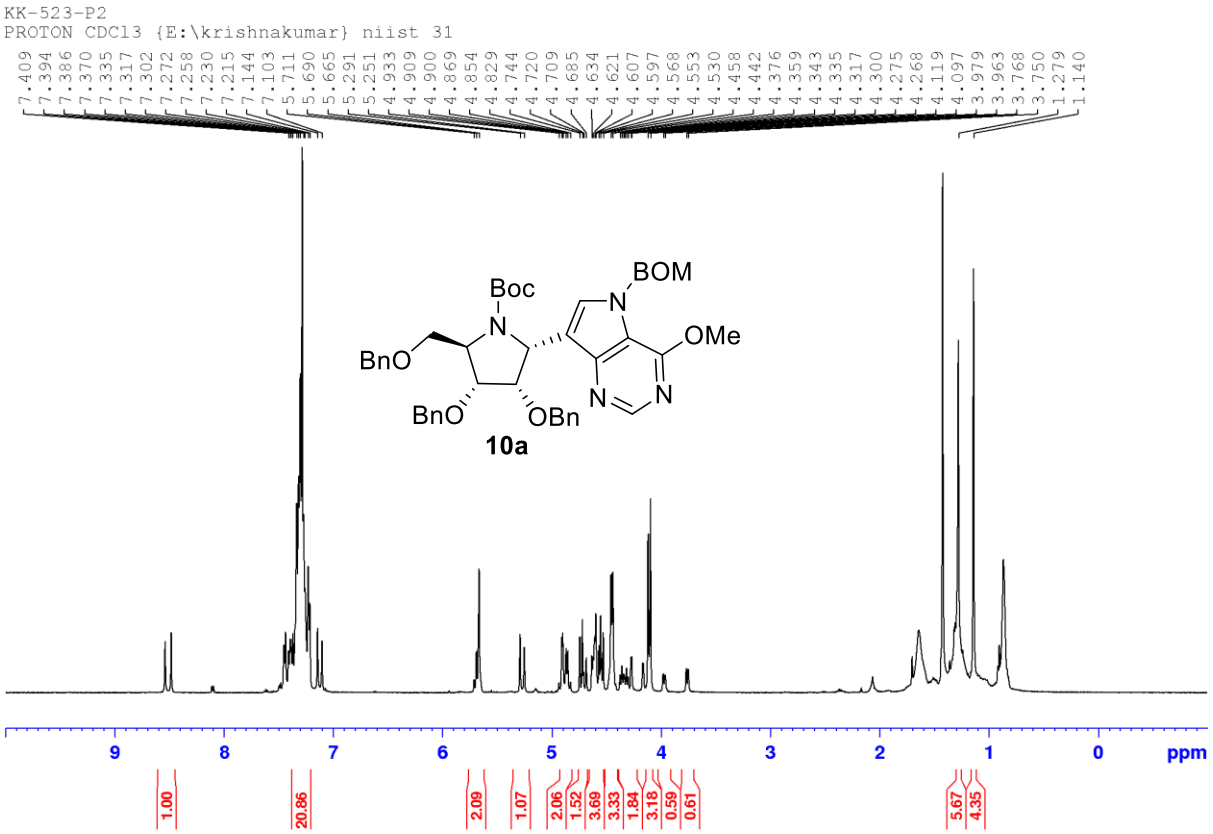

Figure 3.5.8: NMR spectra of compound **22**

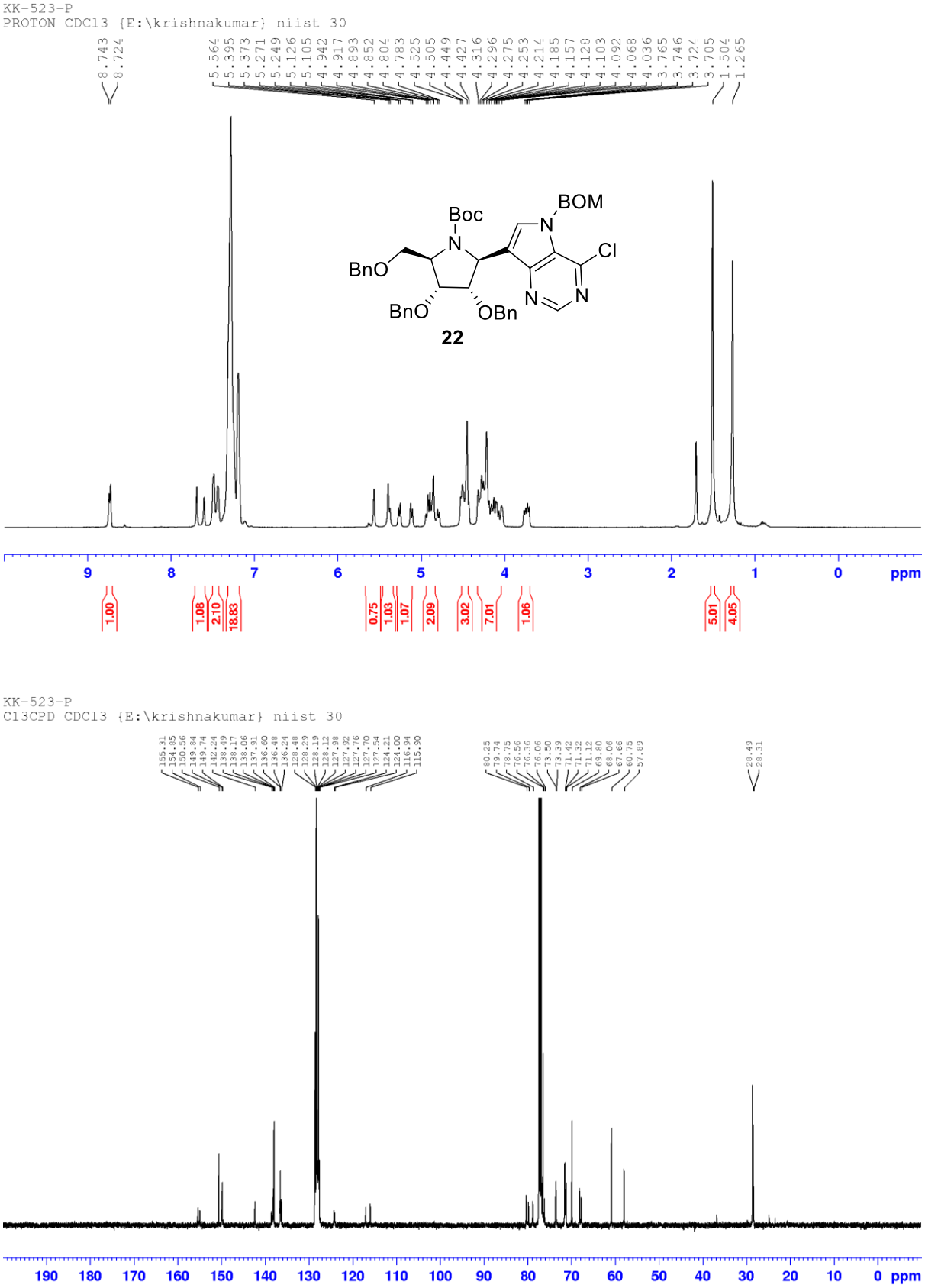

Figure 3.5.9: NMR spectra of compound **25**

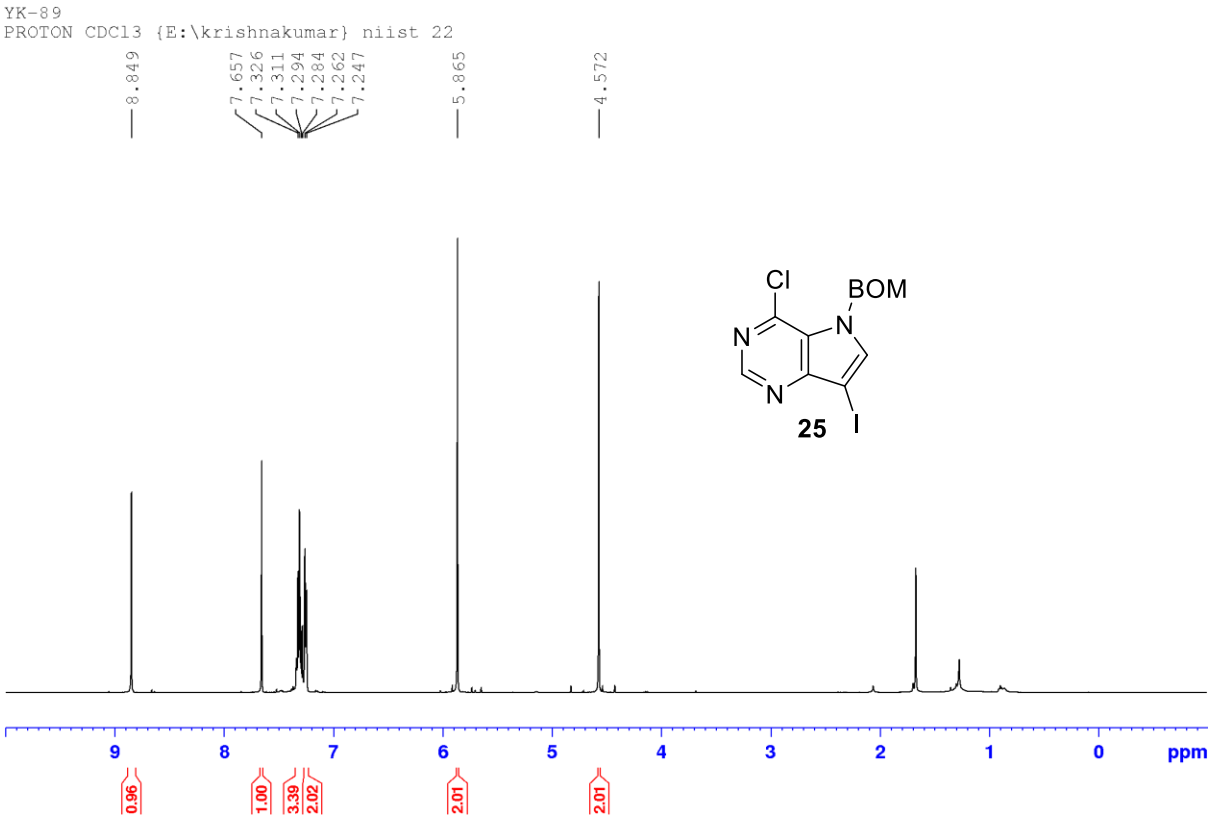

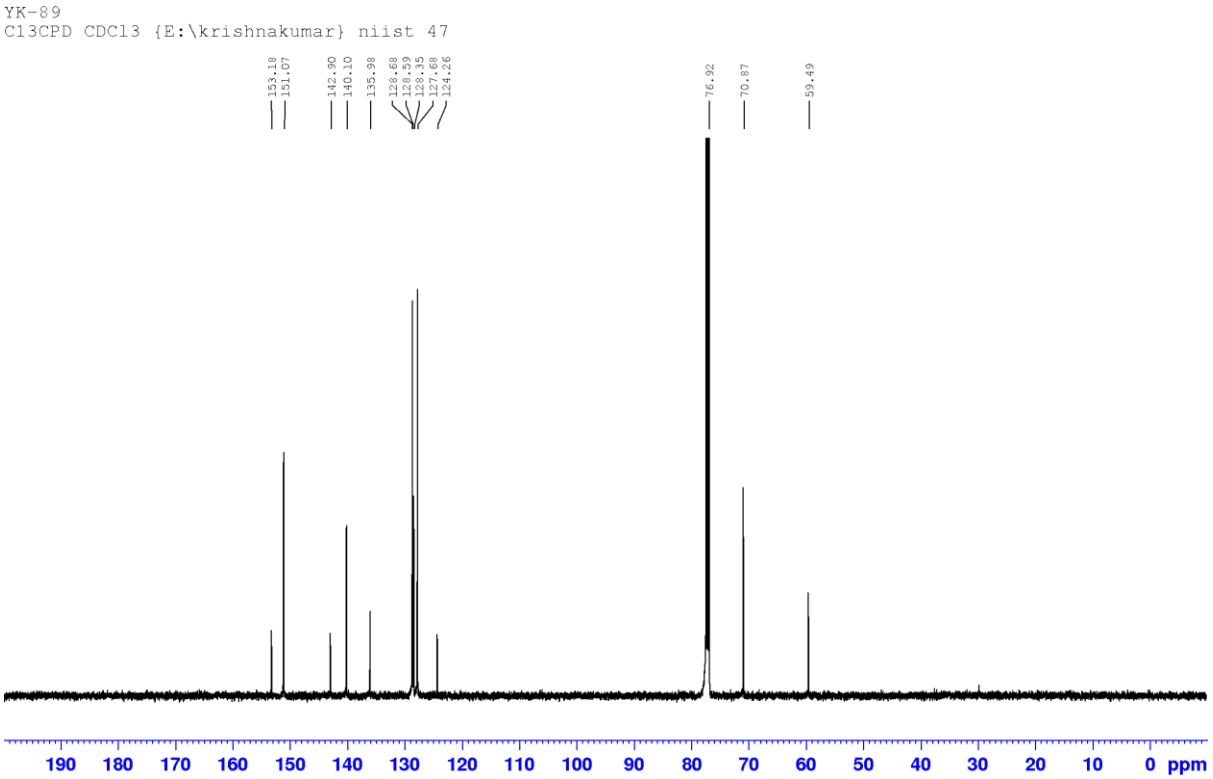

Figure 3.5.10: NMR spectra of deiodo-**25**

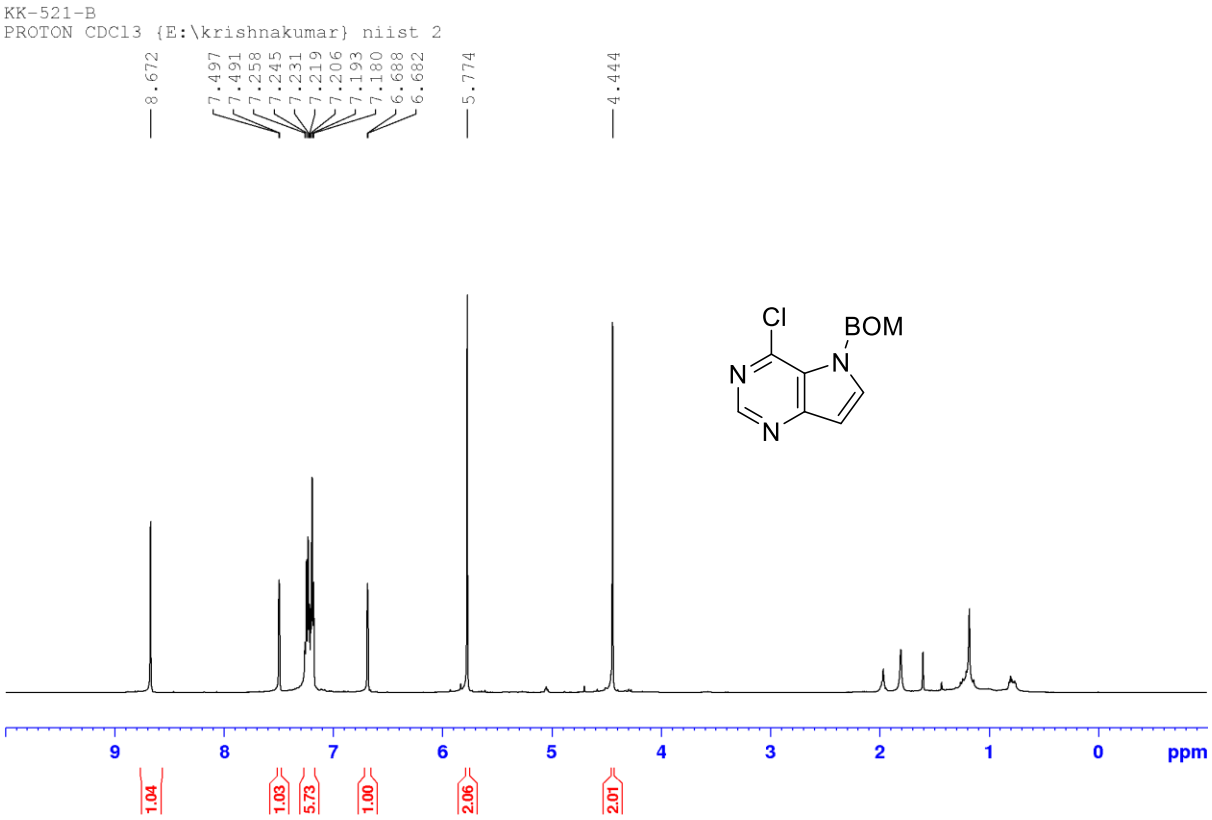

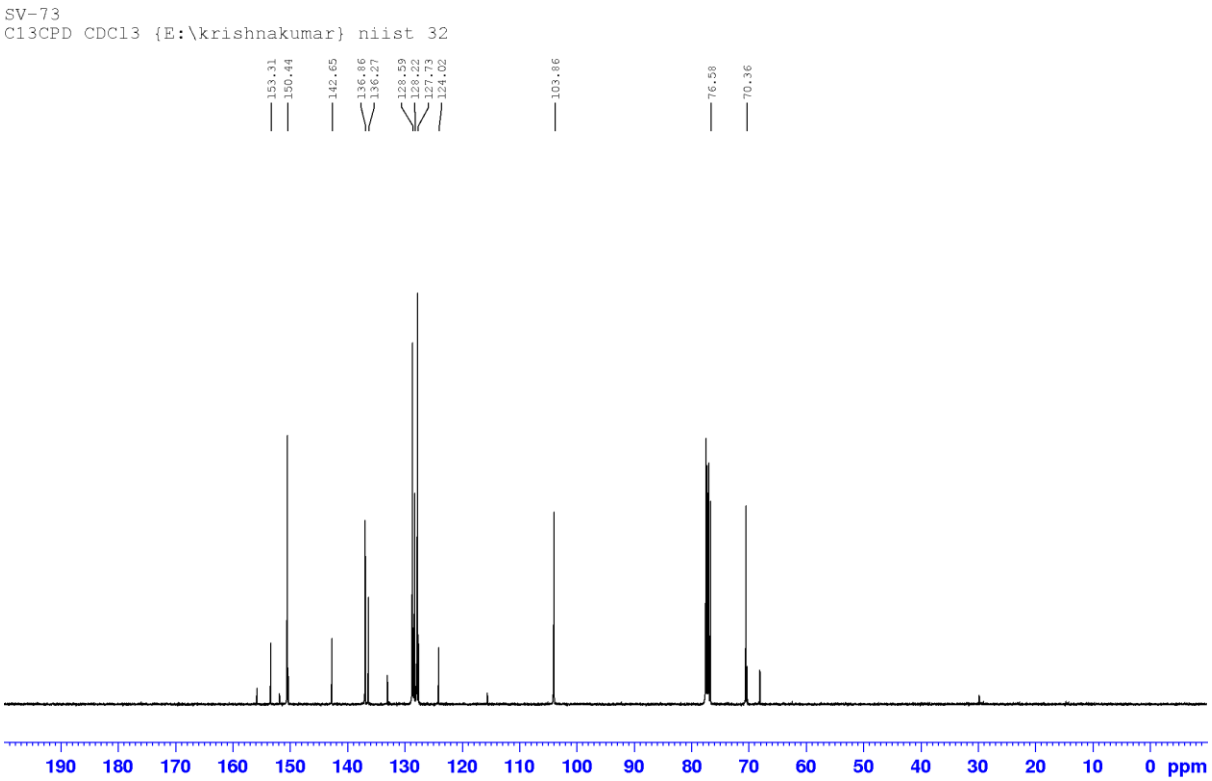

Figure 3.5.11: NMR spectra of compound **26**

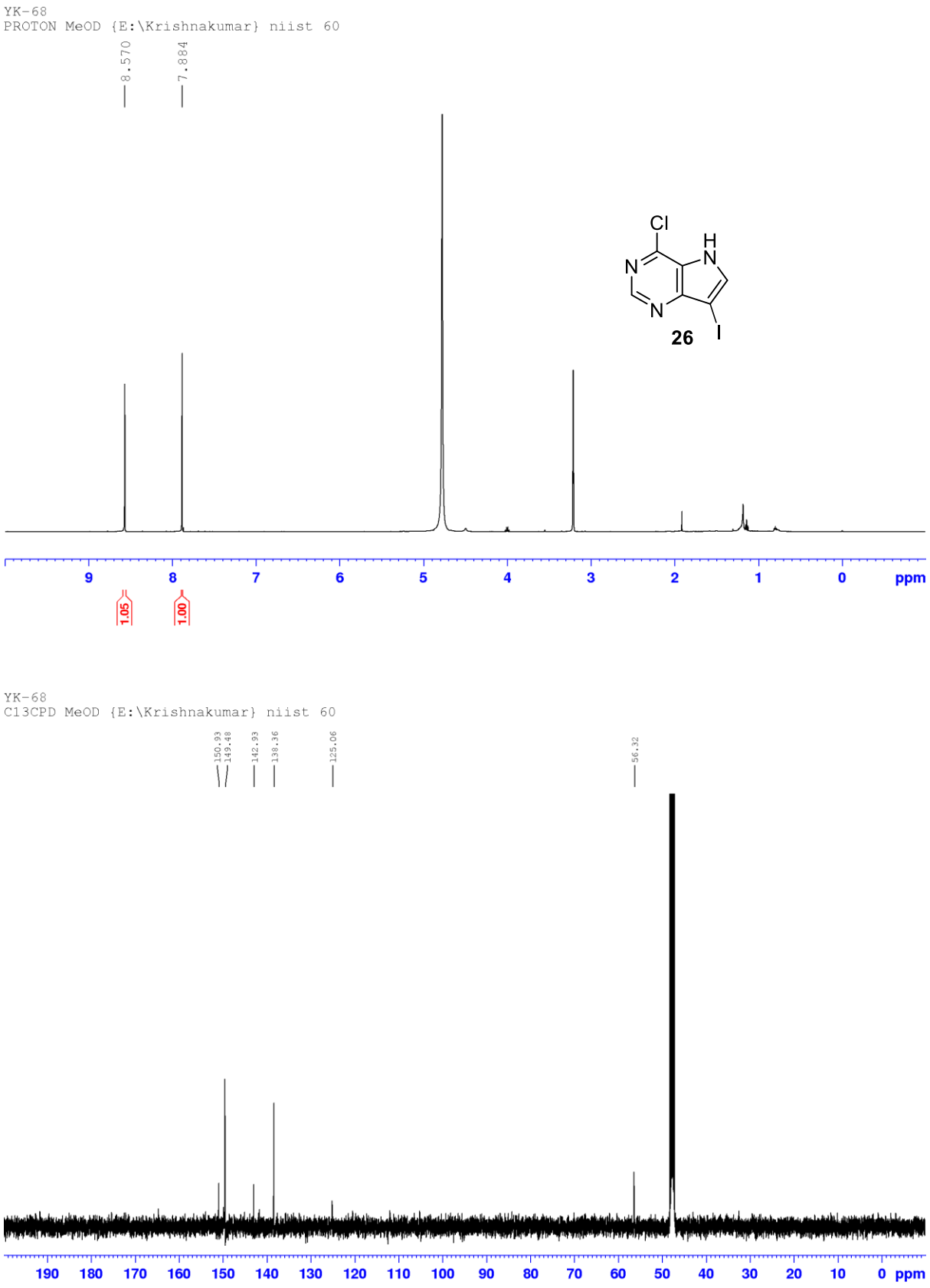

Figure 3.5.12: NMR spectra of compound **28**

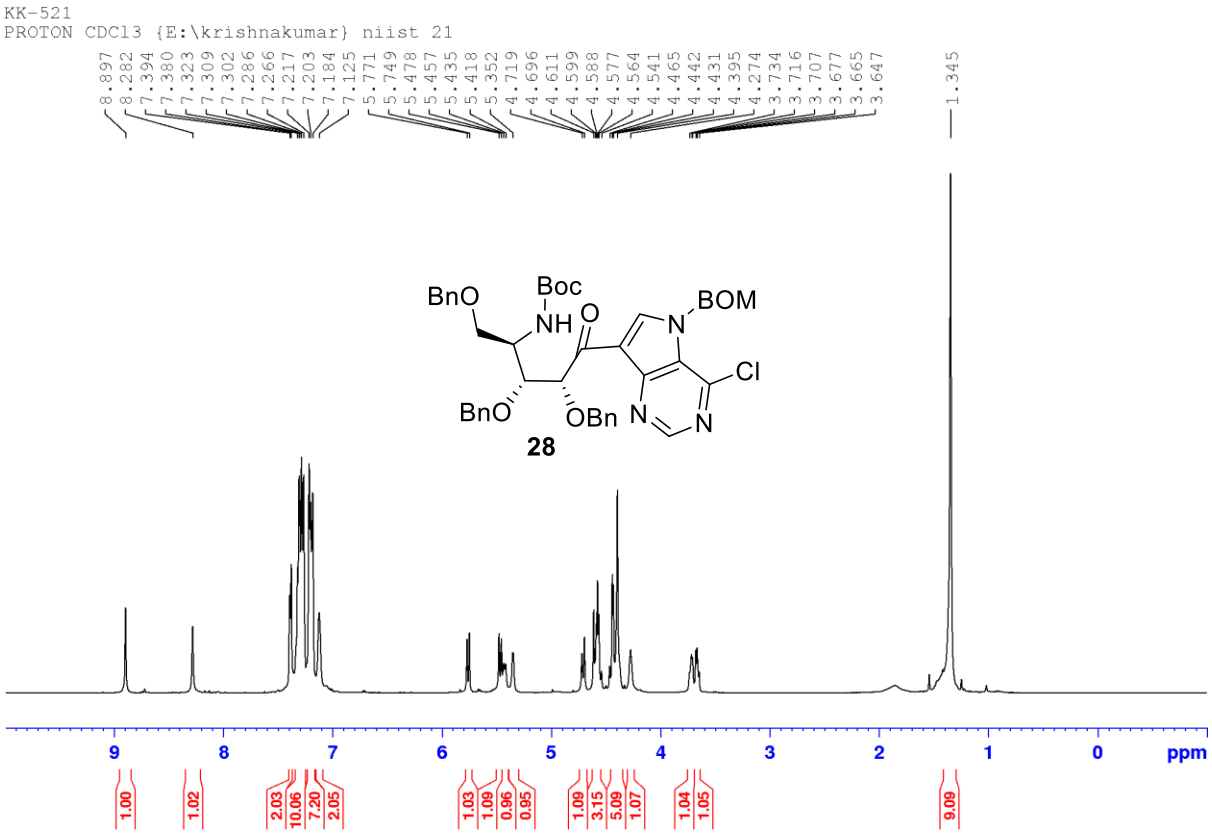

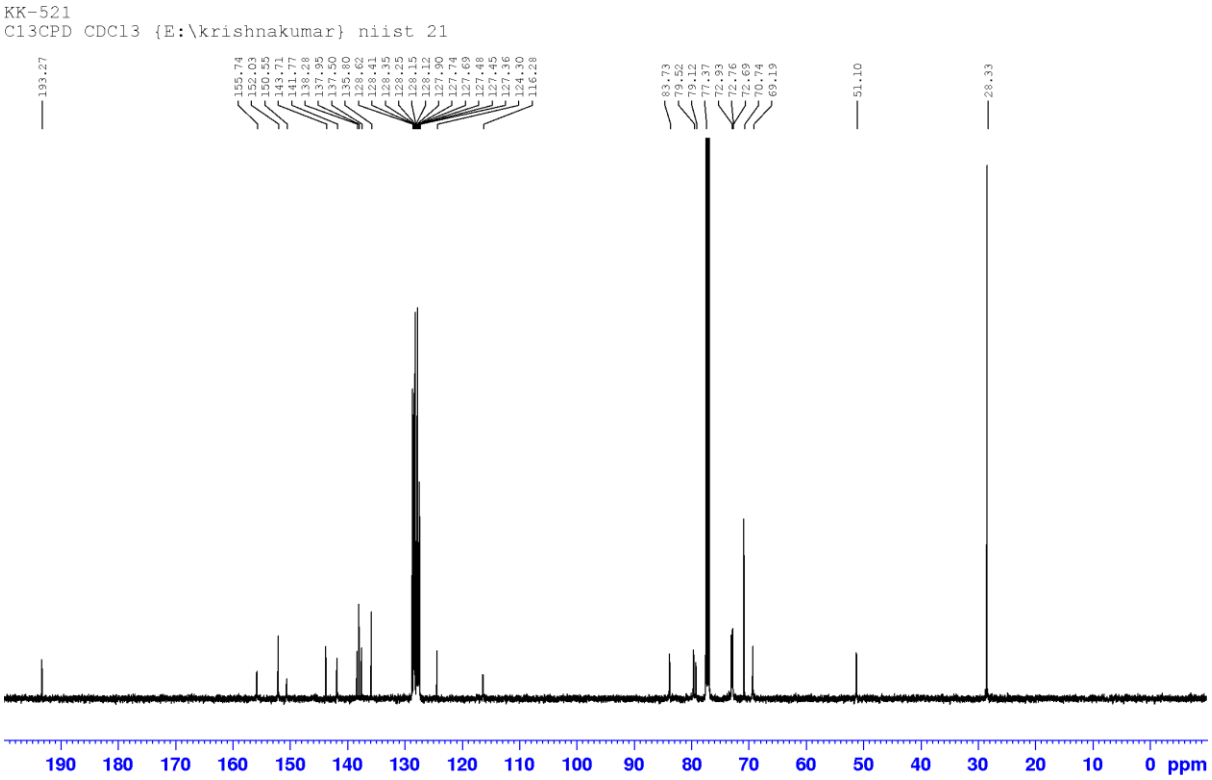

Figure 3.5.13: NMR spectra of compound **30**

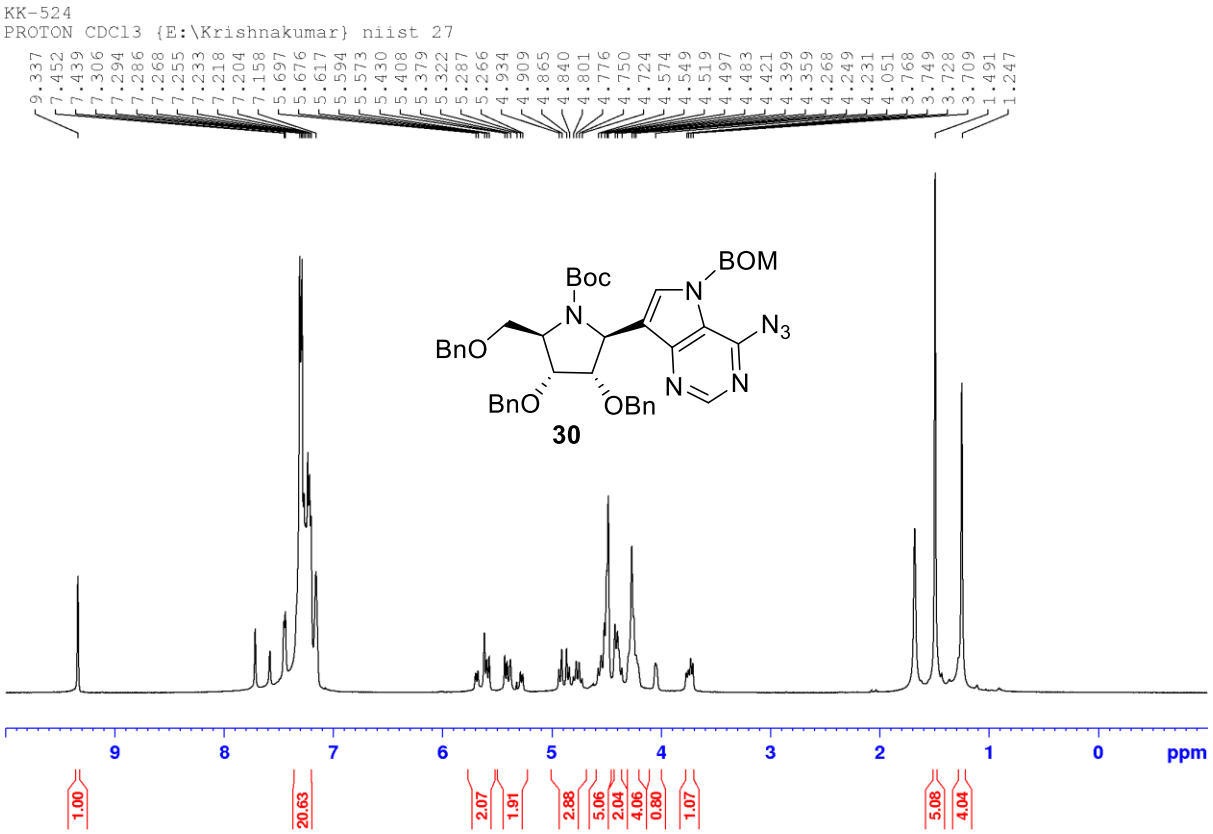

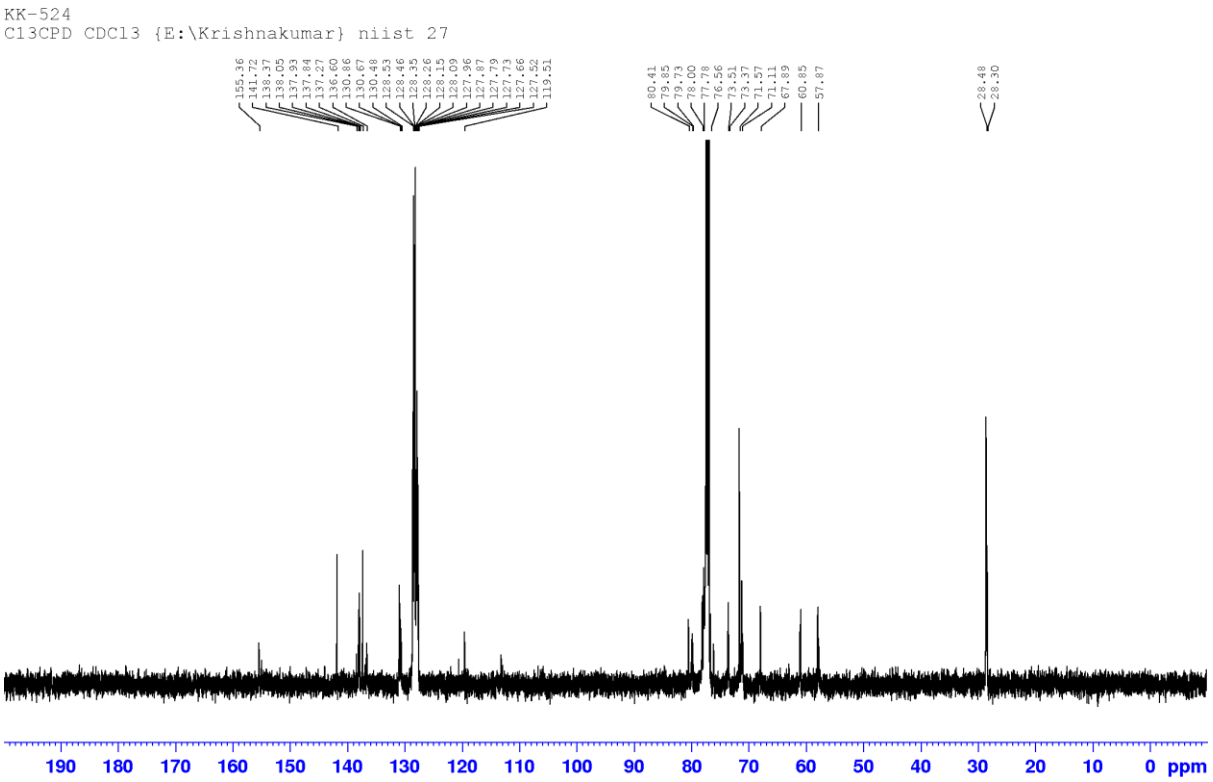

Figure 3.5.14: NMR spectra of Forodesine/Immucillin-H

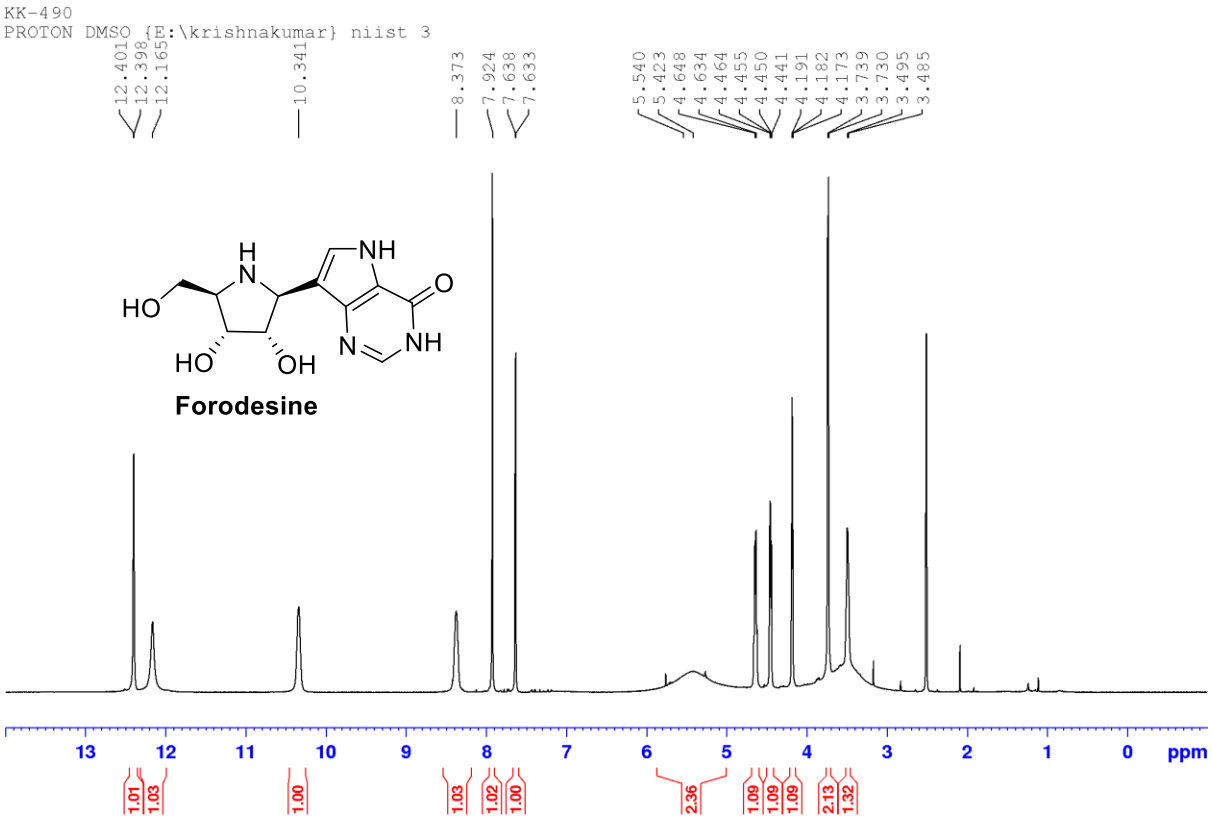

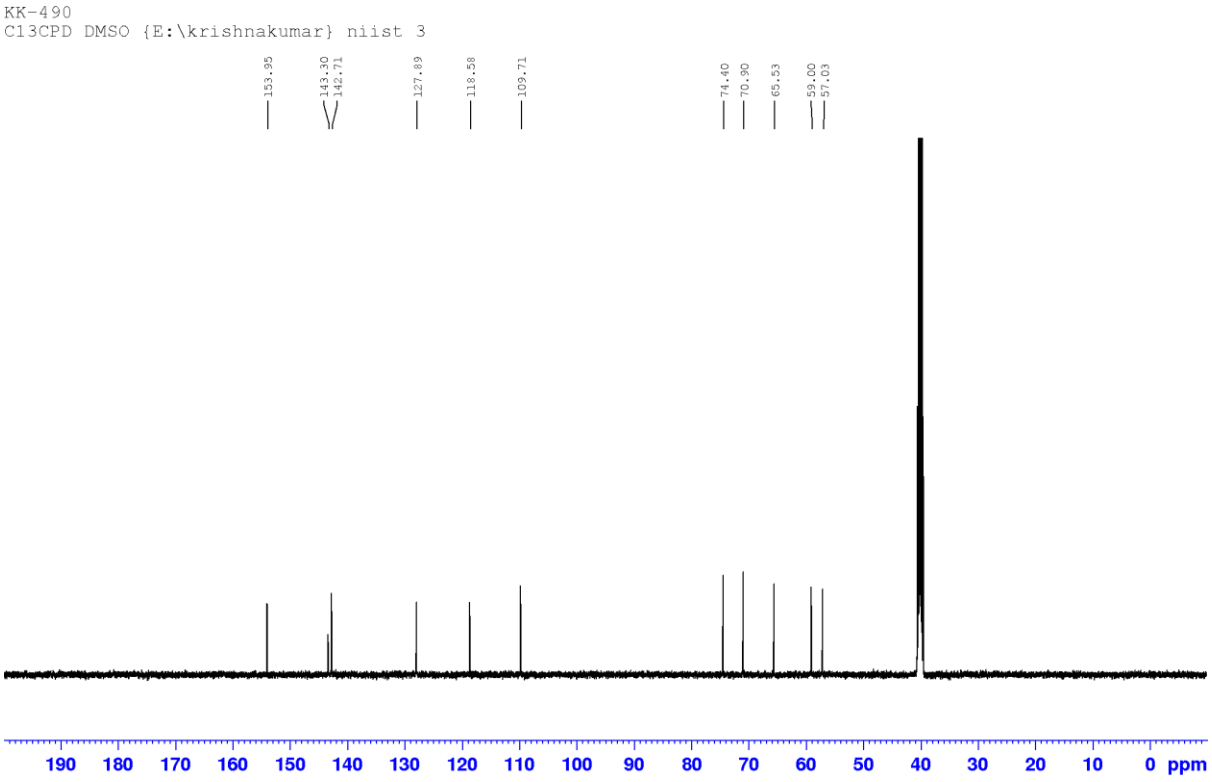

Figure 3.5.15: NMR spectra of Galidesivir/Immucillin-A

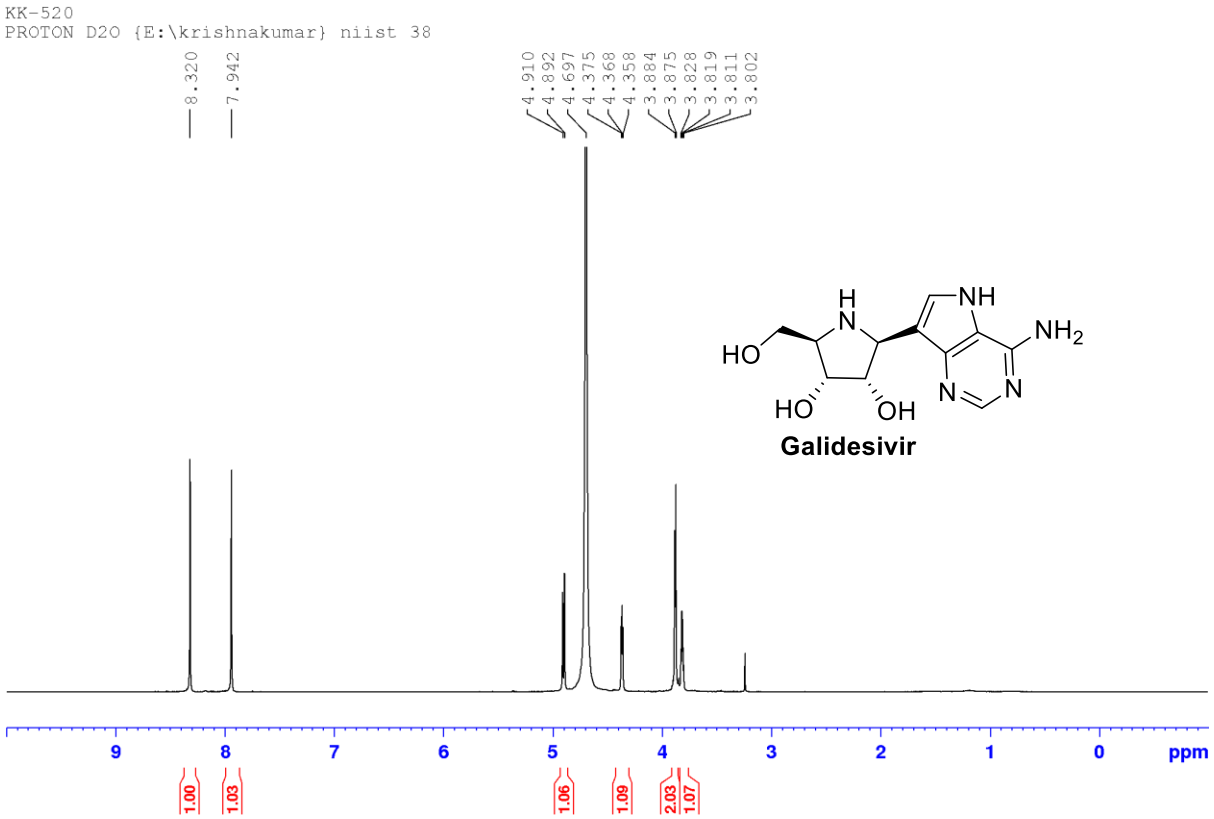

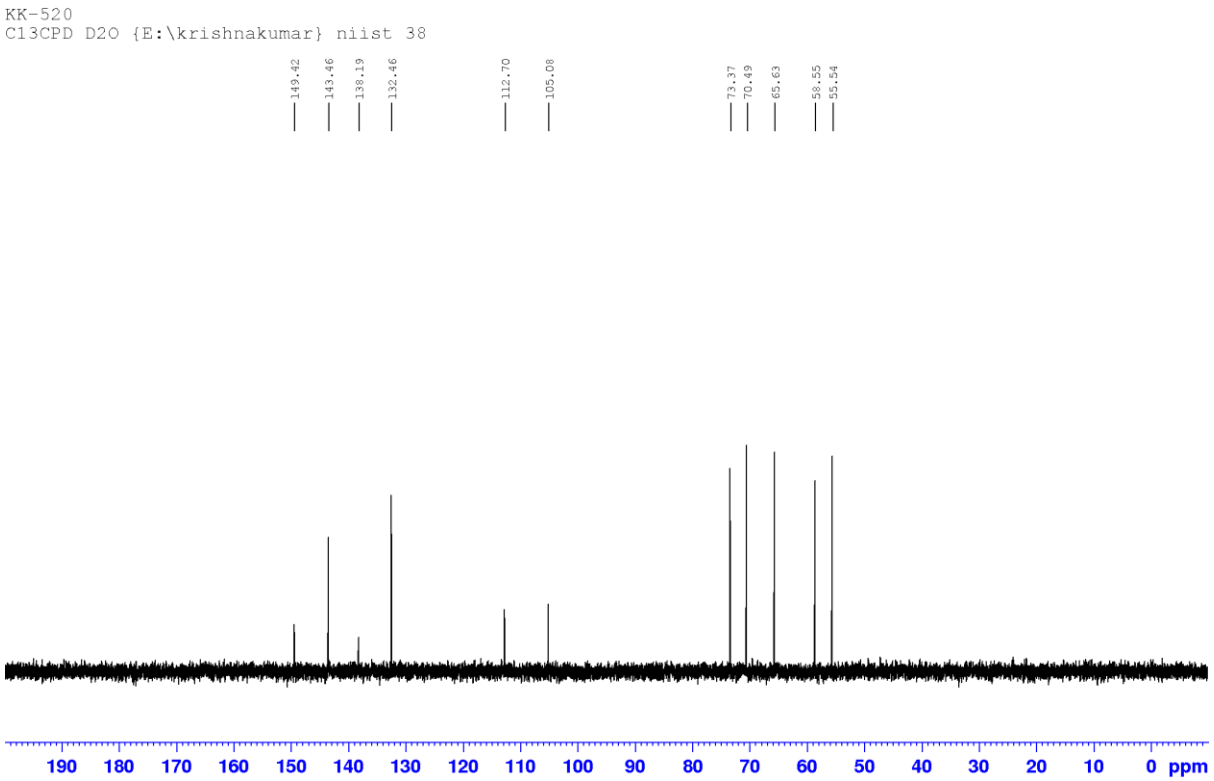

3.6. References

1. Julander, J. G. *et al.* An update on the progress of galidesivir (BCX4430), a broad-spectrum antiviral. *Antiviral Res.* **195**, 105180 (2021).
2. Evans, B. G., Schramm, L. V. & Tyler, C. P. The Immucillins: Design, Synthesis and Application of Transition- State Analogues. *Current Medicinal Chemistry* vol. 22 3897–3909 at https://doi.org/http://dx.doi.org/10.2174/092986732266615082110085 1 (2015).
3. Warren, T. K. *et al.* Protection against filovirus diseases by a novel broad-spectrum nucleoside analogue BCX4430. *Nature* **508**, 402–405 (2014).
4. Eyer, L. *et al.* Antiviral activity of the adenosine analogue BCX4430 against West Nile virus and tick-borne flaviviruses. *Antiviral Res.* **142**, 63–67 (2017).
5. Julander, J. G. *et al.* Efficacy of the broad-spectrum antiviral compound BCX4430 against Zika virus in cell culture and in a mouse model. *Antiviral Res.* **137**, 14–22 (2017).
6. Westover, J. B. *et al.* Galidesivir limits Rift Valley fever virus infection and disease in Syrian golden hamsters. *Antiviral Res.* **156**, 38–45 (2018).
7. Evans, G. B., Tyler, P. C. & Schramm, V. L. Immucillins in Infectious Diseases. *ACS Infect. Dis.* **4**, 107–117 (2018).
8. Zhang, Y., Geng, H., Zhang, J. & He, K. An Update Mini-Review on the Progress of Azanucleoside Analogues. *Chem. Pharm. Bull.* **70**, 469–476 (2022).
9. Taylor, R. *et al.* Activity of Galidesivir in a Hamster Model of SARS-CoV-2. *Viruses* vol. 14 at https://doi.org/10.3390/v14010008 (2022).
10. Li, G. & De Clercq, E. Therapeutic options for the 2019 novel coronavirus (2019-nCoV). *Nat. Rev. Drug Discov.* **19**, 149–150 (2020).
11. Overkleeft, H. S., van Wiltenburg, J. & Pandit, U. K. A facile transformation of sugar lactones to azasugars. *Tetrahedron* **50**, 4215–4224 (1994).
12. Gorantla, J. N., Faseela, A. & Lankalapalli, R. S. Design and synthesis of a novel glycosphingolipid derived from polyhydroxy 2-pyrrolidinone and phytoceramide appended by a 1,2,3-triazole linker. *Chem. Phys. Lipids* **194**, 158–164 (2016).
13. Evans, G. B., Furneaux, R. H., Lewandowicz, A., Schramm, V. L. & Tyler, P. C.

Synthesis of Second-Generation Transition State Analogues of Human Purine Nucleoside Phosphorylase. *J. Med. Chem.* **46**, 5271–5276 (2003).

14. Kamath, V. P., Juarez-Brambila, J. J., Morris, C. B., Winslow, C. D. & Morris, P. E. Development of a practical synthesis of a purine nucleoside phosphorylase inhibitor: BCX-4208. *Org. Process Res. Dev.* **13**, 928–932 (2009).

15. Zhang, M. *et al.* Practical synthesis of immucillins BCX-1777 and BCX-4430. *Org. Chem. Front.* **7**, 3675–3680 (2020).

16. Krasovskiy, A. & Knochel, P. A LiCl-mediated Br/Mg exchange reaction for the preparation of functionalized aryl- and heteroarylmagnesium compounds from organic bromides. *Angew. Chemie - Int. Ed.* **43**, 3333–3336 (2004).

17. Warren, T. K. *et al.* Therapeutic efficacy of the small molecule GS-5734 against Ebola virus in rhesus monkeys. *Nature* **531**, 381–385 (2016).

18. Ren, H., Krasovskiy, A. & Knochel, P. Stereoselective preparation of functionalized acyclic alkenylmagnesium reagents using i-PrMgCl-LiCl. *Org. Lett.* **6**, 4215–4217 (2004).

19. Hermann, A. *et al.* Comprehensive Study of the Enhanced Reactivity of Turbo-Grignard Reagents**. *Angew. Chemie Int. Ed.* **62**, e202302489 (2023).

20. Bambuch, V., Otmar, M., Pohl, R., Masojidkova, M. & Holý, A. C-Functionalization of 9-deazapurines by cross-coupling reactions. *Tetrahedron* **63**, 1589–1601 (2007).

21. Yokoyama, M., Ikenogami, T. & Togo, H. Stereoselective synthesis of C-4′-aminouridines (uracil C-4-amino-D-ribonucleosides). *J. Chem. Soc. Perkin Trans. 1* 2067–2071 (2000) doi:10.1039/B002063J.

22. Yoda, H., Nakajima, T. & Takabe, K. Total synthesis of natural (−)-codonopsinine employing stereoselective reduction of quaternary *α*-hydroxypyrrolidine. *Tetrahedron Lett.* **37**, 5531–5534 (1996).

Synthesis of Iminosugar Analogues of KRN-7000

4.1. Abstract

This chapter details the synthesis of novel iminosugar mimetics of KRN-7000 and its analogs, focusing on the development of aza-C-galactosylceramide through a convergent synthesis approach. Using Turbo Grignard reagent and cross-metathesis strategies, the synthesis aims to replace the natural galactose unit with an iminosugar derivative. Challenges in the synthesis, including difficulties with metal-halogen exchange and optimizing reaction conditions, are addressed. Alternative methods, such as click chemistry, are also explored to achieve the desired linkages. The synthesized compounds are intended to enhance the understanding and application of glycosphingolipids in immunological research and therapy.

4.2. Introduction

Glycosphingolipids (GSLs) are a fascinating class of molecules that act like cellular fingerprints on the surface of our cells. These intricate structures combine a sugar portion (glycan) with a fatty molecule (ceramide). The glycan moieties face outwards, like antennas, and play a crucial role in cellular communication. GSLs orchestrate a variety of essential biological processes through interactions with proteins and other sugars. They act as identification tags, allowing cells to recognize each other and participate in specialized functions like cell adhesion. They can also serve as docking stations for toxins, viruses, and bacteria, influencing how pathogens interact with our cells. Interestingly, GSLs can even influence how other proteins on the cell surface function, impacting processes such as stem cell development, nerve cell differentiation, and even cancer progression.[1–6]

For these reasons, GSLs have become a hot topic in biological research. Scientists are particularly interested in creating well-defined GSLs to understand their specific roles in various biological processes. Since GSLs rely on both the sugar and lipid parts for their function, it's crucial to recreate the entire structure accurately. This will pave the way for

groundbreaking discoveries in biology and potentially lead to novel therapeutic applications.[7–11]

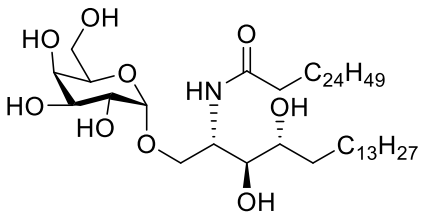

Figure 4.2: Structure of KRN-7000

The story of KRN-7000 begins in the tropical waters near Mauritius, where researchers focused on studying a particular marine sponge called *Agelas mauritianus*. During the 1990s, scientists at Japan's Kirin Brewery Company began investigating extracts from this sponge for their potential biological activities. One of these extracts, named KRN-7000, showed an impressive ability to activate a specific type of immune cell known as invariant natural killer T (iNKT) cells. These iNKT cells play a crucial role in regulating the immune system, acting as a bridge between the innate and adaptive immune systems. KRN-7000, also known as alpha-galactosyl ceramide (α-GalCer), emerged as a potent stimulator of these cells, exhibiting promising immunostimulatory and anti-tumor characteristics. Further studies have revealed its potential to reduce tumor size in animal models, generating interest in its potential use for cancer immunotherapy.[12–16]

The story of KRN-7000 goes beyond its initial discovery. The ability to synthesize the molecule and its analogs has fueled ongoing research. Chemists are now creating modified versions with altered properties, aiming to fine-tune the immune response for specific therapeutic applications. These analogs hold promise for targeting various diseases beyond cancer, including autoimmune disorders and infectious diseases.[17]

4.3. Result and discussions

This chapter aims to synthesize novel iminosugar mimetics of KRN-7000 and its analogs through convergent synthesis.

4.3.1. Turbo Grignard reagent-assisted cross-coupling

Initially, our goal was to create a novel KRN-7000 analog, aza-C-galactosylceramide. To achieve this, we envisioned replacing the natural galactose sugar unit in KRN-7000 with an iminosugar derivative derived from D-galactose. This modified sugar would then be

linked to the ceramide portion *via* a C-glycosidic bond. Leveraging our successful application of Boc-protected lactams in convergent synthesis for previous projects, we planned to employ a similar approach here. The strategy involved the use of a special reagent, the Turbo Grignard reagent. This reagent would facilitate a metal-halogen exchange reaction within a vinyl iodide[18] derived from phytosphingosine, and then it will be added to Boc-protected lactam.

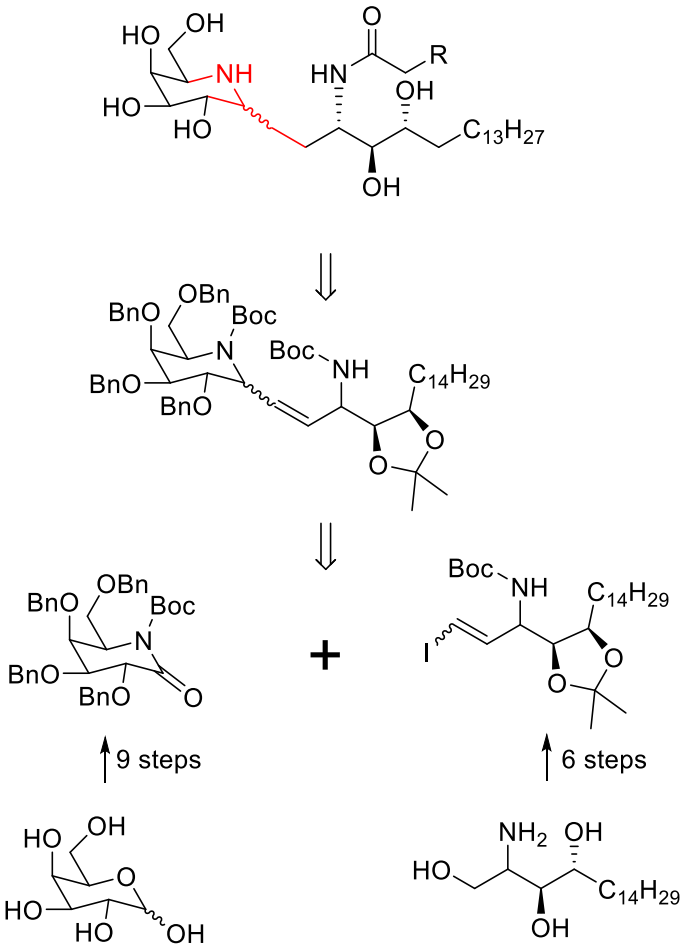

Figure 4.3.1: Synthetic plan for aza-C-galactosylceramide

The crucial stages of the reaction encompassed the application of the Turbo Grignard reagent to facilitate the cross-coupling process between vinyl iodide and lactam. This elegant approach will ultimately result in the targeted synthesis of aza-C-galactosylceramide.

4.3.1.1. Synthesis of N-Boc-protected Lactam *via* D-Galactose Functionalization

The synthesis of Boc-protected *δ*-lactam started with commercially available D-galactose.

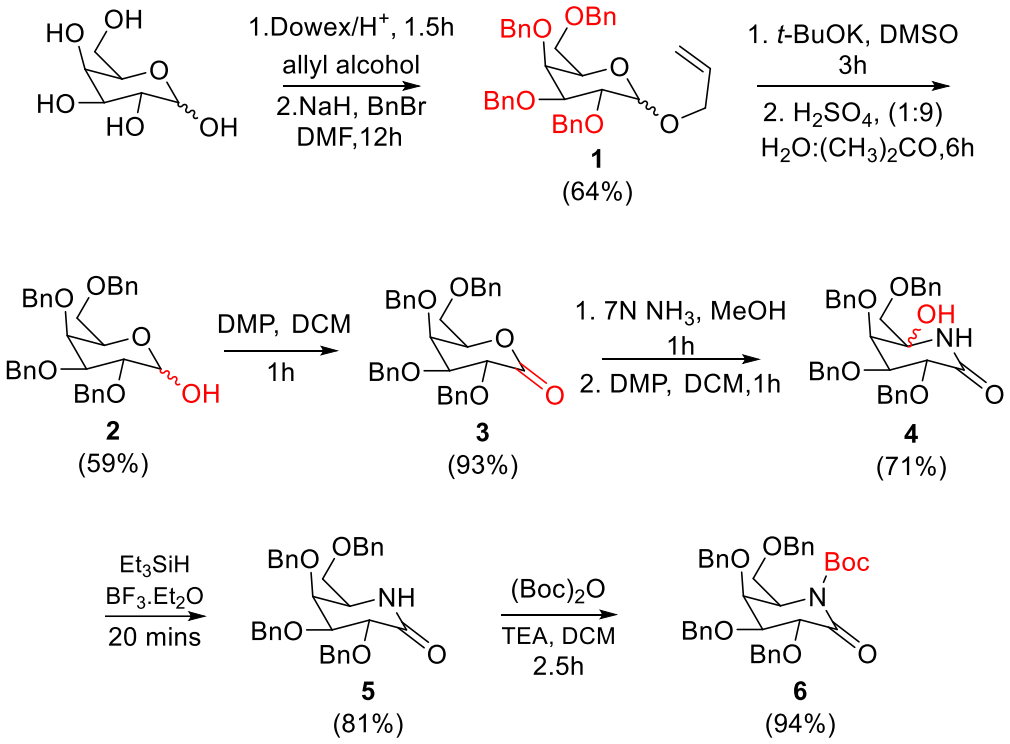

Scheme 4.3.1.1: Synthesis of N-Boc lactam **6**

The synthesis began with selective protection of the D-galactose's anomeric hydroxyl group, forming an allyl ether (1-O-allyl-D-galactose). This was followed by an overnight reaction with benzyl bromide in the presence of sodium hydride (NaH), transforming it into compound **1**. The allyl group was removed by refluxing compound **1** with potassium *tert*-butoxide (*t*-BuOK) followed by hydrolysis with dilute hydrochloric acid (HCl). This resulted in a hemiacetal intermediate **2**. Oxidation of the hemiacetal intermediate **2** using Dess-Martin periodinane, a mild oxidizing agent, converted compound **2** into *δ*-lactone **3**. Treatment of lactone **3** with methanolic ammonia facilitated the conversion to hydroxy-carboxamide, containing a secondary alcohol group. Oxidation with Dess-Martin periodinane transformed the secondary alcohol into a ketone group, forming a keto amide intermediate. This intermediate spontaneously underwent cyclization to yield a mixture of lactam epimers **4**. Finally, reductive amination of the lactam epimer mixture **4** furnished lactam **5**.[19] The synthesis culminated in the N-Boc-protected lactam **6** after treatment with $(Boc)_2O$.

4.3.1.2. Preparation of Phytosphingosine with a Terminal Vinyl Iodide Moiety

Starting from commercially available phytosphingosine, a phytosphingosine side chain functionalized with vinyl iodide was synthesized (Scheme 4.3.1.2a). Initially, the amine

was protected as a *tert*-butyl carbamate **7**, followed by the introduction of a silyl group to protect the primary alcohol temporarily to yield **8**. Later silyl group was removed after isopropylidene protection on the vicinal diol, resulting in an intermediate containing a free primary alcohol **10**.[20] Oxidation of alcohol **10** using Dess-Martin periodinane in the presence of excess $NaHCO_3$ to generate the aldehyde intermediate (**11**, phytosphingosine-1-al). Unfortunately, **11** failed to provide the desired terminal vinyl iodide under subsequent Wittig reaction conditions.

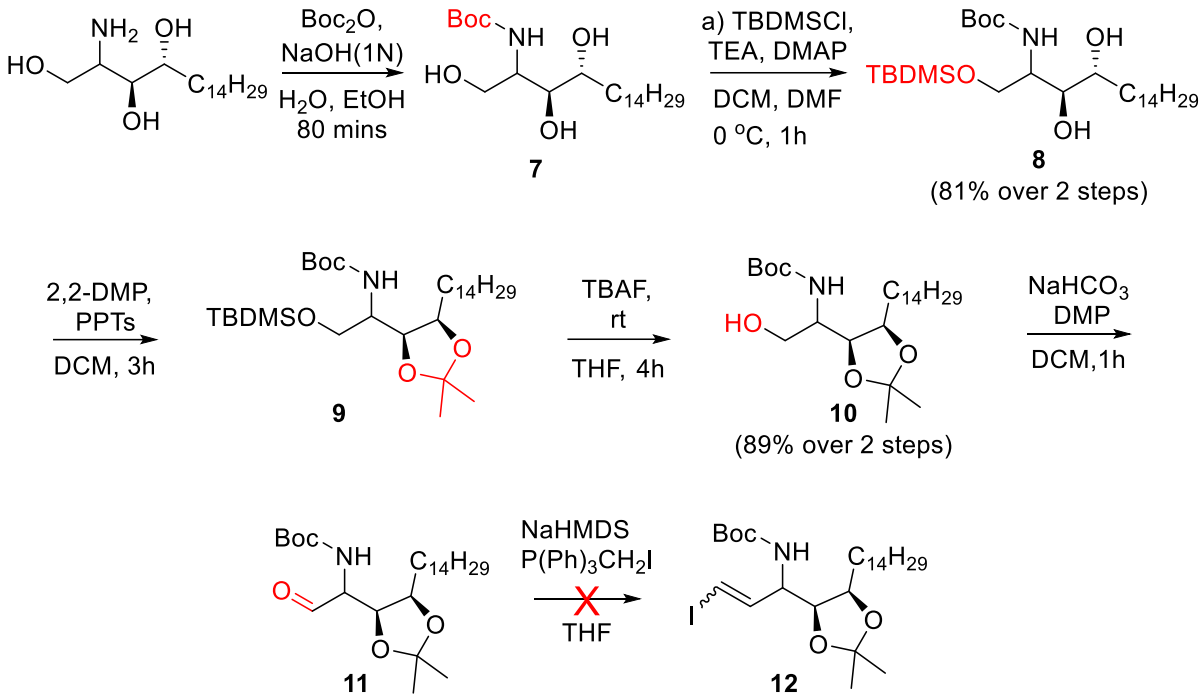

Scheme 4.3.1.2a: Synthesis of vinyl iodide functionalized phytosphingosine **12**

Scheme 4.3.1.2a proved unsuccessful in generating vinyl iodide functionalized phytosphingosine. To address this, we implemented a strategic modification in Scheme 4.3.1.2b by protecting the amine group ($-NH_2$) with a benzyl group and a Boc group. This involved reacting compound **9** with benzyl bromide at subzero temperatures to prevent undesired desilylation by NaH. Subsequently, the silyl group was deprotected using TBAF to obtain primary alcohol **14**. Dess-Martin periodinane oxidation was then performed on alcohol **14** in the presence of excess $NaHCO_3$. This reaction yielded aldehyde **15**, which readily underwent a Wittig reaction with (iodomethyl)triphenylphosphonium iodide to furnish the desired vinyl iodide functionalized phytosphingosine **16** in 38% overall yield over 7 steps.

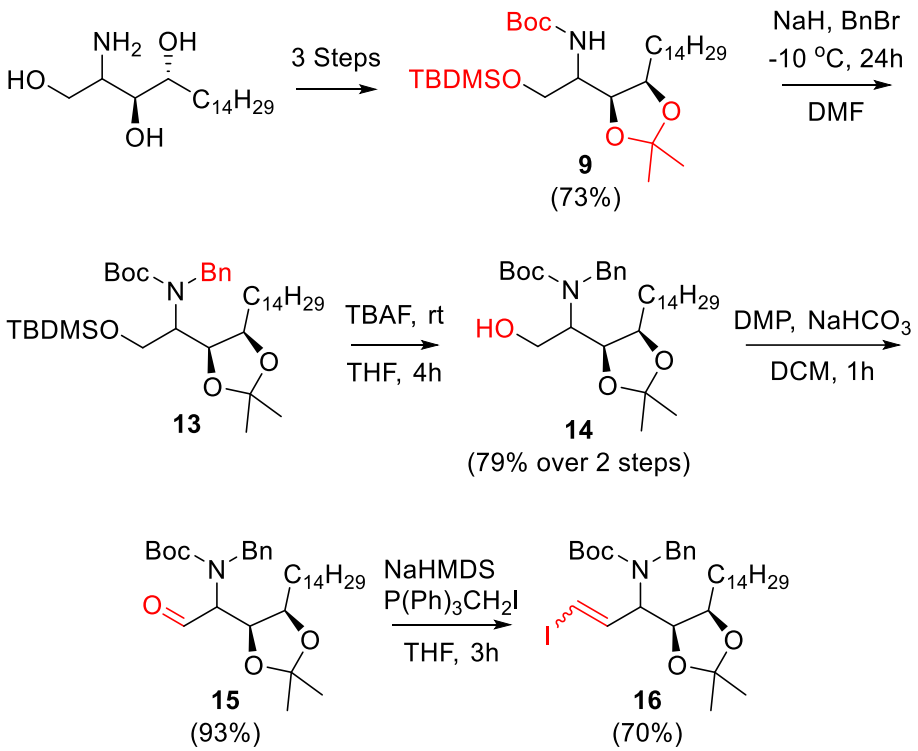

Scheme 4.3.1.2b: Synthesis of vinyl iodide functionalized phytosphingosine **16**

We achieved a variation of the vinyl iodide-functionalized phytosphingosine **18** by employing a different approach. Instead of protecting the vicinal diol with an isopropylidene group, we subjected compound **9** to benzylation. This strategy resulted in the co-benzylation of the diol, providing intermediate **17**. Compound **17** can be efficiently converted to the desired product **18** using the same three-step process described earlier. This approach not only enhances the molecule's stability but also offers the significant benefit of reducing the overall number of synthetic steps (Scheme 4.3.1.2c).

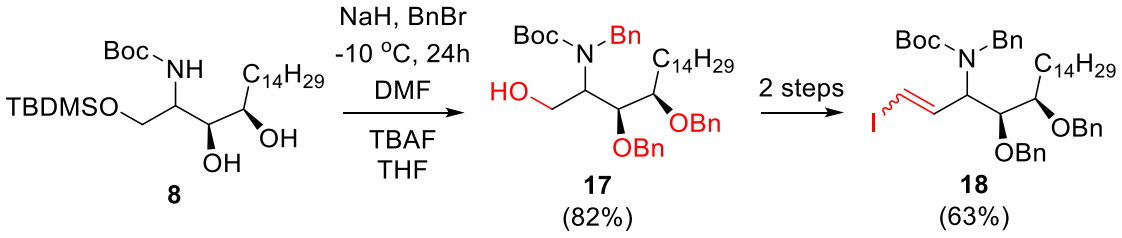

Scheme 4.3.1.2c: Synthesis of vinyl iodide functionalized phytosphingosine **-18**

4.3.1.3. Cross-coupling attempt on N-Boc lactam and vinyl iodide appended phytosphingosine

With both N-Boc lactam **6** and vinyl iodide-functionalized phytosphingosine (compounds **16**/**18**) available, we attempted a cross-coupling reaction mediated by isopropylmagnesium chloride lithium chloride complex (commonly known as the Turbo-Grignard reagent).

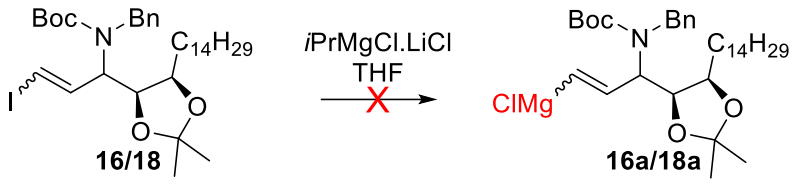

Scheme 4.3.1.3: Magnesium halogen exchange on compound **16/18**

Unfortunately, treatment of the vinyl iodide (**16**/**18**) with the Turbo-Grignard reagent did not result in the anticipated metal-halogen exchange. We explored various reaction conditions like different solvents (THF, MTBE, Et_2O, anisole), temperature (-40, 0 and 27 °C), and time (up to 30 hours) in an effort to promote the exchange, but none were successful.

Since the Turbo-Grignard reagent failed to promote metal-halogen exchange on vinyl iodides **16**/**18**, we explored n-butyllithium (*n*-BuLi) as an alternative.

Table 4.3.1.3: Cross-coupling attempt on N-Boc lactam and vinyl iodide

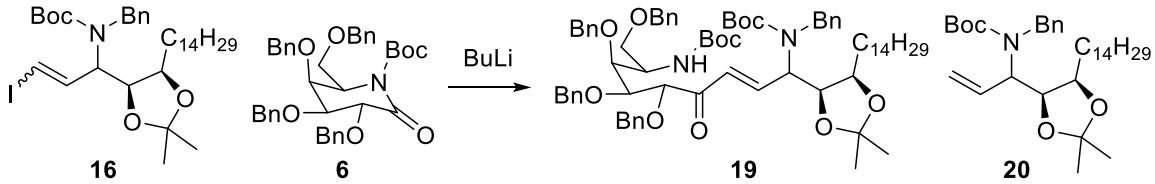

SL. No.	Solvent	Temperature (°C)	Time (h)	Product (17)
1	THF	0	3	Nil
2	THF	-40	3	Nil
3	THF	-78	3	Trace
4	THF	-78	6	Trace
5	Et_2O	-78	3	Nil
6	MTBE: Anisole	-78	3	Trace
7	MTBE	-78	3	Nil

Gratifyingly, treatment of **16** with *n*-BuLi at -78 °C resulted in a rapid metal-halogen exchange. The resulting lithium complex was then reacted with N-Boc lactam **6**. However, the reaction yielded a complex mixture. While column chromatography proved ineffective for purification, preparative TLC provided some fractions. High-resolution mass spectrometry (HRMS) analysis revealed the presence of the desired coupled product, **19** (Figure 4.3.1.3). Unfortunately, attempts to optimize the reaction conditions and improve

the yield for the desired product were unsuccessful. Notably, vinyl iodide **18** completely failed to undergo the cross-coupling reaction.

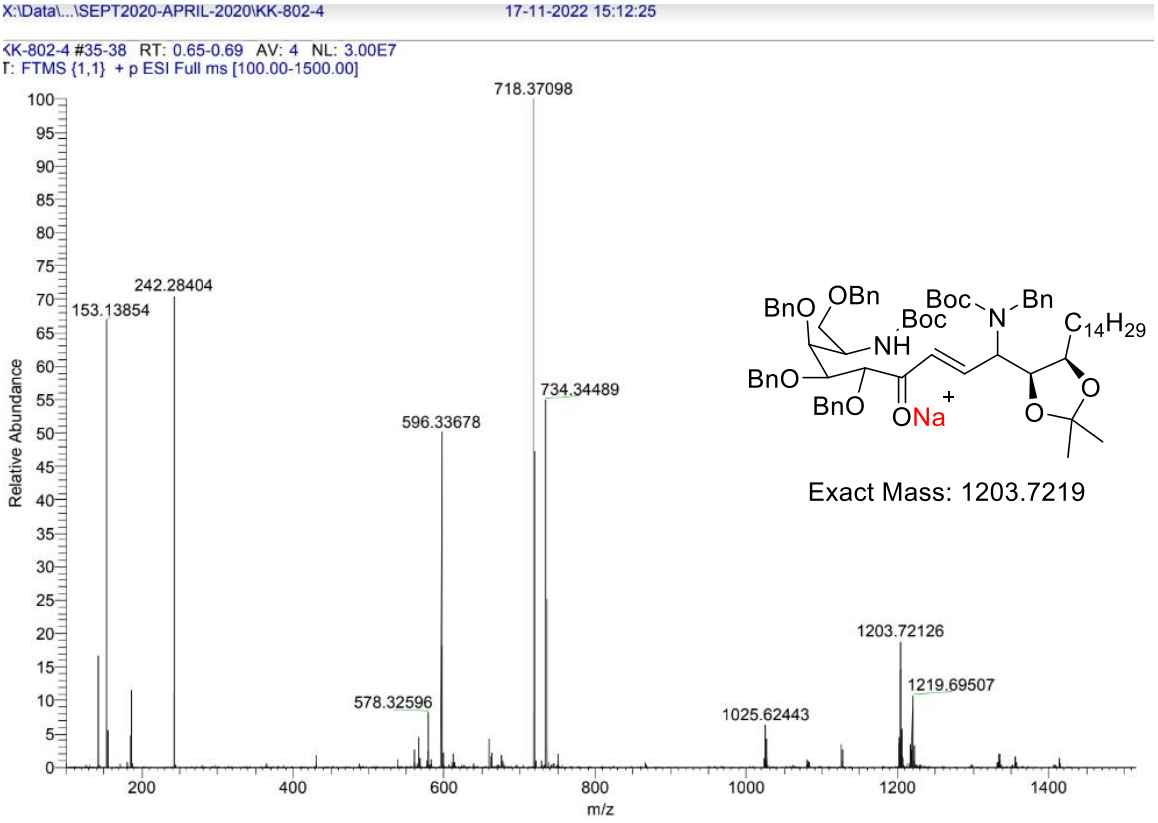

Figure 4.3.1.3: HRMS of compound **19**

4.3.2. cross-coupling through metathesis

Unfortunately, our initial objective of achieving cross-coupling using the Turbo-Grignard reagent fell short. This setback presented a significant hurdle, as there weren't any established alternative methods to synthesize the desired KRN-7000 analog. However, rather than being deterred, we leveraged our chemical knowledge and strategic thinking to design a new KRN-7000 mimetic. This alternative molecule aims to mimic the key functionalities of KRN-7000 but through a synthetic route that is more amenable to our current capabilities.

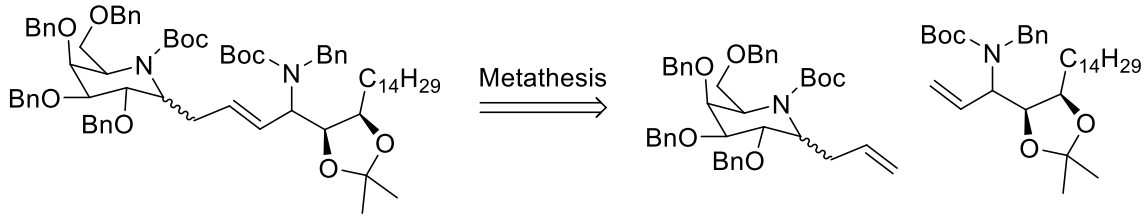

Figure 4.3.2: Synthesis plan for aza-C-galactosylceramide

Cross-metathesis emerges as a new strategy for our KRN-7000 analog synthesis. Unlike the prior method, this approach hinges on connecting the sugar and phytosphingosine portions through a controlled exchange of alkene partners. To achieve this, we strategically need to introduce alkenes into both building blocks.

4.3.2.1. Synthesis of alkenylated aza galactose

For our KRN-7000 analogue synthesis *via* cross-metathesis, we require an alkenylated azagalactose unit. Ideally, the alkene should be positioned at C-1 of the galactose ring for optimal reactivity after the subsequent cross-metathesis step. Considering the readily available reagents and previous experiences, we have opted for a Grignard reaction with allylmagnesium bromide for the alkenylation. This choice avoids potential complications encountered with vinylmagnesium bromide in previous attempts by our team.

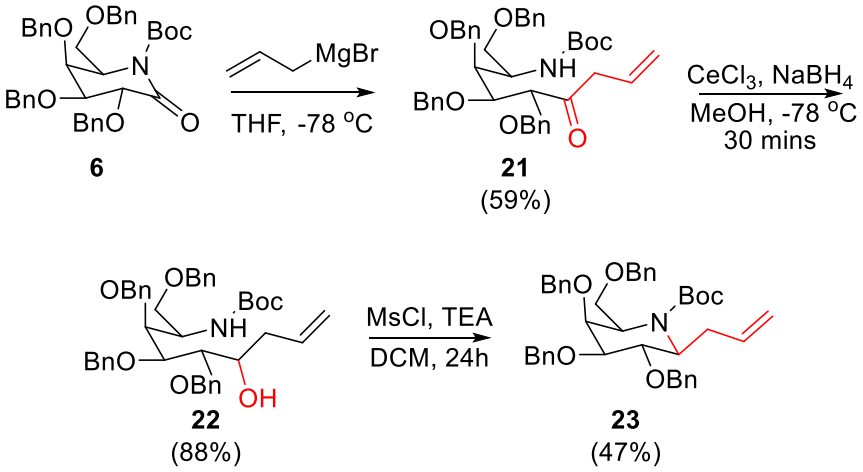

Scheme 4.3.2.1: Synthesis C-1 alkenylated azagalactose

N-Boc lactam **6** reacted with allylmagnesium bromide at -78 °C, but instead of the desired product, we obtained open-chain ketone **21**, similar to observations in a previous experiment discussed in the last chapter. To address this, ketone **21** was subjected to Luche reduction conditions, successfully converting it to the desired secondary alcohol **22**. Subsequent treatment with mesyl chloride promoted a favorable S_N2 reaction, resulting in the formation of C-1 *β*-alkenylated azagalactose **23** with the desired alkene regiochemistry (Scheme 4.3.2.1).

However, a standard $NaCNBH_3$ reduction on **21** followed by cyclization would likely yield an inseparable mixture of α and *β*-alkenylated aza galactoses. The Luche reduction offers

better regioselectivity, directing the reduction to the alcohol intermediate **22** and ultimately affording the C-1 *β*-alkenylated product **23**.

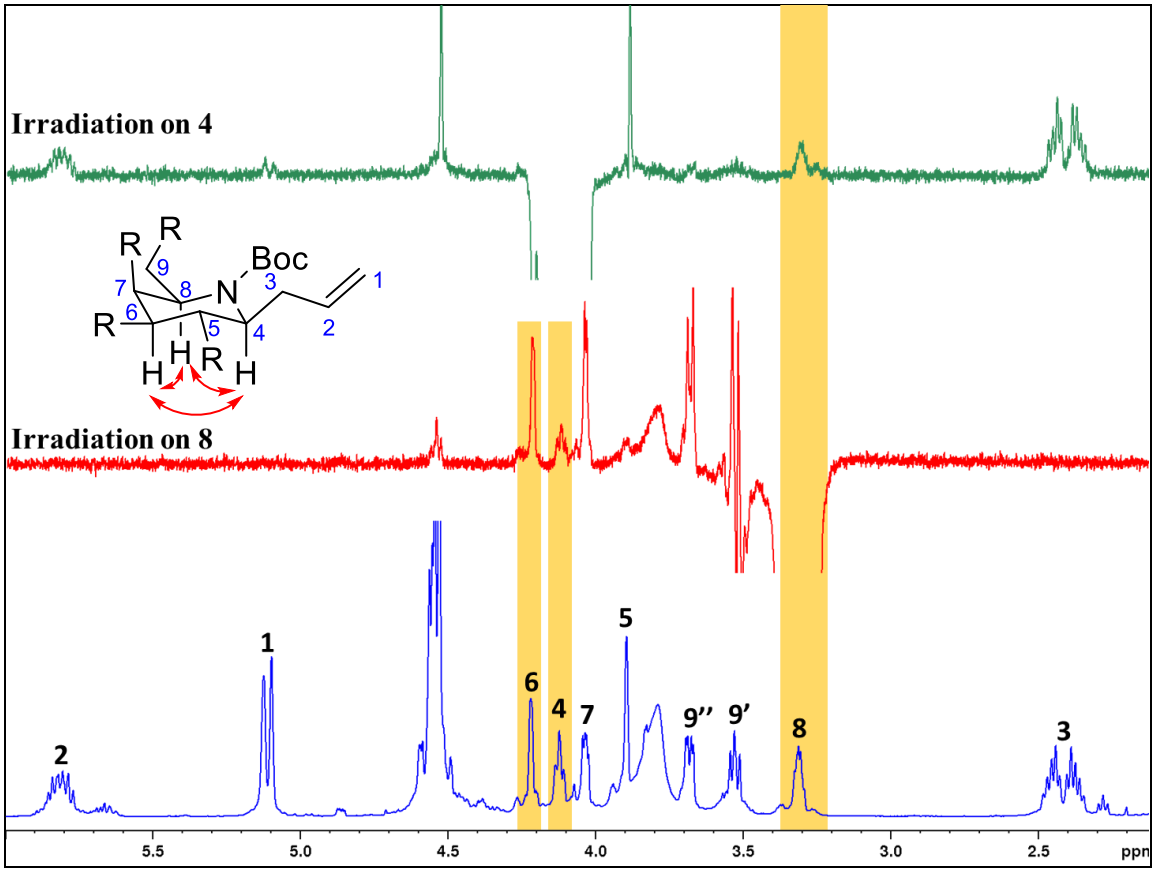

Figure 4.3.2.1: 1D nOe of compound **23**

The regioselectivity of the C-1 *β*-alkenylation in compound **23** was confirmed using a 1D nOe experiment and is shown in Figure 4.3.2.1. In this experiment, irradiating the proton at position 4 (H4) selectively resulted in an enhancement of the signal for the proton at position 8 (H8). Conversely, irradiating H8 led to signal enhancements for both H6 and H4. These observations indicate that all three protons (H4, H6, and H8) are positioned on the same side of the molecule. Since nOe relies on spatial proximity, this confirms that H4 occupies the α-position relative to the anomeric carbon (C-1). Consequently, the alkene moiety in compound **23** must be in the *β*-configuration.

4.3.2.2. Cross-coupling attempt through metathesis

Having successfully obtained the C-1 *β*-alkenylated azagalactose **23**, we turned our attention to the cross-metathesis reaction. To optimize resource utilization, we opted to employ a readily available simple alkene, 3-butenylbenzene, instead of a pre-functionalized

and potentially expensive alkenylated phytosphingosine. Unfortunately, the initial attempt at cross-metathesis using a second-generation Grubb's catalyst proved unsuccessful. We then explored various reaction parameters, including solvent (THF, DCM), temperature, and reaction time, but none of these modifications yielded the desired product

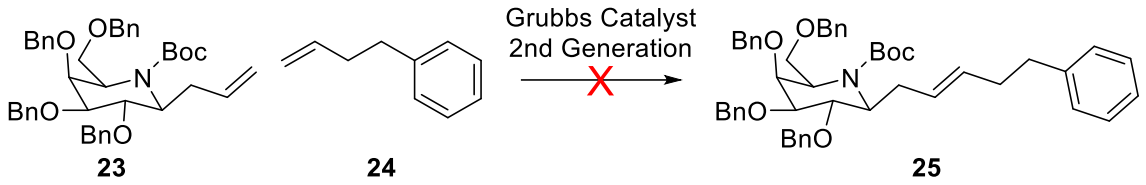

Scheme 4.3.2.2: Cross metathesis attempt

4.3.3. Cross-coupling through Click reaction

Given the challenges encountered with our initial cross-coupling attempts for connecting the sugar and lipid moieties, we have adopted a new strategy. Click chemistry, a powerful tool known for its efficiency and selectivity, now emerges as our preferred approach for forging the desired linkage between these crucial fragments. This method utilizes a copper-catalyzed Huisgen cycloaddition reaction between an azide and an alkyne to form a stable triazole linkage.

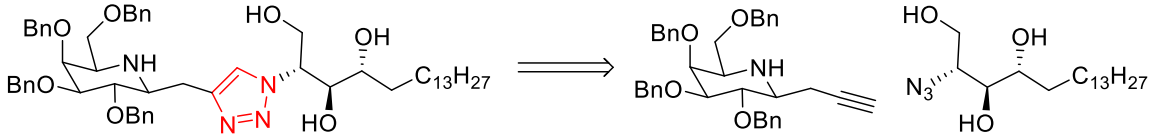

Figure 4.3.3: Click chemistry target

Click chemistry offers several advantages for our KRN-7000 analog synthesis:

- **High Yield and Selectivity:** Click reactions are renowned for their ability to deliver high product yields with excellent regioselectivity. This translates to a more efficient and streamlined synthesis.
- **Mild Reaction Conditions:** Click chemistry typically operates under mild reaction conditions, minimizing the risk of degradation for sensitive sugar and lipid components.

- **Orthogonality:** Click reactions are often orthogonal to many other functional groups commonly found in complex molecules. This allows for selective coupling without affecting other functionalities present in our KRN-7000 analog precursors.

By employing click chemistry as a reliable tool for triazole linkage formation, we aim to achieve a more efficient and robust synthesis of the desired iminosugar analogs of KRN-7000.

4.3.3.1. Synthesis of alkynylated galactose

Similar to the alkenylation strategy, we envisioned employing a Grignard reaction for C-1 alkynylation of the azagalactose unit. However, unlike allylmagnesium bromide, propargyl Grignard reagent (propargylmagnesium bromide) is not readily available in the market due to its limited shelf life. To overcome this hurdle, we opted for in-situ generation of propargyl Grignard reagent from propargyl bromide and magnesium metal.[21,22] This freshly prepared Grignard reagent was then used to treat the N-Boc lactam **6** with the aim of obtaining **28**.

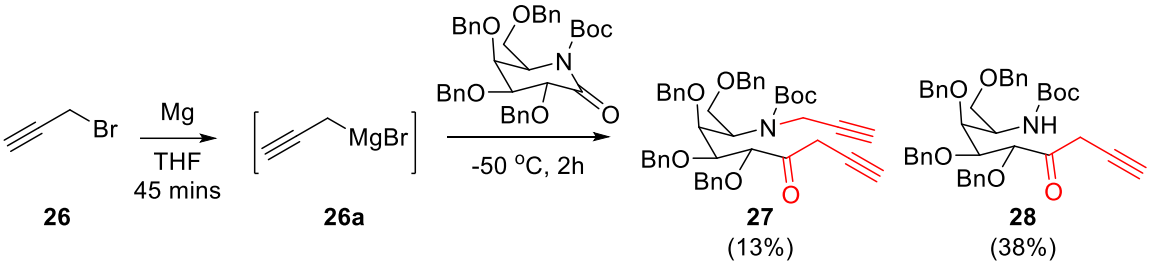

Scheme 4.3.3.1a: Propargylation on N-Boc lactam

Unfortunately, the reaction yielded an unexpected side product **27** in addition to the desired product **28**. This arose from the leftover propargyl bromide reacting with the N-Boc group on the already formed **28**. The challenge lies in achieving a balance: if we wait for the complete conversion of propargyl bromide to the Grignard reagent, the pre-formed propargyl Grignard reagent may decompose, impacting the overall yield. Conversely, using propargyl bromide too early increases the likelihood of the undesired side reaction.

An alternative approach emerged upon further evaluation. While the initial strategy produced the **28**, it required a subsequent reduction cyclization step to furnish the desired intermediate C-1 propargylated aza galactose 29 for click reaction. We recognized an

opportunity to streamline the process. Reacting propargyl Grignard reagent directly with the hemiacetal precursor **2** could potentially yield intermediate **29** after the same reduction cyclization step (Scheme 4.3.3.1b). This approach not only gives an opportunity for late-stage functionalization of sugar but also avoids the formation of the undesired side product **27** observed with the previous method. Since hemiacetal **2** is an intermediate compound for N-Boc lactam synthesis **6**, this streamlined strategy offers a significant reduction in steps (6 steps) and avoids the problematic side reaction.

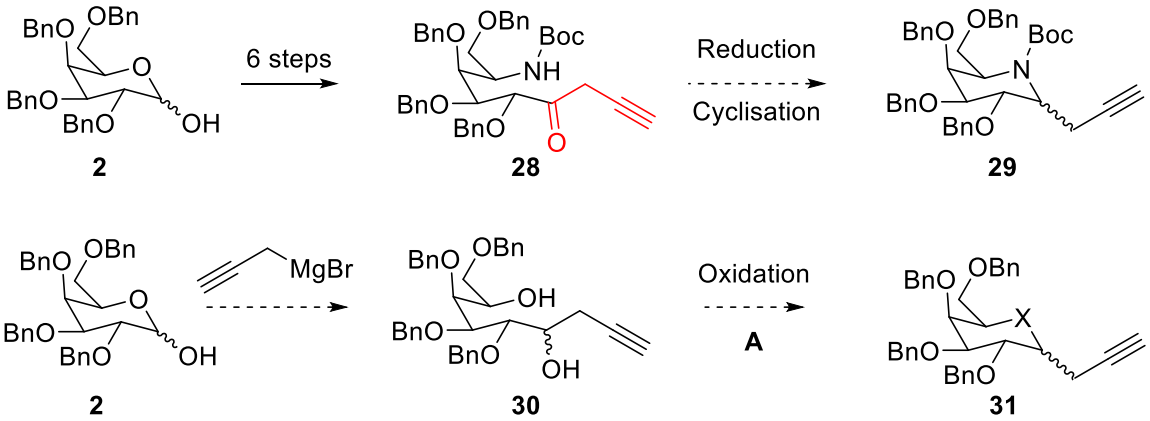

Scheme 4.3.3.1b: the idea of Propargylation on lactol

Following our revised strategy, we treated hemiacetal **2** with the in-situ generated propargyl Grignard reagent. While this approach aimed to achieve the desired C-1 propargylated intermediate **30**, we encountered a similar challenge that had been observed previously. Unreacted propargyl bromide remained in the reaction mixture, leading to the formation of an undesired side product **32** through alkynylation of the product itself.

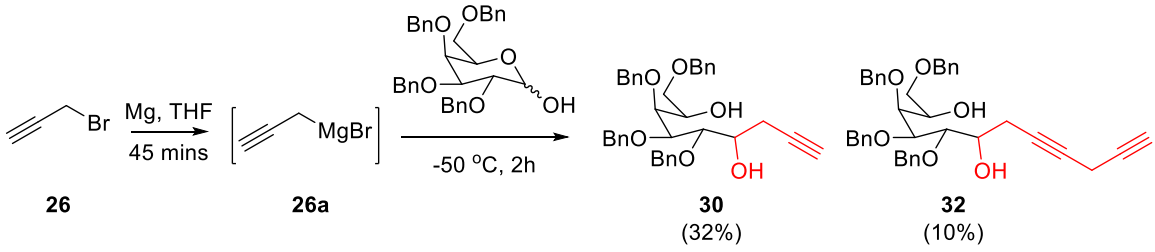

Scheme 4.3.3.1c: Propargylation on lactol

The persistent issue with unreacted propargyl bromide during in-situ Grignard reagent generation prompted us to explore alternative approaches. We implemented the use of trimethylsilyl (TMS)-protected propargyl bromide, anticipating a more stable precursor for

Grignard formation.[23] Unfortunately, the TMS-protected propargyl Grignard reagent failed to react with the hemiacetal **2**. Given this setback, we opted to modify the reaction strategy by changing the sugar partner. Instead of the hemiacetal, we employed lactone **3** (Scheme 4.3.3.1c) for the C-1 alkynylation reaction.

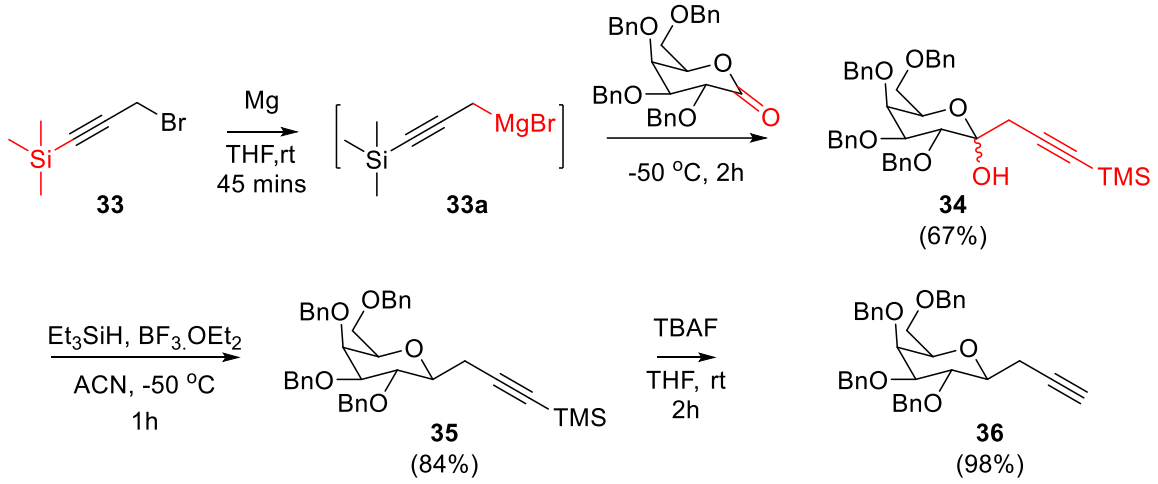

Scheme 4.3.3.1d: Propargylation on lactol

Treatment of lactone **3** with TMS-propargyl Grignard reagent at -50 °C afforded the desired C-1 propargylated hemiketal **34** in 67% yield. This intermediate served as a key precursor for the synthesis of the KRN-7000 oxy-sugar derivative. To achieve this, hemiketal **34** was first reduced to **35** using Kishi reduction conditions. Subsequent fluoride ion mediated desilylation afforded the click reaction partner, C-1 propargylated galactose **36**.

4.3.3.2. Synthesis of KRN-7000 analog

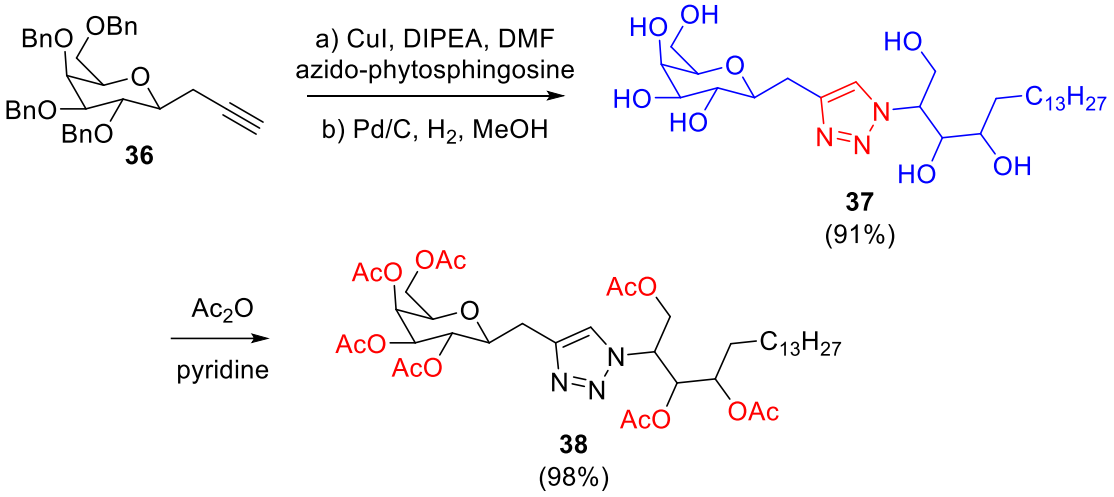

Scheme 4.3.3.2: Synthesis of KRN-7000 analogue

C-1propargylated galactose **36** readily underwent a copper-catalyzed click reaction (CuI) with azido-phytosphingosine in the presence of DIPEA (Scheme 4.3.3.2). Finally, global deprotection *via* Pd/C reduction furnished the KRN-7000 analogue **37** in excellent yield. To facilitate NMR characterization, the final product was acetylated using acetic anhydride to **38**.

^{1}H NMR techniques were used to confirm the *β*-C glycosylation at the C-1 position of the KRN-7000 analogue. Coupling constant values obtained from spectroscopic analysis played a key role in this confirmation (Figure 4.3.3.2).

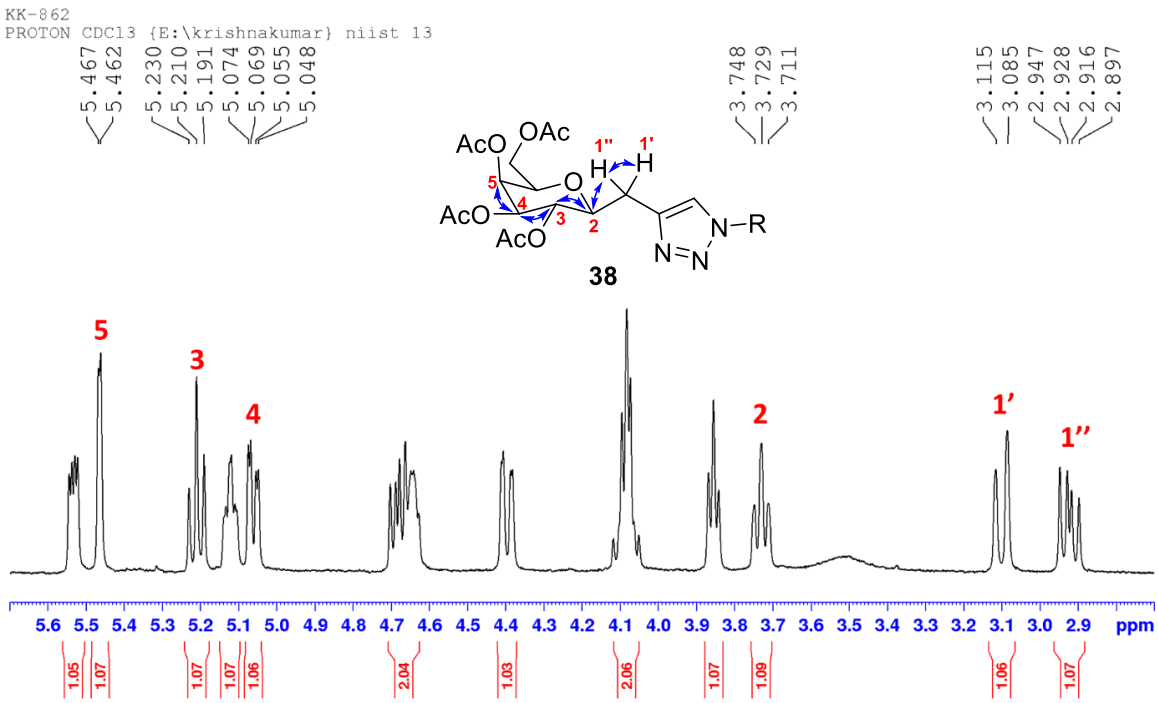

Figure 4.3.3.2: 1D nOe of compound **38**

Additionally, COSY analysis identifies the relationships between neighbouring protons in the molecule. It indeed helped to confirm the respective positions of the protons. H1" appeared as a doublet of doublets (dd), indicating interactions with two other protons. It has a geminal coupling with proton 1' and vicinal coupling with H2 were quantified by their coupling constants, which were 15.3 Hz and 9.6 Hz, respectively. Interestingly, both H2 and H3 protons appeared as triplets instead of doublets of doublets, suggesting a similar chemical environment for these protons. Furthermore, their respective coupling constants of 9.3 Hz and 9.8 Hz supported the idea of an axial-axial orientation for these hydrogens.

These coupling constants and multiplicities provide strong evidence for the *β*-orientation of the side chain (as an axial C-1 hydrogen is a characteristic feature of *β*-glycosidic bonds).

4.3.3.3. Synthesis of iminosugar analogue of KRN-7000

We initially envisioned synthesizing the C-1propargylated azagalactose derivative by oxidizing hemiketal **34** to a diketone intermediate. This intermediate would then be subjected to a double reductive amination to introduce the nitrogen atom and complete the azagalactose unit. Unfortunately, despite exploring various oxidation strategies, we were unable to obtain the desired diketone. This setback precluded the synthesis of the C-1 propargylated azagalactose using this planned route.

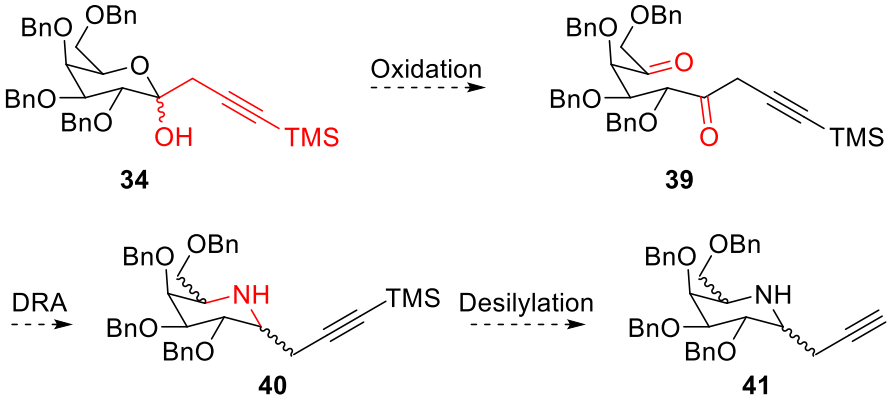

Scheme 4.3.3.3a: Proposed synthesis of C-1 propargylated azagalactose

Following the challenges encountered with C-1 propargylation, we opted for a strategic shift towards N-propargylation of the lactam moiety. This approach leverages the lone pair of electrons on the nitrogen atom of **5** to directly react with propargyl bromide *via* an S_N2 reaction, efficiently yielding click reaction partner **42**. This intermediate readily underwent a successful cycloaddition (click reaction) with azido-phytosphingosine under standard conditions, forming the triazole-linked product **43**.

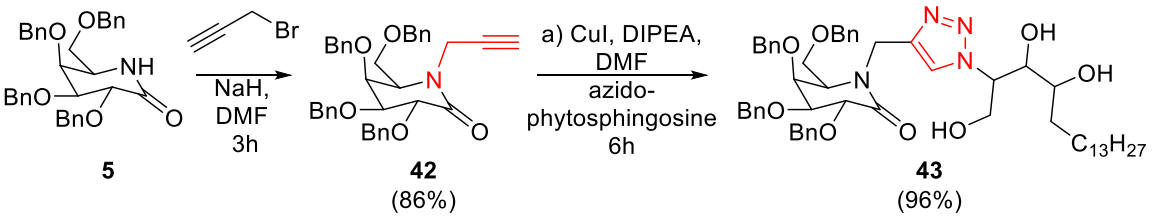

Scheme 4.3.3.3b: Click reaction with N-propargylated azagalactolactam

From this key intermediate **43**, we were able to diversify the synthesis and generate two distinct KRN-7000 glycomimetic analogs. Direct deprotection of **42** using Pd/C reduction yielded a lactam derivative of KRN-7000, compound **44**. Conversely, selective reduction of the amide carbonyl in **43** with borane-dimethyl sulfide (BH_3-DMS) followed by debenzylation afforded the C-1 deoxy iminosugar derivative (**45**) of KRN-7000.

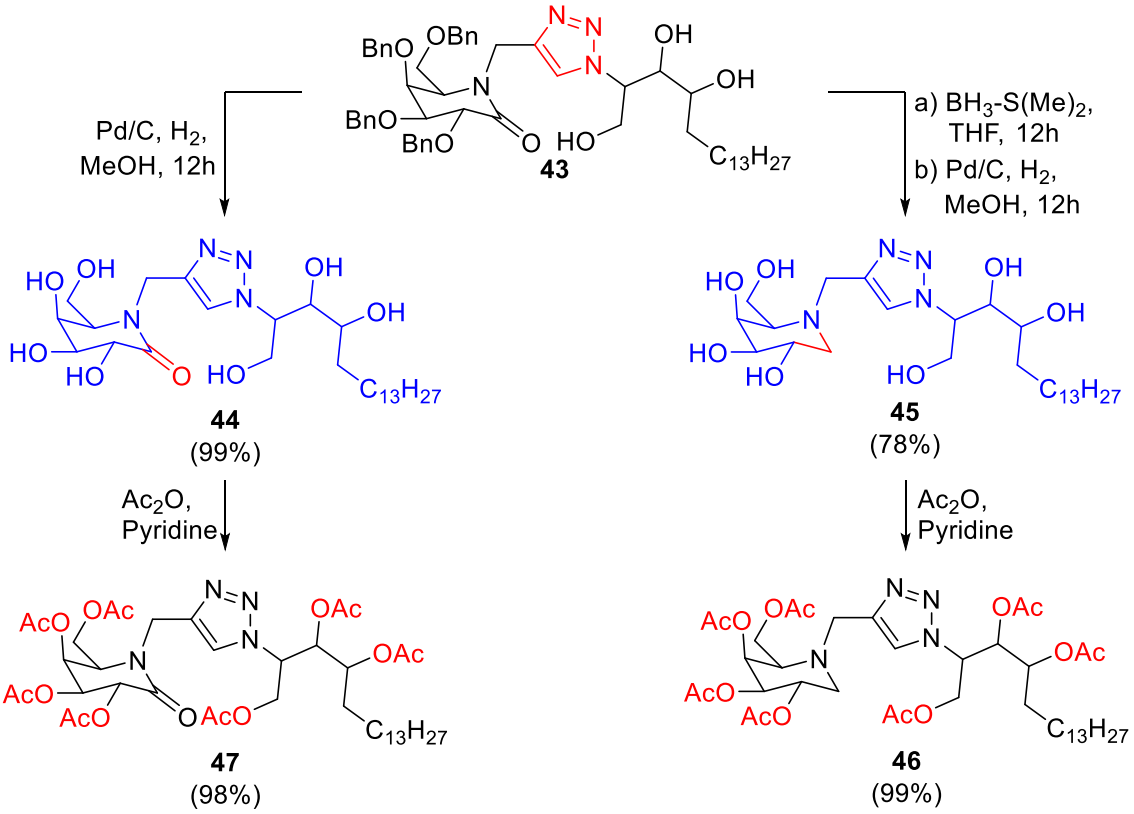

Scheme 4.3.3.3c: Synthesis of iminosugar analog of KRN-7000

While our goal was to synthesize the iminosugar C-glycosidic analogue of KRN-7000, we encountered several challenges during the C-1 propargylation step. However, by strategically adapting a different approach and employing click reaction, we were able to successfully synthesize novel KRN-7000 analogues. These analogues offer valuable alternatives for further investigation and potential development.

4.4. Conclusions

The synthesis of KRN-7000 analogues explored multiple avenues to achieve iminosugar glycomimetics of KRN-7000. Initial attempts using cross-coupling reactions, including Turbo Grignard reagents and metathesis, proved unsuccessful. Challenges arose with

controlling the reactivity of in-situ generated propargyl Grignard reagents during C-1 propargylation. However, this approach ultimately yielded the desired C-1 propargylated galactose intermediate using a lactone precursor and synthesised a KRN-7000 analogue with triazole linker

To overcome limitations with C-1 propargylation, the synthetic strategy shifted towards N-propargylation of the lactam moiety. This approach efficiently provided a click reaction partner through a direct S_N2 reaction. Subsequent click reaction with azido-phytosphingosine successfully furnished two novel KRN-7000 analogs

Despite encountering setbacks with the initial turbo Grignard reaction, cross-metathesis, and C-1 propargylation strategy, the successful application of N-propargylation and click reaction paves the way for the development of novel KRN-7000 analogs with potential biological applications. Future efforts can focus on refining the C-1 propargylation approach and exploring the biological activity of the newly synthesized KRN-7000 analogs.

4.5. Materials and methods

4.5.1. General experimental conditions:

^{1}H and ^{13}C NMR spectra were obtained using a Bruker ASCEND^{TM}-500 spectrometer at 500 and 125 MHz, respectively. $CDCl_3$ and CD_3OD solvents were used to record the spectra. The NMR data is presented as chemical shifts in ppm (δ) along with integration, coupling constant in Hz, and multiplicity (s = singlet, bs= broad singlet, d = doublet, t = triplet, m = multiplet, dd = doublet of doublet, etc.). The HR-ESI-MS analysis was performed on a Thermo Scientific Exactive-LCMS instrument using the electrospray ionization method. The ions are reported in m/z using an Orbitrap analyzer. Optical rotation was measured on a JASCO P-2000 polarimeter. The reactions were monitored by silica gel G-60 F_{254} aluminum TLC plates, and the compounds were made visible by a short wavelength lamp; the TLC plate was charred after spraying with 15% sulfuric acid in ethanol. Chromatographic separations were carried out by conventional column chromatography on silica gel (100 - 200 mesh). The reagents were purchased at the highest commercial quality and used without further purification.

4.5.2. General procedure for debenzylation

To prepare the respective product, a solution of benzyl-protected intermediate in 5 mL of MeOH was added with Pd/C and a few drops of conc. HCl, followed by purging H_2 gas for 2 minutes. The reaction mixture was stirred overnight under an H_2 atmosphere. The resulting mixture was filtered through a Celite® pad after being diluted with MeOH. The filtrate was concentrated and precipitated in DCM to obtain the desired product.

4.5.3. General procedure for Acetylation reaction

Corresponding polyalcohol (15 mg) was dissolved in pyridine (1 mL), and then acetic anhydride (0.5 mL) was added at room temperature. After 6 h, the reaction mixture was neutralized with saturated $NaHCO_3$(aq) solution and extracted with EtOAc (20 mL x 2). The organic layer was washed with distilled water and dried with anhydrous Na_2SO_4. The resulting mixture was concentrated, and the residue was purified using hexane: EtOAc by silica gel column chromatography to obtain the corresponding acetylated product.

4.5.4. Synthesis of propargyl magnesium bromide

Vigorously stirring a blend of Mg turnings (10 mmol, 240 mg, 1.6 equiv.) and $HgCl_2$ (0.02 mmol, 5.4 mg, 0.003 equiv.) in 3 mL of Et_2O took place for approximately 10 mins at room temperature under an argon atmosphere. Subsequently, a small quantity of the corresponding propargylic bromide solution (6 mmol, 1.5 equiv.) in 6 mL of Et_2O was introduced. As the reaction mixture began to bubble, it was cooled to 0 ºC, and the remaining propargylic bromide solution was added dropwise *via* a pressure-equalizing funnel. The reaction mixture was stirred for 1 hour, transitioning from 0 ºC to room temperature.

4.5.5. General condition for C-1 propargylation

A thoroughly dried corresponding sugar derivative (1.48 mmol, 1 equiv.) was dissolved in dry Et_2O (4 mL) under an argon atmosphere. The solution was cooled to -50 °C, and freshly prepared propargyl magnesium bromide solution in THF (~9 mL, 6 mmol, 4 equiv.) was transferred using a cannula, and the stirring was continued at -50 °C. After 2 hours, the reaction mixture was quenched with 2 mL of MeOH and was allowed to warm to room temperature. The reaction mixture was partitioned between EtOAc (50 mL) and distilled water (50 mL). The aqueous layer was extracted with EtOAc (50 mL x 2), and the combined organic layers were dried over anhydrous Na_2SO_4 and concentrated under reduced pressure.

The residue was then purified through column chromatography using hexane/EtOAc to obtain the corresponding propargylated compound.

4.5.6. Other experimental procedures

(3R,4S,5S,6R)-3,4,5-tris(benzyloxy)-6-((benzyloxy)methyl)tetrahydro-2H-pyran-2-ol (2): The hemiacetal compound **2** was synthesized using the Overkleeft protocol[19] and confirmed by comparison of the NMR data. ^{1}H-NMR ($CDCl_3$) δ 7.37 (30H, m), 5.32 (1H, m), 4.97 (2H, m), 4.84 (2H, m), 4.76 (3H, m), 4.69 (1H, m), 4.63 (1H, m), 4.51 (1H, m), 4.44 (1H, m), 4.20 (1H, m), 4.07 (1H, m), 3.97 (2H, m), 3.91 (1H, m), 3.80 (1H, t, *J*=8.55 Hz), 3.63 (1H, m), 3.57 (1H, m), 3.51 (1H, m) ppm; ^{13}C-NMR ($CDCl_3$) δ 138.65, 138.56, 138.50, 138.41, 138.26, 137.87, 137.75, 128.46, 128.43, 128.35, 128.32, 128.28, 128.20, 128.04, 128.02, 127.98, 127.86, 127.80, 127.79, 127.66, 127.60, 127.54, 97.80, 91.91, 82.21, 80.75, 78.75, 76.61, 75.11, 74.76, 74.69, 74.59, 73.63, 73.58, 73.52, 73.50, 72.99, 72.96, 69.52, 69.09, 68.95 ppm; HR-ESI-MS: $[M+Na]^+$ calculated for $C_{34}H_{36}O_6Na$ was m/z 563.2410, found 563.2419.

(3R,4S,5S,6R)-3,4,5-tris(benzyloxy)-6-((benzyloxy)methyl)tetrahydro-2H-pyran-2-one (3): A solution of hemiacetal **2** (5 g, 9.2 mmol, 1 equiv.) was dissolved in DCM (200 mL), followed by the addition of Dess-Martin periodinane (DMP) (5.88 g, 13.8 mmol, 1.5 equiv.). The reaction mixture was stirred for 2 h at room temperature under an argon atmosphere. After the reaction was complete, as indicated by TLC, the mixture was quenched with saturated $Na_2S_2O_3$(aq) (50 mL) and saturated $NaHCO_3$(aq) (50 mL), it was then extracted with DCM (2 x 100 mL). The combined organic extracts were dried over anhydrous Na_2SO_4 and concentrated. The resulting product was purified by column chromatography using hexane/EtOAc to afford **3** (4.63 g, 93% yield). ^{1}H-NMR ($CDCl_3$) δ 7.36 (2H, m), 7.45 (16H, m), 7.27 (2H, m), 5.22 (1H, d, *J*=11.01 Hz), 4.97 (1H, d, *J*=11.26 Hz), 4.80 (2H, t, *J*=12.76 Hz), 4.72 (1H, d, *J*=11.86 Hz), 4.64 (1H, d, *J*=11.31 Hz), 4.51 (3H, m), 4.37 (1H, m), 4.20 (1H, s), 3.92 (1H, dd, *J* =1.07, 9.59 Hz), 3.72 (2H, m) ppm; ^{13}C-NMR ($CDCl_3$) δ 170.04, 137.81, 137.56, 137.42, 128.54, 128.53, 128.50, 128.40, 128.05, 128.02, 128.00, 127.95, 127.91, 127.86, 127.57, 80.16, 77.35, 75.33, 74.77, 73.70, 72.86, 72.57, 67.55 ppm; HR-ESI-MS: $[M+Na]^+$ calculated for $C_{34}H_{34}O_6Na$ was m/z 561.2253, found 561.2245.

(3R,4S,5R)-3,4,5-tris(benzyloxy)-6-((benzyloxy)methyl)-6-hydroxypiperidin-2-one (4): A solution of lactone, **3** (4 g, 7.4 mmol, 1 equiv.) was dissolved in 7N NH_3 in MeOH (20 mL)

and stirred for 1 h, a white precipitate was formed, and the reaction mixture was evaporated to dryness. DCM (150 mL) was added followed by Dess−Martin periodinane (DMP) (4.72 g, 11.13 mmol, 1.5 equiv.), and the reaction mixture was stirred for 1 h at rt under an argon atmosphere. After the completion of the reaction indicated by TLC, the reaction mixture was quenched with saturated $Na_2S_2O_3$(aq) (50 mL), saturated $NaHCO_3$ (aq) (50 mL), and extracted with DCM (2 × 100 mL), the organic extracts were dried over anhydrous Na_2SO_4 and concentrated. Purification by column chromatography using hexane/EtOAc afforded **4** as a colorless viscous liquid (3.64 g, 71% yield over 2 steps). ^{1}H-NMR ($CDCl_3$) δ 7.46 (2H, m), 7.33 (17H, m), 7.24 (2H, m), 6.52 (1H, s), 5.21 (1H, d, J =11.28 Hz), 4.97 (1H, d, J =11.45 Hz), 4.85 (2H, d, J =11.49 Hz), 4.74 (1H, m), 4.61 (1H, d, J =11.30 Hz), 4.54 (3H, m), 4.41 (2H, m), 3.97 (1H, s), 3.88 (1H, s), 3.49 (1H, d, J =8.81 Hz), 3.56 (1H, d, J =8.82 Hz) ppm; ^{13}C-NMR ($CDCl_3$) δ 171.97, 138.40, 138.27, 137.80, 136.84, 128.64, 128.61, 128.57, 128.48, 128.47, 128.40, 128.34, 128.27, 128.18, 128.10, 127.99, 127.91, 127.87, 127.83, 127.64, 127.62, 127.60, 82.13, 77.97, 77.66, 76.73, 75.16, 74.63, 73.84, 73.34, 73.07 ppm; HR-ESI-MS: $[M+Na]^+$ calculated for $C_{34}H_{35}NO_6Na$ was m/z 576.2362, found 576.2381.

(3R,4S,5S,6R)-3,4,5-tris(benzyloxy)-6-((benzyloxy)methyl)piperidin-2-one (5): To a solution of **4** (2 g, 3.6 mmol, 1 equiv.) in ACN (50 mL) was added 13 mL formic acid, and $NaCNBH_3$ (360 mg, 7.22 mmol, 2 equiv.), and then the reaction mixture was stirred at 60 °C under an argon atmosphere for 2 h. The reaction mixture was cooled to 0 °C, quenched with saturated aqueous $NaHCO_3$ (100 mL), and extracted with EtOAc (3 × 100 mL), and the organic layers were washed with H_2O (2 × 50 mL), dried over anhydrous Na_2SO_4, and concentrated. Purification by column chromatography using hexane/EtOAc afforded compound **5** (1.57 g, 81% yield) as a white solid. ^{1}H-NMR ($CDCl_3$) δ 7.33 (20H, m), 6.02 (1H, s), 5.21 (1H, d, J =11.15 Hz), 4.88 (2H, m), 4.78 (2H, m), 4.51 (3H, m), 4.04 (1H, d, J =7.82 Hz), 3.94 (1H, t, J =8.04 Hz), 3.61 (3H, m), 3.30 (1H, t, J =8.11 Hz) ppm; ^{13}C-NMR ($CDCl_3$) δ 171.80, 138.35, 138.24, 137.74, 136.75, 128.66, 128.40, 128.32, 128.27, 128.18, 128.10, 127.93, 127.65, 127.62, 127.60, 82.07, 77.96, 77.64, 76.73, 75.15, 74.59, 73.85, 73.37, 73.12 ppm; HR-ESI-MS $[M+Na]^+$ calculated for $C_{34}H_{35}NO_5Na$ was m/z 560.2413, found 560.2417.

***tert*-butyl(2R,3S,4S,5R)-3,4,5-tris(benzyloxy)-2-((benzyloxy)methyl)-6-oxopiperidine -1-carboxylate (6):** The compound **5** (2.7 g, 5.0 mmol, 1 equiv.) was dissolved in DCM (50 mL). $(Boc)_2O$ (2.19 g, 10 mmol, 2 equiv.), Et_3N (1.55 mL, 11.0 mmol, 2.2 equiv.) and

DMAP (0.61 mg, 0.5 mmol, 0.1 equiv.) was added then stirred at room temperature for 3 h. The reaction mixture was quenched with water (50 mL), and the product was extracted in DCM (2 x 50 mL). The organic layer was dried using anhydrous Na_2SO_4, concentrated under reduced pressure, and purified using silica gel column chromatography to obtain compound **6** as a colorless viscous liquid (3 g, 94% yield). ^{1}H-NMR ($CDCl_3$) δ 7.45 (2H, d, J =7.20 Hz), 7.30 (17H, m), 7.20 (2H, d, J=7.30 Hz), 5.16 (1H, d, J =11.06 Hz), 4.74 (2H, t, J =7.60 Hz), 4.71 (1H, m), 4.67 (2H, m), 4.57 (1H, d, J =12.01 Hz), 4.46 (1H, d, J =9.35 Hz), 4.39 (3H, s), 4.11 (1H, dd, J =2.43, 9.33 Hz), 4.02 (1H, m), 3.48 (1H, m), 3.43 (1H, m), 1.50 (9H, s) ppm; ^{13}C-NMR ($CDCl_3$) δ 171.10, 152.51, 138.37, 138.29, 137.94, 137.44, 128.45, 128.40, 128.35, 128.27, 128.25, 127.88, 127.84, 127.77, 127.67, 127.59, 127.57, 83.33, 79.99, 74.91, 74.31, 73.34, 72.86, 72.48, 68.94, 56.48, 28.02 ppm; HR-ESI-MS: $[M+Na]^+$ calculated for $C_{39}H_{43}NO_7Na$ was m/z 660.2937, found 660.2929.

***tert*-butyl((3S,4R)-1-((*tert*-butyldimethylsilyl)oxy)-3,4-dihydroxyoctadecan2yl) carbamate (8):** Phytosphingosine (954 mg, 2.7 mmol, 1 equiv.) was added to 1 N NaOH (aq) (4.5 mL, 4 mmol, 1.5 equiv.), and the mixture was diluted with a solution of water-ethanol (1:2, 36 mL). Then, $(Boc)_2O$ (956 mg, 4 mmol, 1.5 equiv.) was added and stirred at room temperature for 1h. The reaction mixture was quenched with saturated aqueous NH_4Cl (50 mL) and extracted in EtOAc (100 mL x 3). The organic layer was washed with distilled water (2 x 50 mL) and brine (50 mL). It was then dried using anhydrous Na_2SO_4 and concentrated under reduced pressure to obtain a crude syrup. It was dissolved in a 10 mL solution of dry DCM and dry DMF (4:1) and cooled to 0 °C. Triethylamine (0.625 mL, 4 mmol, 1.5 equiv.) TBDMSCl (688 mg, 4 mmol, 1.5 equiv.) and DMAP (28 mg, 0.27 mmol, 0.1 equiv.) were added into the reaction mixture by maintaining an inert argon atmosphere. After 2 h, the reaction mixture was quenched with saturated aqueous NH_4Cl (50 mL) and extracted in DCM (100 mL x 3). The organic layer was washed with distilled water (3 x 50 mL) and brine (50 mL). The concentration of organic layer and silica gel column chromatography purification afforded **8** as a colorless viscous liquid (1.16 g, 81% yield over 2 steps). ^{1}H-NMR ($CDCl_3$) δ 5.21 (1H, d, J =8.43 Hz), 3.91 (1H, d, J =9.85 Hz), 3.82 (1H, bs), 3.75 (1H, m), 3.58 (2H, m), 3.25 (1H, bs), 2.93 (1H, bs), 1.67 (2H, m), 1.43 (9H, s), 1.24 (24H, s), 0.89 (9H, s), 0.86 (3H, t, J =6.77 Hz), 0.09 (6H, s) ppm; ^{13}C-NMR ($CDCl_3$) δ 155.67, 79.63, 76.01, 73.38, 62.81, 51.60, 33.43, 31.93, 29.70, 29.67, 29.64, 29.62, 29.37, 28.38, 25.96, 25.82, 22.69, 18.16, 14.12, -5.54, -5.64 ppm; HR-ESI-MS: $[M+Na]^+$ calculated for $C_{29}H_{61}NO_5SiNa$ was m/z 554.4217, found 554.4212.

***tert*-butyl(2-((*tert*-butyldimethylsilyl)oxy)-1-((4S,5R)-2,2-dimethyl-5-tetradecyl-1,3-dioxolan-4-yl)ethyl)carbamate (9):** A solution of **8** (126 mg, 0.24 mmol, 1 equiv.) in dry DCM (5 mL) was prepared to which 2,2-dimethoxy propane (232 µL, 1.9 mmol, 8 equiv.) and PPTS (3 mg, 0.02 mmol, 0.1 equiv.) were added at 0 °C. The mixture was slowly warmed to room temperature and stirred for 3 hours. MeOH (5 mL) was added to the reaction mixture and stirred for one more hour. The solvents were then evaporated, and the residue was purified using silica gel chromatography to obtain compound **9** as a colorless liquid (122 mg) in 90% yield. ^{1}H-NMR ($CDCl_3$) δ 4.67 (1H, d, J =9.74 Hz), 4.00 (2H, m), 3.78 (1H, d, J =9.66 Hz), 3.69 (1H, t, J =8.68 Hz), 3.60 (1H, d, J =9.50 Hz), 1.48 (3H, m), 1.38 (13H, m), 1.22 (25H, m), 0.84 (9H, s), 0.81 (3H, t, J =6.90 Hz), -0.00 (6H, s) ppm; ^{13}C-NMR ($CDCl_3$) δ 155.07, 107.80, 79.39, 77.94, 75.52, 62.91, 50.77, 31.93, 29.69, 29.66, 29.54, 29.37, 29.09, 28.35, 26.25, 25.94, 25.90, 22.69, 18.35, 14.12, -5.48 ppm; HR-ESI-MS: $[M+Na]^+$ calculated for $C_{32}H_{65}NO_5SiNa$ was m/z 594.4530, found 594.4535.

***tert*-butyl(1-((4S,5R)-2,2-dimethyl-5-tetradecyl-1,3-dioxolan-4-yl)-2-hydroxyethyl) carbamate (10):** A solution of **9** (98 mg, 0.17 mmol) in THF (5 mL) was stirred with a solution of TBAF in THF (0.514 mL, 0.51 mmol, 3 equiv.) at room temperature for 3 hours. The reaction mixture was then quenched with 10 mL of saturated aqueous NH_4Cl and extracted with 3 x 25 mL of EtOAc. The combined organic extracts were dried over anhydrous Na_2SO_4 and concentrated. Purification by column chromatography using hexane/EtOAc afforded compound **10** (77 mg, 99% yield) as a white solid. ^{1}H-NMR ($CDCl_3$) δ 4.99 (1H, d, J =8.40 Hz), 4.18 (1H, t, J =6.21 Hz), 4.10 (1H, d, J =5.59 Hz), 3.80 (3H, m), 2.40 (1H, s), 1.58 (3H, s), 1.46 (13H, s), 1.26 (25H, m), 0.90 (3H, t, J =6.62 Hz) ppm; ^{13}C-NMR ($CDCl_3$) δ 155.42, 108.07, 79.75, 78.14, 77.87, 63.80, 51.08, 31.93, 29.69, 29.66, 29.61, 29.58, 29.52, 29.36, 29.20, 28.35, 27.63, 26.76, 25.29, 22.69, 14.12 ppm; HR-ESI-MS: $[M+Na]^+$ calculated for $C_{26}H_{51}NO_5Na$ was m/z 480.3665, found 480.3674.

***tert*-butylbenzyl(1-((4S,5R)-2,2-dimethyl-5-tetradecyl-1,3-dioxolan-4-yl)-2 hydroxyethyl)carbamate (14):** To a solution of compound **9** (300 mg, 0.52 mmol, 1 equiv.) in DMF (4 mL) at -10°C, NaH (60% suspension in mineral oil) (31.4 mg, 0.8 mmol, 1.5 equiv.) was added and the resulting mixture was stirred for 30 minutes. At the same temperature, benzyl bromide (0.1 mL, 0.8 mmol, 1.5 equiv.) was added dropwise and stirring was continued. After 24 h, the reaction mixture was quenched with ice and extracted with EtOAc (2 × 25 mL). The organic extracts were dried over anhydrous Na_2SO_4 and concentrated to obtain a crude syrup. It was redissolved in THF (5 mL) and added TBAF

solution in THF (2 mL, 2 mmol, 4 equiv) at room temperature and stirred for 4 hours. The reaction mixture was then quenched with 10 mL of saturated aqueous NH_4Cl and extracted with 3 x 25 mL of EtOAc. The combined organic extracts were dried over anhydrous Na_2SO_4 and concentrated. Purification by column chromatography using hexane/EtOAc afforded compound **14** (227 mg, 79% yield over 2 steps) as a viscous liquid. HR-ESI-MS $[M+Na]^+$ calculated for $C_{33}H_{57}NO_5Na$ was m/z 570.4134, found 570.4136.

***tert*-butylbenzyl(1-((4S,5R)-2,2-dimethyl-5-tetradecyl-1,3-dioxolan-4-yl)-2-oxoethyl) carbamate (15):** A solution of **14** (122 mg, 0.22 mmol, 1 equiv.) was dissolved in 5 mL of DCM. $NaHCO_3$ (84 mg, 1 mmol, 4.5 equiv.) was added followed by Dess-Martin periodinane (DMP) (142 mg, 0.33 mmol, 1.5 equiv.). the reaction mixture was stirred for 1 h at room temperature. It was quenched with 10 mL of saturated $Na_2S_2O_3$(aq) and 10 mL of water. The mixture was then extracted with 3 x 25 mL of DCM. The combined organic extracts were dried over anhydrous Na_2SO_4 and concentrated. The resulting product was purified using hexane/EtOAc by column chromatography, which resulted in the formation of **15** (113 mg, 81% yield) as a viscous liquid. ^{1}H-NMR ($CDCl_3$) δ 9.72 (1H, s), 7.30 (5H, m), 4.75 (1H, m), 4.44 (1H, t, J =6.08 Hz), 4.14 (1H, d, J =14.91 Hz), 3.97 (1H, m), 1.47 (14H, m), 1.28 (26H, m), 0.90 (3H, t, J =6.72 Hz) ppm; ^{13}C-NMR ($CDCl_3$) δ 198.92, 155.94, 128.89, 128.79, 128.70, 127.91, 127.86, 127.71, 108.55, 107.16, 81.14, 77.78, 64.85, 50.34, 31.94, 29.71, 29.67, 29.60, 29.50, 29.48, 29.38, 28.23, 22.70, 14.14 ppm; HR-ESI-MS: $[M+Na]^+$ calculated for $C_{33}H_{55}NO_5Na$ was m/z 568.3978, found 568.3983.

***tert*-butylbenzyl(1-((4S,5R)-2,2-dimethyl-5-tetradecyl-1,3-dioxolan-4-yl)-3-iodoallyl) carbamate (16):** A solution of (Iodomethyl)triphenylphosphonium iodide (3.5 g, 6.6 mmol, 2.5 equiv.) in dry THF (50 mL) was stirred for 10 minutes at room temperature. Then, a solution of NaHMDS in THF (9.3 mL, 9.3 mmol, 3.5 equiv.) was slowly added to it at room temperature under a nitrogen atmosphere. After stirring for 45 mins, a solution of compound **15** (1.45 g, 2.6 mmol, 1 equiv.) in dry THF (10 mL) was added to the reaction mixture using a cannula and stirring was continued at rt for 3h. It was quenched with saturated aqueous NH_4Cl (50 mL) and extracted with EtOAc (100 mL x 2). The organic layer was washed with excess water, dried over anhydrous Na_2SO_4, concentrated, and purified by column chromatography using hexane/ethyl acetate, which yielded the compound **16** (1.23 g, 70% yield) as a viscous liquid. ^{1}H-NMR ($CDCl_3$) δ 7.16 (5H, m), 6.50 (2H, m), 4.82 (1H, s), 4.37 (3H, m), 4.03 (1H, d, J =8.50 Hz), 1.52 (2H, s), 1.40 (12H, m), 1.21 (27H, m), 0.81 (3H, t, J =6.80 Hz) ppm; ^{13}C-NMR ($CDCl_3$) δ 155.27, 136.92,

128.00, 126.90, 126.51, 107.77, 79.79, 77.78, 31.94, 29.71, 29.67, 29.62, 29.59, 29.52, 29.49, 29.38, 28.34, 27.10, 24.88, 22.71, 14.14 ppm; HR-ESI-MS: $[M+Na]^+$ calculated for $C_{34}H_{56}INO_4Na$ was m/z 692.3152, found 692.3161.

***tert*-butylbenzyl((3S,4R)-3,4-bis(benzyloxy)-1-hydroxyoctadecan-2-yl)carbamate (17) :** To a solution of compound **9** (600 mg, 1.12 mmol, 1 equiv.) in DMF (10 mL) at -10°C, NaH (60% suspension in mineral oil) (135 mg, 5.6 mmol, 5 equiv.) was added, and the resulting mixture was stirred for 30 minutes. To it, benzyl bromide (0.535 mL, 4.5 mmol, 1.7 equiv.) was added dropwise and stirred for 30 h. The reaction mixture was quenched with ice and extracted with EtOAc (2 × 100 mL). The organic extracts were dried over anhydrous Na_2SO_4 and concentrated to obtain a crude syrup. It was the redissolved in THF (10 mL) then added a solution of TBAF in THF (4.5 mL, 4.5 mmol, 4 equiv.) and stirred at room temperature for 3 hours. The reaction mixture was then quenched with 10 mL of saturated aqueous NH_4Cl and extracted with 3 x 50 mL of EtOAc. The combined organic extracts were dried over anhydrous Na_2SO_4 and concentrated. Purification by column chromatography using hexane/EtOAc afforded compound **17** (620 mg, 80% yield over 2 steps) as a colorless viscous liquid. ^{1}H-NMR ($CDCl_3$) δ 7.31 (15H, m), 4.86 (1H, d, J =11.04 Hz), 4.66 (3H, m), 4.45 (2H, m), 4.20 (1H, m), 3.89 (2H, m), 3.56 (2H, m), 1.72 (1H, m), 1.51 (10H, s), 1.31 (24H, s), 0.92 (3H, t, J =6.75 Hz) ppm; ^{13}C-NMR ($CDCl_3$) δ 156.60, 138.75, 138.50, 128.62, 128.45, 128.38, 128.30, 128.18, 127.94, 127.74, 127.62, 127.45, 80.96, 80.84, 78.69, 73.80, 72.55, 64.09, 60.79, 52.71, 31.97, 30.66, 29.76, 29.71, 29.41, 28.46, 26.75, 22.74, 14.18 ppm; HR-ESI-MS: $[M+Na]^+$ calculated for $C_{44}H_{65}NO_5Na$ was m/z 710.4760, found 710.4781.

***tert*-butyl benzyl((3S,4R)-3,4-bis(benzyloxy)-1-oxooctadecan-2-yl)carbamate (17a):** A solution of **17** (261 mg, 0.38 mmol, 1 equiv.) was dissolved in 5 mL of DCM. To the solution, $NaHCO_3$ (143 mg, 1.7 mmol, 4.5 equiv.) and Dess-Martin periodinane (DMP) (241 mg, 0.57 mmol, 1.5 equiv.) were added. The mixture was stirred for 1 h at room temperature until the reaction was complete, as indicated by TLC. Then, the mixture was quenched with 10 mL of saturated $Na_2S_2O_3$(aq) extracted with 3 x 25 mL of DCM. The combined organic extracts were dried over anhydrous Na_2SO_4 and concentrated. The resulting product was purified using hexane/EtOAc by column chromatography, which led to the compound **17a** (208 mg, 80% yield) as a viscous liquid. ^{1}H-NMR ($CDCl_3$) δ 9.54 (1H, s), 7.29 (15H, m), 4.55 (3H, m), 4.42 (2H, m), 4.18 (1H, mm), 3.85 (1H, m), 3.65 (1H, m), 1.71 (1H, m), 1.47 (10H, s), 1.30 (24H, s), 0.91 (3H, t, J =6.80 Hz) ppm; ^{13}C-NMR

($CDCl_3$) δ 198.41, 155.64, 138.59, 138.07, 128.52, 128.42, 127.99, 127.85, 127.75, 127.63, 127.46, 81.14, 79.94, 78.89, 73.01, 65.82, 52.47, 31.96, 30.87, 29.79, 29.74, 29.70, 29.67, 29.40, 28.31, 26.64, 22.73, 14.16 ppm; HR-ESI-MS: $[M+Na]^+$ calculated for $C_{44}H_{63}NO_5Na$ was m/z 708.4604, found 708.4608

***tert*-butylbenzyl((4S,5R)-4,5-bis(benzyloxy)-1-iodononadec-1-en-3-yl)carbamate (18):** A solution of (Iodomethyl)triphenylphosphonium iodide (293 mg, 0.82 mmol, 3 equiv.) in dry THF (4 mL) was stirred for 10 minutes at room temperature. Then, a solution of NaHMDS in THF (1.1 mL, 1.1 mmol, 4 equiv.) was slowly added at room temperature under a nitrogen atmosphere. The resulting solution was stirred for 45 mins. To it, a solution of compound **17a** (187 mg, 0.27 mmol, 1 equiv.) in dry THF (2 mL) was added using a cannula. The reaction mixture was stirred for 6 hours, and then quenched with saturated aqueous NH_4Cl (5 mL) and extracted with EtOAc (25 mL x 2). The organic layer was washed with water, dried over anhydrous Na_2SO_4, concentrated, and purified by column chromatography using hexane/ethyl acetate, which yielded compound **18** (140 mg, 63% yield) as a viscous liquid. ^{1}H-NMR ($CDCl_3$) δ 7.19 (15H, m), 6.51 (2H, m), 4.62 (2H, m), 4.43 (2H, m), 4.33 (3H, m), 3.90 (1H, s), 3.35 (1H, m), 1.45 (11H, m), 1.19 (24H, s), 0.81 (3H, t, J =6.74 Hz) ppm; ^{13}C-NMR ($CDCl_3$) δ 155.21, 138.98, 137.96, 128.29, 128.26, 128.20, 127.83, 127.60, 127.43, 126.99, 126.75, 80.34, 73.66, 72.18, 62.80, 51.90, 31.96, 30.18, 29.79, 29.75, 29.71, 29.41, 28.47, 26.41, 22.73, 14.17 ppm; HR-ESI-MS: $[M+Na]^+$ calculated for $C_{45}H_{64}INO_4Na$ was m/z 832.3778, found 832.3792.

***tert*-butyl (1,3,4,5-tetrakis(benzyloxy)-6-oxonon-8-en-2-yl)carbamate (21):** To a solution of **6** (212 mg, 0.33 mmol) in dry THF (5 mL), allyl magnesium bromide (1.2 mL, 0.83 mmol, 2.5 equiv.) was added at -78 °C. After 6h, it was quenched with excess sat. aq. NH_4Cl and extracted with EtOAc (50 mL x 2). The organic layer was washed with distilled water and dried over anhydrous Na_2SO_4. The residue was concentrated and then purified by silica gel column chromatography using hexane: EtOAc to obtain compound **21** (133 mg) in 59% yield (pale yellow viscous liquid). ^{1}H-NMR ($CDCl_3$) δ 7.29 (20H, m), 5.82 (1H, m), 5.12 (1H, d, J =10.20 Hz), 4.98 (2H, m), 4.54 (9H, m), 4.21 (2H, m), 4.08 (1H, s), 3.94 (1H, m), 3.63 (2H, m), 3.32 (2H, m), 1.45 (9H, s) ppm; ^{13}C-NMR ($CDCl_3$) δ 208.66, 155.52, 138.21, 138.13, 137.83, 137.36, 130.56, 128.44, 128.37, 128.32, 128.28, 128.24, 128.10, 127.93, 127.75, 127.72, 127.65, 127.62, 118.60, 84.66, 79.77, 78.72, 73.59, 73.38, 73.00, 69.26, 44.27, 28.42 ppm; HR-ESI-MS: $[M+Na]^+$ calculated for $C_{42}H_{49}NO_7Na$ was m/z 702.3407, found 702.3410.

***tert*-butyl (1,3,4,5-tetrakis(benzyloxy)-6-hydroxynon-8-en-2-yl)carbamate (22):** To compound **21** (160 mg, 0.23 mmol, 1 equiv.) in MeOH (3 mL), $CeCl_3$ (87 mg, 0.35 mmol, 1.5 equiv.) was added and cooled to -78 °C. To it sodium borohydride (22 mg, 0.59 mmol, 2.5 equiv.) was added and stirred for 10 mins. The reaction mixture was quenched with 1 M NaH_2PO_4 (20 mL) and extracted in DCM (25 mL x 3). The organic layer was dried over anhydrous Na_2SO_4 and passed through a silica plug to yield 141 mg (88%) of the reduced product **22** as a colorless viscous liquid. ^{1}H-NMR ($CDCl_3$) δ 7.21 (20H, m), 5.67 (1H, m), 4.96 (3H, m), 4.79 (1H, m), 4.68 (1H, m), 4.61 (2H, s), 4.47 (2H, m), 4.36 (2H, m), 3.93 (2H, m), 3.84 (1H, d, J=6.88 Hz), 3.71 (2H, m), 3.54 (2H, m,), 2.91 (1H, m), 2.27 (1H, m), 2.17 (1H, m), 1.35 (9H, s) ppm; ^{13}C-NMR ($CDCl_3$) δ 155.61, 138.28, 138.04, 137.84, 134.39, 128.42, 128.39, 128.34, 128.00, 127.74, 127.72, 127.63, 127.58, 117.30, 86.78, 85.60, 82.55, 82.31, 79.31, 73.29, 71.84, 71.61, 69.11, 51.70, 37.38, 29.72, 28.40 ppm; HR-ESI-MS: $[M+Na]^+$ calculated for $C_{42}H_{51}NO_7Na$ was m/z 704.3563, found 704.3573.

***tert*-butyl(2S,3S,4R,5S,6R)-2-allyl-3,4,5-tris(benzyloxy)-6-((benzyloxy)methyl) piperidine -1-carboxylate (23):** The secondary alcohol **22** (159 mg, 0.23 mmol, 1 equiv.), was dissolved in dry DCM (5 mL) and cooled to 0 °C. Triethylamine (0.227 mL, 1.6 mmol, 7 equiv.) was added. To it mesyl chloride (0.108 mL, 1.4 mmol, 6 equiv.) was added dropwise while maintaining an inert argon atmosphere. The reaction mixture was allowed to warm to room temperature and stirred for 24 h. It was quenched with saturated aqueous NH_4Cl (5 mL) and extracted in DCM (20 mL x 3). The organic layer was washed with distilled water (2 x 20 mL), and brine (20 mL). The concentration of organic layer and purification by silica gel column chromatography afforded **23** as a colorless viscous liquid (49 mg, 47% yield). ^{1}H-NMR ($CDCl_3$) δ 7.24 (20H, m), 5.69 (1H, m), 4.99 (2H, d, J=12.85 Hz), 4.43 (6H, m), 4.09 (1H, m), 4.00 (1H, m), 3.91 (1H, m), 3.77 (1H, s), 3.65 (3H, bs), 3.57 (1H, m), 3.41 (1H, m), 3.19 (1H, m), 2.34 (1H, m), 2.26 (1H, m), 1.18 (9H, s) ppm; ^{13}C-NMR ($CDCl_3$) δ 155.72, 138.36, 137.96, 137.90, 134.96, 128.46, 128.37, 128.32, 128.21, 127.77, 127.61, 127.53, 116.79, 83.66, 83.36, 82.21, 81.05, 79.15, 73.23, 71.59, 71.39, 69.27, 52.15, 33.13, 29.72, 28.42 ppm; HR-ESI-MS: $[M+Na]^+$ calculated for $C_{42}H_{49}NO_6Na$ was m/z 686.3458, found 686.3461.

***tert*-butyl prop-2-yn-1-yl(1,3,4,5-tetrakis(benzyloxy)-6-oxonon-8-yn-2-yl)carbamate (27):** The conditions employed for the preparation of this compound were those described in the synthesis of propargyl magnesium bromide and General condition for C-1 propargylation, **27** was afforded as a sticky solid (43 mg, 13% yield). ^{1}H-NMR ($CDCl_3$) δ

7.42 (4H, m), 7.32 (14H, m), 7.15 (2H, d, *J* =6.58 Hz), 5.07 (1H, d, *J* =9.68 Hz), 4.93 (1H, d, *J* =11.52 Hz), 4.59 (3H, m), 4.48 (1H, d, *J* =11.80 Hz), 4.40 (3H, m), 4.32 (1H, m), 4.23 (1H, m), 4.19 (1H, d, *J* =9.45 Hz), 4.09 (1H, d, *J* =9.27 Hz), 3.63 (1H, m), 3.51 (1H, m), 2.59 (2H, m), 2.41 (2H, m), 2.04 (1H, s), 1.70 (1H, s), 1.48 (9H, s) ppm; ^{13}C-NMR ($CDCl_3$) *δ* 188.53, 155.44, 138.08, 137.99, 137.62, 137.36, 128.86, 128.42, 128.36, 128.27, 128.18, 127.94, 127.90, 127.80, 127.73, 127.66, 127.49, 95.47, 85.20, 81.49, 80.73, 79.51, 79.43, 76.16, 74.73, 73.94, 72.95, 72.68, 70.33, 69.31, 49.45, 28.43, 19.30, 17.64 ppm; HR-ESI-MS: $[M+Na]^+$ calculated for $C_{45}H_{49}NO_7Na$ was m/z 738.3407, found 738.3398.

***tert*-butyl (1,3,4,5-tetrakis(benzyloxy)-6-oxonon-8-yn-2-yl)carbamate (28):** The conditions employed for the preparation of this compound were those described in the synthesis of propargyl magnesium bromide and the General condition for C-1 propargylation, which afforded **28** as a sticky solid (121 mg, 38% yield). ^{1}H-NMR ($CDCl_3$) *δ* 7.25 (20H, m), 5.21 (1H, m), 5.08 (1H, d, *J* =8.75 Hz), 4.75 (2H, m), 4.62 (2H, m), 4.51 (1H, m), 4.43 (2H, m), 4.35 (2H, m), 4.20 (1H, d, *J* =4.09 Hz), 3.94 (1H, m), 3.88 (1H, m), 3.64 (1H, m), 3.50 (1H, m), 3.39 (1H, m), 2.52 (1H, bs), 1.64 (1H, bs), 1.35 (9H, s) ppm; ^{13}C-NMR ($CDCl_3$) *δ* 170.47, 152.03, 138.50, 138.27, 137.87, 137.51, 128.51, 128.44, 128.19, 128.14, 127.94, 127.90, 127.86, 127.80, 127.72, 127.48, 127.44, 127.33, 83.04, 78.11, 77.70, 74.25, 74.22, 73.34, 72.98, 71.50, 71.33, 57.36, 27.95 ppm; HR-ESI-MS: $[M+Na]^+$ calculated for $C_{42}H_{47}NO_7Na$ was m/z 700.3250, found 700.3266.

1,3,4,5-tetrakis(benzyloxy)non-8-yne-2,6-diol (30): The conditions employed for the preparation of this compound were those described in the synthesis of propargyl magnesium bromide and the General condition for C-1 propargylation, **30** was afforded as a sticky solid (172 mg, 32% yield). ^{1}H-NMR ($CDCl_3$) *δ* 7.31 (20H, m), 4.79 (4H, m), 4.67 (1H, m), 4.57 (1H, m), 4.48 (2H, m), 3.98 (5H, m), 3.55 (2H, m), 3.08 (2H, m), 2.44 (3H, m), 2.01 (1H, m) ppm; ^{13}C-NMR ($CDCl_3$) *δ* 138.04, 137.94, 137.75, 137.69, 128.54, 128.48, 128.43, 128.40, 128.28, 128.22, 128.11, 128.08, 128.06, 128.02, 127.87, 127.72, 80.90, 80.87, 79.08, 77.92, 75.19, 74.48, 73.74, 73.33, 70.75, 70.66, 70.11, 69.17, 24.15, 18.91 ppm; HR-ESI-MS: $[M+Na]^+$ calculated for $C_{37}H_{40}O_6Na$ was m/z 603.2723, found 603.2735.

(3R,4S,5S,6R)-3,4,5-tris(benzyloxy)-6-((benzyloxy)methyl)-2-(3-(trimethylsilyl)prop-2-yn-1-yl)tetrahydro-2H-pyran-2-ol (34): The conditions employed for the preparation of this compound were those described in the synthesis of propargyl magnesium bromide

and the General condition for C-1 propargylation, **34** was afforded as a viscous liquid (647 mg, 67% yield). ^{1}H-NMR ($CDCl_3$) δ 7.22 (20H, s), 4.87 (2H, t, J =12.33 Hz), 4.67 (1H, d, J =11.51 Hz), 4.62 (2H, m), 4.50 (1H, d, J =11.51 Hz), 4.41 (1H, d, J =11.81 Hz), 4.35 (1H, d, J =11.79 Hz), 4.04 (1H, t, J =6.35 Hz), 3.94 (3H, m), 3.54 (1H, t, J =8.38 Hz), 3.47 (1H, t, J =7.20 Hz), 3.00 (1H, s), 2.67 (1H, d, J =16.81 Hz), 2.43 (1H, d, J =16.81 Hz), 1.17 (1H, s), 0.00 (9H, s) ppm; ^{13}C-NMR ($CDCl_3$) δ 138.98, 138.43, 138.09, 138.07, 128.51, 128.48, 128.43, 128.23, 127.98, 127.86, 127.76, 127.67, 127.60, 127.46, 100.87, 97.13, 88.99, 80.92, 77.53, 75.64, 74.63, 74.60, 73.47, 72.46, 70.72, 68.67, 31.00, 0.00 ppm; HR-ESI-MS: $[M+Na]^+$ calculated for $C_{40}H_{46}O_6SiNa$ was m/z 673.2961, found 673.2969.

trimethyl(3-((2S,3S,4R,5S,6R)-3,4,5-tris(benzyloxy)-6-((benzyloxy)methyl) tetrahydro-2H-pyran-2-yl)prop-1-yn-1-yl)silane (35): A solution of compound **34** (203 mg, 0.3 mmol, 1 equiv.) in ACN (10 mL) was prepared. Et_3SiH (498 µL, 3.0 mmol, 10 equiv.) and BF_3-OEt_2 (116 µL, 0.93 mmol, 3 equiv.) were added to the solution at -50 °C and stirred for 1h. The reaction mixture was then treated with saturated aqueous $NaHCO_3$ (10 mL) and extracted with EtOAc (2 × 30 mL). The extracts were washed with brine (25 mL), dried over anhydrous Na_2SO_4, and concentrated. The resulting crude mixture was purified using hexane/EtOAc by column chromatography, and **35** was obtained as a colorless viscous liquid (166 mg, 84% yield). ^{1}H-NMR ($CDCl_3$) δ 7.21 (1H, m), 4.86 (2H, t, J =10.28 Hz), 4.67 (1H, d, J =11.71 Hz), 4.59 (2H, t, J =9.43 Hz), 4.50 (1H, d, J =11.61 Hz), 4.41 (1H, d, J =11.76 Hz), 4.33 (1H, d, J =11.74 Hz), 3.90 (1H, s), 3.82 (1H, t, J =9.25 Hz), 3.50 (4H, m), 3.27 (1H, m), 2.56 (2H, m), 0.00 (9H, s) ppm; ^{13}C-NMR ($CDCl_3$) δ 138.91, 138.39, 138.26, 137.90, 128.37, 128.34, 128.09, 128.06, 127.94, 127.69, 127.65, 127.58, 127.50, 127.25, 103.56, 86.36, 84.46, 77.78, 77.61, 77.16, 75.49, 74.41, 73.94, 73.43, 72.06, 68.72, 23.53, 0.00 ppm; HR-ESI-MS: $[M+Na]^+$calculated for $C_{40}H_{46}O_5SiNa$ was m/z 657.3012, found 657.3027.

(2R,3S,4R,5S,6S)-3,4,5-tris(benzyloxy)-2-((benzyloxy)methyl)-6-(prop-2-yn-1-yl) tetrahydro-2H-pyran (36): A solution of **35** (130 mg, 0.2 mmol) in THF (5 mL) was stirred with a solution of TBAF in THF (800 µL, 0.8 mmol, 4 equiv.) at room temperature for 2 h. The reaction mixture was then quenched with 5 mL of saturated aqueous NH_4Cl and extracted with 3 x 15 mL of EtOAc. The combined organic extracts were dried over anhydrous Na_2SO_4 and concentrated. Purification by column chromatography using hexane/EtOAc afforded compound **36** (112 mg, 98% yield). ^{1}H-NMR ($CDCl_3$) δ 7.35 (20H, m), 5.01 (2H, d, J =11.26 Hz), 4.81 (1H, d, J =11.71 Hz), 4.73 (2H, m), 4.67 (1H, d, J=11.71

Hz), 4.55 (1H, d, *J* =11.81 Hz), 4.47 (1H, d, *J*=11.76 Hz), 4.05 (1H, s), 3.93 (1H, t, *J* =9.30 Hz), 3.65 (4H, m), 3.44 (1H, t, *J* =7.70 Hz), 2.73 (1H, d, J=16.91 Hz), 2.59 (1H, m), 2.03 (1H, s), 1.66 (1H, s) ppm; ^{13}C-NMR ($CDCl_3$) δ 138.91, 138.35, 138.31, 138.01, 128.49, 128.45, 128.44, 128.22, 128.20, 128.01, 127.85, 127.80, 127.70, 127.57, 127.46, 84.62, 81.09, 77.82, 77.72, 75.54, 74.40, 73.73, 73.56, 72.19, 69.89, 68.85, 22.24 ppm; HR-ESI-MS: $[M+Na]^+$ calculated for $C_{37}H_{38}O_5Na$ was m/z 585.2617, found 585.2630.

(2R,3S,4R,5S,6S)-2-(acetoxymethyl)-6-((1-(1,3,4-triacetoxyoctadecan-2-yl)-1H-1,2,3-triazol-4-yl)methyl)tetrahydro-2H-pyran-3,4,5-triyl triacetate (38): A solution of compound **36** (90 mg, 0.16 mmol, 1 equiv.) and azido phytosphingosine (55 mg, 0.16 mmol, 1 equiv.) in 4 mL of DMF was made at 0 °C. To this mixture, CuI (61 mg, 0.32 mmol, 2 equiv.) and DIPEA (84 µL, 0.48 mmol, 3 equiv.) were added and stirred for 1 h under a nitrogen atmosphere. Once the starting materials were completely consumed (as indicated by TLC), the reaction mixture was quenched with 20 mL of saturated aqueous NH_4Cl and extracted with 3 x 30 mL of EtOAc. The combined organic extracts were dried over anhydrous Na_2SO_4 and concentrated. The resulting triazole was purified by column chromatography using hexane/EtOAc and obtained as a colorless sticky solid. Upon debenzylation (mentioned in the general procedure for debenzylation) it yielded compound **37** as a colorless crystalline solid (79 mg, 91% yield over 2 steps, $[\alpha]_D^{26}$ = +10.96° (c = 1, MeOH), HR-ESI-MS $[M+H]^+$ calculated for $C_{27}H_{52}N_3O_8$ was m/z 546.3749, found 546.3765). **37** (15 mg) was acetylated for NMR purposes (General acetylation procedure) and yielded **38** as a colorless viscous liquid (22.6 mg, 98% yield). ^{1}H-NMR ($CDCl_3$) δ 7.66 (1H, s), 5.53 (1H, dd, *J* =3.51, 7.54 Hz), 5.46 (1H, d, *J* =2.91 Hz), 5.21 (1H, t, *J* =9.84 Hz), 5.13-5.10 (1H, m), 5.06 (1H, dd, *J* =3.04, 9.93 Hz), 4.66 (2H, m), 4.40 (1H, dd, J=2.22, 11.98 Hz), 4.08 (2H, m), 3.85 (1H, t, *J* =6.61 Hz), 3.73 (1H, t, *J* =9.23 Hz), 3.10 (1H, d, *J* =15.17 Hz), 2.92 (1H, dd, *J* =9.66, 15.26 Hz), 2.18 (3H, s), 2.13 (3H, s), 2.09 (3H, s), 2.06 (3H, s), 2.04 (3H, s), 2.03 (3H, s), 2.00 (3H, s), 1.68 (2H, s), 1.53 (2H, q, *J* =6.85 Hz), 1.27 (24H, m), 0.89 (3H, t, *J* =6.70 Hz) ppm; ^{13}C-NMR ($CDCl_3$) δ 170.43, 170.25, 170.23, 170.21, 170.14, 169.88, 169.45, 144.14, 122.05, 74.16, 72.07, 72.03, 71.04, 69.24, 67.70, 61.97, 61.30, 58.90, 31.90, 29.67, 29.64, 29.59, 29.50, 29.38, 29.33, 29.19, 28.65, 28.58, 25.23, 22.67, 20.83, 20.78, 20.67, 20.65, 20.62, 20.58, 20.55, 14.08 ppm; HR-ESI-MS: $[M+H]^+$ calculated for $C_{41}H_{66}N_3O_{15}$ was m/z 840.4488, found 840.4506.

(3R,4S,5S,6R)-3,4,5-tris(benzyloxy)-6-((benzyloxy)methyl)-1-(prop-2-yn-1-yl) piperidin-2-one (42): Compound **5** (220 mg, 0.4 mmol, 1 equiv.) was dissolved in 5 mL

of DMF, and then 2 equiv. 60% NaH (32.7 mg, 0.8 mmol) was added while stirring the mixture at 0°C under a nitrogen atmosphere. Then, Propargyl bromide (0.111 µL, 1 mmol, 2.5 equiv.) was added, and the reaction mixture was stirred for 6 h. Once a non-polar product was formed as indicated by TLC, the reaction mixture was quenched with 25 mL of H_2O and then extracted twice with 50 mL of EtOAc. The combined organic extract was then dried over anhydrous Na_2SO_4 and concentrated. The residue was then purified through column chromatography using hexane/EtOAc to obtain compound **42** as a viscous liquid (203 g, 86% yield). ^{1}H-NMR ($CDCl_3$) δ 7.33-7.25 (20H, m), 5.27 (1H, s), 4.99 (1H, d, *J* =17.53 Hz), 4.85 (2H, s), 4.65 (1H, m), 4.56-4.45 (5H, m), 4.14 (1H, s), 3.95-3.79 (3H, m), 2.21 (1H, s), 1.26 (2H, s) ppm; ^{13}C-NMR ($CDCl_3$) δ 159.96, 145.62, 137.89, 137.31, 135.84, 128.57, 128.56, 128.48, 128.08, 128.01, 127.83, 127.74, 127.52, 127.30, 107.17, 79.44, 73.53, 71.97, 71.90, 71.36, 70.12, 68.67, 57.10, 35.45 ppm; HR-ESI-MS: $[M+Na]^+$ calculated for $C_{37}H_{38}NO_5Na$ was m/z 598.2569, found 598.2575.

(3R,4S,5S,6R)-3,4,5-tris(benzyloxy)-6-((benzyloxy)methyl)-1-((1-(1,3,4-trihydroxy octadecan-2-yl)-1H-1,2,3-triazol-4-yl)methyl)piperidin-2-one (43): A solution of compound **42** (1 g, 1.73 mmol, 1 equiv.) and azido phytosphingosine (595 mg, 1.73 mmol, 1 equiv.) in 25 mL of DMF was made at 0 °C. To this mixture, CuI (661 mg, 3.47 mmol, 2 equiv.) and DIPEA (904 µL, 5.21 mmol, 3 equiv.) were added and stirred for 12 h under a nitrogen atmosphere. The starting materials were completely consumed, as indicated by TLC. The reaction mixture was then quenched with 50 mL of saturated aqueous NH_4Cl and extracted with 3 x 75 mL of EtOAc. The combined organic extracts were dried over anhydrous Na_2SO_4 and concentrated. The resulting triazole was purified by column chromatography using hexane/EtOAc and obtained **43** as a colorless sticky solid (1.53 g, 96% yield). ^{1}H-NMR ($CDCl_3$) δ 7.74 (1H, s), 7.23-7.13 (20H, m), 4.89 (2H,m), 4.73 (1H, s), 4.63 (1H, t, *J* =12.45 Hz), 4.55-4.36 (6H, m), 4.27 (1H, s), 4.14 (1H, d, *J* =6.20 Hz), 4.07 (1H, s), 3.98-3.83 (6H, m), 3.72 (1H, d, *J* =5.94 Hz), 3.43-3.33 (2H, m), 2.12 (2H, s), 1.48 (1H, m),1.38- 1.15 (26H, m), 0.80 (3H, t, *J* =6.46 Hz) ppm; ^{13}C-NMR ($CDCl_3$) δ 169.66, 137.96, 137.93, 137.74, 137.68, 128.47, 128.40, 128.33, 127.90, 127.83, 127.73, 127.56, 78.66, 75.03, 74.75, 73.61, 73.48, 73.38, 72.86, 72.42, 70.43, 63.03, 61.12, 58.76, 40.61, 32.65, 31.96, 29.75, 29.71, 29.40, 25.89, 22.73, 14.17 ppm; HR-ESI-MS: $[M+H]^+$ calculated for $C_{55}H_{75}N_4O_8$ was m/z 919.5579, found 919.5611.

(2R,3S,4R,5S)-2-(acetoxymethyl)-1-((1-(1,3,4-triacetoxyoctadecan-2-yl)-1H-1,2,3-triazol-4-yl)methyl)piperidine-3,4,5-triyl triacetate (46): A solution of **43** (400 mg, 0.43

mmol, 1 equiv.) in anhydrous THF (15 mL) was prepared. BH_3-DMS (1.087 mL, 2.175 mmol, 5 equiv.) was added dropwise to the solution at 0 °C under an argon atmosphere. The reaction mixture was stirred at room temperature for 12 hours. The mixture was then cooled to 0 °C, and ethanol (5 mL) was added to stop the reaction. The solvent was removed under reduced pressure. The remaining mixture was partitioned between EtOAc (100 mL) and distilled water (100 mL). The aqueous layer was extracted thrice with EtOAc (100 mL each time). The organic layers were combined, dried using anhydrous Na_2SO_4, and concentrated under reduced pressure. The residue was then passed through a small plug of silica to remove polar impurities. It was upon debenzylation (mentioned in the general procedure for debenzylation) yielded compound **45** as a pale yellow solid (184.9 mg, 78% yield over 2 steps, $[\alpha]_D^{25}$ = +10.0° (*c* = 1, MeOH), HR-ESI-MS $[M+H]^+$ calculated for $C_{27}H_{53}N_4O_7$ was m/z 545.3909, found 545.3936). **45** (15 mg) was acetylated for NMR purposes (General acetylation procedure) and yielded **46** as a colorless viscous liquid (22.6 mg, 99% yield). ^{1}H-NMR ($CDCl_3$) δ 7.80 (1H, s), 5.49 (2H, m), 5.22 (1H, m), 5.16 (1H, t, *J* =7.14 Hz), 4.85 (1H, d, *J* =9.83 Hz), 4.71 (1H, dd, *J* =7.55, 11.82 Hz), 4.63 (1H, dd, *J* =4.77, 10.87 Hz), 4.58 (1H, s), 4.40 (1H, d, *J* =12.07 Hz), 4.15 (1H, t, *J* =9.59 Hz), 4.06 (1H, d, *J* =15.52 Hz), 3.95 (1H, d, *J* =15.58 Hz), 3.21 (1H, dd, *J* =4.03, 11.25 Hz), 2.85 (1H, m), 2.40 (1H, t, *J* =10.63 Hz), 2.15 (3H, s), 2.14 (3H, s), 2.06 (3H, s), 2.04 (3H, s), 2.03 (6H, s), 1.99 (3H, s), 1.70 (2H, m), 1.57 (2H, m), 1.25 (24H, m), 0.88 (3H, t, *J* =6.51 Hz) ppm; ^{13}C-NMR ($CDCl_3$) δ 170.6, 170.4, 170.3, 170.2, 170.15, 170.11, 169.5, 142.0, 122.4, 71.9, 71.8, 71.2, 67.7, 67.4, 61.7, 61.0, 59.0, 57.3, 53.0, 47.4, 31.9, 29.7, 29.6, 29.6, 29.5, 29.4, 29.3, 29.2, 28.4, 25.2, 22.6, 20.9, 20.86, 20.84, 20.81, 20.7, 20.69, 20.60, 14.1 ppm; HR-ESI-MS: $[M+H]^+$ calculated for $C_{41}H_{67}N_4O_{14}$ was m/z 839.4648, found 839.4657.

(2R,3S,4S,5R)-2-(acetoxymethyl)-6-oxo-1-((1-(1,3,4-triacetoxyoctadecan-2-yl)-1H-1,2,3-triazol-4-yl)methyl)piperidine-3,4,5-triyl triacetate (47): Compound **43** (250 mg, 0.43 mmol, 1 equiv.) was on debenzylation (mentioned in the general procedure for debenzylation) yielded compound **44** as a colorless solid (150 mg, 99% yield, $[\alpha]_D^{26}$ = +24.16° (*c* = 1, MeOH), HR-ESI-MS $[M+H]^+$ calculated for $C_{27}H_{51}N_4O_8$ was m/z 558.3629, found 558.3641). **44** (15 mg) was acetylated for NMR purposes (General acetylation procedure) and yielded **47** as a colorless viscous liquid (22.6 mg, 99% yield). ^{1}H-NMR ($CDCl_3$) δ 7.82 (1H, s), 5.69 (1H, s), 5.48 (1H, d, *J*=10.30 Hz), 5.41 (2H, d, *J* =10.25 Hz), 5.35 (1H, d, *J* =15.46 Hz), 5.11 (1H, t, *J* =7.05 Hz), 4.62 (1H, dd, *J* =7.23,

12.03 Hz), 4.55 (1H, dd, *J* =4.93, 11.18 Hz), 4.49 (1H, m), 4.44 (1H, d, *J* =12.06 Hz), 4.29 (2H, m), 3.99 (1H, m), 2.17 (3H, s), 2.12 (6H, s), 2.06 (3H, s), 2.05 (3H, s), 2.04 (3H, s), 2.03 (3H, s), 1.72 (2H, s), 1.55 (H, m), 1.25 (23H, s), 0.88 (3H, t, *J* =6.50 Hz) ppm; ^{13}C-NMR ($CDCl_3$) δ 170.6, 170.3, 170.2, 170.3, 170.1, 169.7, 169.7, 169.4, 166.2, 143.3, 123.0, 71.7, 71.6, 69.3, 68.9, 66.6, 61.4, 61.0, 59.1, 53.9, 38.7, 31.9, 29.7, 29.7, 29.6, 29.5, 29.4, 29.4, 29.3, 28.6, 25.2, 22.7, 20.8, 20.7, 20.6, 14.1 ppm; HR-ESI-MS: $[M+H]^+$ calculated for $C_{41}H_{65}N_4O_{15}$ was m/z 853.4441, found 853.4445.

Figure 4.5.7.1: NMR spectra of *α,β* mixture of compound **2**

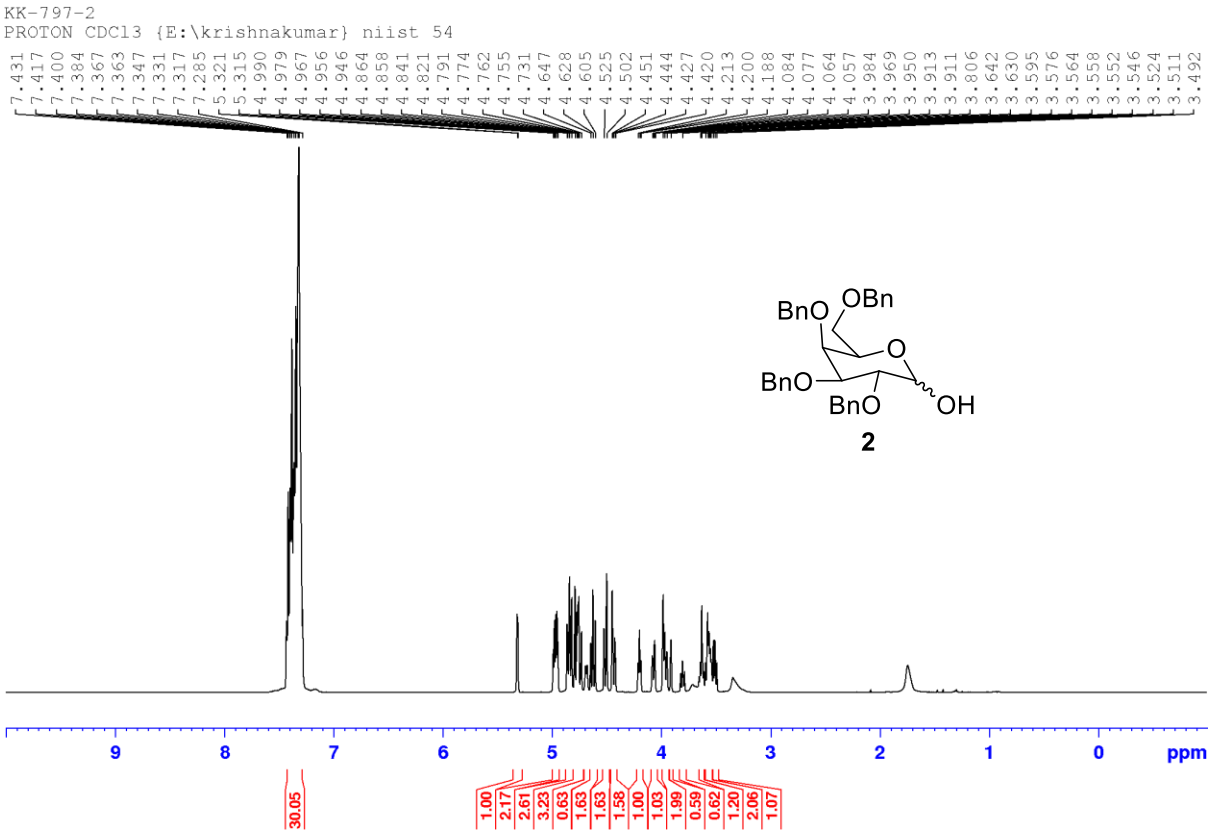

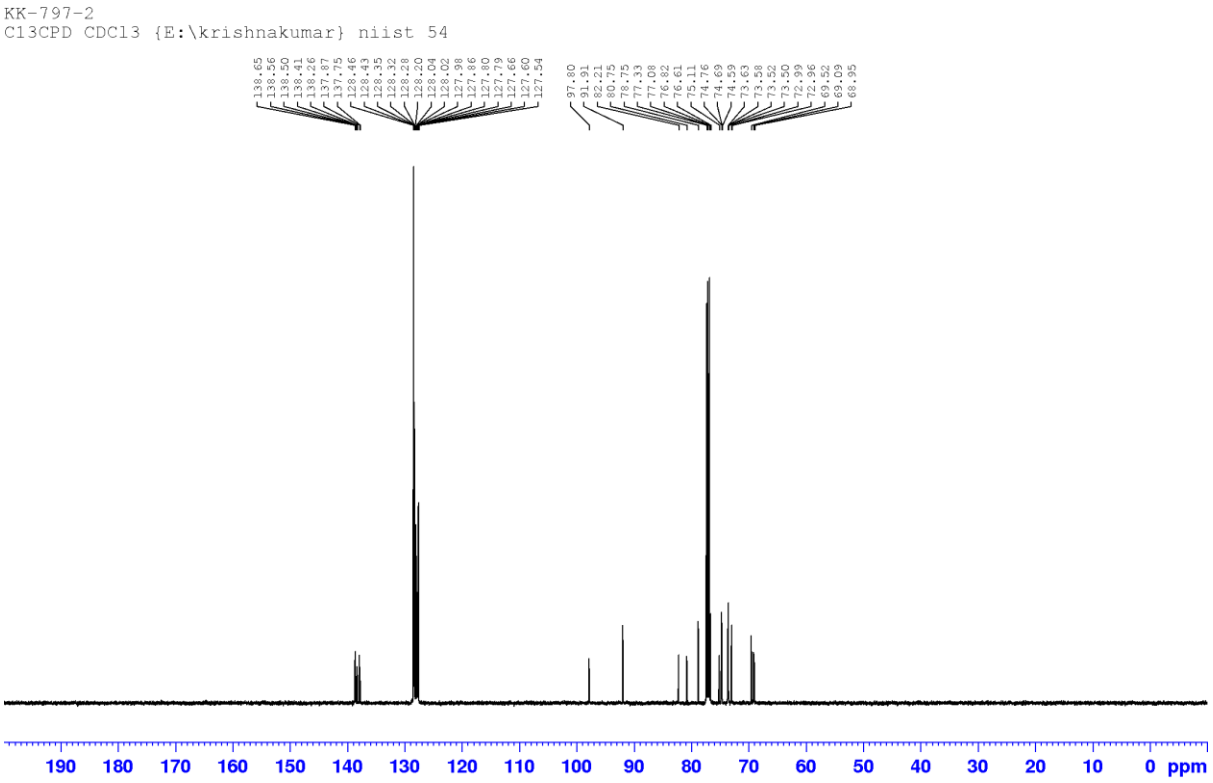

Figure 4.5.7.2: NMR spectra of compound **3**

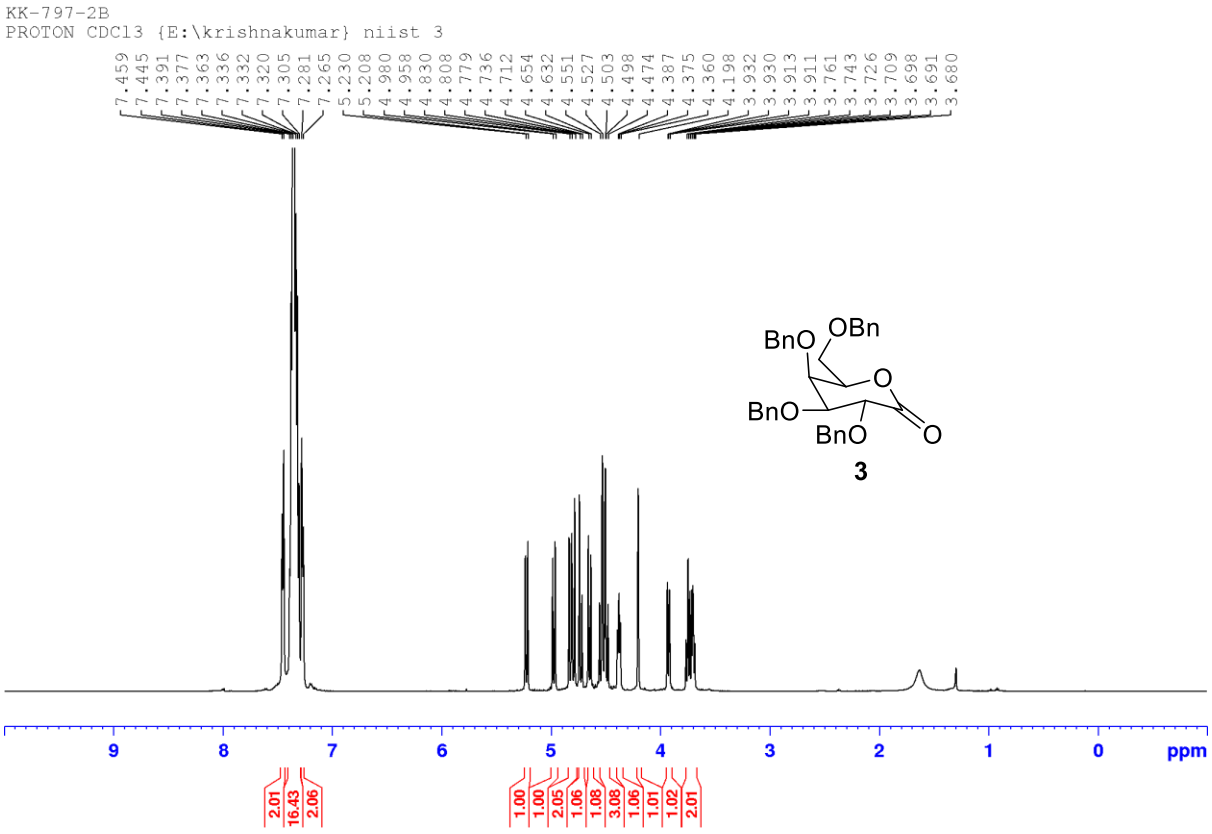

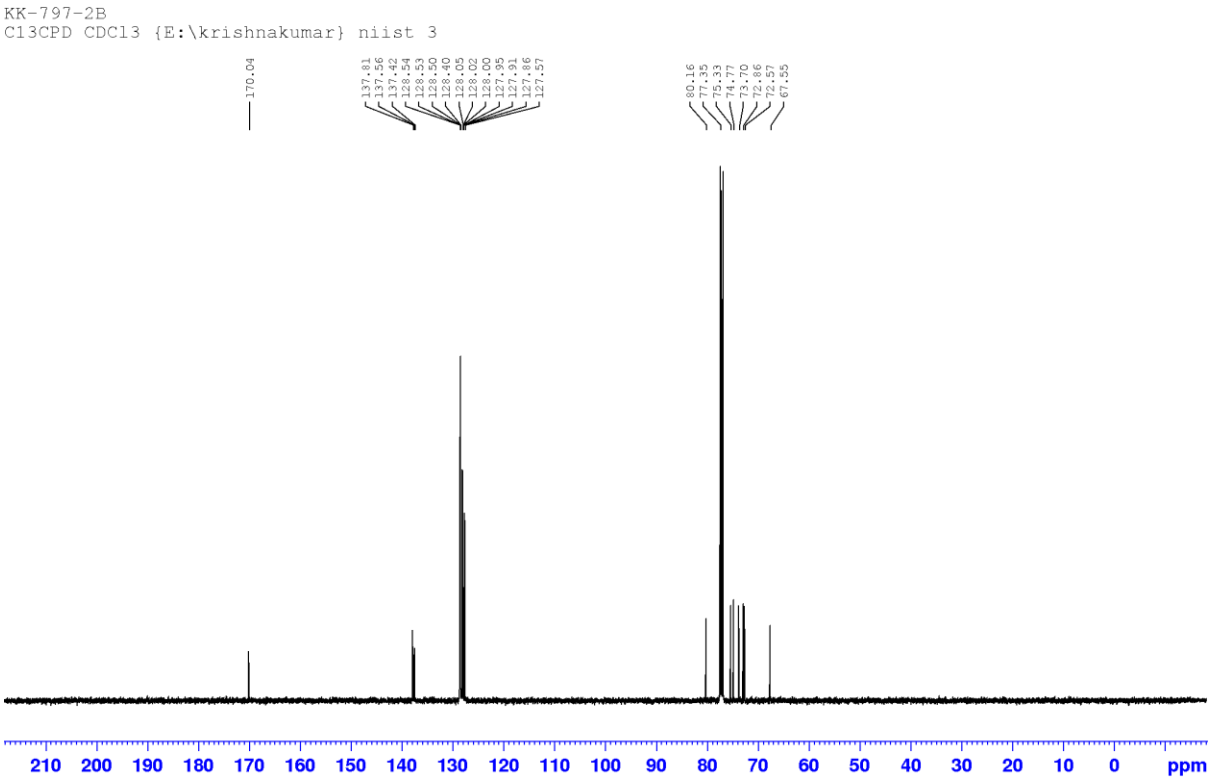

Figure 4.5.7.3: NMR spectra of compound **4**

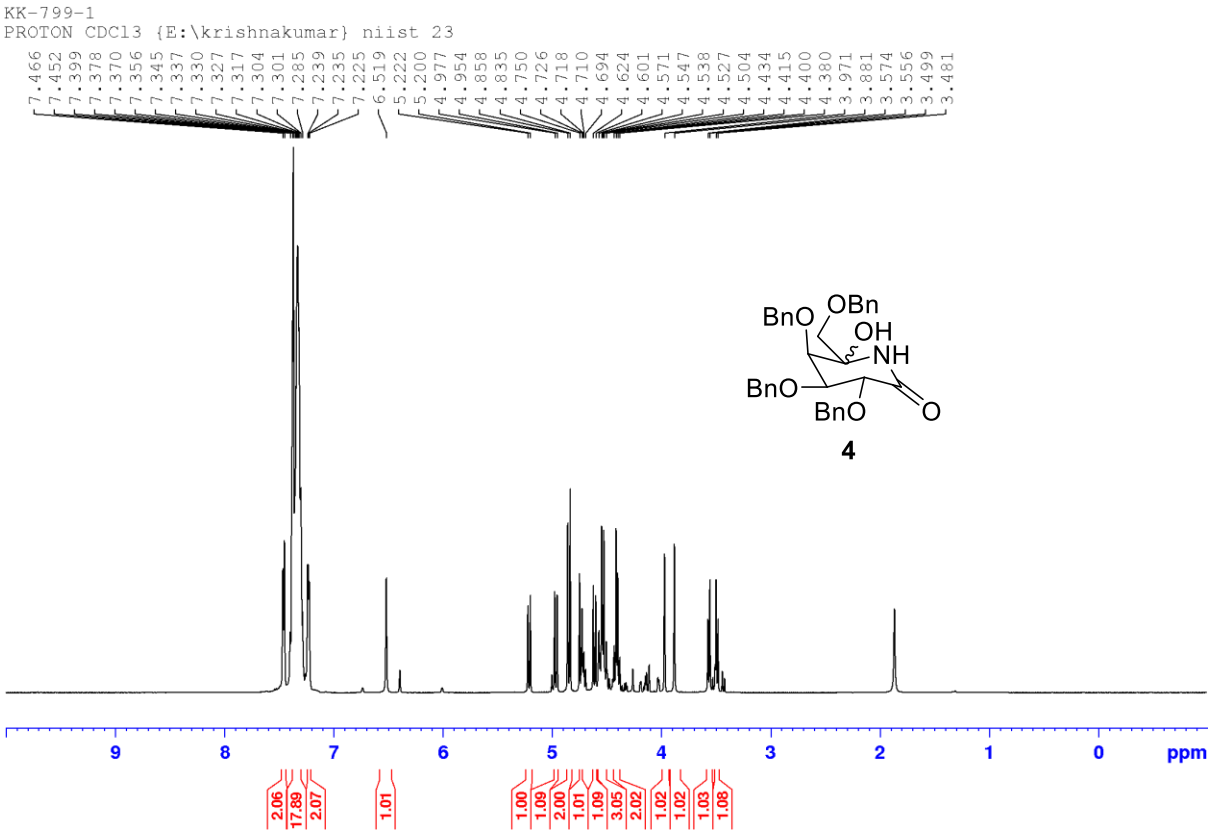

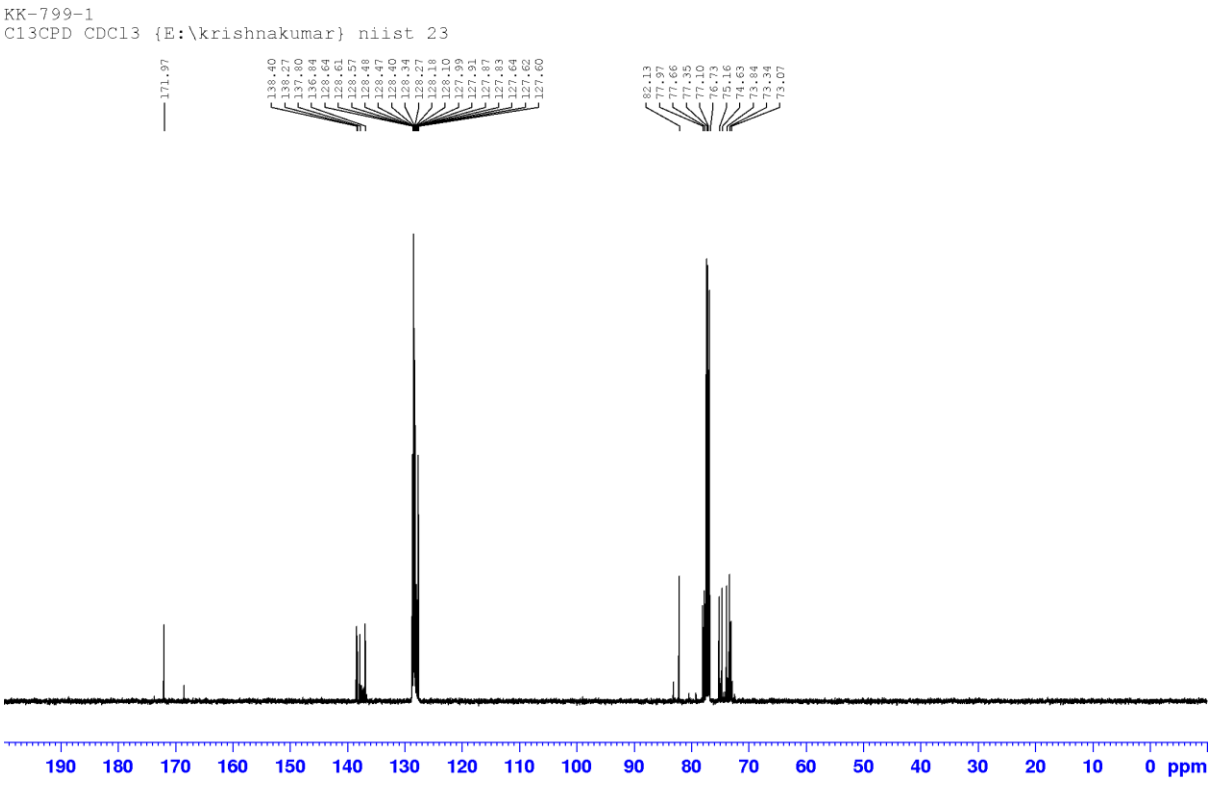

Figure 4.5.7.4: NMR spectra of compound **5**

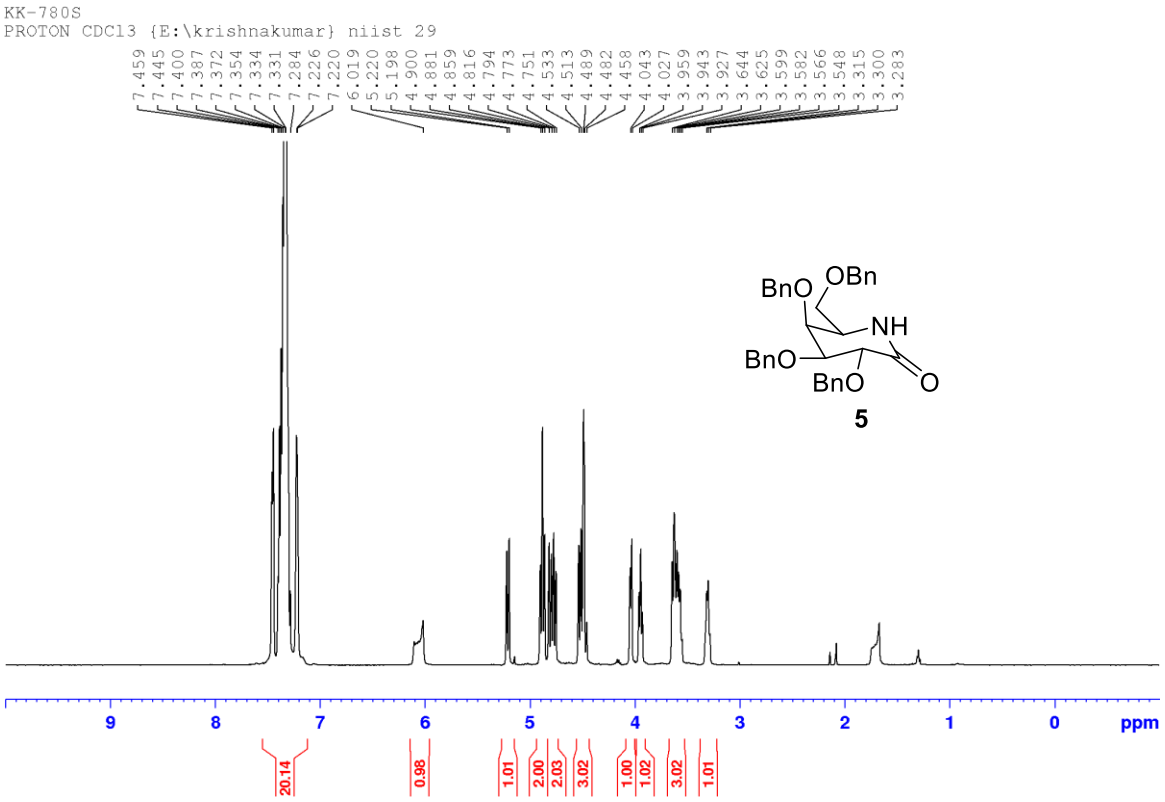

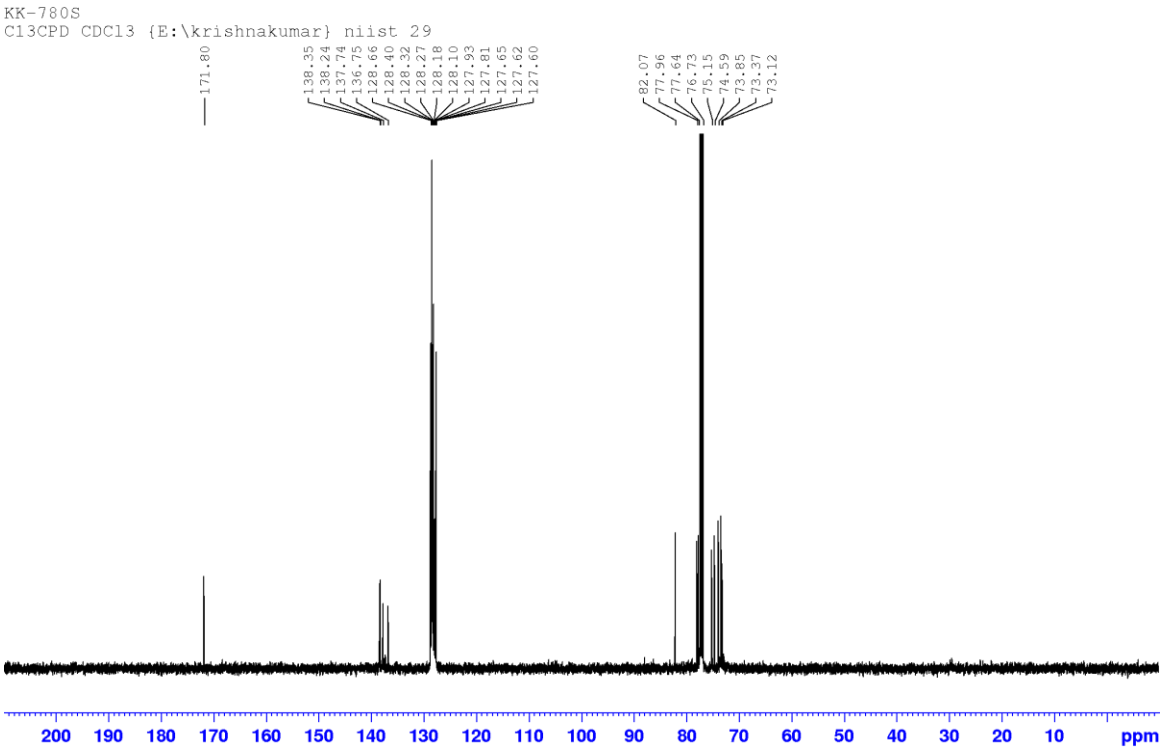

Figure 4.5.7.5: NMR spectra of compound **6**

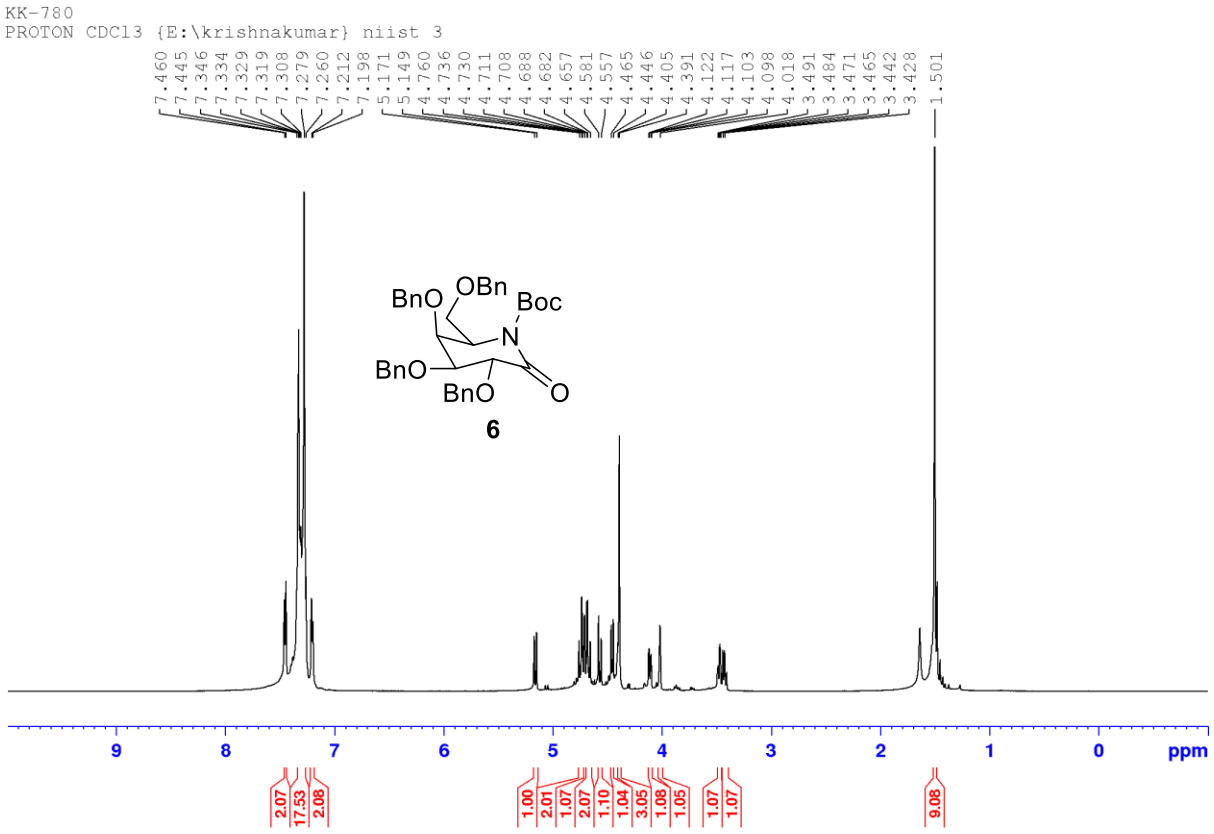

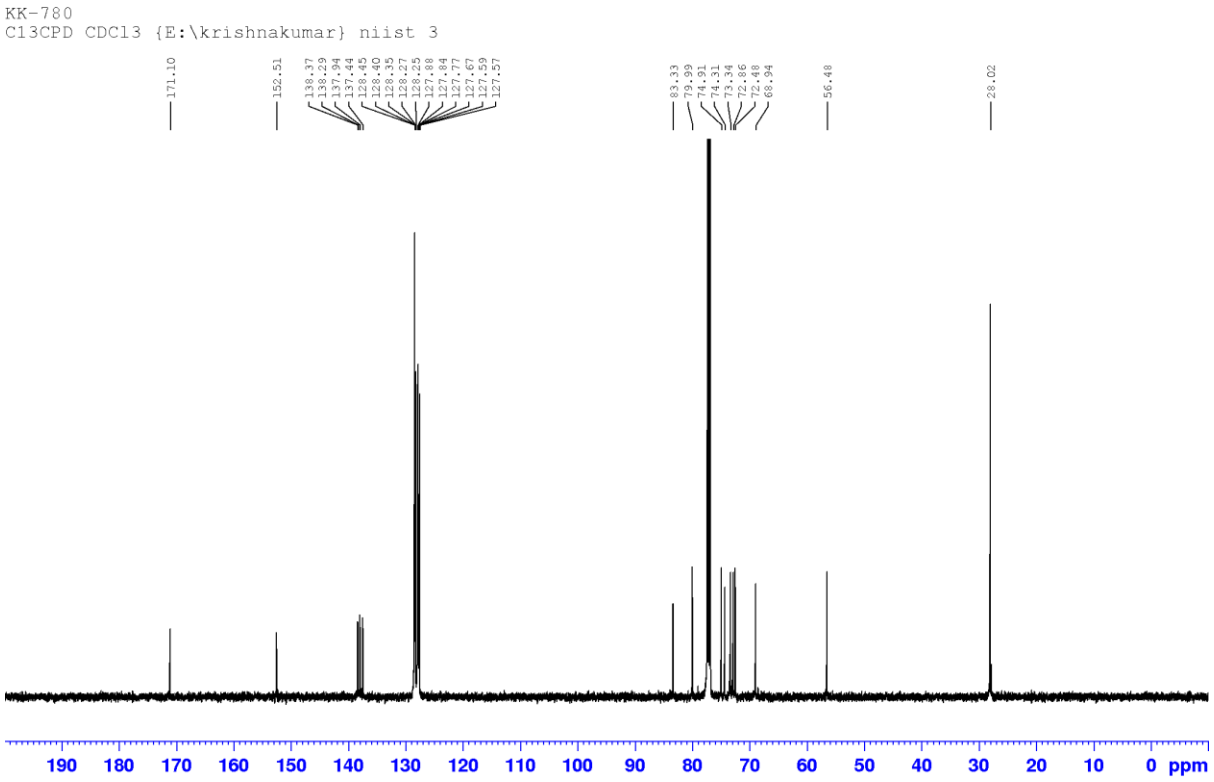

Figure 4.5.7.6: NMR spectra of compound **8**

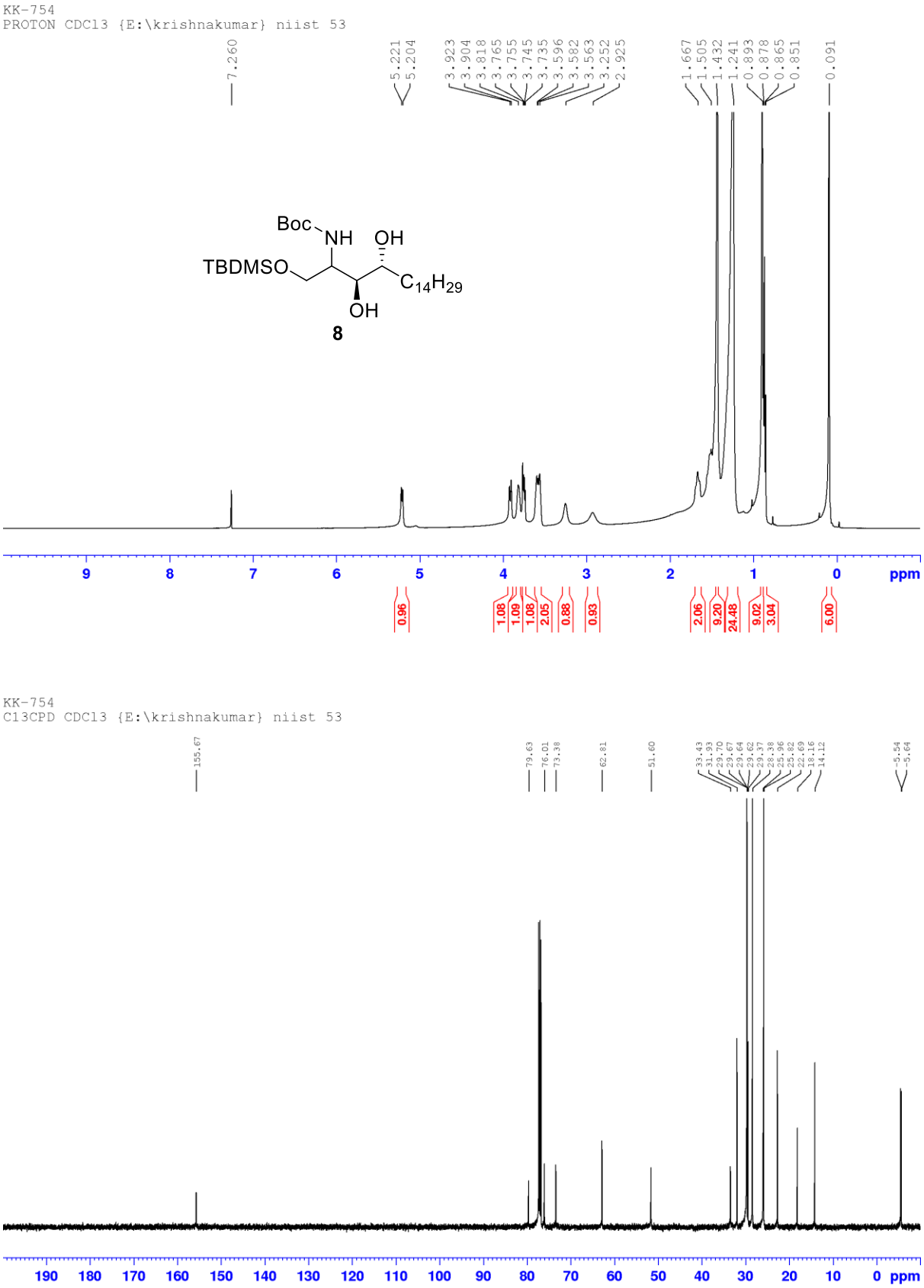

Figure 4.5.7.7: NMR spectra of compound **9**

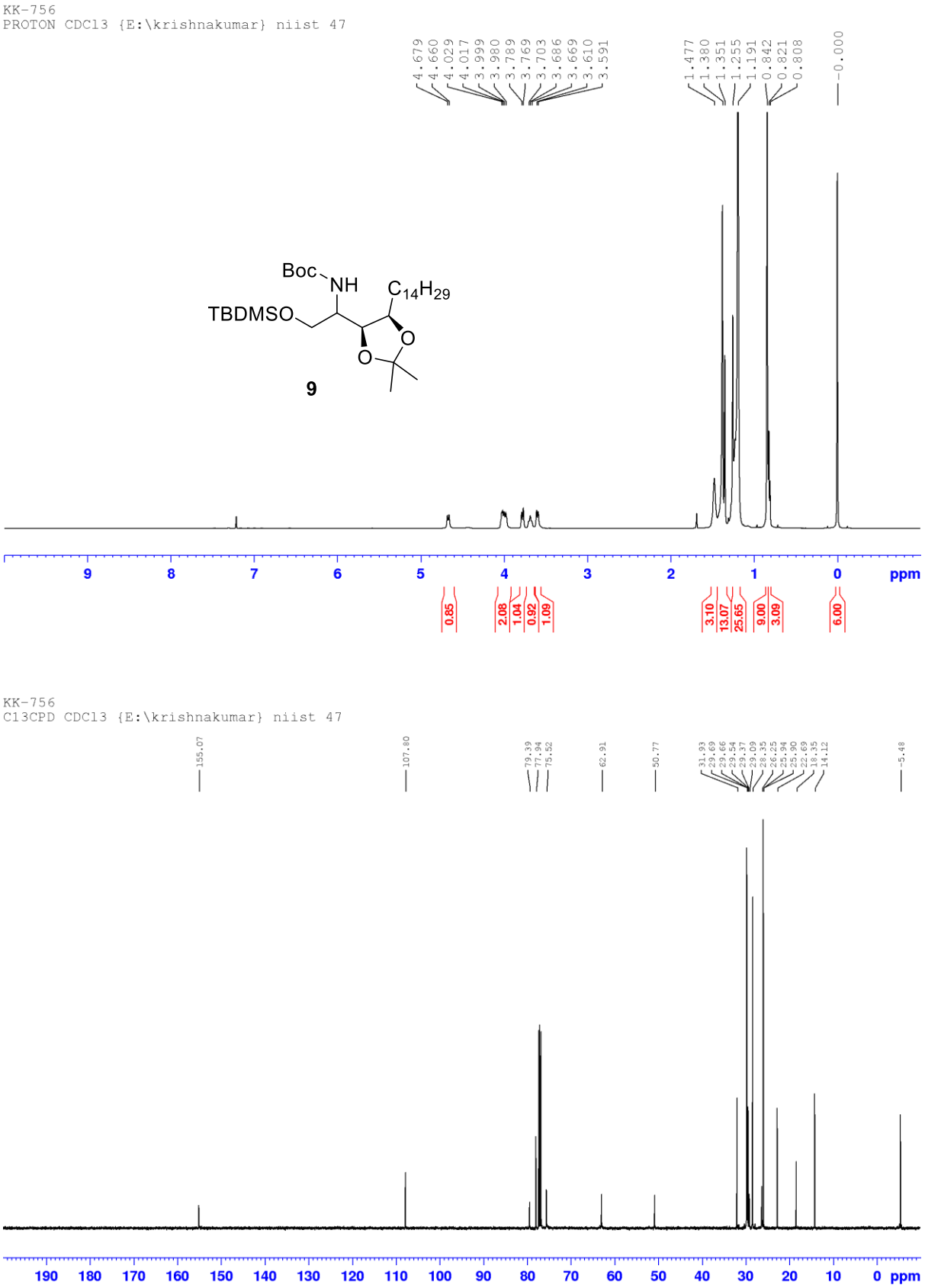

Figure 4.5.7.8: NMR spectra of compound **10**

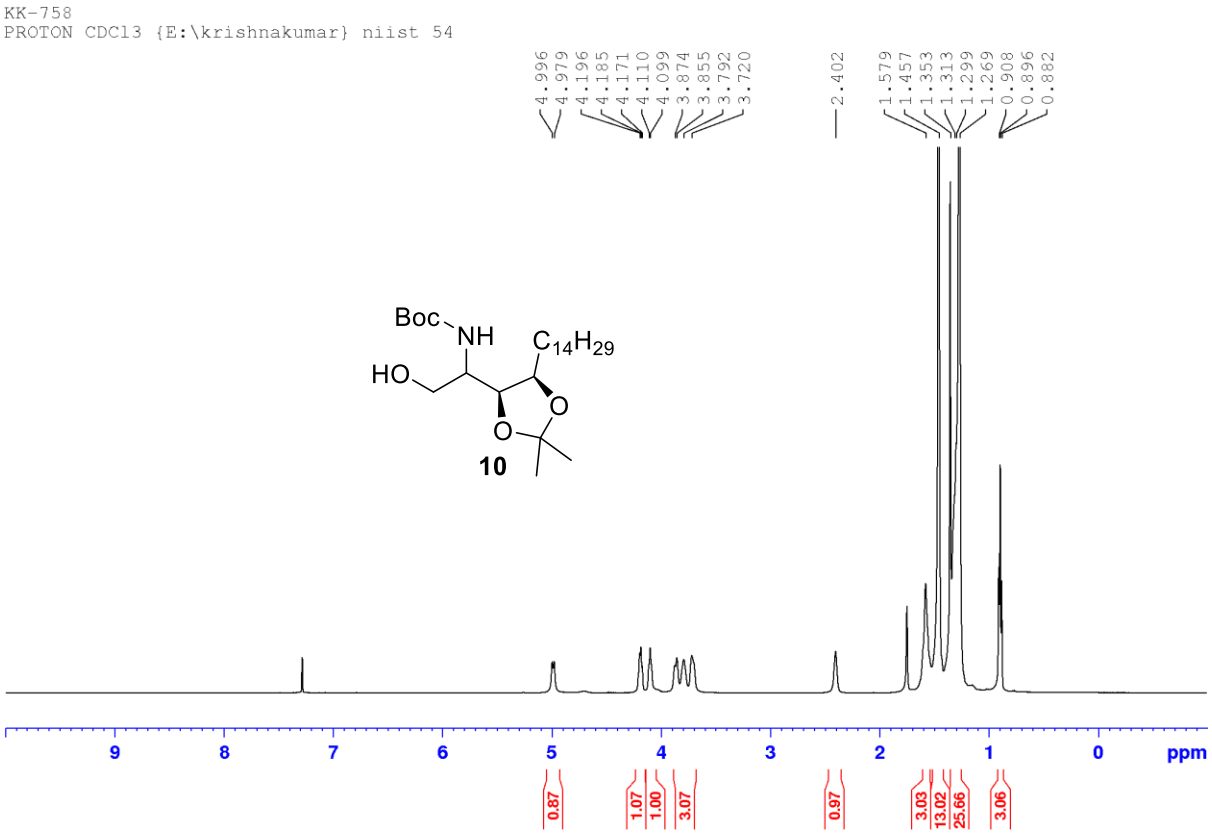

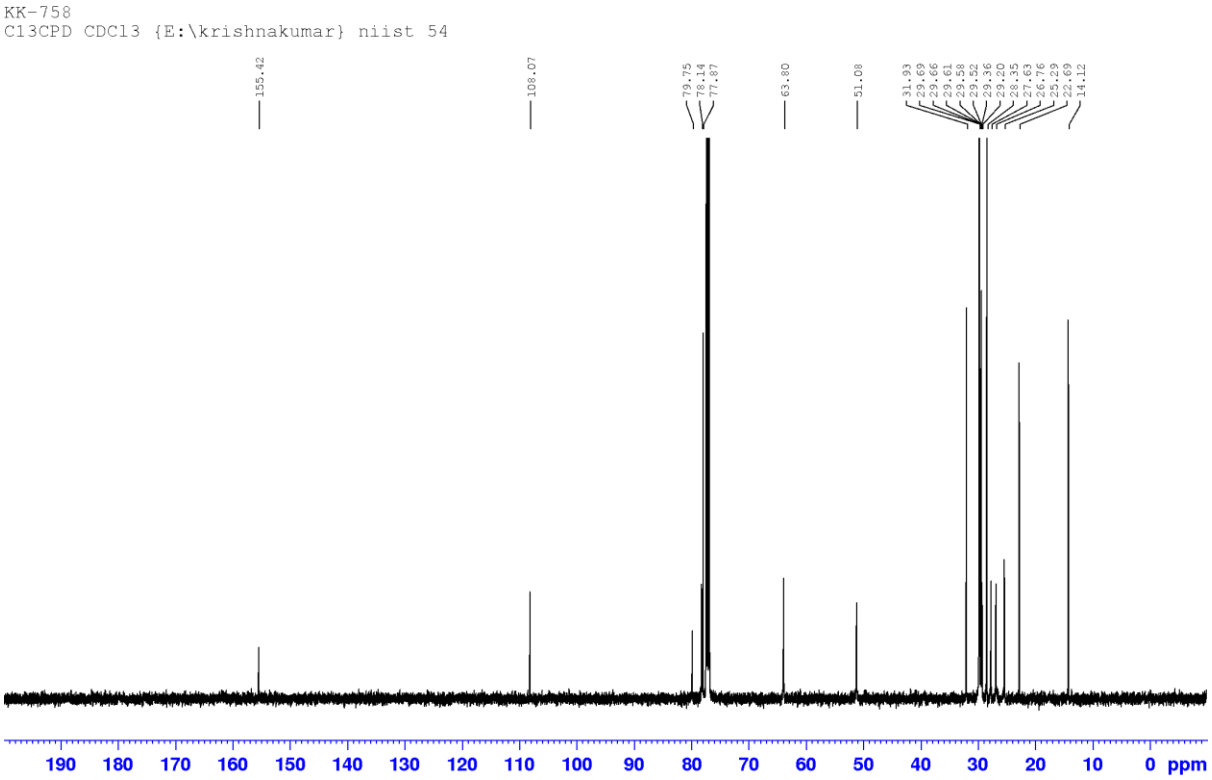

Figure 4.5.7.9: NMR spectra of compound **15**

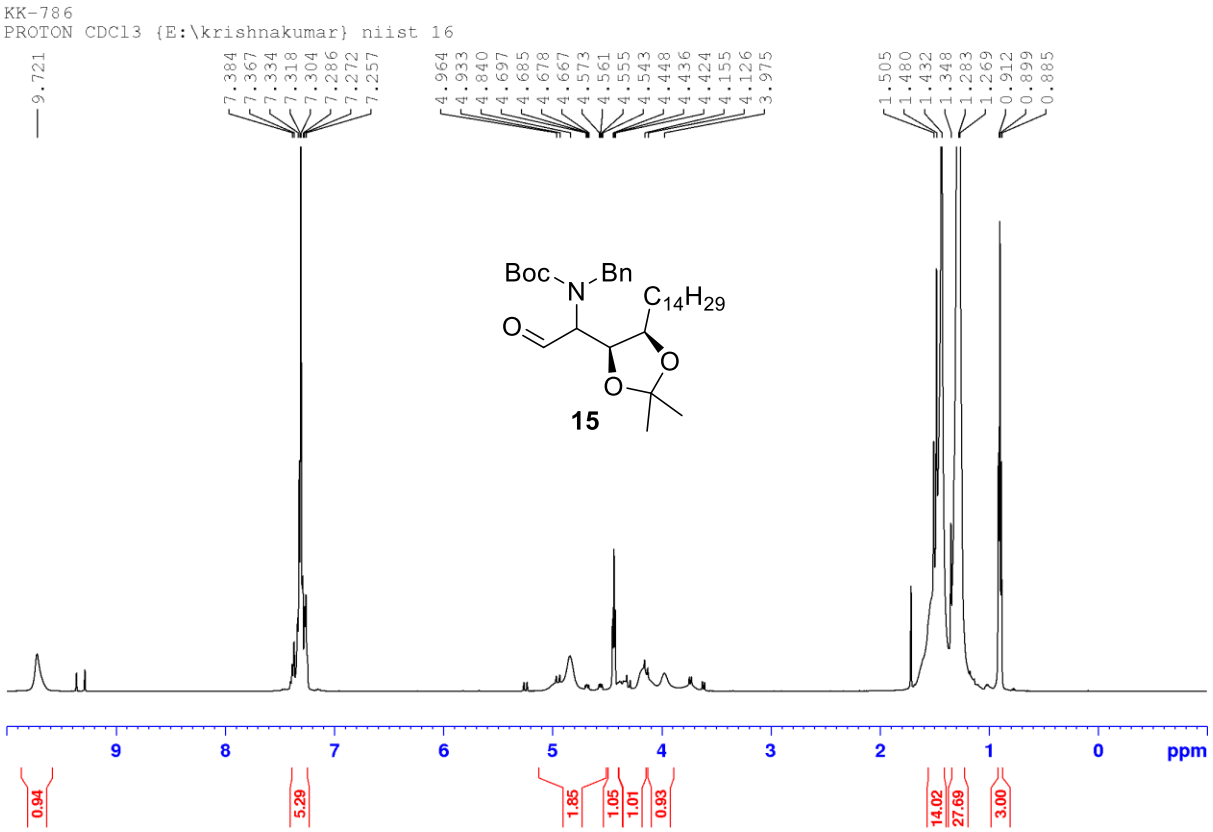

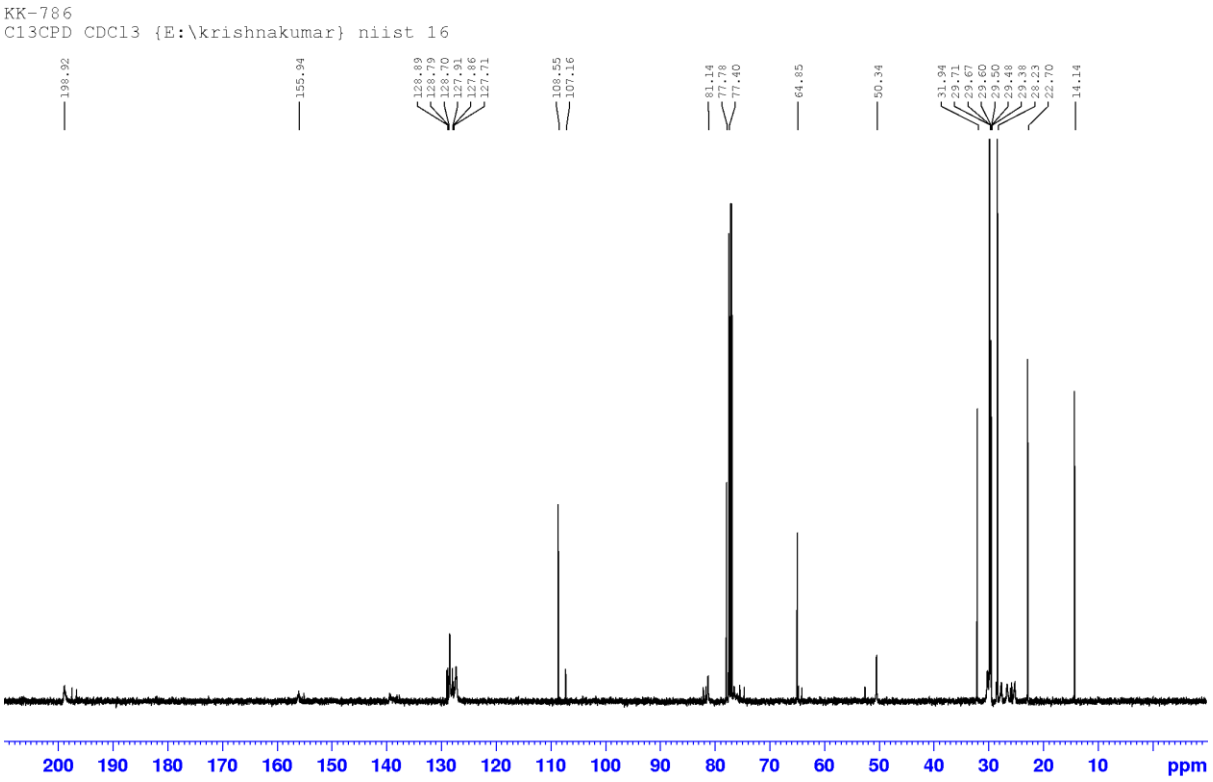

Figure 4.5.7.10: NMR spectra of compound **16**

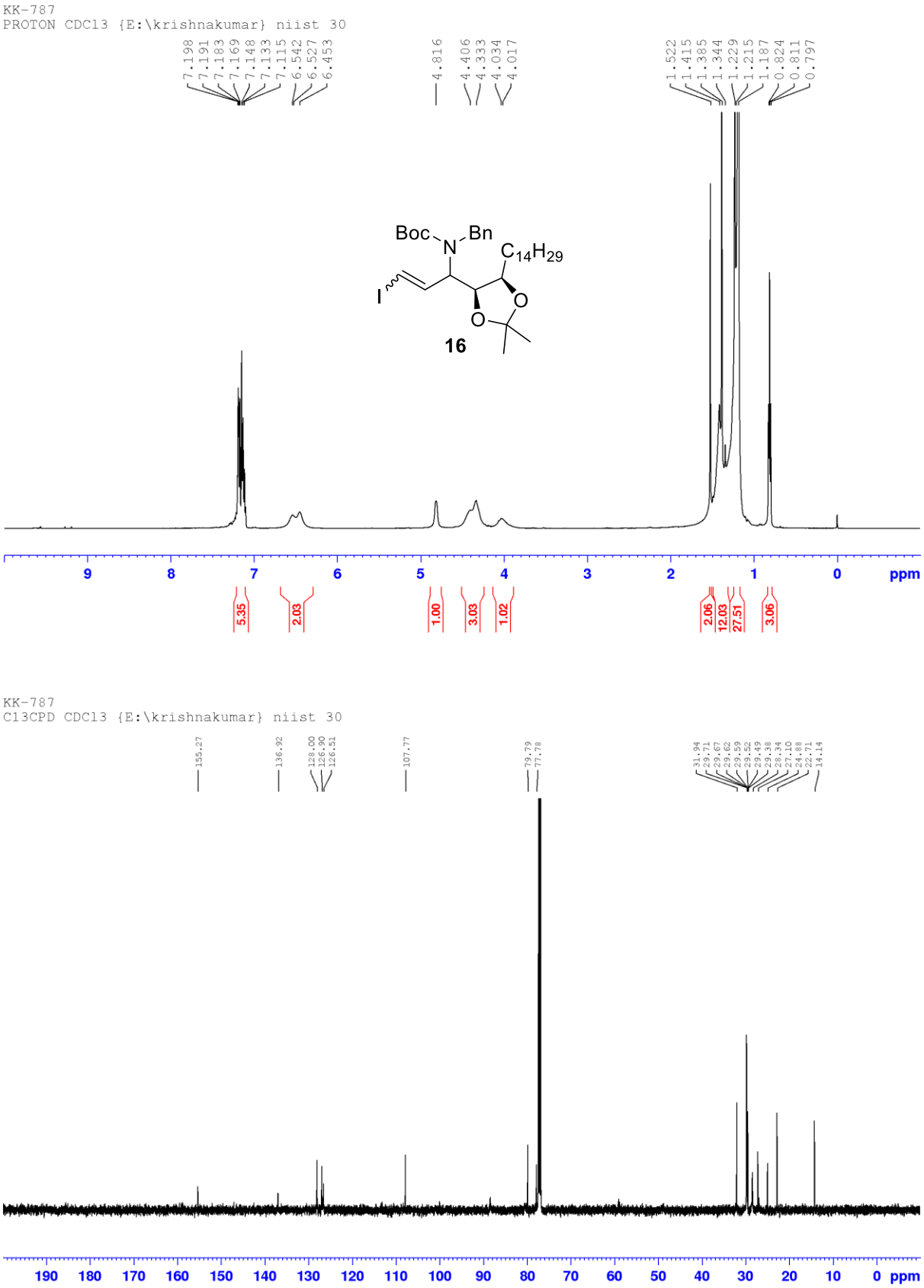

Figure 4.5.7.11: NMR spectra of compound **17**

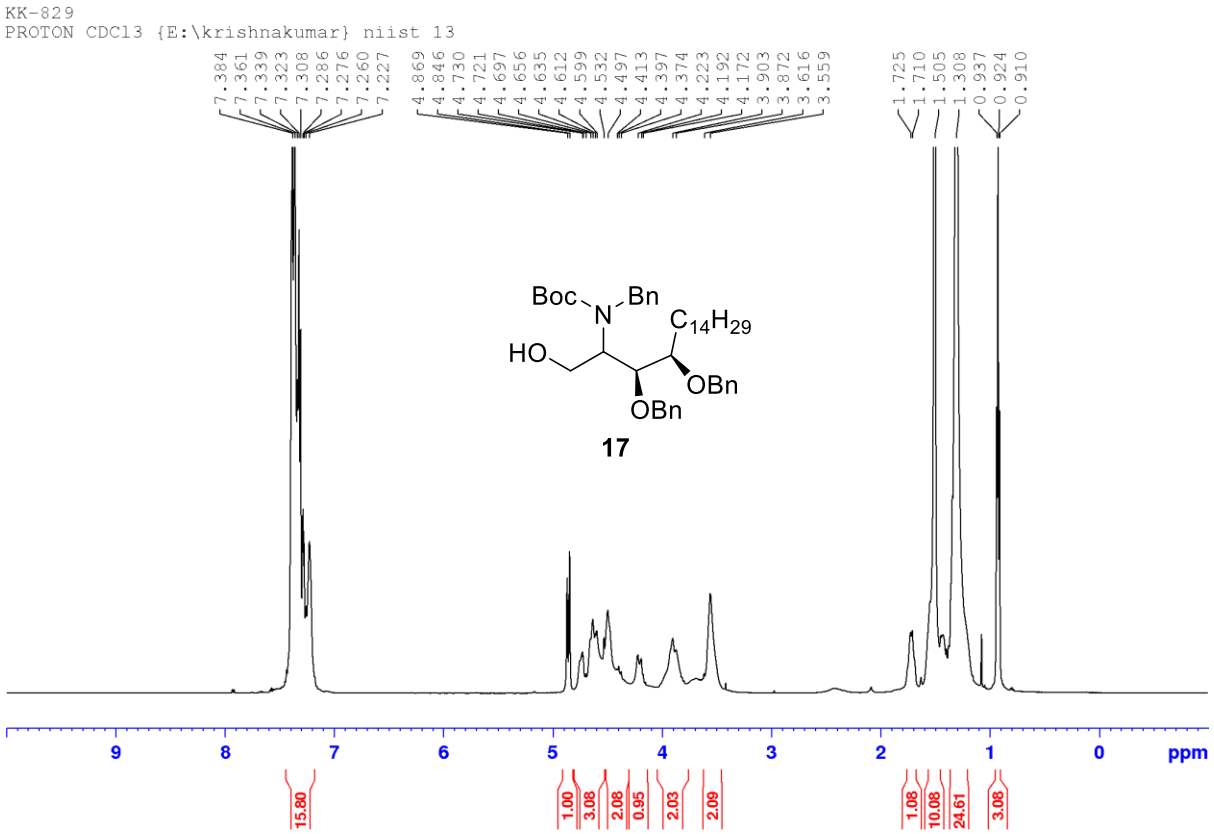

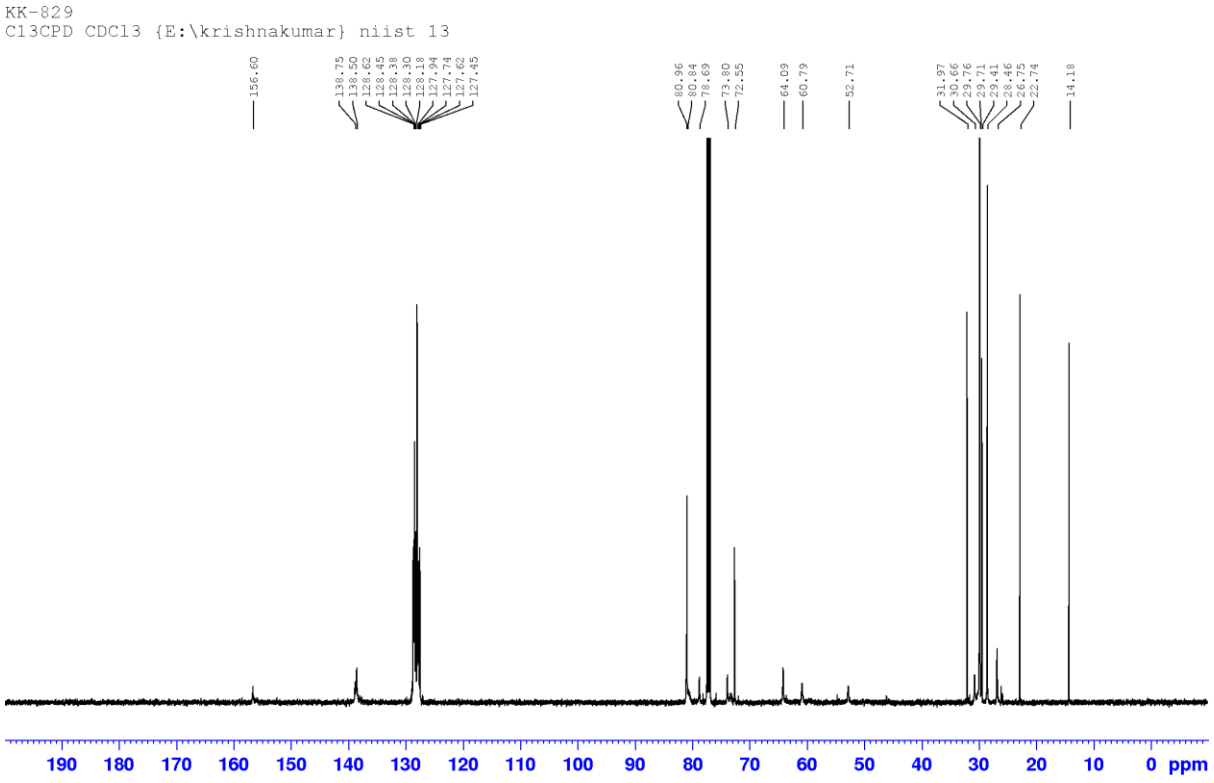

Figure 4.5.7.12: NMR spectra of compound **17a**

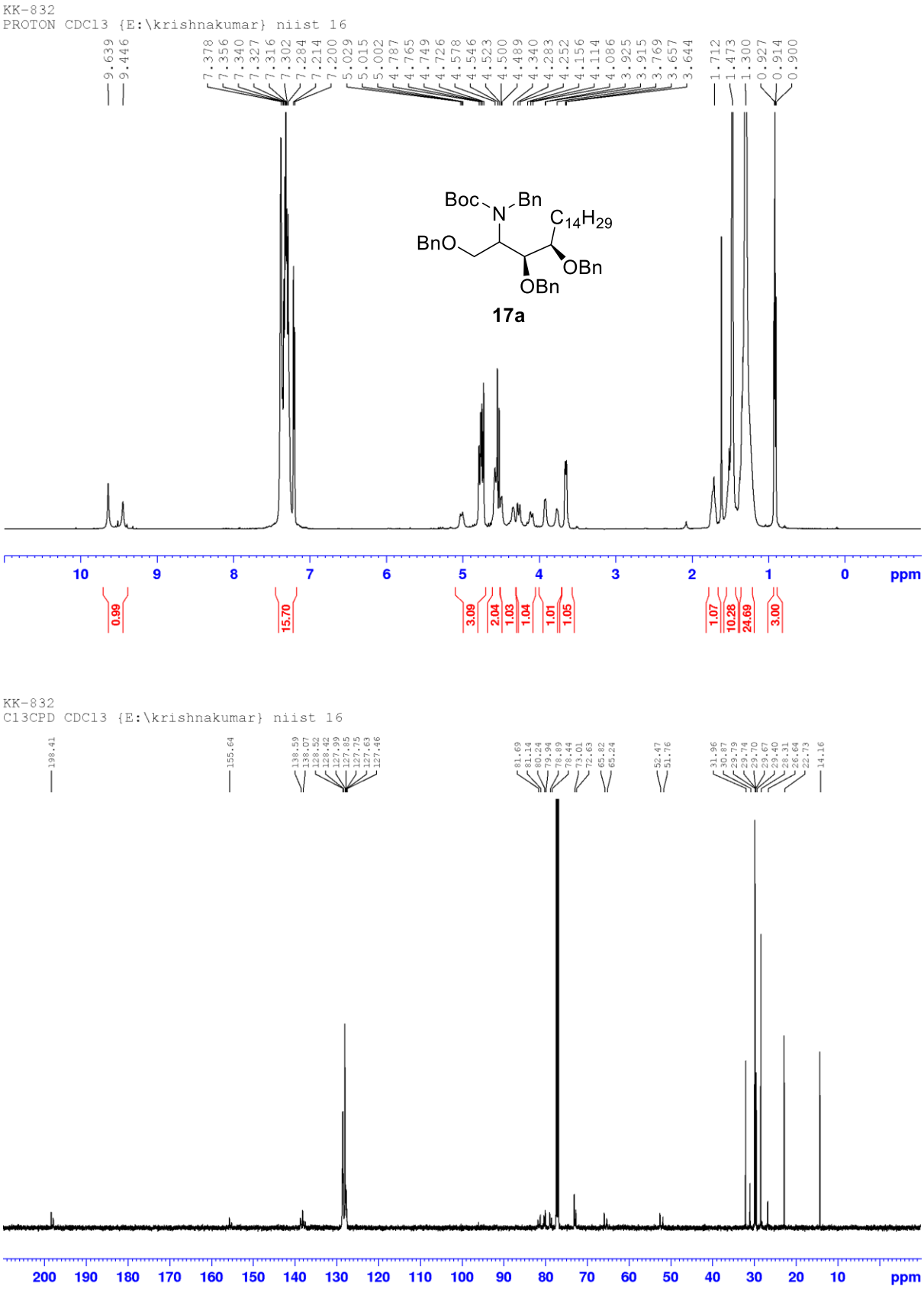

Figure 4.5.7.13: NMR spectra of compound **18**

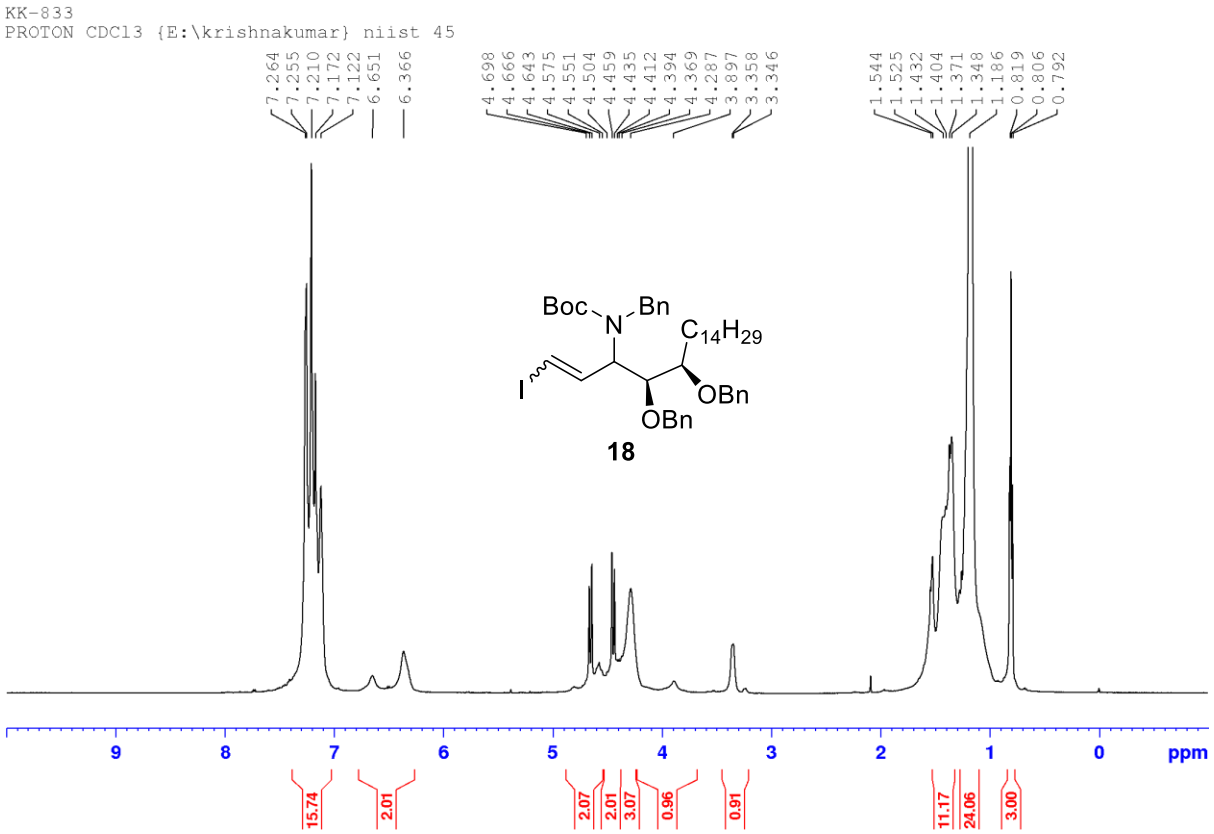

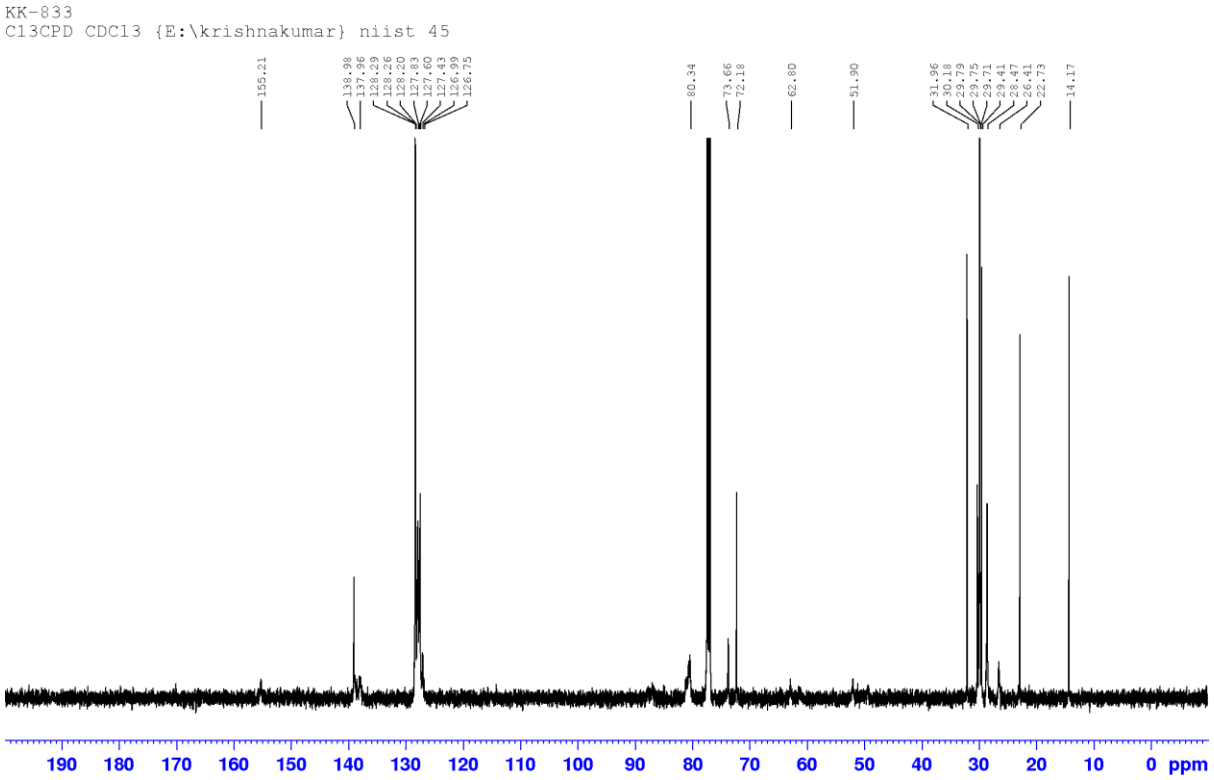

Figure 4.5.7.14: NMR spectra of compound **21**

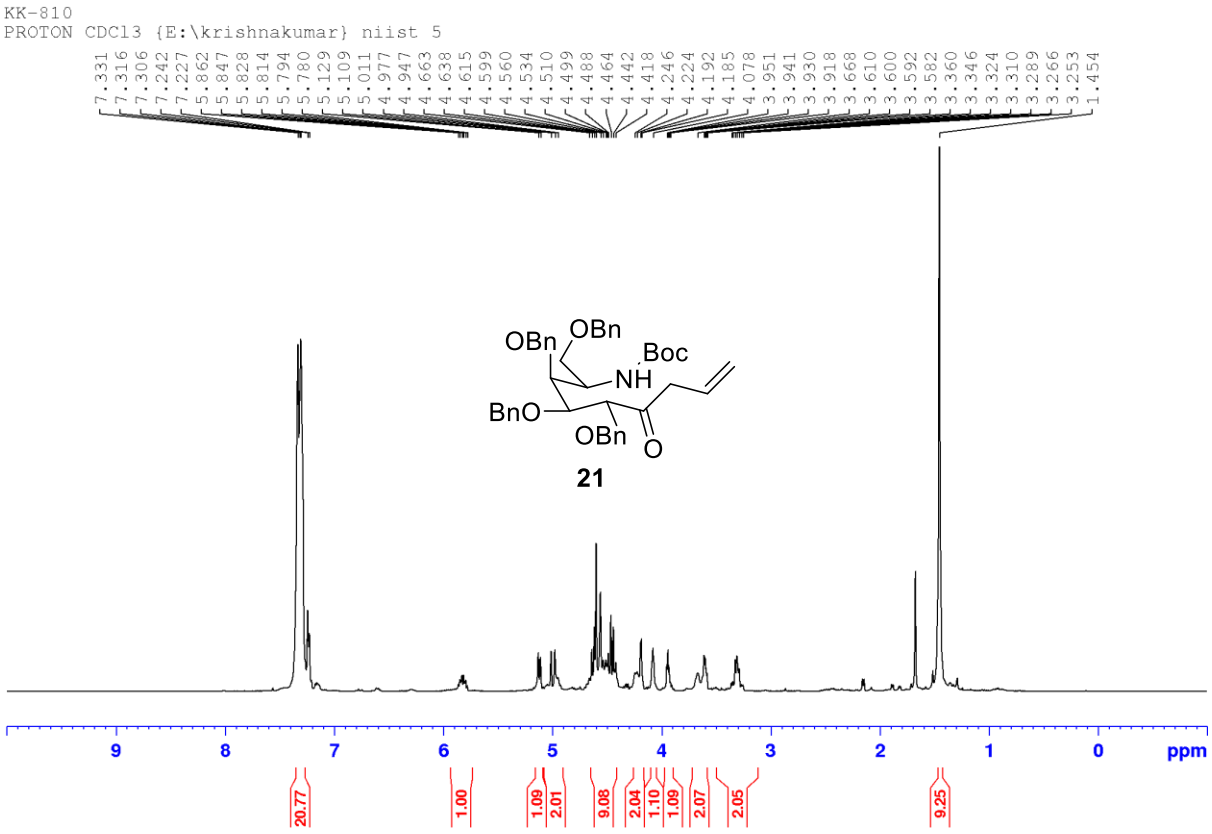

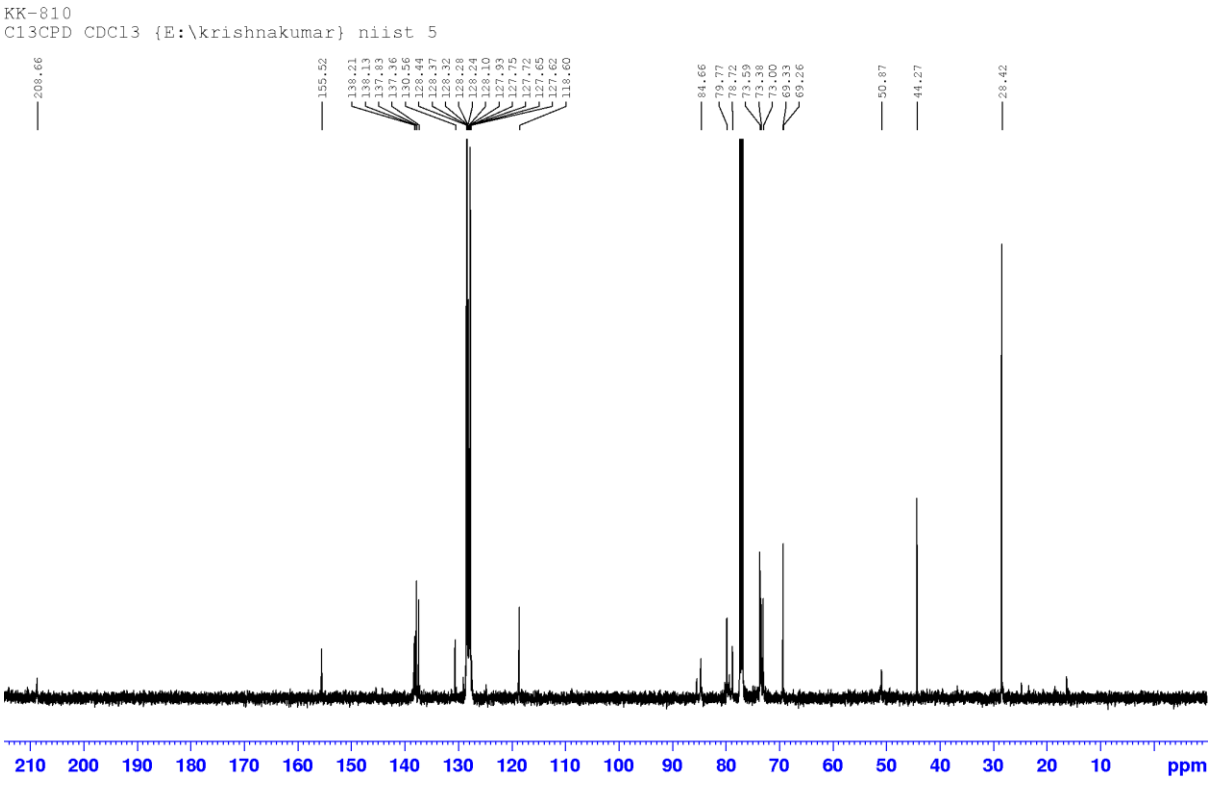

Figure 4.5.7.15: NMR spectra of compound **22**

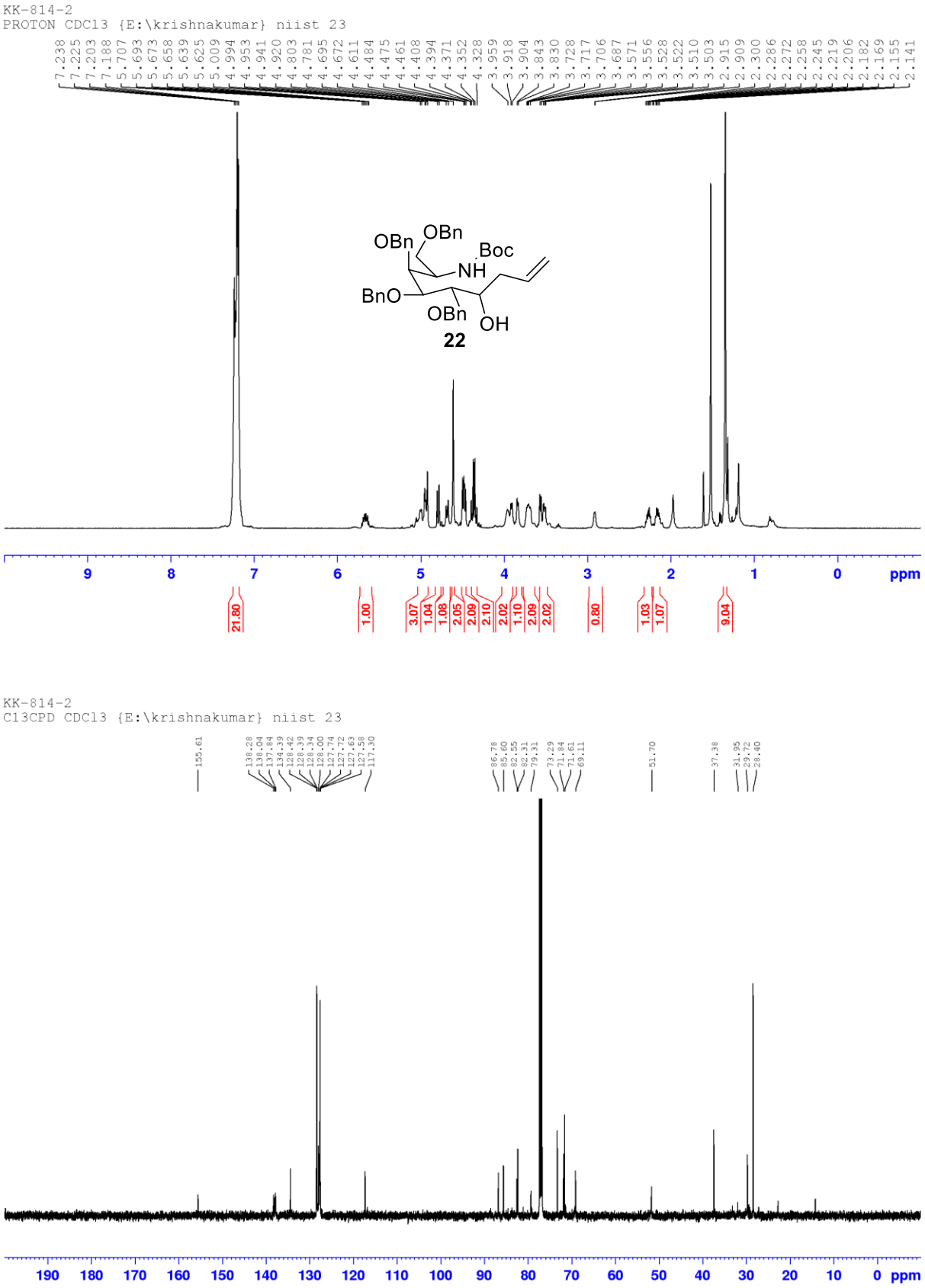

Figure 4.5.7.16: NMR spectra of compound **23**

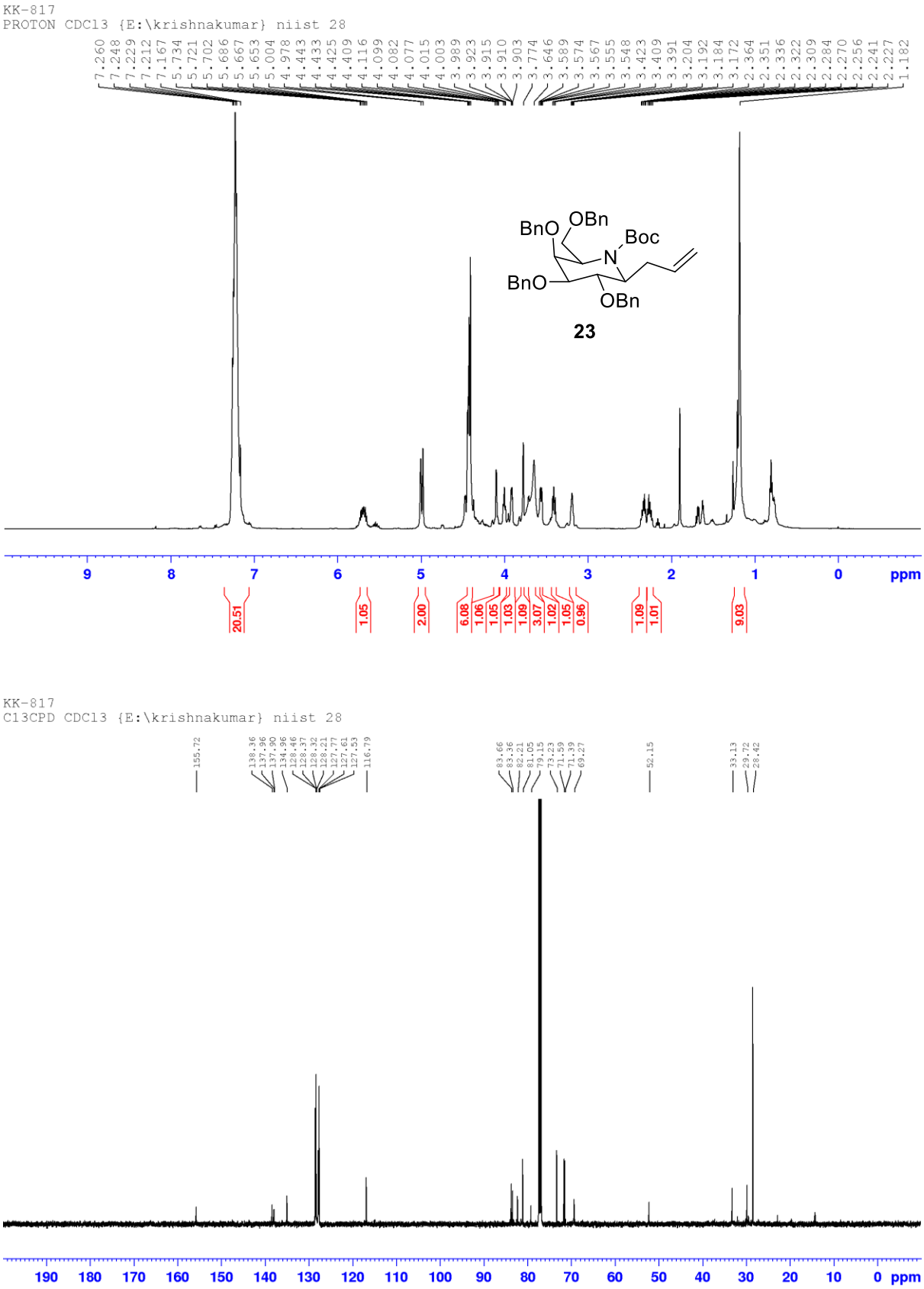

Figure 4.5.7.17: NMR spectra of compound **27**

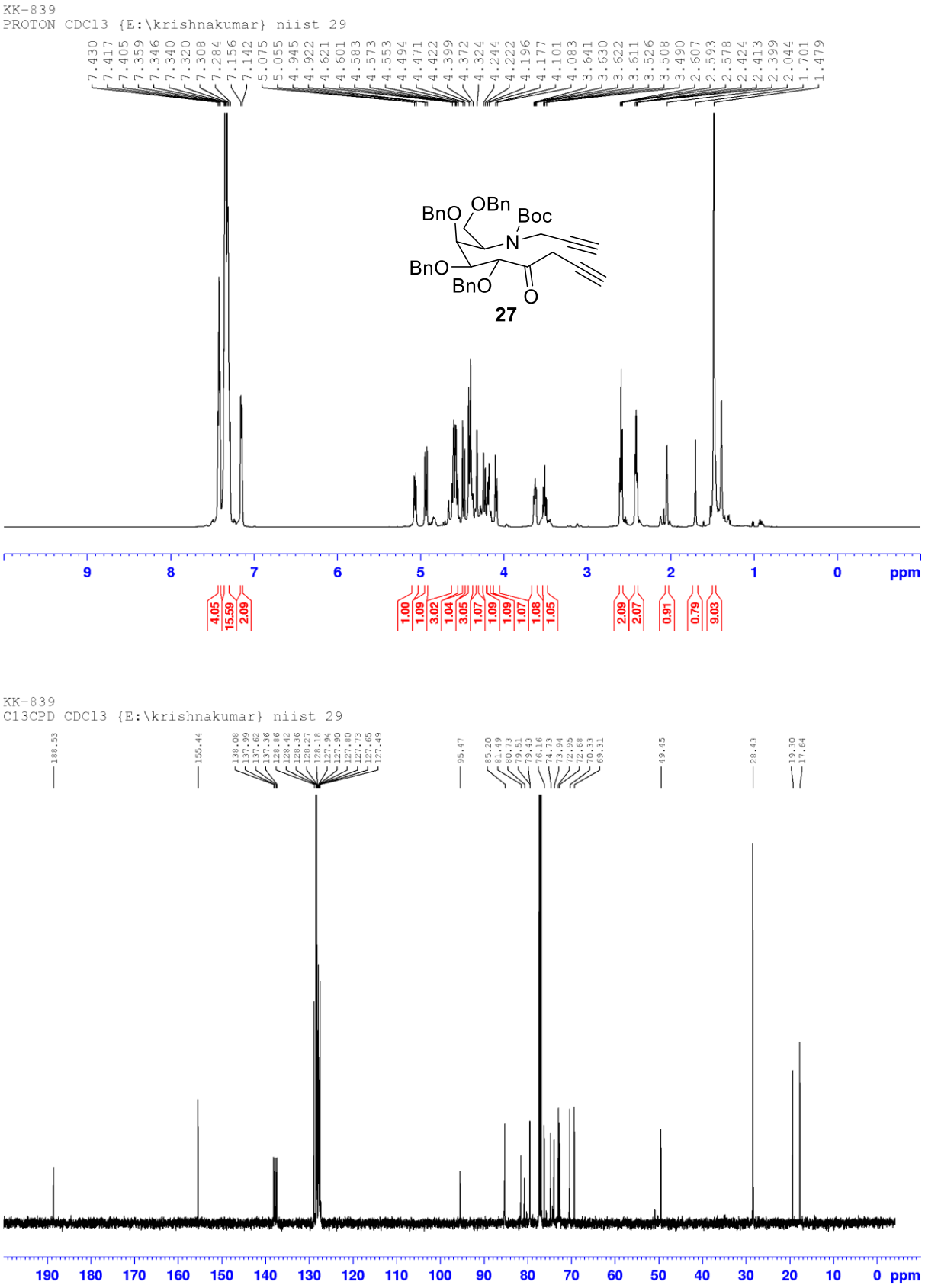

Figure 4.5.7.18: NMR spectra of compound **28**

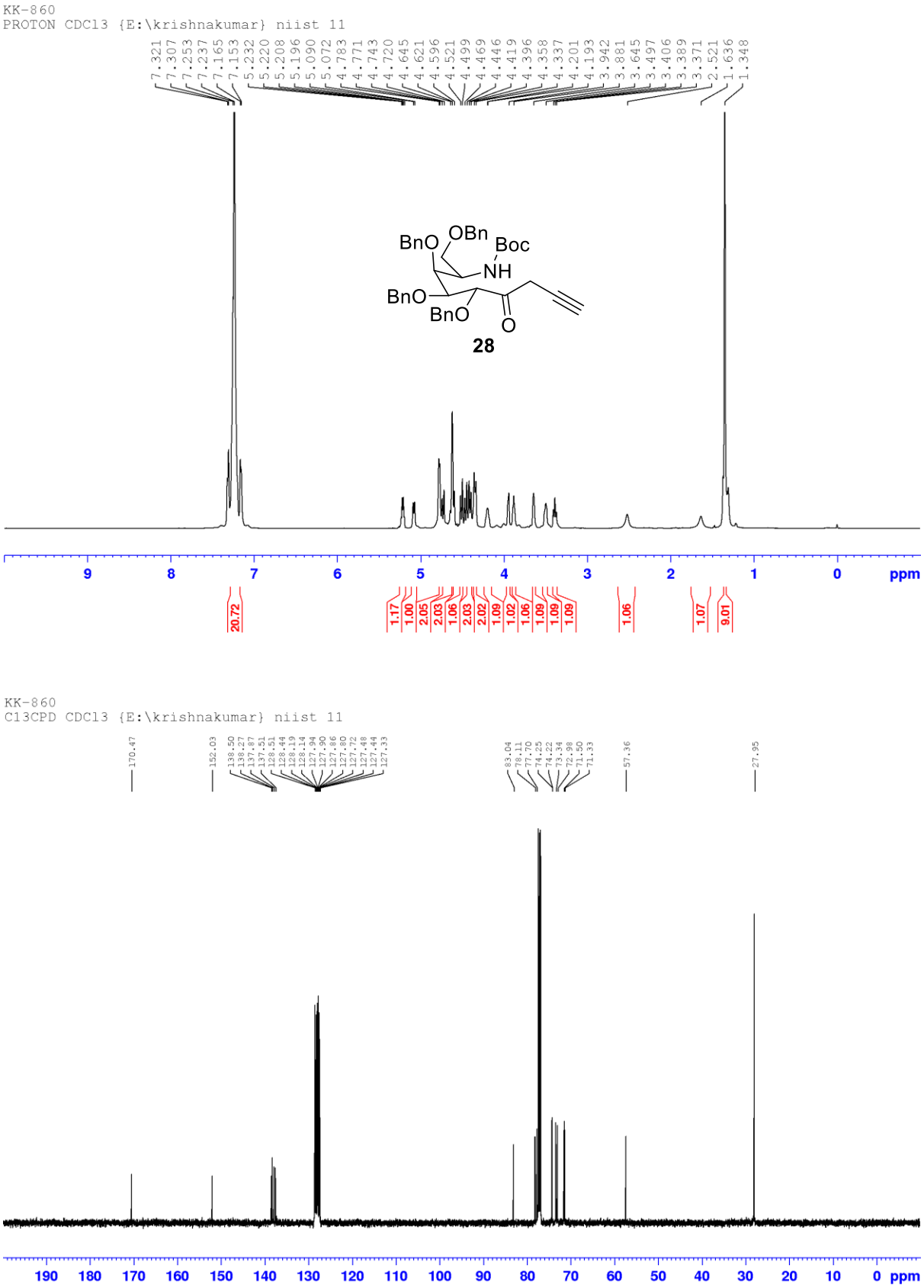

Figure 4.5.7.19: NMR spectra of compound **30**

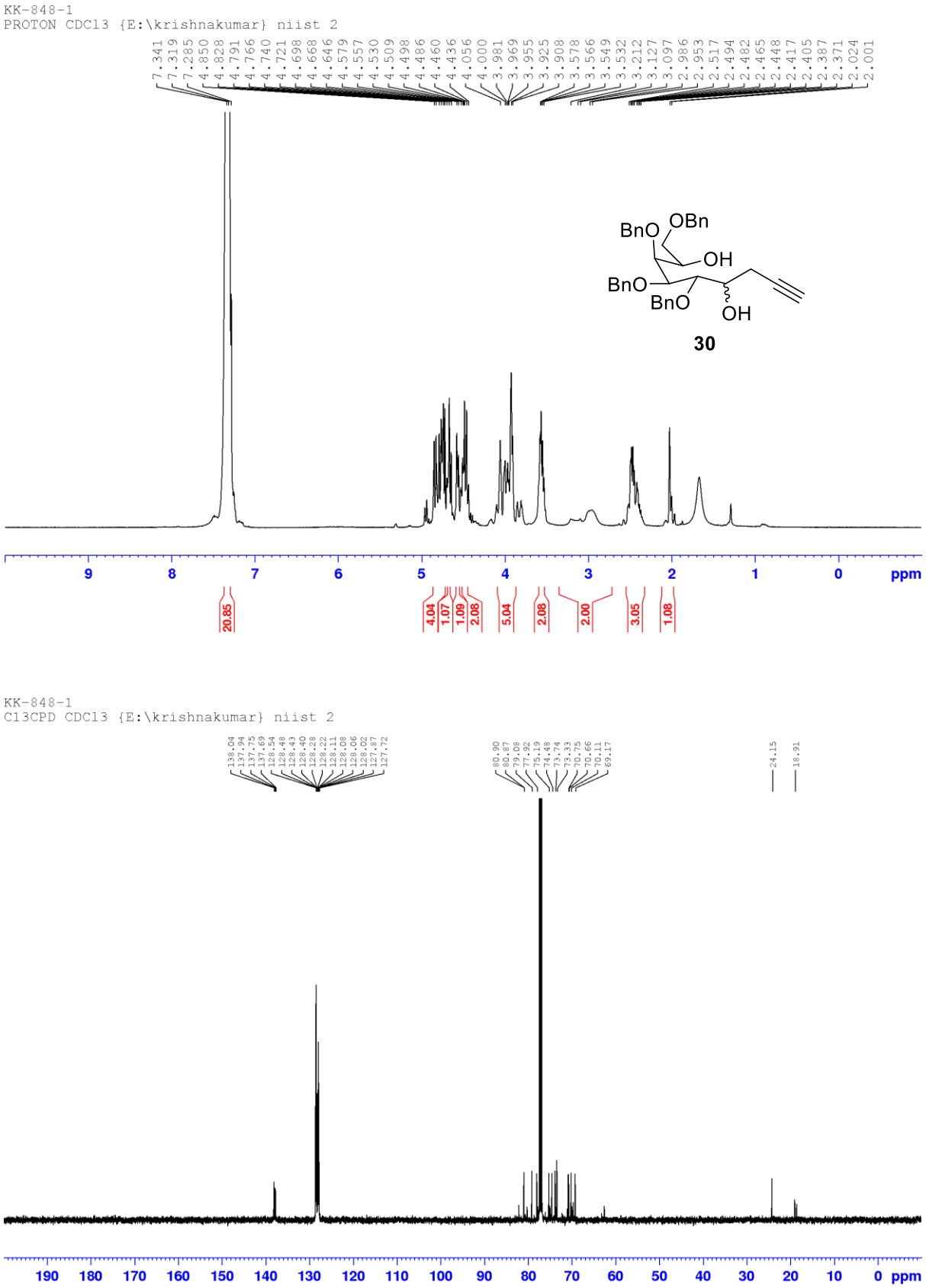

Figure 4.5.7.20: NMR spectra of compound **34**

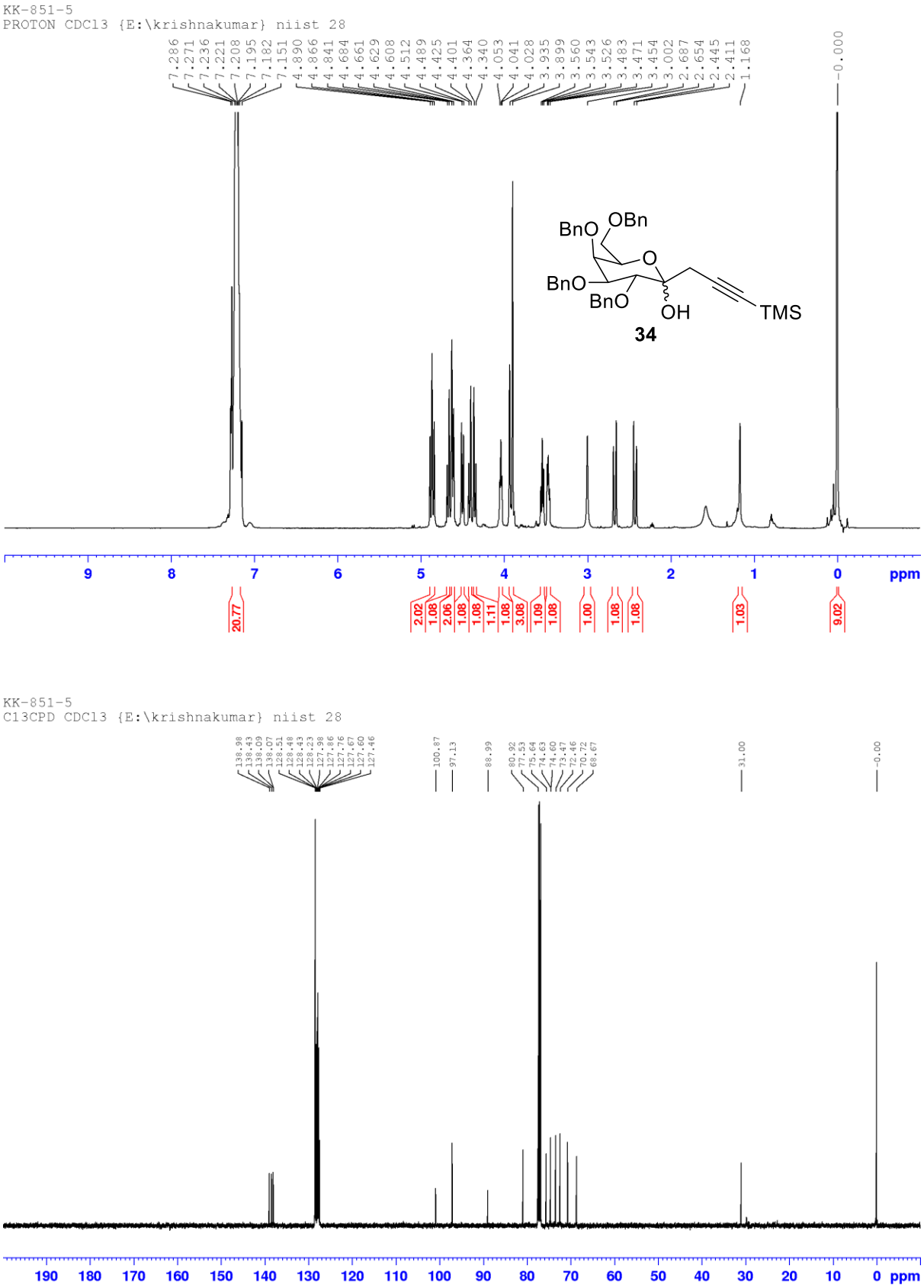

Figure 4.5.7.21: NMR spectra of compound **35**

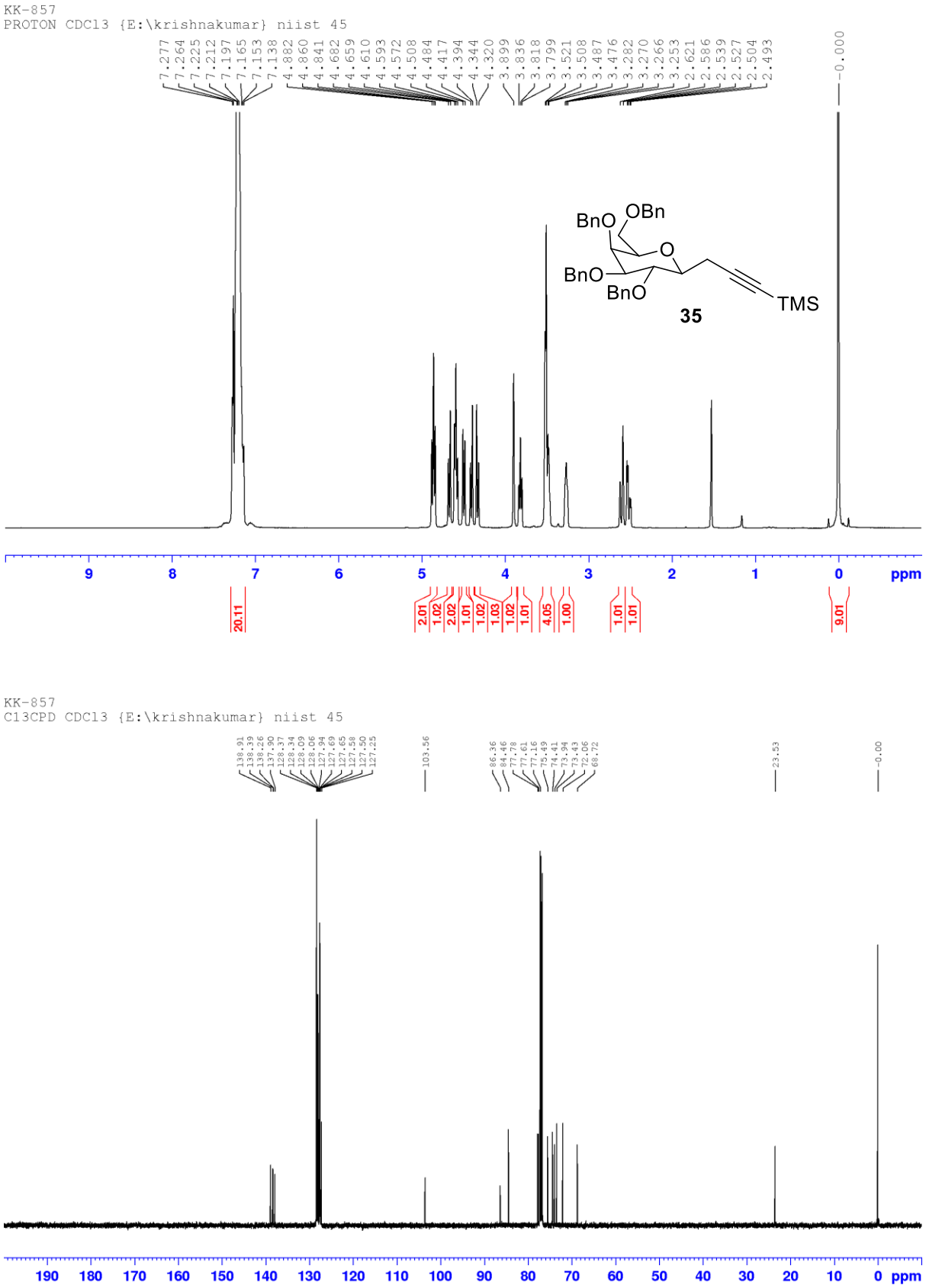

Figure 4.5.7.22: NMR spectra of compound **36**

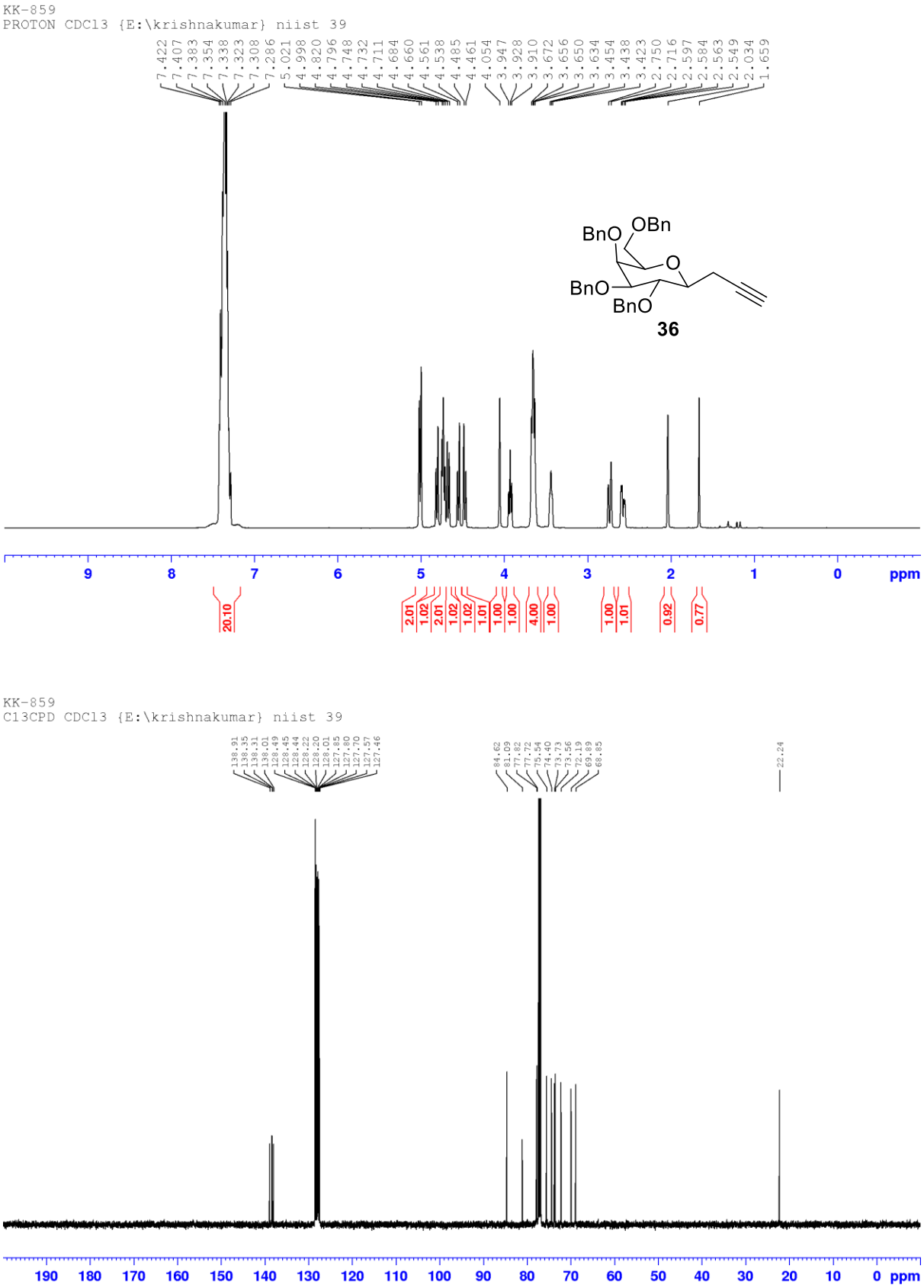

Figure 4.5.7.23: NMR spectra of compound **38**

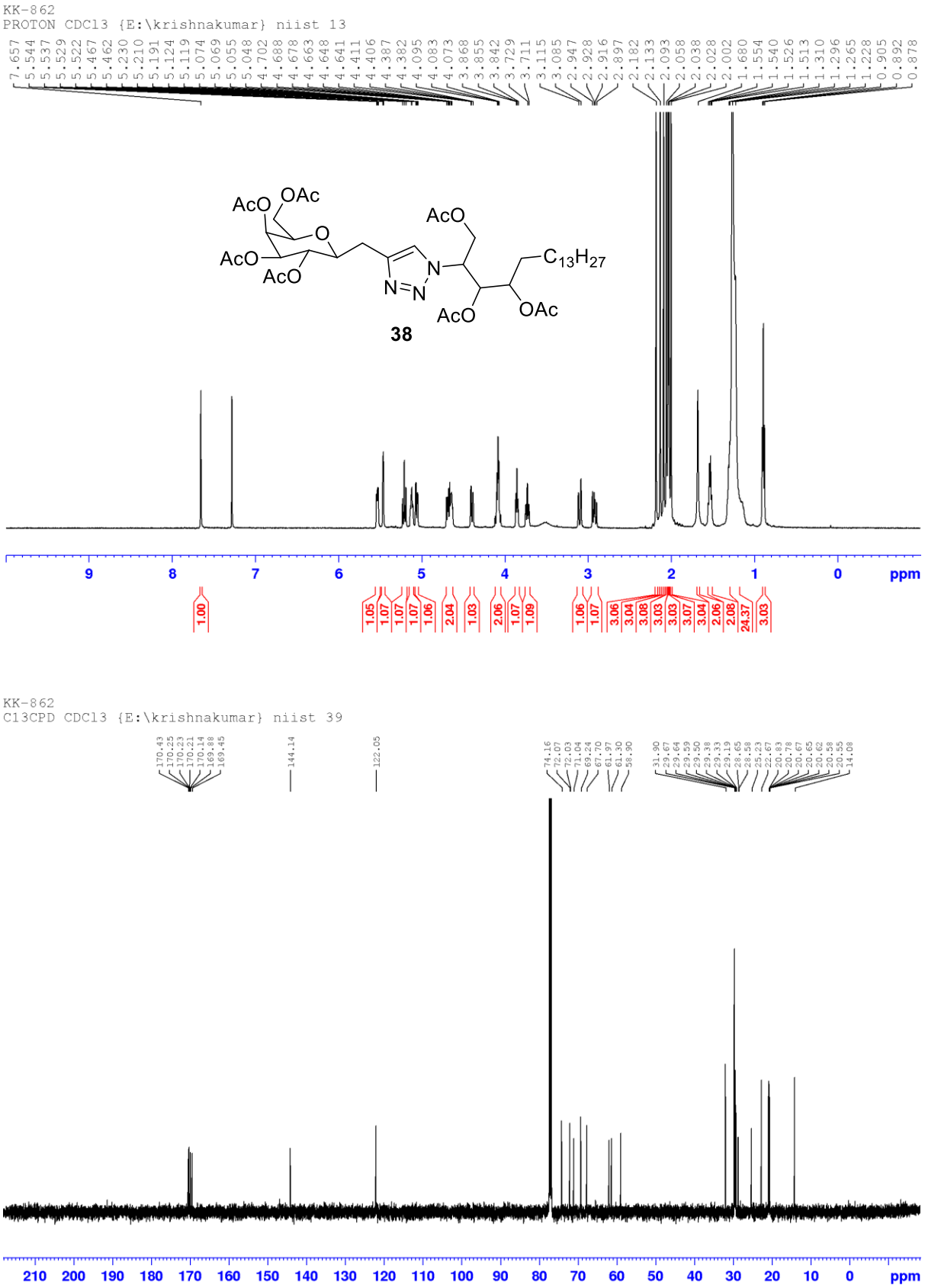

Figure 4.5.7.24: NMR spectra of compound **42**

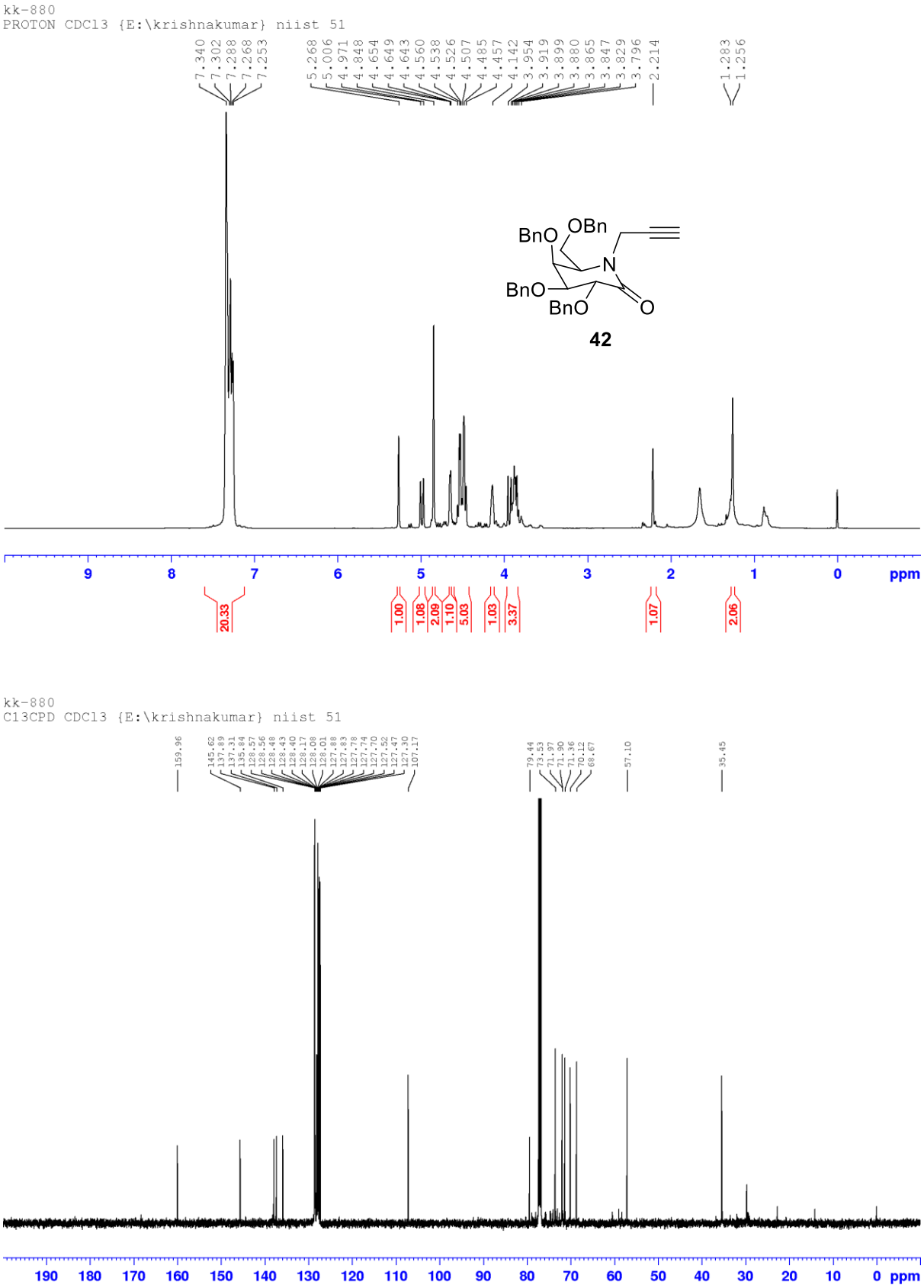

Figure 4.5.7.25: NMR spectra of compound **43**

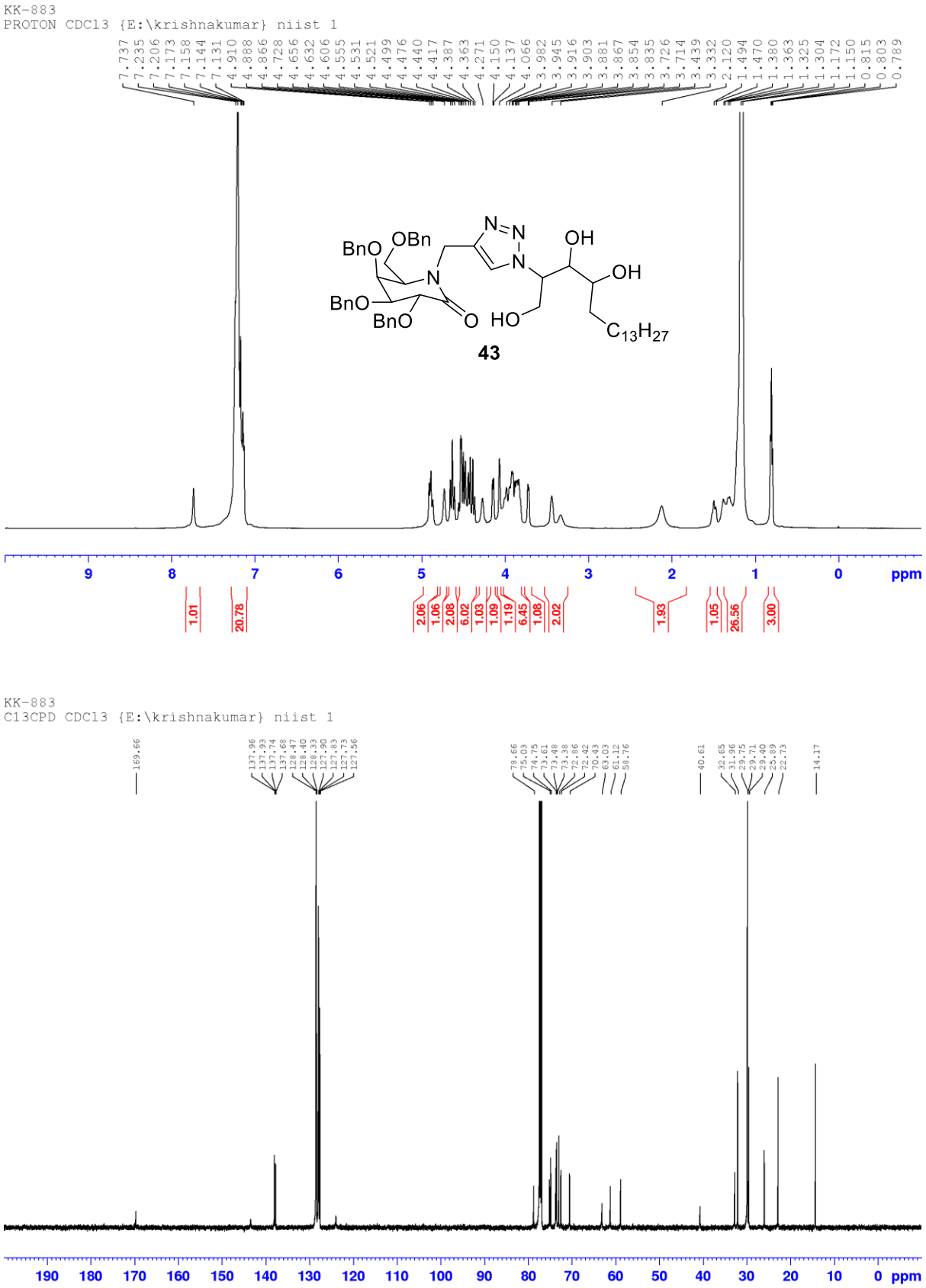

Figure 4.5.7.26: NMR spectra of compound **46**

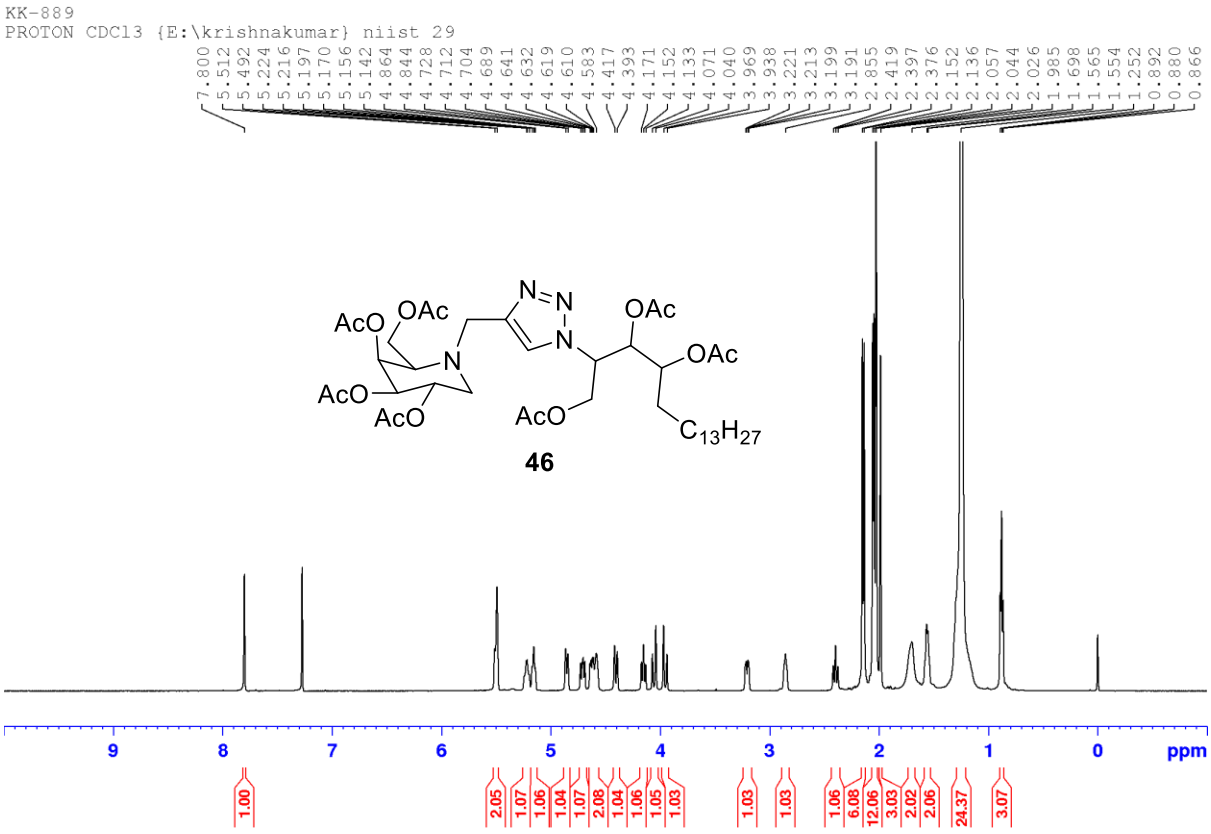

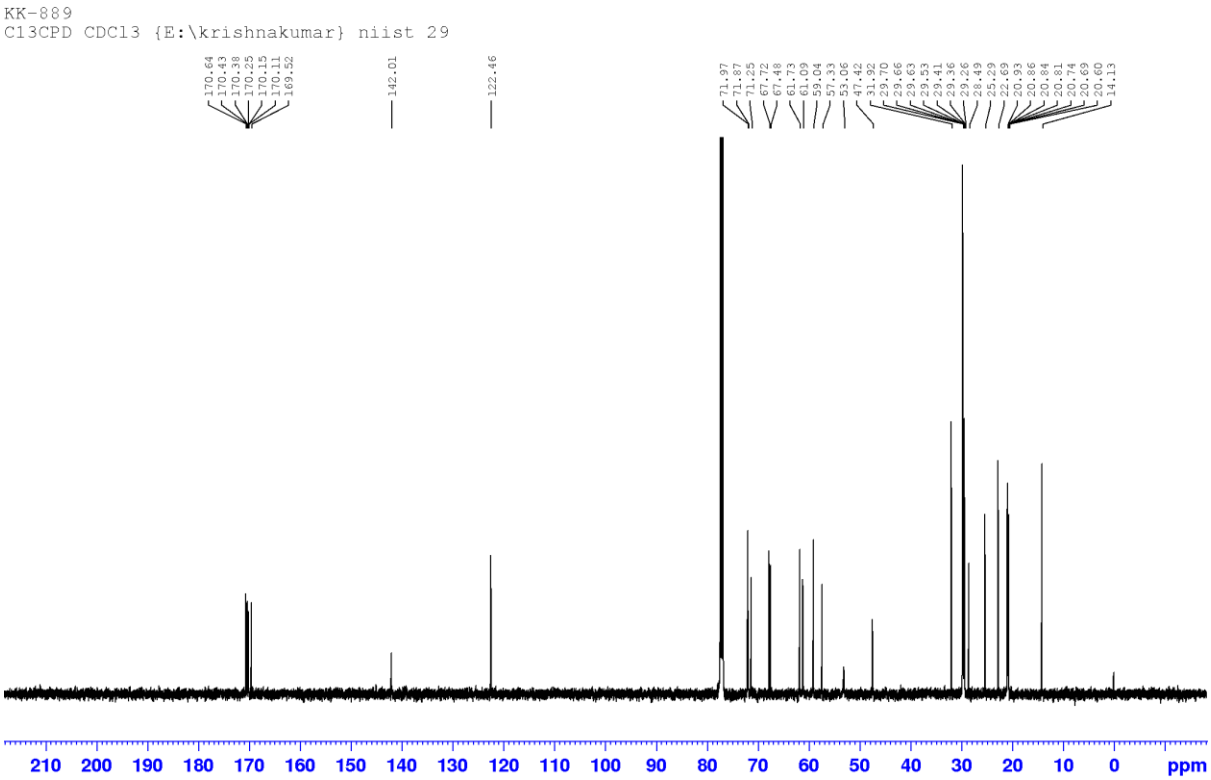

Figure 4.5.7.27: NMR spectra of compound **47**

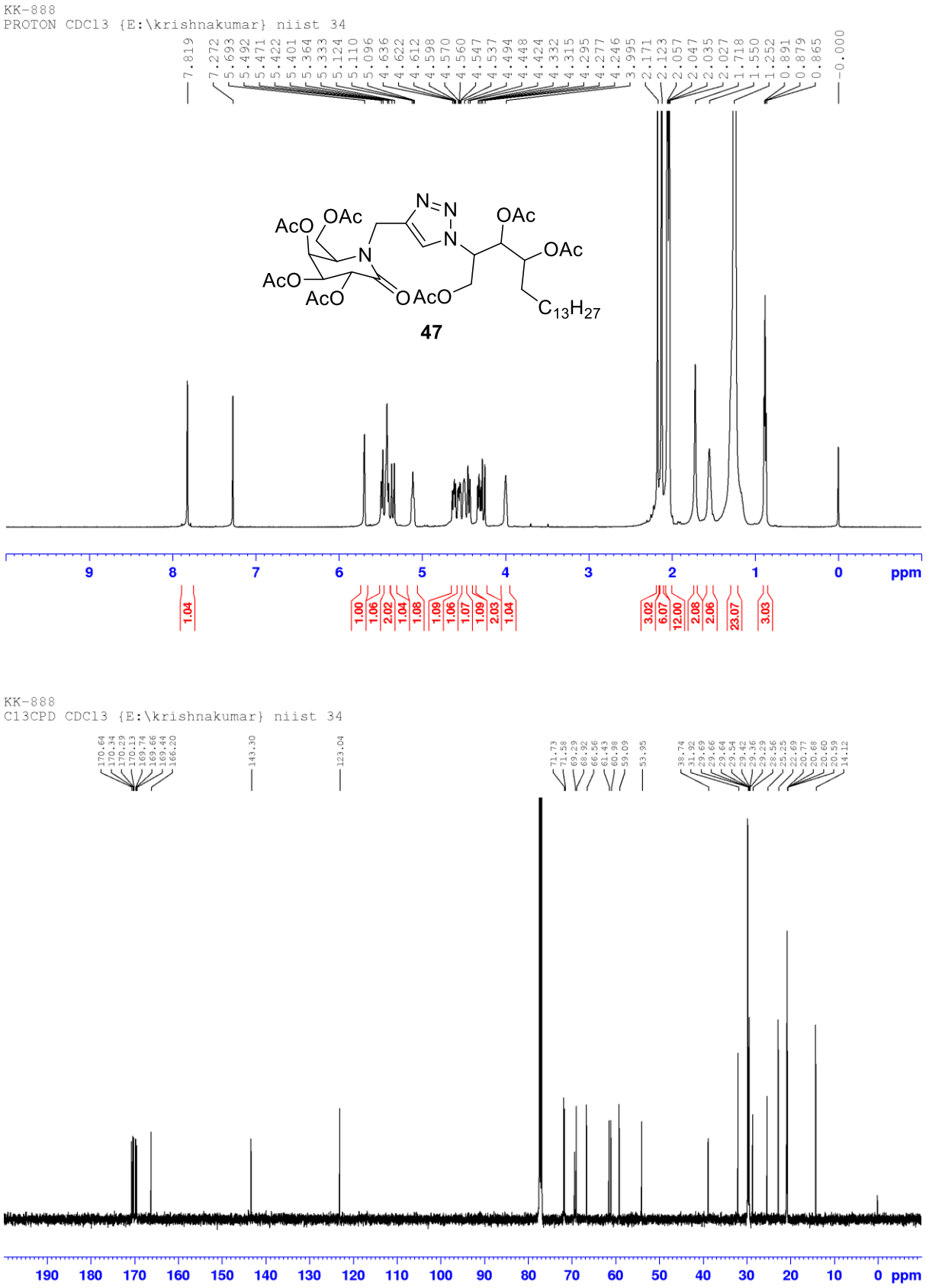

4.6. References

1. Kulkarni, R., Wiemer, E. A. C. & Chang, W. Role of lipid rafts in pathogen-host interaction-a mini review. *Front. Immunol.* **12**, 815020 (2022).
2. Avota, E. *et al.* The manifold roles of sphingolipids in viral infections. *Front. Physiol.* **12**, 715527 (2021).
3. Yagi-Utsumi, M. *et al.* The double-layered structure of amyloid-*β* assemblage on GM1-containing membranes catalytically promotes fibrillization. *ACS Chem. Neurosci.* **14**, 2648–2657 (2023).
4. Dong, M., Masuyer, G. & Stenmark, P. Botulinum and tetanus neurotoxins. *Annu. Rev. Biochem.* **88**, 811–837 (2019).
5. Lopez, P. H. H. & Schnaar, R. L. Gangliosides in cell recognition and membrane protein regulation. *Curr. Opin. Struct. Biol.* **19**, 549–557 (2009).
6. Nakayama, H., Nagafuku, M., Suzuki, A., Iwabuchi, K. & Inokuchi, J. The regulatory roles of glycosphingolipid-enriched lipid rafts in immune systems. *FEBS Lett.* **592**, 3921–3942 (2018).
7. Yeh, S.-C. *et al.* Glycolipid GD3 and GD3 synthase are key drivers for glioblastoma stem cells and tumorigenicity. *Proc. Natl. Acad. Sci.* **113**, 5592–5597 (2016).
8. Inokuchi, J. & Nagafuku, M. Gangliosides in T cell development and function of mice. *Glycoconj. J.* **39**, 229–238 (2022).
9. Vasques, J. F. *et al.* Gangliosides in nervous system development, regeneration, and pathologies. *Neural Regen. Res.* **18**, 81–86 (2023).
10. Voelkel-Johnson, C. Sphingolipids in embryonic development, cell cycle regulation, and stemness–Implications for polyploidy in tumors. in *Seminars in cancer biology* vol. 81 206–219 (Elsevier, 2022).
11. Liang, Y.-J. Glycosphingolipids in human embryonic stem cells and breast cancer stem cells, and potential cancer therapy strategies based on their structures and functions. *Glycoconj. J.* **39**, 177–195 (2022).
12. Zhang, L. & Donda, A. Alpha-galactosylceramide/CD1d-antibody fusion proteins redirect invariant natural killer T cell immunity to solid tumors and promote prolonged therapeutic responses. *Front. Immunol.* **8**, 4–6 (2017).
13. Huang, S.-L. *et al.* Mechanisms and Clinical Trials of Hepatocellular Carcinoma Immunotherapy. *Front. Genet.* **12**, 691391 (2021).
14. Wieland Brown, L. C. *et al.* Production of α-galactosylceramide by a prominent member of the human gut microbiota. *PLoS Biol.* **11**, e1001610 (2013).
15. Natori, T., Koezuka, Y. & Higa, T. Agelasphins, novel α-galactosylceramides from the marine sponge Agelas mauritianus. *Tetrahedron Lett.* **34**, 5591–5592 (1993).

16. Wagner, M. & Koyasu, S. A 3D Skin Melanoma Spheroid-Based Model to Assess Tumor-Immune Cell Interactions. *Bio-protocol* **10**, e3839 (2020).

17. Chen, X. *et al.* α-Galactosylceramide and its analog OCH differentially affect the pathogenesis of ISO-induced cardiac injury in mice. *Acta Pharmacol. Sin.* **41**, 1416–1426 (2020).

18. Ren, H., Krasovskiy, A. & Knochel, P. Stereoselective preparation of functionalized acyclic alkenylmagnesium reagents using i-PrMgCl-LiCl. *Org. Lett.* **6**, 4215–4217 (2004).

19. Overkleeft, H. S., van Wiltenburg, J. & Pandit, U. K. A facile transformation of sugar lactones to azasugars. *Tetrahedron* **50**, 4215–4224 (1994).

20. Gorantla, J. N., Faseela, A. & Lankalapalli, R. S. Design and synthesis of a novel glycosphingolipid derived from polyhydroxy 2-pyrrolidinone and phytoceramide appended by a 1,2,3-triazole linker. *Chem. Phys. Lipids* **194**, 158–164 (2016).

21. Llobat, A., Escorihuela, J., Fustero, S. & Medio-Simón, M. Diastereoselectivity of the Addition of Propargylic Magnesium Reagents to Fluorinated Aromatic Sulfinyl Imines. *Org. Lett.* **23**, 3691–3695 (2021).

22. Suero, M. G., De la Campa, R., Torre-Fernández, L., García-Granda, S. & Flórez, J. Enantioselective Multicomponent Synthesis of Fused 6–5 Bicyclic 2-Butenolides by a Cascade Heterobicyclisation Process. *Chem. Eur. J.* **18**, 7287–7295 (2012).

23. Alicea-Matías, E. & Soderquist, J. A. Asymmetric Propargylboration of Aldimines and Ketimines with the Borabicyclo [3.3. 2] decanes: Novel Entries to Allenyl Carbinamines, Amino Acids, and Their α-Methyl Counterparts. *Org. Lett.* **19**, 336–339 (2017).

ABSTRACT

Name of the student: **Krishnakumar K A** Registration No.: **10CC18J39003**
Faculty of study: **Chemical Sciences** Year of Submission: **2024**
AcSIR academic centre/CSIR Lab: **CSIR-NIIST** Name of the Supervisor: **Dr. Ravi Shankar L**
Title of the thesis: **Development of Novel Synthetic Strategies for Iminosugar-Based Glycomimetics**

This thesis introduces the foundational concepts of glycomimetics, emphasizing their critical roles in various biological processes and therapeutic applications. **Chapter 1** underscores the necessity of synthetic glycomimetics to overcome the inherent limitations of natural carbohydrates, such as metabolic instability and poor bioavailability. It highlights the therapeutic potential of these synthetic analogs, particularly immucillins like Immucillin-H and Immucillin-A, in the treatment of T-cell malignancies and viral infections. By setting the stage with a thorough exploration of the current landscape and advancements in glycomimetic research, this chapter provides the necessary context for the detailed synthetic strategies and innovative approaches discussed in the subsequent chapters.

Chapter-2 describes a novel approach to synthesizing forodesine, a potent iminosugar with immunosuppressive properties. The strategy focuses on the independent synthesis of the key subunits – a lactam derived from d-ribose and a pyrrolopyrimidine unit – followed by their coupling in a final step. Challenges were encountered in the synthesis of the lactam precursor using previously reported methods. The research described here addressed these limitations by exploring alternative reaction conditions and protecting group strategies. The pyrrolopyrimidine unit was successfully synthesized from readily available starting materials. However, the crucial cross-coupling reaction between the lactam and pyrrolopyrimidine unit proved unsuccessful using initial attempts. A different approach was then explored, employing ribose-aldehyde as the sugar partner. This strategy ultimately yielded the desired cross-coupled product. Subsequent double reductive amination reactions furnished an iminosugar derivative. While this compound possessed the correct N-substitution and pyrrolopyrimidine core, it exhibited a stereochemical configuration distinct from the target forodesine molecule. Despite not achieving the direct synthesis of forodesine, this study successfully identified a route to access a stereoisomer of the forodesine precursor. Further optimization is needed to improve the yield of this key intermediate for the complete synthesis of forodesine.

Chapter-3 describes a novel and efficient method for synthesizing galidesivir (Immucillin-A), a broad-spectrum antiviral drug effective against various RNA viruses. The key lies in first obtaining forodesine (Immucillin-H), a precursor molecule. To achieve this, the chapter presents a revised strategy using lactam as the coupling partner, leading to a more controlled and efficient forodesine synthesis. This approach overcomes challenges encountered in previous cross-coupling reactions by utilizing a Grignard reaction for a crucial step. This streamlined approach improves yield and scalability of the forodesine synthesis. The method offers a viable pathway for galidesivir production, facilitating its potential application in combating significant viral infections. This chapter also highlights key innovations that contribute to this efficient synthesis. These include using a Boc protecting group to activate the lactam carbonyl group and overcome limitations in cross-coupling reactions. Additionally, the chapter describes the advantages of employing the turbo-Grignard reagent for chemoselective cross-coupling, with the added benefit of compatibility with THF solvent. Most significantly, the work establishes a unified intermediate for the synthesis of both forodesine and galidesivir, bypassing limitations of existing methods that rely on forodesivir as the starting material. The chapter even proposes a possible explanation for the observed stereoselectivity during intermediate formation, involving anchimeric assistance. Overall, this work paves the way for streamlined galidesivir production and opens doors for the exploration of novel immucillin derivatives with potential therapeutic applications.

Chapter-4 describes the synthesis of novel iminosugar analogs of KRN-7000, a potent immune stimulator. The main strategy involved replacing the natural galactose sugar unit in KRN-7000 with an iminosugar derivative and linking it to the ceramide portion through a C-glycosidic bond. Initial attempts focused on cross-coupling reactions using Turbo Grignard reagents and metathesis. However, these methods encountered challenges, particularly with controlling the reactivity of propargyl Grignard reagents. Click chemistry emerged as a successful alternative strategy. The chapter details the synthesis of C1-propargylated galactose and N-propargylated lactam intermediates. Both intermediates readily underwent click reactions with azido-phytosphingosine to afford KRN-7000 analogs with triazole linkers. Although the desired C1-propargylated azagalactose intermediate remained elusive, the chapter successfully produced novel KRN-7000 analogs using click chemistry. These analogs hold promise for further investigation and potential development in the field of immunology.

List of publications

List of publications emanating from the thesis work

1. Synthesis of Immucillins BCX-1777 and BCX-4430 from a Common Precursor. **Krishnakumar K. A.**, & Lankalapalli R. S. ***European Journal of Organic Chemistry*****,** ***2022***(25), (DOI:10.1002/ejoc.202200428)

List of patents

1. A PROCESS FOR THE SYNTHESIS OF BCX-1777 AND BCX-4430
   Indian Patent Application No**. 202111061664** (Date of filing: 29/12/2021)
   International Application No. **PCT/IN2022/051135** (Date of filing: 29/12/2022)
   Lankalapalli Ravi Shankar, **Karunakaran Anitha Krishnakumar**, Suresh Sanjay Varma, Velickakathu Omanakuttan Yadhukrishnan, Kapiya Sangeeth, Chekrain Valappil Shihas Ahammed, Bernard Prabha, Thangarasu Arun Kumar, Doddramappa Doddamani Shridevi, John Jubi, Kokkuvayil Vasu Radhakrishnan, Ayyappanpillai Ajayaghosh

List of publications not related to thesis

1. Cu (I)-azidopyrrolo [3, 2-d] pyrimidine Catalyzed Glaser–Hay Reaction under Mild Conditions. Thangarasu A. K., Yadhukrishnan V. O., **Krishnakumar K. A**., Varma S. S., & Lankalapalli R. S. ***ACS Organic & Inorganic Au*****, 2021**. *2*(1), 3-7. (DOI: 10.1021/acsorginorgau.1c00015).

2. Enzyme based bioelectrocatalysis over laccase immobilized poly-thiophene supported carbon fiber paper for the oxidation of D-ribofuranose to D ribonolactone. Thadathil D. A., Varghese A., Ahamed C. V. S., **Krishnakumar K. A**., Varma S. S., Lankalapalli R. S., & Radhakrishnan K. V. ***Molecular Catalysis*****, 2022** (*524)*, 112314. (DOI:10.1016/j.mcat.2022.112314)

3. NMR-based Phytochemical Profiling of Palmyra Palm Syrup Infused with Dry Ginger, Black Pepper, and Long Pepper. Athira A. S., Kiruthika R., Ingaladal N., **Krishnakumar K. A.,** Raveena N. K., Gopika B., Reshma M.V & Lankalapalli, R. S. ***Current Nutraceuticals*****, 2023**. *4*(1). (DOI: 10.2174/2665978604666230112144757)+

Poster presentation

1. Isolation of bio-active metabolites from rhizophore of Mangroove's associated bacterial strains and their antibacterial effect on human pathogens., 32nd KSC, 2020. **Krishnakumar K. A.**, Vikas G., Jesmina A. S., Dileep Kumar B. S., & Ravi Shankar Lankalapalli* (Poster presentation).

ISOLATION OF BIO-ACTIVE METOBOLITES FROM RHIZOPHORE SOIL OF MANGROOVE'S ASSOCIATED BACTERIAL STRAINS AND THEIR ANTIBACTERIAL EFFECT ON HUMAN PATHOGENS

Krishnakumar K. A.,[#,†] Vikas G.,[#,†] Jesmina A. S.,[‡] Dileep Kumar B. S.,[‡] and Ravi Shankar Lankalapalli[†]

[†]*Chemical Sciences and Technology Division,* [‡]*Agro-Processing and Technology Division, and* [†‡]*Academy of Scientific & Innovative Research (AcSIR), CSIR-National Institute for Interdisciplinary Science and Technology (CSIR-NIIST), Thiruvananthapuram-695019, Kerala, India.*

[#]These authors contributed equally to this work.

Introduction: Due to emergence of multidrug-resistant strains of bacteria and fungi, there is an ever-increasing demand for novel antibiotics with broad antimicrobial spectra. Soil is a rich source of microorganisms, which include neutral, beneficial and harmful organisms. One of the most important beneficial organisms are belonging to *Actinomycetes*, a diverse group of free living saprobic mycelial bacteria present abundantly in the soil, maintaining the structure and integrity of soil. Marine ecosystem constitutes oceans, the deep sea and the sea floor, estuaries and lagoons, salt marsh and intertidal zones, coral reefs and mangrove swamps. Mangrove soils are a brimful resource of microorganisms, and due to the dynamic physicochemical environment, microorganisms surviving in this area are equipped with various biomolecules, which has many potential applications in pharmaceutical industry. Moreover, many microorganisms isolated from mangroves are reported. In this context, we are screening all the bacterial strains including, *Streptomyces* being the major interest from soil sediments of selected mangroves. The Mangrove species chosen for this study include ***Excoecaria agallocha,*** and ***Avicennia officinalis*** that are some of the most abundant species available in Kerala coastal region.

Materials and methods: Soil samples were collected from Ayram Thengu (9.125579° N, 76.47731° E) of the Coastal region in kollam, Kerala, India and bought to the laboratory.1g of such soil were suspended in 9 ml sterile distilled water and was vortexed for a few minutes. From this, a wire loop of the suspension was streaked on Starch Casein Agar(SCA) plates in triplicates and incubated at 28±2°C for 14 to 28 days. The emerging colonies with different morphological characteristics were selected and the purified strains were

maintained on SCA slants. The viability of the strains was checked in NA, PDA and SCA, where SCA was the best, hence further storage and maintenance of the culture was done in SCA.

The bacterial pathogens used for antibacterial studies were *Bacillus cereus* MTCC 1305, , *Mycobacterium smegmatis* MTCC 993, *Staphylococcus aureus* MTCC 902, , (all Gram positive) and *Escherichia coli* MTCC 2622, *Klebsiella pneumoniae* MTCC 109, *Proteus mirabilis* MTCC 425, *Pseudomonas aeruginosa* MTCC 2642, *Salmonella typhi* MTCC 3216, (all Gram negative). All the bacterial strains were procured from Microbial Type Culture Collection and Gene Bank (MTCC), CSIR-Institute of Microbial Technology (IMTECH), Chandigarh, India.

Results and discussion: In this study, a Streptomyces strain designated as ATEA-1 and ATAO-1 showing a broad-spectrum antibacterial activity against *Staphylococcus aureus, Mycobacterium smegmatis, Bacillus cereus* and *Pseudomonas aeruginosa,* also later showing inhibition against *Escherichia coli*, *Klebsiella pneumoniae*, *Proteus mirabilis*, *Salmonella typhi.* Further the metabolite in crude form was isolated by fermenting in a Starch Casein Broth after 6 days of incubation. The fermented broth was extracted using ethyl acetate and then evaporated under vacuum and concentrated. The crude extract was also subjected to antagonistic studies, of which ATEA-1 and ATAO-1 produced metabolic extract showed promising activity against the specified human pathogens. By optimizing a new media for growth and by statistical analysis we enhanced the production of the metabolite. When the characterization is complete we will get a clear idea of the compounds in metabolite.

References:

1. Sharifi, M., & Bipinraj, N. K. (2019). Isolation and Identification of Actinomycetes with Anticandida Activity from Mangrove Soil. *Biosciences Biotechnology Research Asia*, *16*(3).

2. Das, A., Bhattacharya, S., Mohammed, A. Y. H., & Rajan, S. S. (2014). In vitro antimicrobial activity and characterization of mangrove isolates of streptomycetes effective against bacteria and fungi of nosocomial origin. *Brazilian Archives of Biology and Technology*, *57*(3), 349-356.

3 Sweetline, C., Usha, R., & Palaniswamy, M. (2012). Antibacterial activity of actinomycetes from Pichavaram Mangrove of Tamil Nadu. *Applied Journal of Hygiene*, *1*(2), 15-18.

EurJOC
European Journal of Organic Chemistry

Research Article
doi.org/10.1002/ejoc.202200428

Chemistry Europe
European Chemical Societies Publishing

www.eurjoc.org

Special Collection

Synthesis of Immucillins BCX-1777 and BCX-4430 from a Common Precursor

K. A. Krishnakumar[a, b] and Ravi S. Lankalapalli*[a, b]

Dedicated to the students in my lab for their perseverance during the COVID-19 pandemic

A convergent route for the synthesis of BCX-1777 and BCX-4430 from a Boc-protected 2-pyrrolidinone, derived from 2,3,5-tri-*O*-benzyl-D-ribonolactone, and a dihalogenated pyrrolopyrimidine as the key starting materials is reported. A chemoselective cross-coupling was achieved from the two key starting materials in 79% yield. Luche reduction and mesylation resulted in the stereoselective formation of an advanced intermediate in 77% yield over two steps, which served as a precursor for synthesizing BCX-1777 and BCX-4430 in 38% (over 10 steps) and 32% (over 11 steps) overall yields, respectively, from 2,3,5-tri-*O*-benzyl-D-ribonolactone.

Introduction

Nucleoside analogues are the mainstay of therapeutic modalities in treating viral infections.[1] SARS-CoV-2 or COVID-19 infection led to a global endeavor in repurposing nucleoside-based drugs that resulted in remdesivir and molnupiravir as FDA-approved drugs (Figure 1), and many more are at various stages of developmental studies as potential hits for novel antivirals. BCX-4430 (aka galidesivir or immucillin A, Figure 1), a *C*-nucleoside analogue, is a broad-spectrum antiviral agent that disrupts viral RNA-dependent RNA polymerase.[2] BCX-4430, initially intended for hepatitis C virus, displayed *in vivo* antiviral activity against several serious pathogens, including Ebola, Marburg, Zika, Yellow fever, Rift Valley fever, and *in vitro* against more than 20 RNA viruses.[3] BCX-4430 was repurposed for COVID-19 by BioCryst Pharmaceuticals. Though the Phase I clinical studies displayed promising results with a dose-dependent decline in viral levels, and the drug was found to be safe and well-tolerated, it was not pursued further for COVID-19. However, BCX-4430 is in advanced clinical development to treat Marburg viral disease,[3] the same family as Ebola with high fatality. A related adenosine analogue, BCX-1777 (aka Forodesine or immucillin H, Figure 1), serves as a purine nucleoside phosphorylase inhibitor that produces selective suppression of T-cells, inducing apoptosis.[4] In Japan, BCX-1777 is sold under the brand name Mundesine® for the treatment of relapsed or refractory peripheral T-cell lymphoma.

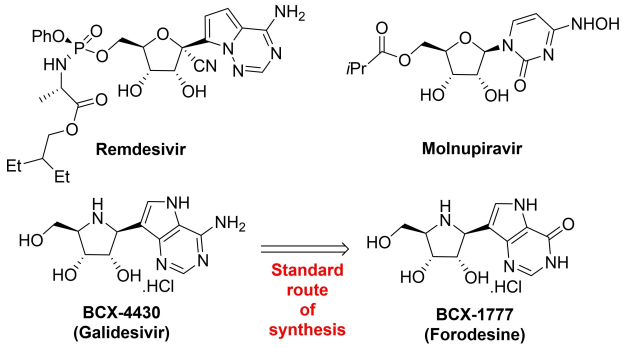

Figure 1. Repurposed nucleoside-based drugs used against COVID-19 (top) and compounds BCX-4430 and BCX-1777.

On the synthetic front, most of the reports for obtaining BCX-4430 rely on the intermediacy of BCX-1777 with the key step for *C*-nucleoside synthesis being C–C bond formation between iminoribitol and aglycon moieties. In a linear synthesis, an imine derived from an N-halo amine, obtained from D-gulono-1,4-lactone,[5] by base-catalyzed elimination, was utilized in the addition reaction with excess lithiated acetonitrile to afford a cyanomethyl C-glycoside derivative (Figure 2A), which culminated in BCX-1777 with an overall yield of 3.7% in 20 steps.[6,7] In a convergent route, adding a lithiated 9-deazahypoxanthine derivative, derived from isoxazole,[8] to an imine afforded *C*-nucleoside in the key step (Figure 2B), providing BCX-1777 in an overall yield of 19% in 14 steps.[9] Coupling the stable tri-*O*-benzyl cyclic nitrone, derived from D-ribose, with lithiated 9-deazahypoxanthine derivative furnished hydroxylamine as separable diastereoisomers of β:α (7:1) (Figure 2C), which resulted in BCX-1777 in an overall yield of 8% in 11 steps.[10] Cross-coupling of a stable aza-sugar lactam (Figure 2D), derived from L-pyroglutamic acid, with lithiated 9-deazahypoxanthine followed by reduction furnished a mixture of β:α (4:1) of BCX-1777 in an overall yield of 14% from 10 steps.[11] A detailed comparison of reported syntheses for BCX-1777 and BCX-4430 are provided in Table S1 (Supporting Information). As

[a] *K. A. Krishnakumar, Dr. R. S. Lankalapalli*
Chemical Sciences and Technology Division,
CSIR-National Institute for Interdisciplinary
Science and Technology (CSIR-NIIST),
Thiruvananthapuram 695019,
Kerala, India
E-mail: ravishankar@niist.res.in
[b] *K. A. Krishnakumar, Dr. R. S. Lankalapalli*
Academy of Scientific & Innovative Research (AcSIR),
Ghaziabad 201002, India

Supporting information for this article is available on the WWW under https://doi.org/10.1002/ejoc.202200428

Part of a joint special collection highlighting research from CSIR Institutes.

Research Article
doi.org/10.1002/ejoc.202200428

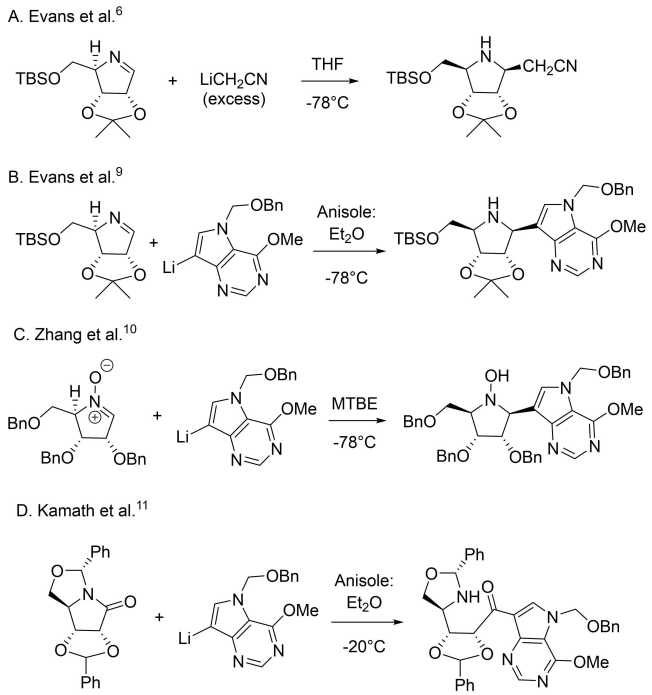

Figure 2. Key cross-coupling steps in synthesis of BCX-1777.

stated earlier, the synthesis of BCX-4430 was dependent on BCX-1777 that involved seven linear steps, including the incorporation of amine in the C-6 position of the purine.[2,10] To the best of our knowledge, the only report of a standalone synthetic route of BCX-4430 without dependence on the synthesis of BCX-1777 involved a tetrahydroxy tetrahydrofuran chiral intermediate, and by using a highly advanced chiral aminobenzyl-2-naphthol as the amine source.[12]

We report herein a novel process for synthesizing BCX-1777 and BCX-4430 in an expedient manner that is advantageous over the reported routes that rely on synthesis of an advanced common intermediate **9** (Scheme 2). In the present process, the key chemoselective cross-coupling step to afford compound **8** involves two key starting materials, a stable Boc-protected lactam **3** that is produced in five steps from 2,3,5-tri-*O*-benzyl-D-ribonolactone **1**, and a suitably dihalogenated pyrrolo[3,2-*d*]pyrimidine **7**, obtained from 9-deazahypoxanthine **5** in three steps. Compared to the imine D-ribose precursor employed in cross-coupling (Figure 2), lactam **3** serves as a convenient and stable starting material. A subsequent stereoselective reaction afforded the advanced intermediate **9** that serves as a common precursor to facilitate a standalone process for the synthesis of BCX-4430 and BCX-1777. The overall yield of BCX-1777 and BCX-4430 was 38% in 10 steps and 32% in 11 steps, respectively, from 2,3,5-tri-*O*-benzyl-D-ribonolactone **1**. Furthermore, the chloro substituent of advanced intermediate **9** can be substituted with various amines to provide adenosine receptor agonists,[13] and 6-S-immucillin-H.[14]

Results and Discussion

The synthetic strategy of adding metallated species to Boc-protected γ-lactam, followed by stereoselective reduction of the ketone, and subsequent cyclization by S_N2 displacement via mesylation to afford pyrrolidine as an epimeric mixture i.e. an addition-reduction-cyclization process was applied in several total synthesis reports.[15–22] Accordingly, 2,3,5-tri-*O*-benzyl-D-ribonolactone **1** was converted by established conditions in our lab[23] to Boc-protected γ-lactam **3** (Scheme 1), and applied here as a key starting material for cross-coupling reaction.[24] Next, we envisaged a metallated-9-deazahypoxanthine and a chloro substituent in C-6 position by chemoselective halogen-metal exchange with Grignard reagent under controlled conditions. Synthesis of 9-deazahypoxanthine **5** by reported method suffered setback in our hands,[25] hence, we adopted a novel condition in the presence of sodium methoxide for its synthesis (Scheme 1), by heating. Though 9-deazahypoxanthine **5** was obtained in a low yield, the duration of the reaction by heating to 12 hours is an advantage compared to the reported method which takes several days. 9-Deazahypoxanthine **5**, by known conditions,[9] was converted in three steps to dihalogenated pyrrolo[3,2-*d*]pyrimidine **7** (Scheme 1) that serves as the second key starting material. Alteration of the sequence of reactions from intermediate **6**, i.e., BOM protection followed by iodination with NIS led to a complex mixture.

The effect of LiCl additive on the rate of Br/Mg exchange was spectacular in the preparation of functionalized heteroarylmagnesium compounds,[26] which was applied successfully in the key cross-coupling step in nucleoside synthesis of

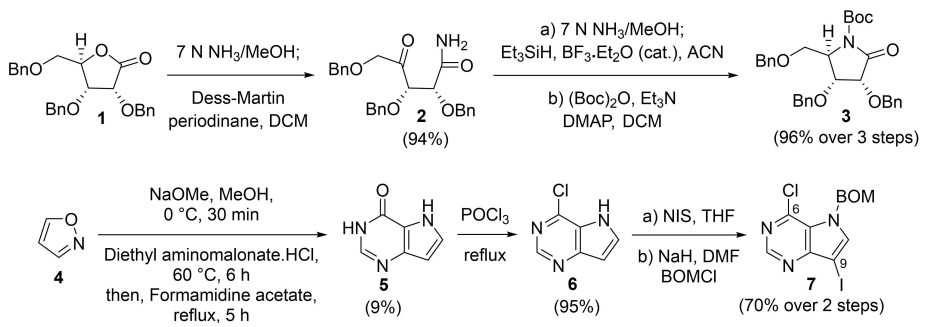

Scheme 1. Synthesis of Boc-protected γ-lactam **3** and dihalogenated pyrrolo[3,2-*d*]pyrimidine **7**.

remdesivir.[27] Initial attempts for cross-coupling lactam **3** were made with bromo-9-deazahypoxanthine derivative with chloro substituent in C-6 position using the commercially available *i*PrMgCl·LiCl reagent, but the expected bromo-metal exchange was sluggish. However, treatment of iodide **7** with *i*PrMgCl·LiCl reagent indicated a faster Mg exchange as observed by TLC, even at −50 °C, and an immediate addition of lactam **3** after 5 min led to a chemoselective addition reaction to afford intermediate **8** (Scheme 2). Purification of intermediate **8** led to a separable mixture of open- and closed-chain products as observed by the presence and absence of ketone carbonyl peak in ^{13}C NMR, respectively. The closed-chain compound **8** underwent a stereoselective reaction under Kishi reduction conditions using triethylsilane to afford the desired pyrrolidine **9** along with the formation of an open-chain product **8**. Repeated attempts on open-chain compound **8** under Kishi reduction conditions and variations failed to afford pyrrolidine **9**. Attempts of Boc group deprotection of compound **8** with trifluoroacetic acid to form an imine followed by reduction was also not fruitful. Hence, mesylation of the 2° alcohol, by reduction of ketone for ring-closing to afford pyrrolidine was envisaged. Accordingly, the compound **8** mixture was treated with catalytic $BF_3.Et_2O$ for converting closed-chain product to open-chain product, confirmed by ^{13}C NMR. Application of Luche reduction conditions on compound **8** afforded the 2° alcohol, which upon treatment with mesyl chloride facilitated the formation of pyrrolidine **9** and its C-1′ epimer in 77% and 10% yields over two steps, respectively. To determine the stereochemistry at C-1′ position, compound **9** was treated with sodium methoxide and the resulting C-6 methoxy substituted product exhibited a specific optical rotation of +56.7°, which was in agreement with the reported value of +56.2°, with the desired *'S'* configuration at C-1′ position (see the Supporting Information).[10] The undesired '*R*' configuration at C-1′ position exhibited a specific optical rotation of +20.4°, which was in agreement with the reported value of +21.7° (see the Supporting Information).[10]

Based on the overall addition–reduction–cyclization synthetic strategy for the synthesis of pyrrolidine in literature, *vide supra*, reduction of ketone by $NaBH_4$ is considered as the stereoselective step, which was explained by transition state models.[18,21] Accordingly, Cram's non-chelation or five-membered Ce^{3+} chelation model (TS-1, Path A, Scheme 3) favors the formation of mesylate **A** that leads to undesirable C-1′ epimer of compound **9**. In a six-membered Ce^{3+} chelation model (TS-2, Path A, Scheme 3), hydride attack from si face delivers the formation of desired mesylate **B** and subsequent cyclization affords compound **9**. However, under Luche reduction conditions, possible coordination of methoxyborohydride with the oxygen atom of C-2′ OBn group next to the reaction site to deliver hydride from re face to afford the undesired mesylate **A** cannot be ruled out, a rationale disregarded in reports involving addition-reduction-cyclization synthetic strategy. A substrate analogous to mesylate **A** led to a reaction outcome that supports anchimeric assistance, from unpublished results in our lab (Scheme S1, see the Supporting Information). Cyclization of mesylate **A** is hindered by the steric factor, which prompts the positioning of mesylate group (**I**) to facilitate S_N2 attack by C-2′

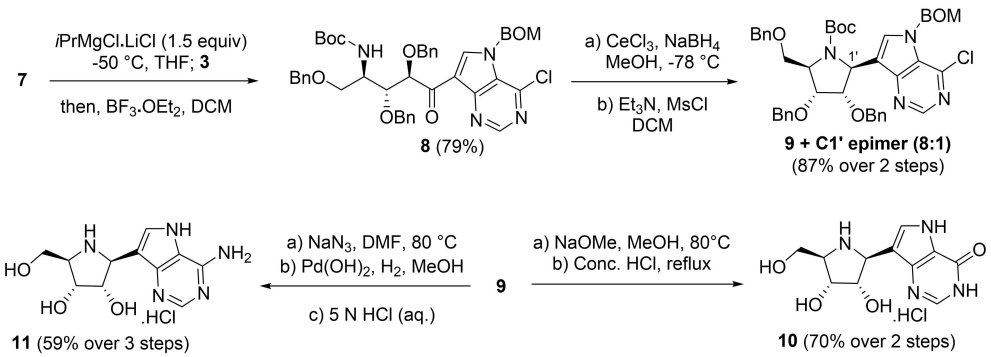

Scheme 2. Synthesis of BCX-1777 (**10**) & BCX-4430 (**11**).

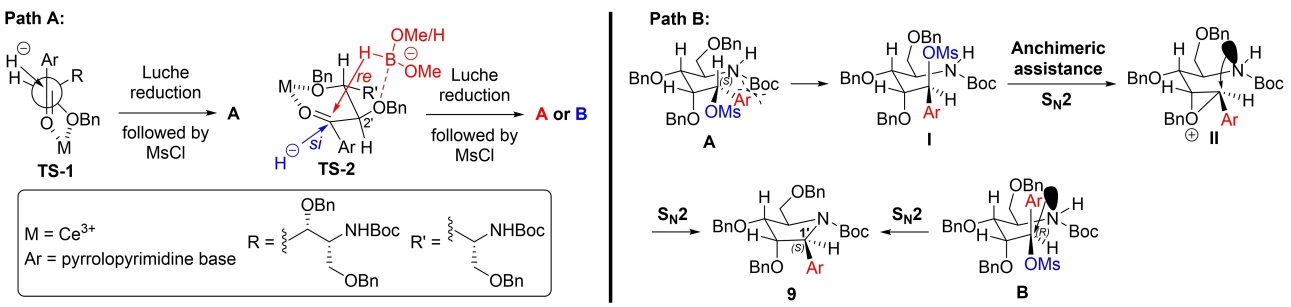

Scheme 3. Plausible pathways for stereoselective formation of compound **9**.

OBn group by anchimeric assistance (**II**) and subsequent unhindered and facile S_N2 attack by NHBoc group affords the desired compound **9** (Path B, Scheme 3). On the other hand, an apparent S_N2 attack by NHBoc with mesylate **B** affords compound **9**. As envisaged, compound **9** served as an advanced intermediate that provided BCX-1777 (**10**) in 70% yield over two steps, C-6 substitution by methoxide followed by global deprotection in the presence of concentrated HCl. Secondly, compound **9** was treated with sodium azide for C-6 substitution, followed by a reduction in the presence of $Pd(OH)_2/H_2$ in methanol for three days to effect global deprotection, and subsequent treatment with 5 N HCl afforded BCX-4430 (**11**) in 59% yield over three steps.

Conclusion

In summary, a standalone process for synthesizing BCX-1777 and BCX-4430 from a common intermediate is described against the existing routes that rely on BCX-1777 as the starting material for the synthesis of BCX-4430. An addition-reduction-cyclization synthetic strategy was undertaken to afford the common intermediate, with chemoselective and stereoselective steps. We proposed the role of anchimeric assistance for stereoselectivity that facilitates even the undesired mesylate to afford the desired configuration of compound **9** at the C-1′ position. The advanced common intermediate offers an opportunity to vary the chloro substituent in the C-6 position with other nucleophiles to afford novel immucillin derivatives. The present work was applied for a process patent application (No. 202111061664), filed in December 2021.

Experimental Section

***tert*-Butyl (2*R*,3*R*,4*R*)-1,3,4-tris(benzyloxy)-5-(5-((benzyloxy)methyl)-4-chloro-5*H*-pyrrolo[3,2-*d*]pyrimidin-7-yl)-5-oxopentan-2-yl)carbamate (8)**: Thoroughly dried compound **7** (1.9 g, 4.78 mmol, 1.5 equiv.) was taken in a 100 mL round-bottomed flask and dissolved in dry THF (20 mL) under argon atmosphere. The solution was cooled to −50 °C and 1.3 M *i*PrMgCl·LiCl solution in THF (3.67 mL, 4.78 mmol, 1.5 equiv.) was transferred using a cannula. After 10 min, lactam **3** (1.65 g, 3.18 mmol, 1 equiv.) in 5 mL of THF was transferred via cannula and the stirring was continued at −50 °C. After 3 hours, the reaction mixture was quenched with 2 mL of MeOH and was allowed to warm to room temperature. The reaction mixture was partitioned between EtOAc (200 mL) and distilled water (200 mL). The aqueous layer was extracted with EtOAc (100 mL×3) and the combined organic layers were dried over anhydrous Na_2SO_4, and concentrated under reduced pressure. The resulting crude pale yellow colored syrup was dried under vacuum, dissolved in DCM (25 mL), and cooled to −20 °C under argon atmosphere. Catalytic amount of $BF_3.OEt_2$ was added, after 30 min, the reaction mixture was quenched by adding saturated aqueous $NaHCO_3$ solution (10 mL), and extracted in EtOAc (150 mL). Organic layers were dried over anhydrous Na_2SO_4, and concentrated under reduced pressure. Silica gel column purification (30% EtOAc in hexane to 40% EtOAc in hexane) of the crude pale yellow colored syrup afforded 1.63 g of compound **8** as a colorless viscous liquid in 79% yield (Yield calculated on the basis of isolated compound **8** and recovered lactam **3** (0.29 g)).

(3*R*,4*R*,5*R*)-*tert*-Butyl 3,4-bis(benzyloxy)-5-((benzyloxy)methyl)-2-(5-((benzyloxy)methyl)-4-chloro-5*H*-pyrrolo[3,2-*d*]pyrimidin-7-yl)-2-hydroxypyrrolidine-1-carboxylate (9): To compound **8** (1.45 g, 1.83 mmol, 1 equiv.) in MeOH (25 mL), $CeCl_3$ (0.68 g, 2.74 mmol, 1.5 equiv.) was added and cooled to −78 °C, and sodium borohydride (0.17 g, 4.58 mmol, 2.5 equiv.) was added and stirred for 10 mins. The reaction mixture was quenched with 1 M NaH_2PO_4 (20 mL) and extracted in DCM (100 mL×3). The organic layer was dried over anhydrous Na_2SO_4, and passed through a silica plug to yield 1.4 g (96.3%) of the reduced product as a colorless viscous liquid. The reduced product was dissolved in dry DCM (30 mL) and cooled to 0 °C, and added triethylamine (1.72 mL, 12.35 mmol, 7 equiv.), mesyl chloride (0.82 mL, 10.58 mmol, 6 equiv.) was added dropwise into the reaction mixture by maintaining an inert argon atmosphere. The reaction mixture was allowed to warm to room temperature and stirred. After 20 hours, the reaction mixture was quenched with saturated aqueous NH_4Cl (100 mL), and extracted in DCM (100 mL×3). The organic layer was washed with distilled water (2×50 mL), and brine (50 mL). Concentration of organic layer and purification by silica gel column chromatography (20% EtOAc in hexane to 30% EtOAc in hexane) afforded a separable mixture of compound **9** as a colorless viscous liquid (1.09 g, 76.8% yield over 2 steps), and C1′ epimer as a colorless viscous liquid (0.14 g, 9.9% yield over 2 steps), culminating in an 8:1 ratio of compound **9** and its C1′ epimer.

Forodesine hydrochloride (10, BCX-1777): To a solution of compound **9** (0.2 g, 0.26 mmol) in MeOH (3 mL) was added NaOMe (0.07 g, 1.29 mmol, 5 equiv.) and heated under reflux. After 30 hours, the solvent was completely evaporated and the residue was partitioned between DCM (25 mL) and distilled water (25 mL). The organic layer was washed with brine (25 mL) and dried over anhydrous Na_2SO_4, and passed through a small plug of silica to remove polar impurities. The resulting filtrate was concentrated to afford a colorless viscous liquid (0.19 g), dissolved in MeOH (0.5 mL), and added concentrated hydrochloric acid (3 mL). The resulting mixture was heated to boil, after 72 hours, the solvent was removed under reduced pressure to afford a brownish red colored solid, which was dissolved in MeOH (0.5 mL) and diluted with DCM until a white precipitate was obtained. The precipitate was filtered and washed with DCM, and dried to afford 0.055 g of BCX-1777 (**10**, 70% yield over 2 steps) as a white powder, and an overall yield of 38% from 2,3,5-tri-*O*-benzyl-D-ribonolactone over 10 steps.

Galidesivir hydrochloride (11, BCX-4430): To compound **9** (0.2 g, 0.26 mmol, 1 equiv.) in DMF (3 mL), NaN_3 (0.08 g, 1.29 mmol, 5 equiv.) was added and stirred at 80 °C. After 10 hours, the reaction mixture was cooled to room temperature and poured into ice, and the product was extracted using DCM (3×20 mL). The organic layer was washed with distilled water (5×60 mL) to remove DMF, and dried over anhydrous Na_2SO_4, and passed through a small plug of silica to remove polar impurities to afford a colorless viscous liquid (0.18 g), which was dissolved in MeOH (3 mL) and $Pd(OH)_2/C$ (20% w/w) was added (0.2 g). H_2 gas was purged through the reaction mixture for 5 mins and the suspension was stirred for 5 days under H_2 atmosphere. The reaction mixture was filtered through celite (2 g) and the solvent was completely evaporated. To the resulting mixture aqueous 5 N HCl (3 mL) was added and stirred at room temperature. After 30 mins, the solvent was evaporated to afford a brown colored solid, which was purified by C18 column chromatography (0.001 M HCl (aq.)) to afford 0.046 g of BCX-4430 (**11**, 59 % yield over 3 steps) as a white powder, and an overall yield of 32% from 2,3,5-tri-*O*-benzyl-D-ribonolactone over 11 steps.

Acknowledgements

This work was financially supported by Council of Scientific and Industrial Research (CSIR), India (Project number: HCP-29).

Conflict of Interest

The authors declare no conflict of interest.

Data Availability Statement

The data that support the findings of this study are available in the supplementary material of this article.

Keywords: Antiviral agents · Chemoselectivity · Immucillins · Nucleosides · Stereoselectivity

[1] M. I. Elzagheid, *Mini-Rev. Org. Chem.* **2021**, *18*, 672–679.
[2] T. K. Warren, J. Wells, R. G. Panchal, K. S. Stuthman, N. L. Garza, S. A. van Tongeren, L. Dong, C. J. Retterer, B. P. Eaton, G. Pegoraro, S. Honnold, S. Bantia, P. Kotian, X. Chen, B. R. Taubenheim, L. S. Welch, D. M. Minning, Y. S. Babu, W. P. Sheridan, S. Bavari, *Nature* **2014**, *508*, 402–405.
[3] J. G. Julander, J. F. Demarest, R. Taylor, B. B. Gowen, D. M. Walling, A. Mathis, Y. S. Babu, *Antiviral Res.* **2021**, *195*, 105180.
[4] A. Korycka, J. Blonski, T. Robak, *Mini-Rev. Med. Chem.* **2007**, *7*, 976–983.
[5] G. W. J. Fleet, J. C. Son, *Tetrahedron* **1988**, *44*, 2637–2647.
[6] G. B. Evans, R. H. Furneaux, G. J. Gainsford, V. L. Schramm, P. C. Tyler, *Tetrahedron* **2000**, *56*, 3053–3062.
[7] B. A. Horenstein, R. F. Zabinski, V. L. Schramm, *Tetrahedron Lett.* **1993**, *34*, 7213–7216.
[8] R. H. Furneaux, P. C. Tyler, *J. Org. Chem.* **1999**, *64*, 8411–8412.
[9] G. B. Evans, R. H. Furneaux, T. L. Hutchison, H. S. Kezar, P. E. Morris, V. L. Schramm, P. C. Tyler, *J. Org. Chem.* **2001**, *66*, 5723–5730.
[10] M. Zhang, F. Xue, J. Ou, Y. Huang, F. Lu, B. Zhou, Z. Zheng, X.-Y. Liu, W. Zhong, Y. Qin, *Org. Chem. Front.* **2020**, *7*, 3675–3680.
[11] V. P. Kamath, J. Xue, J. J. Juarez-Brambila, P. E. Morris, *Tetrahedron Lett.* **2009**, *50*, 5198–5200.
[12] X. Xu, *Process for Preparation of Anti-Ebola Virus Agent BCX4430*, **2015**, CN 104513249 A.
[13] D. Kumar Ojha, R. N. Prasad, H. Rao, Y. Gupta, U. Agrawal, P. Chand, *J. Indian Chem. Soc.* **2014**, *91*, 1451–1457.
[14] G. A. Kicska, P. C. Tyler, G. B. Evans, R. H. Furneaux, W. Shi, A. Fedorov, A. Lewandowicz, S. M. Cahill, S. C. Almo, V. L. Schramm, *Biochemistry* **2002**, *41*, 14489–14498.
[15] T. Ohta, A. Hosoi, S. Nozoe, *Tetrahedron Lett.* **1988**, *29*, 329–332.
[16] T. Sengoku, Y. Satoh, M. Takahashi, H. Yoda, *Tetrahedron Lett.* **2009**, *50*, 4937–4940.
[17] C.-M. Si, Z.-Y. Mao, Y.-W. Liu, Z.-T. Du, B.-G. Wei, G.-Q. Lin, *Org. Chem. Front.* **2015**, *2*, 1485–1499.
[18] M. Yokoyama, T. Ikenogami, H. Togo, *J. Chem. Soc., Perkin Trans. 1* **2000**, 2067–2071.
[19] K. Tatsuta, T. Hirabayashi, M. Kojima, Y. Suzuki, T. Ogura, *J. Antibiot.* **2004**, *57*, 291–297.
[20] H. Imamura, A. Shimizu, H. Sato, Y. Sugimoto, S. Sakuraba, S. Nakajima, S. Abe, K. Miura, I. Nishimura, K. Yamada, H. Morishima, *Tetrahedron* **2000**, *56*, 7705–7713.
[21] H. Yoda, T. Nakajima, K. Takabe, *Tetrahedron Lett.* **1996**, *37*, 5531–5534.
[22] N. Ikota, *Tetrahedron Lett.* **1992**, *33*, 2553–2556.
[23] J. N. Gorantla, A. Faseela, R. S. Lankalapalli, *Chem. Phys. Lipids* **2016**, *194*, 158–164.
[24] H. S. Overkleeft, J. van Wiltenburg, U. K. Pandit, *Tetrahedron* **1994**, *50*, 4215–4224.
[25] R. H. Furneaux, P. C. Tyler, *J. Org. Chem.* **1999**, *64*, 8411–8412.
[26] A. Krasovskiy, P. Knochel, *Angew. Chem., Int. Ed.* **2004**, *43*, 3333–3336.
[27] T. K. Warren, R. Jordan, M. K. Lo, A. S. Ray, R. L. Mackman, V. Soloveva, D. Siegel, M. Perron, R. Bannister, H. C. Hui, N. Larson, R. Strickley, J. Wells, K. S. Stuthman, S. A. van Tongeren, N. L. Garza, G. Donnelly, A. C. Shurtleff, C. J. Retterer, D. Gharaibeh, R. Zamani, T. Kenny, B. P. Eaton, E. Grimes, L. S. Welch, L. Gomba, C. L. Wilhelmsen, D. K. Nichols, J. E. Nuss, E. R. Nagle, J. R. Kugelman, G. Palacios, E. Doerffler, S. Neville, E. Carra, M. O. Clarke, L. Zhang, W. Lew, B. Ross, Q. Wang, K. Chun, L. Wolfe, D. Babusis, Y. Park, K. M. Stray, I. Trancheva, J. Y. Feng, O. Barauskas, Y. Xu, P. Wong, M. R. Braun, M. Flint, L. K. McMullan, S.-S. Chen, R. Fearns, S. Swaminathan, D. L. Mayers, C. F. Spiropoulou, W. A. Lee, S. T. Nichol, T. Cihlar, S. Bavari, *Nature* **2016**, *531*, 381–385.

Manuscript received: April 10, 2022
Revised manuscript received: May 25, 2022
Accepted manuscript online: May 27, 2022